Orbital Transfer Vehicle
3000 LBF Thrust Chamber Assembly
Hot Fire Test Program

Interim Report
Contract/Task Order NAS 3-23772-C.2
NASA CR 182145
September 1988

Prepared For:
National Aeronautics and Space Administration
NASA Lewis Research Center

Aerojet
TechSystems
Company

1. Report No.	2. Government Accession No.	3. Recipient's Catalog No.
NASA CR-182145		

4. Title and Subtitle	5. Report Date
Orbital Transfer Vehicle 3000 lbf Thrust Chamber Assembly Hot-Fire Test Program Interim Report	March 1988
	6. Performing Organization Code
7. Author(s)	8. Performing Organization Report No.
Judy Schneider and Warren R. Hayden	
	10. Work Unit No. 506-42-21 S2583
9. Performing Organization Name and Address Aerojet TechSystems Company Highway 50 and Aerojet Road PO Box 13400 Sacramento, CA 95813	11. Contract or Grant No. Interim - Contractor Report
	13. Type of Report and Period Covered
12. Sponsoring Agency Name and Address National Aeronautics & Space Administration Washington, D.C. 20546	14. Sponsoring Agency Code

15. Supplementary Notes

Task Order Manager: Tamara A. Smith
NASA Lewis Research Center
Cleveland, Ohio 44135

16. Abstract

The Aerojet Orbital Transfer Vehicle (OTV) Thrust Chamber Assembly (TCA) concept consists of a hydrogen cooled chamber, an annular injector, and an oxygen cooled centerbody. This report documents the hot fire testing of a heat sink version of the chamber with only the throat section using hydrogen cooling. Hydraulic performance of the injector and cooled throat were verified by water flow testing prior to TCA assembly. The cooled throat was proof tested to 3000 psia to verify the integrity of the co-deposited EF Nickel-Cobalt closeout. The first set of hot fire tests were conducted with a heat sink throat to obtain heat flux information. After demonstration of acceptable heat fluxes, the heat sink throat was replaced with the LH2 cooled throat section.

Fourteen tests were conducted with a heat sink chamber and throat at chamber pressures of 85 to 359 psia. The injector face was modified at this time to add more face coolant flow. Ten tests were then conducted at chamber pressures of 197 to 620 psia. To run higher chamber pressure tests, the heat sink throat was replaced by the LH2 cooled throat. Seven tests were conducted at chamber pressures of 513 to 2104 psia. Actual heat fluxes at the higher (2000 psia) chamber pressure range were 23% higher than the average of 10 Btu/in**2 predicted. Heat flux was directly proportional to chamber pressure and showed little change with mixture ratio. Energy release efficiencies (ERE) were calculated to range from 100.5 to 104.8%. Data scatter hampered the performance correlations at higher chamber pressures as did the lack of steady state data. Additional work is recommended to modify the injector element for better wall compatibility. The cooled throat hardware was in excellent condition at the completion of testing.

17. Key Words (Suggested by Author(s))	18. Distribution Statement
	Unlimited

19. Security Classif. (of this report)	20. Security Classif. (of this page)	21. No. of pages	22. Price*
UNCLASSIFIED	UNCLASSIFIED	222	

*For sale by the National Technical Information Service, Springfield, Virginia 22161

FOREWORD

This document represents the final report to the National Aeronautics and Space Administration for work performed under Task Order C.2 to contract NAS 3-23772. The task work span was from December 1984 to March 1988. Task work was initiated by Len Schoenman, the Project Engineer, and carried through completion of testing by the Task Leader, Deena Berkman. The OTV Engine program at ATC was transferred from the Research Group to Advanced Engineering in 1986. Warren Hayden was assigned as Project Engineer after the program transfer with Judy Schneider as Thrust Chamber Assembly (TCA) Task Leader.

This is a summary report in that all material discussed herein was presented to NASA program personnel at oral presentations or in the contractually required monthly reports submitted while the work was in progress.

The authors wish to acknowledge the assistance of Deena Berkman and Len Schoenman for providing material, review, and comments during report preparation and for the analysis assistance from Jack Ito, Karen Niiya, Blake Cathroe, Dick Ewen, Felix Chen, and Sal Buccella.

Orbital Transfer Vehicle
3000 lbF Thrust Chamber Assembly
Hot-Fire Test Program

NASA CR-182145

INTERIM REPORT

Prepared By:

Judy Schneider and Warren Hayden
Aerojet TechSystems Company

For

National Aeronautics and Space Administration

September 1988

NASA-Lewis Research Center
Contract NAS 3-23772

Contract/Task Order NAS 3-23772-C.2

TABLE OF CONTENTS

TABLE OF CONTENTS (cont.)

TABLE OF CONTENTS (cont.)

LIST OF TABLES (cont.)

LIST OF FIGURES (cont.)

LIST OF FIGURES (cont.)

LIST OF FIGURES

LIST OF TABLES

LIST OF FIGURES (cont.)

LIST OF FIGURES (cont.)

I. INTRODUCTION

A. BACKGROUND

The thrust chamber test program documented in this report supports the NASA-OAST plans for development of a new Orbit Transfer Vehicle (OTV) to be operational in the late 1990's. Critical to the economical operation of a space based OTV is a new O_2/H_2 rocket engine with capabilities superior to available engines. Table I summarizes the available engine characteristics and those required of a new engine. In total, these requirements represent a substantial advance in the state-of-the-art and a considerable challenge to rocket engine designers. Aerojet Techsystems Company (ATC) has selected a unique engine cycle and thrust chamber configuration in response to these requirements.

In a conventional expander cycle engine hydrogen is routed through passages in the combustion chamber wall where it both cools the wall and acquires sufficient thermal energy to power the turbine drives of pumps for both the hydrogen and oxygen flow circuits. It is then routed to the injector for combustion. This cycle is fairly simple, plumbing is straightforward, and it offers good performance potential. Since all propellant is burned in the combustion chamber it does not have the losses of open cycles. Its limitations are related to dependence on only one working fluid for turbine drive energy. High turbopump and engine chamber pressures require the hydrogen to exit the regen chamber at temperatures very near to the design limits for the chamber liner. For copper alloy based chambers this is 1000 degrees F. A marked improvement in engine operating flexibility and high chamber pressure capability is available if oxygen can be used as a working fluid driving the turbine on the oxidizer circuit Turbine Pump Assembly (TPA). This reduces the demands on the hydrogen circuit and allows for the turbopumps to be designed without inter-propellant seals or mechanical gear train connections. This new engine cycle proposed by Aerojet for the OTV, is called the dual expander engine cycle.

The purpose of the test program documented in this report is to evaluate the TCA design proposed for the OTV dual expander engine cycle. The ATC thrust chamber design which was proposed for the OTV engine included a hydrogen cooled outerchamber and throat, an annular 2-row injector, and an inner body with oxygen regenerative cooling. For the actual thrust chamber assembly that was

Table I
Technology Goals for the New OTV Engine

Parameters	Available Engine System Characteristics	Requirements for a New Engine: October 1986 NASA Goals and/or Requirements	Requirements for a New Engine: 1987 Updated Goals or Requirements
Basing	Earth	Not Specified	Space
Human-rating	No	Not Specified	Yes
Design Criteria	Not Specified	Not Specified	Fail Operational, Fail Safe
Propellants - Fuel	Hydrogen	Hydrogen	Hydrogen
- Oxidizer	Oxygen	Oxygen	Oxygen
Vacuum Thrust (Design Point)	15,000 lbf	10,000 - 25,000 lbf*	7500 lbf (per engine)
Number of Engines per Vehicle		Not Specified	2 Minimum
Engine Mixture Ratio, O/F (Design Point)	5.0	6.0	6.0
Engine Mixture ratio Range, O/F	4.4 to 5.6	5 - 7	5 - 7
Propellant Inlet Temperature -			
Hydrogen	38.3°R	37.8°R	37.8°R
Oxygen	175.3°R	162.7°R	162.7°R
Gimbal	±4.0 Degrees	±6.0 Degrees (Sq. Pattern)	±20 degrees Pitch & Yaw
Aerobraking Design Criteria	The engine must be compatible with aeroassist return of the vehicle to low-earth orbit.		
Vacuum Specific Impulse	444 lbf-sec/lbm	520 lbf-sec/lbm	490 lbf-sec/lbm
Vacuum Thrust Throttling Ratio	No Throttling	30:1	10:1
Net Positive Suction Head (NPSH)-			
Hydrogen	133.0 ft-lbf/lbm	0	15 ft-lbf/lbm
Oxygen	16.7 ft-lbf/lbm	0	2 ft-lbf/lbm
Weight	290 lbm	360 lbm	360 lbm (2 engines)
Length	70.1 in.	40	TBD
Reliability (90% Confidence Level)	0.9982	1.0	.9997
Operational Life	3 Starts, 4000 sec	500 Starts, 20 Hours	500 Starts, 20 Hours
Service Free-Life		100 Starts, 4 Hours	100 Starts, 4 Hours
Start Cycle		Chilldown with propulsive dumping of propellants, tankhead start, pumped idle operation, autogenous tank pressurization required	

Updated 3 November 1987

*Vehicle engine set total thrust must be in this range

tested, the cooled outerbody, centerbody, and throat section were replaced with copper billets machined to the dimensions of the original design. This hardware served as a heat sink chamber suitable for injector testing at low (<1000 psia) chamber pressures. For higher chamber pressures the heat sink copper throat was replaced with a hydrogen cooled throat. Use of the cooled throat allowed test times of nearly 2 seconds before any melting would occur in the heat sink combustor.

The cooled throat was fabricated from a NAS-Z copper alloy billet with machined coolant channels of 0.010 inches width. The channels were closed out with a specially developed electroformed Nickel-Cobalt co-deposited alloy. This was the first successful application of this closeout material. It has material properties approximately three times those of a pure nickel closeout.

B. SCOPE OF WORK

The Contractor shall provide the necessary personnel to fabricate a LH_2 cooled throat section, to conduct hot fire test evaluation and the data analysis for a fully variable thrust, thrust chamber assembly using gaseous hydrogen and gaseous oxygen as propellants.

Specific Subtasks

The Contractor shall accomplish the scope of work by performance of the specific subtasks which follow. The effort shall be conducted in accordance with "Work Plan for Thrust Chamber Assembly," dated June 1983, submitted in response to Contract Task Order NAS 3-23772-A.3.

Subtask I - Cooled Throat Fabrication

The Contractor shall fabricate one LH_2 cooled throat section, PN 1197112-9. The completed throat section shall be subjected to non-destructive testing to evaluate the structural integrity of the closeout bond and welds. In addition, the throat section shall be subjected to a pressure of 6500 psia with proof and leak check. A water flow check shall be performed.

Subtask II - Proof and Leak-Testing and Installation of Hardware Instrumentation

The assembled heat sink thrust chamber (fabricated in Task Order NAS 3-23772-C.1) shall be subjected to a 3500 psia proof pressure test and a leak test prior to installing the instrumentation.

The hardware shall then be instrumented with the thermocouples shown in Assembly Drawing 1197110 and discussed in Section 3.0. Additional pressure and flow measuring instrumentation shall be added during final installation on the test stand.

Subtask III - Cold Flow and Igniter Checkout Tests

A series of propellant cold flow tests using the heat sink hardware as listed in the Test plan shall be conducted to establish the flow system and injector hydraulic characteristics for use in feed system flow control to obtain proper thrust and mixture ratio conditions in subsequent tests.

A series of ignition checkout tests as listed in the Test Plan shall be conducted using two types of ignition approaches: direct spark ignition and spark torch ignition (ignitor fabricated in Task Order NAS3-23772-C.1). One approach shall be selected for use in subsequent tests.

Subtask IV - Low Pressure Performance, Stability, and Heat Transfer Testing

A series of tests, as listed in the Test Plan, shall be conducted in which thrust, chamber pressure and mixture ratio are systematically varied. These short duration tests will use the heat sink chamber assembly including the heat sink copper throat. The maximum operating pressure will be in accordance with the heat sink capabilities of the throat.

Subtask V - High Pressure Performance, Stability, and Heat Transfer Testing

A series of tests, as listed in the Test Plan, shall be conducted in which the heat sink throat will be replaced by the LH_2 cooled throat. Testing will be conducted to operating pressures of approximately 2400 psi. The test durations and types of data recorded are discussed in the Test Plan and data presentation as listed in Table III of the Test Plan.

Subtask VI - Test Data Analysis and Documentation

The results of the testing shall be analyzed and documented by writing and delivering an interim report. A review of the work shall be presented at the NASA Lewis Research Center. The data to be included shall be as follows:

1) Low Pressure Ignition
   a) Direct Spark
   b) Oxidizer-Rich Torch
2) Combustion Stability
   a) With Resonator Cavities
   b) Without Resonator Cavities
3) Chamber Thermal Characteristics
   a) Total Heat Load to Centerbody
   b) Total Heat Load to Outer Chamber
   c) Local Heat Flux at Selected Stations
   d) Injector Face Cooling
   e) Resonator Cavity Cooling
4) Thrust Chamber Performance
   a) C* Combustion Efficiency at Chamber Pressure and Mixture Ratio Conditions Tested
   b) Thrust-Based Energy Release Efficiency at the Test Conditions

II. HARDWARE AND FACILITY

1.0 Hardware Description

1.1 Injector:

1.1.1 Design

Injector design goals are listed in Table 1.1.1-I. These goals were selected to achieve the overall operational goals defined for the OTV engine (Table I). Use of gaseous phase propellants was selected based on results of the work performed under NASA Contract NAS-3-14379 (Reference 3) as the best approach for providing the capability for wide range throttling and Mixture Ratio (MR) operations. In order to evaluate the injector design best suited for meeting the OTV requirements, three of ATC's element designs (Figure 1.1.1-1) were evaluated. The pre-mix triplet element was selected as offering the highest energy release efficiency in the MR range of interest (5 to 7).

Specific design parameters for the injector are listed in Table 1.1.1-II. These parameters were identified by performing a system analysis of the OTV engine. The overall design goals are utilized to determine specific information on flowrates, pressure and temperature of the propellants being delivered to the injector. Nominal operational parameters for thrust, chamber pressure, specific impulse, and Mixture Ratio were selected as a design point. Stability analysis of the injector design provided the dimensions of the acoustic cavities to ensure stable operation. Dimensions of the injector face were determined by the OTV engine design, specifically: chamber design, chamber contraction ratio, and injector element. Figure 1.1.1-2 shows the injector which consists of 72 pre-mix triplet elements arranged in two rows. The injector face encompasses the annular space between the regen-cooled chamber ID and the centerbody OD.

The ignition mechanism, also referred to as a "torch igniter" consists of a aviation type spark plug with separately plumbed fuel and oxidizer lines providing an oxidizer rich flame through the core (Figure 1.1.1-3). The igniter assembly is introduced through one of the acoustic cavities. The acoustic cavities, used to ensure combustion stability, are located around the circumference of the injector

TABLE 1.1.1-I

INJECTOR DESIGN GOALS

• **Energy Release Efficiency**	**>99.5%**
• Throttling	15:1 min
• **Mixture Ratio (MR)**	**5-7**
• Uniform and Predictable Combustion Chamber Heat Flux at High Contraction Ratio (16:1)	10 Btu/sec $in.^2$
• **Stable Combustion**	**CPIA 247***
• Pressure Drop	<15% of Pc
• **Cycle Life**	**500 Cycles**
• Operating Life	20 Hours
• **Fabrication**	**Low Cost**
• Proof Pressure	3500 psi

*Compliance with Combustion Guidelines Chemical Propulsion Information Agency (CPIA)

PREMIX TRIPLET PROVIDES HIGHEST ERE IN SHORTEST LENGTH CHAMBER

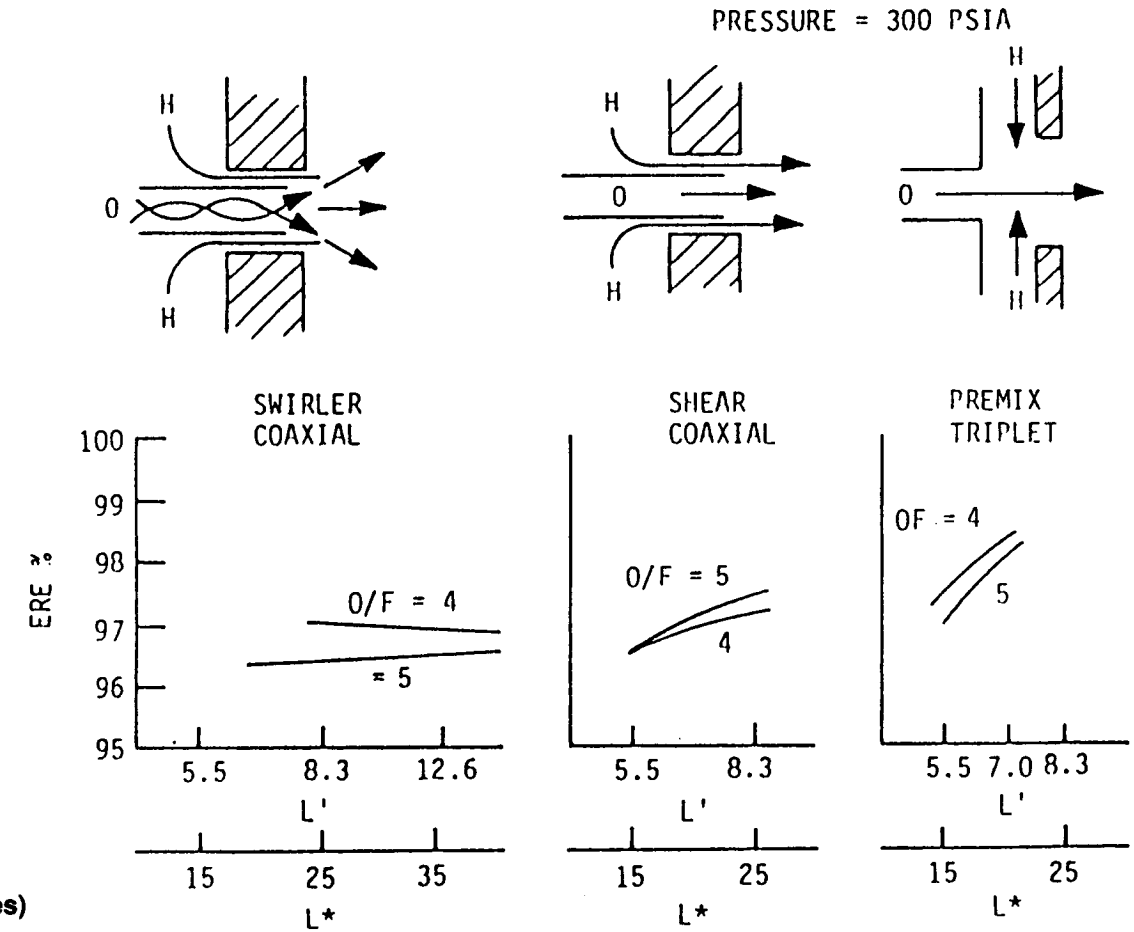

Nomenclature:

H	Hydrogen (GH2)
O	Oxidizer (GO2)
L'	Barrel Length (inches)
L*	Characteristic Chamber Length (Inches)
O/F	Mixture Ratio

Figure 1.1.1-1. Performance Test Results for Gas-Gas Combustion

TABLE 1.1.1-II

OTV INJECTOR DESIGN PARAMETERS

I. DESIGN PARAMETERS (Nominal)

A. Thrust, lbf (vacuum) - 3000

B. Chamber Pressure, psia - 2000

C. Propellants

1. Fuel - GH_2

a. $\dot{\omega}$ = .893 lb/sec

b. P = 2300 psia

c. T = 509°F or 969°R

2. Oxidizer - GO_2

a. $\dot{\omega}$ = 5.36 lb/sec

b. P = 2300 psia

c. T = 800°R (design)

D. M.R. = 6.0

E. Injector Face O.D. = 5.60 in.

F. Injector Face I.D. = 4.00 in.

G. Isp =480 sec

H. Resonator Cavity

1. 12 Partitions

2. .3 Wide x 1.3 Deep

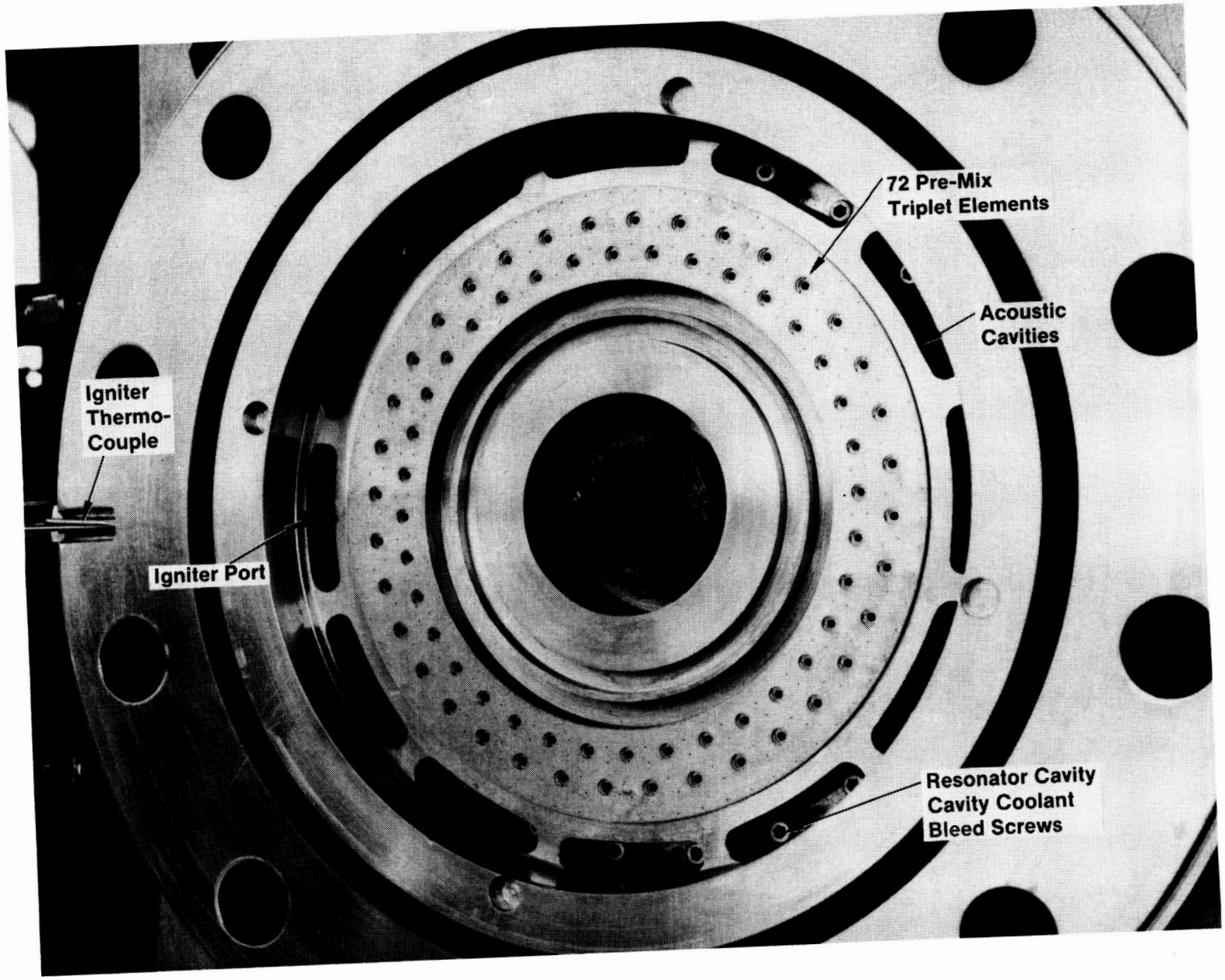

Figure 1.1.1-2. OTV Injector

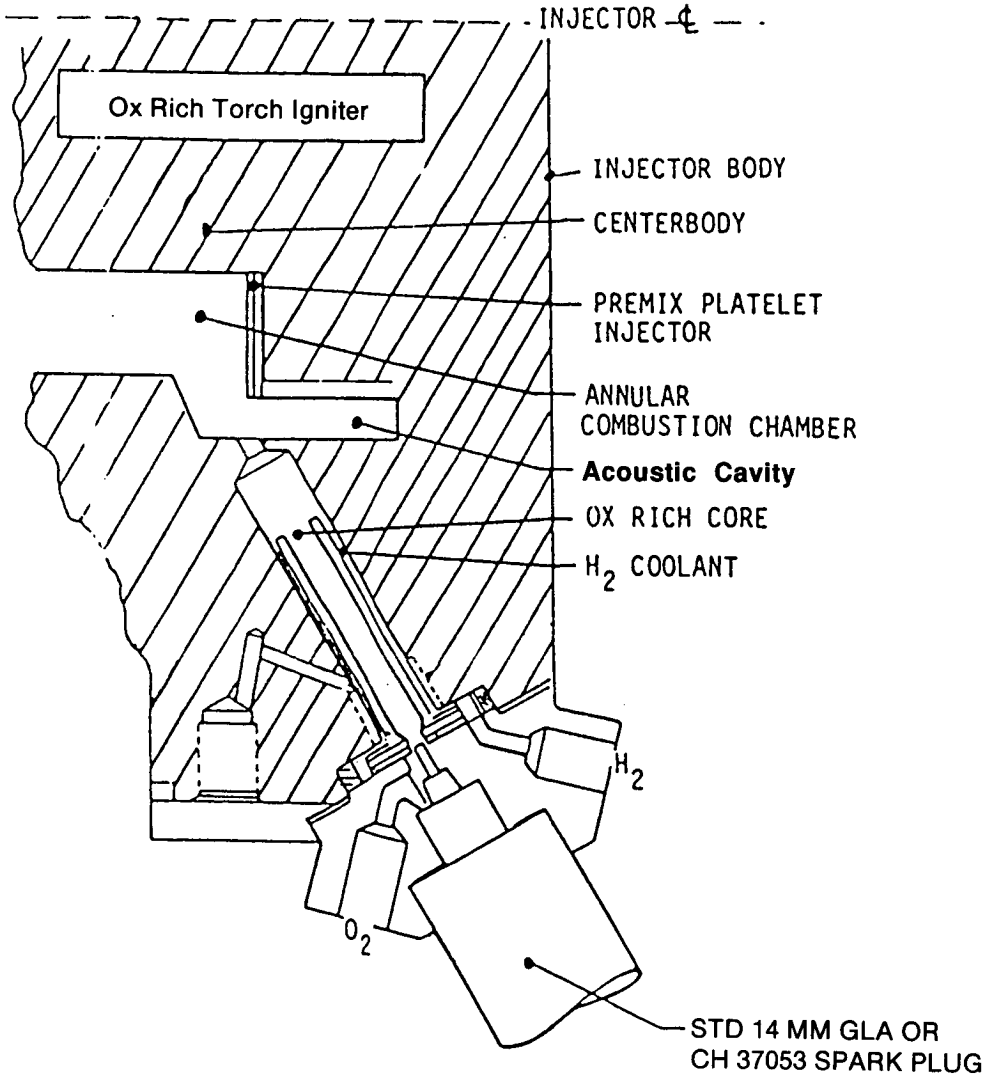

Figure 1.1.1-3. OTV Torch Igniter

circumference of the injector face as shown in Figure 1.1.1-3. Further discussion of the igniter design and test results is contained in Section 4.1.

1.1.2 Fabrication

The injector assembly, illustrated in Figure 1.1.2-1, consists of a machined manifold with a diffusion bonded stack of thin Nickel platelets forming the individual injector elements.

Figure 1.1.2-2 shows the machined injector manifold, prior to diffusion bonding of the platelets. Two annular manifolds furnish the fuel to the injector elements through cross drilled holes. Figure 1.1.2-3 shows a detail of the cross drilling. The oxidizer enters from the top of the injector manifold, and is fed to the elements by drilled metering holes. This design eliminates the need for numerous brazed tubes to isolate the fuel and oxidizer. Pre-mixing of the fuel and oxidizer occurs in the injector platelet stack (illustrated in Figured 1.1.2-4) before exiting into the combustion chamber and igniting.

A 0.61" stack of 10 Nickel 200 platelets, shown individually in Figure 1.1.2-5, forms the injector elements. Chemical milling generates the flow paths in each platelet. After the milling process, the Nickel platelets are diffusion bonded in a stack to a Nickel 200 manifold. Hydrogen bleed holes between the elements are used for face cooling.

The finished injector with lines and manifolds welded in place is shown in Figure 1.1.2-6.

1.1.3 Cold Flow Tests

A series of cold flow tests was conducted to evaluate injector flow nonuniformity induced by the manifolds and inlet line configuration. Data were generated by collecting the flow from selected individual fuel and oxidizer elements. Flow was captured by a specially fabricated collector tube and measured by a rotometer. The water supply was pressurized to simulate the injector manifold pressures expected over a range of operating conditions. Inlet pressure was monitored by a manometer gauge. Figure 1.1.3-1 provides the measured flow

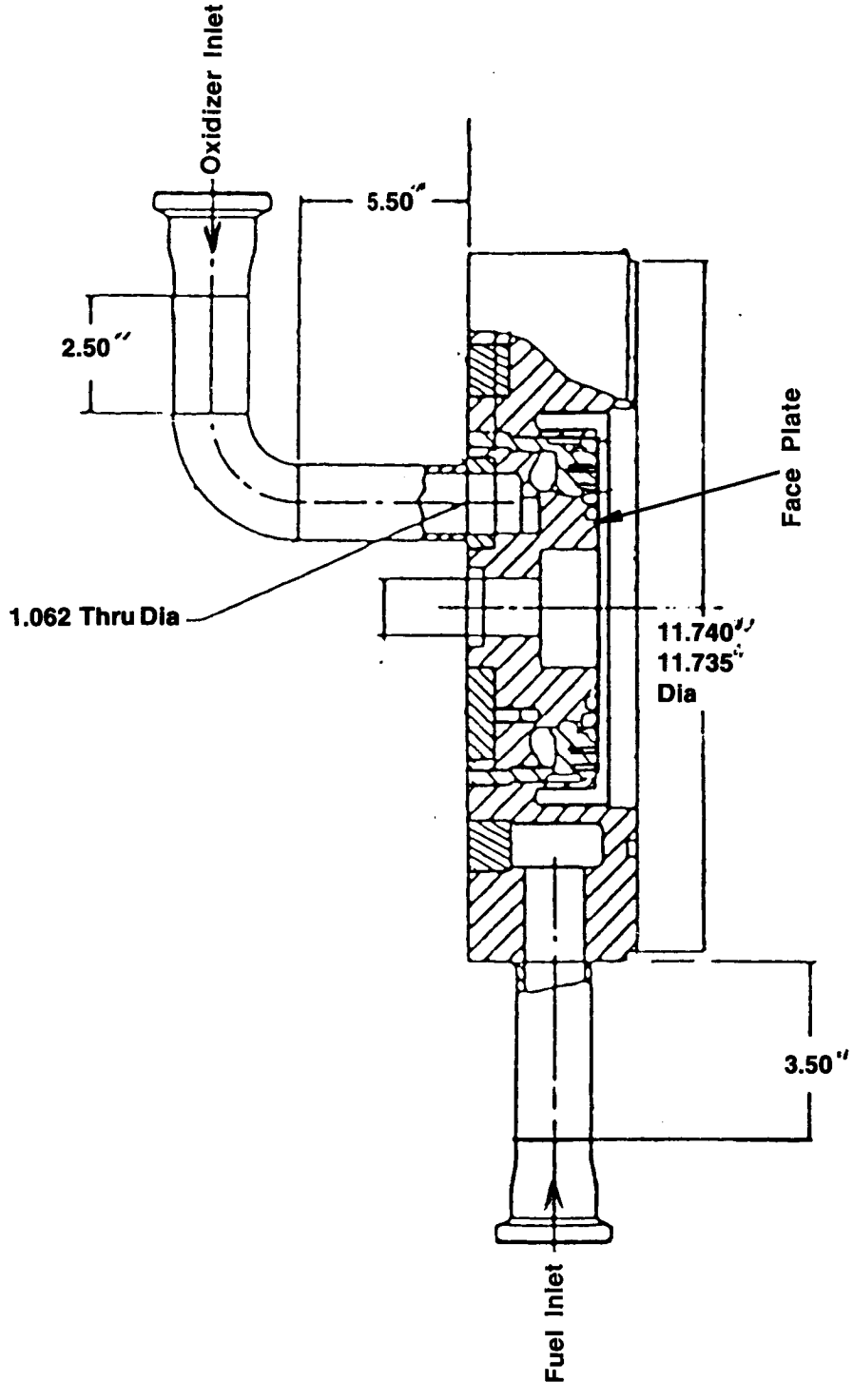

Figure 1.1.2-1. Injector Assembly

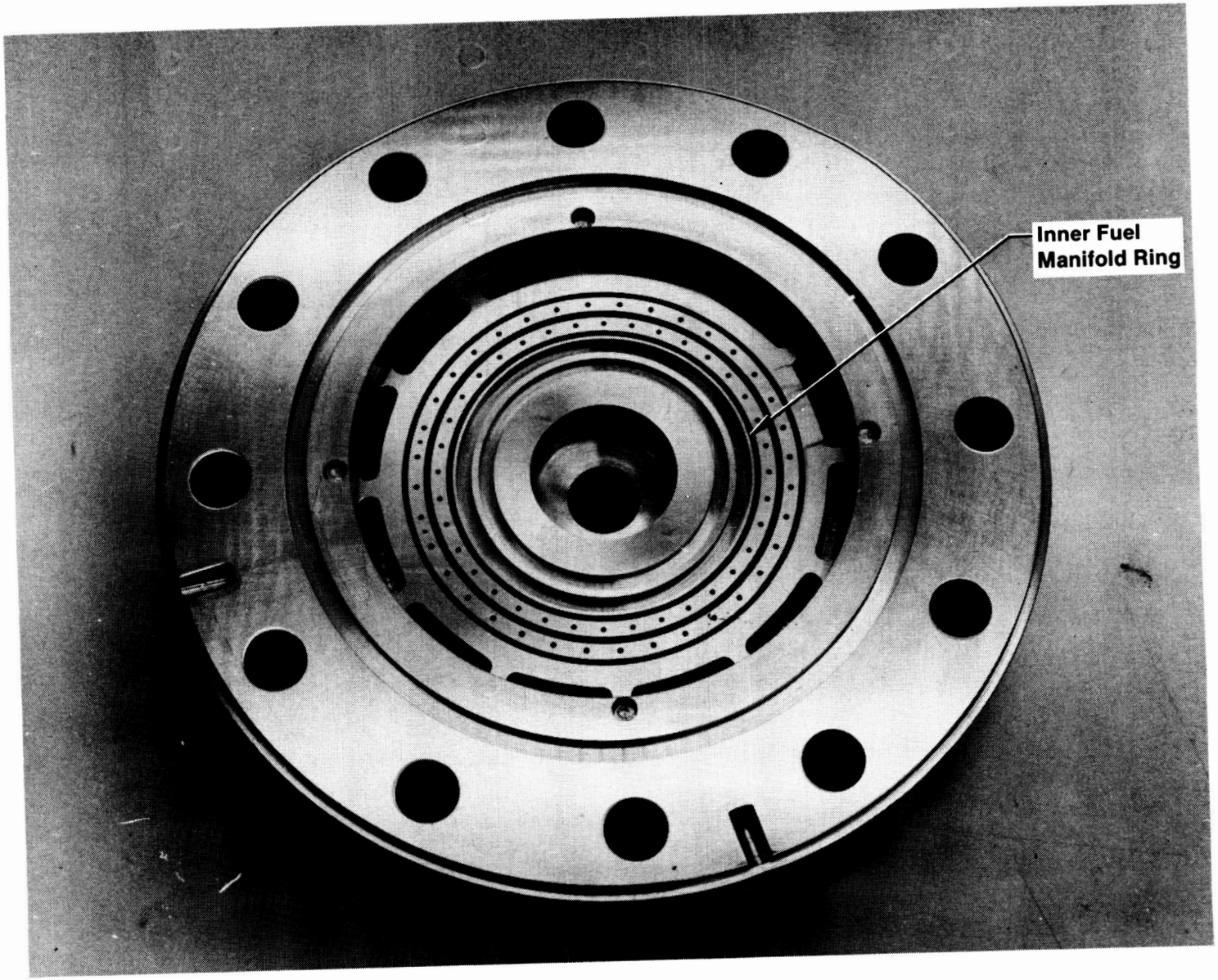

Figure 1.1.2-2. Machined Injector Manifold Prior to Diffusion Bonding

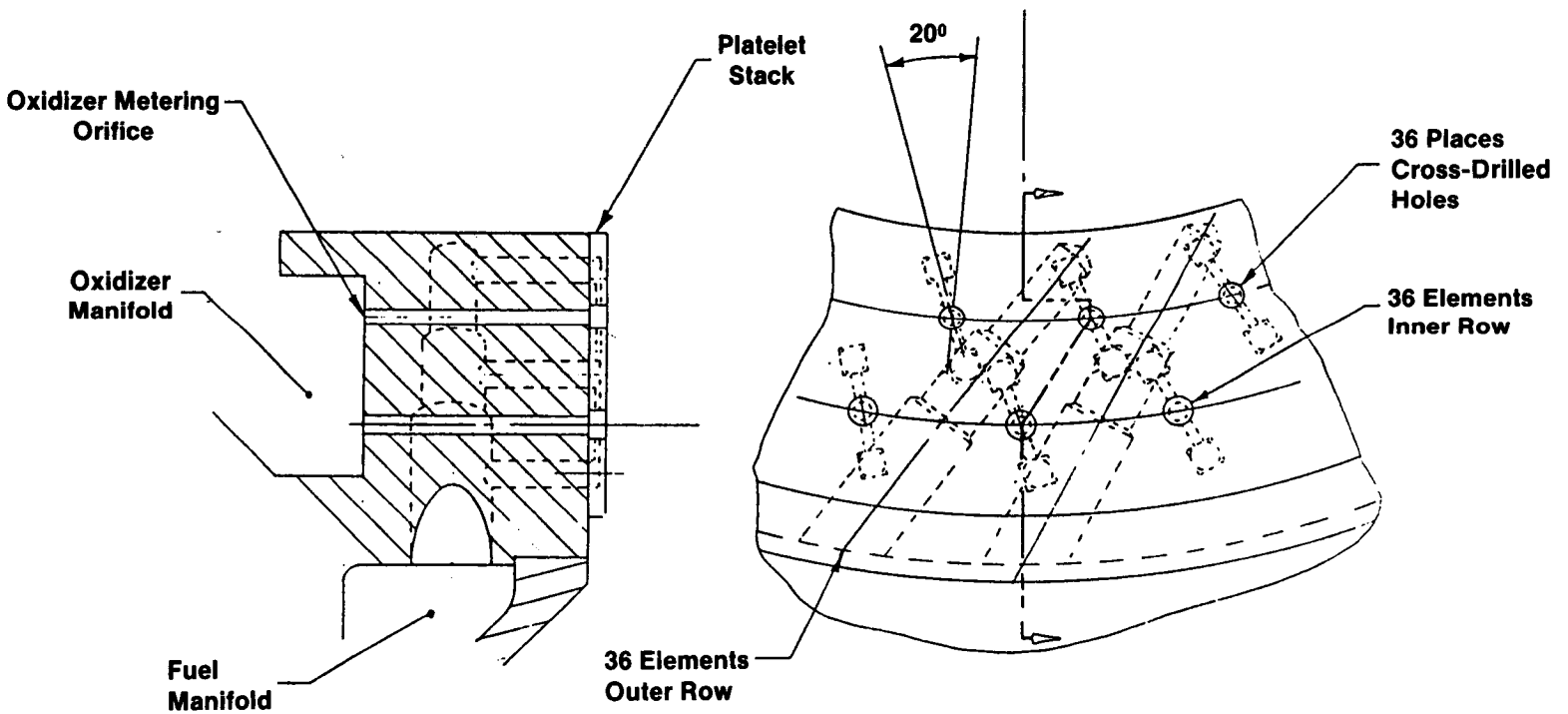

Figure 1.1.2-3. Premix Element Injection Pattern

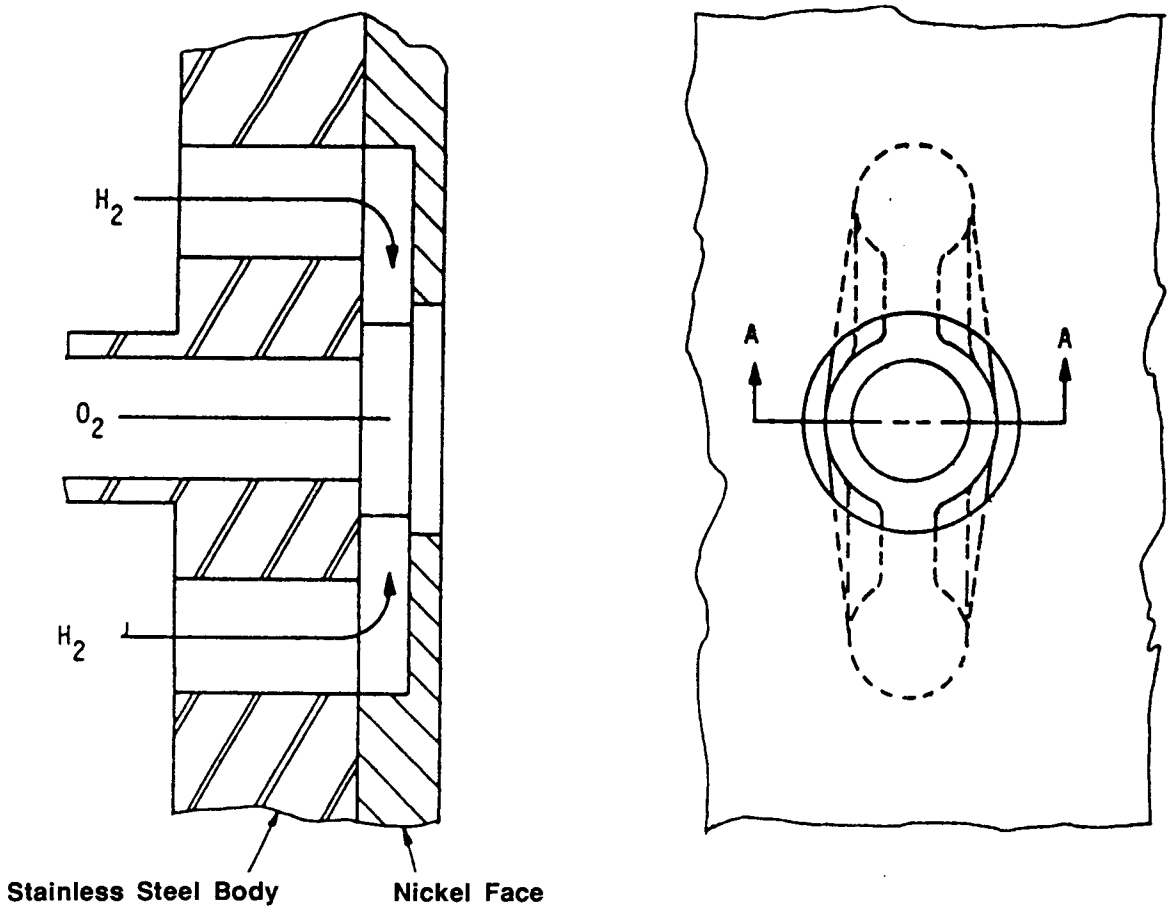

Figure 1.1.2-4. Modified "I" Premix Injector Element

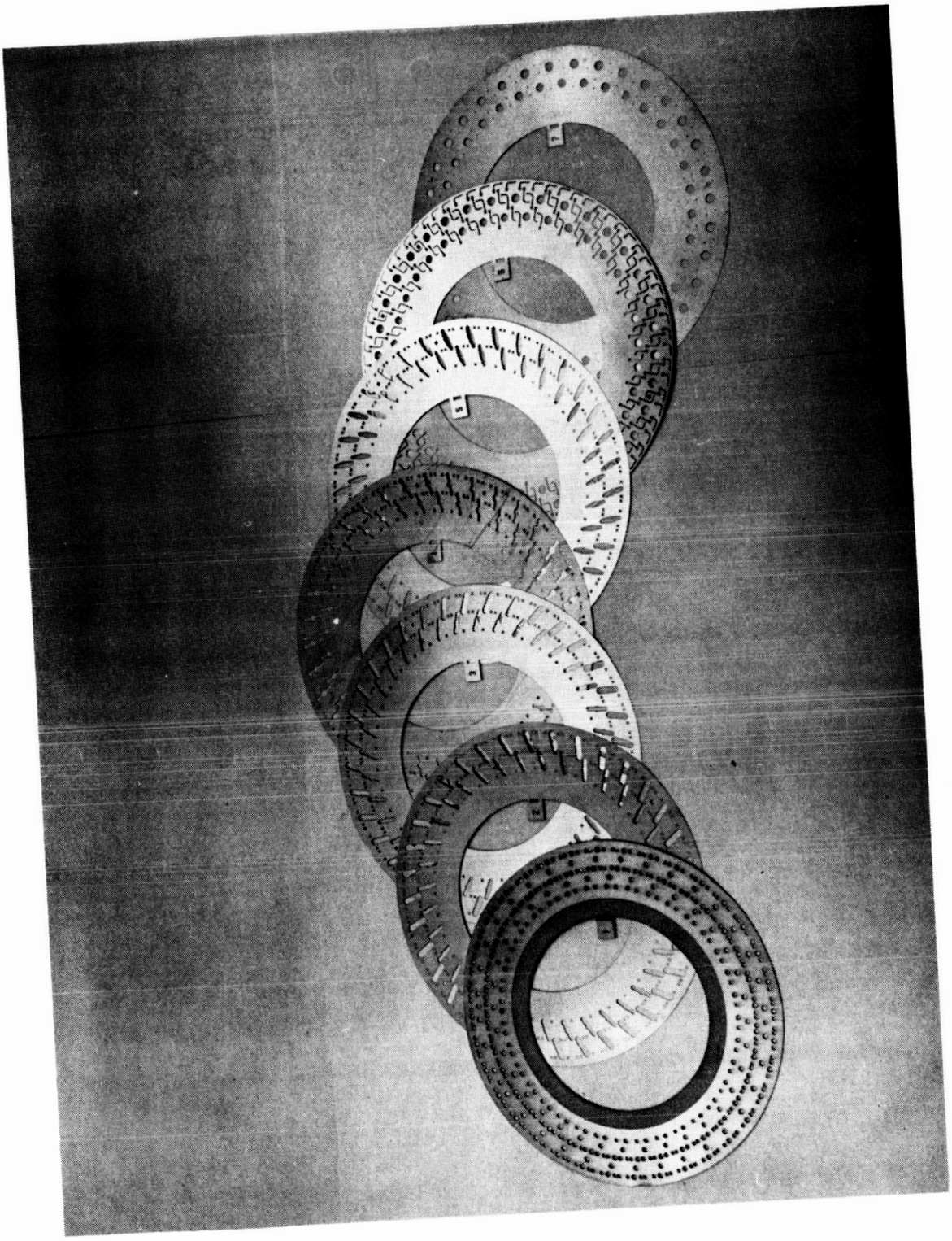

Figure 1.1.2-5. Injector Platelets

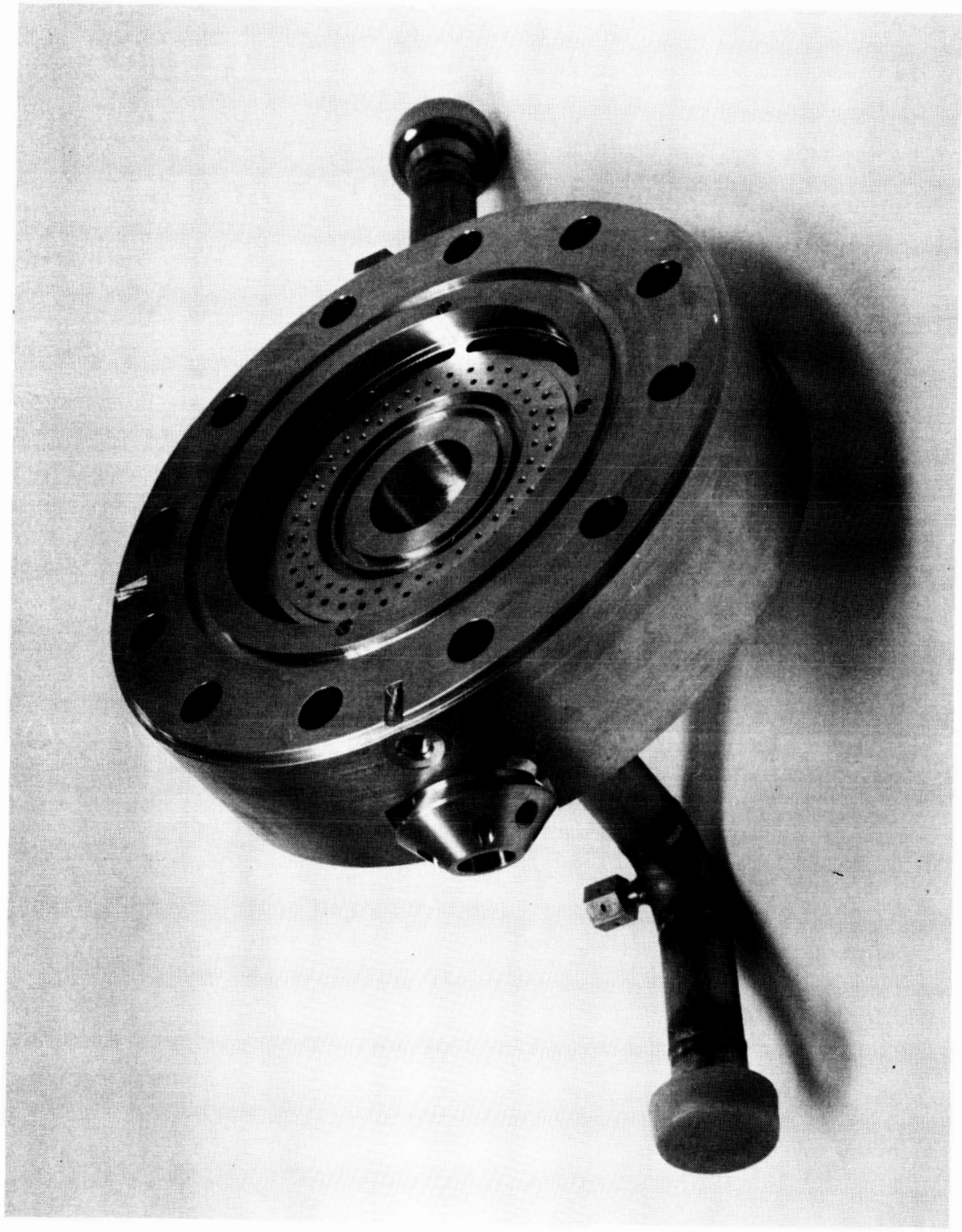

Figure 1.1.2-6. Injector Assembly

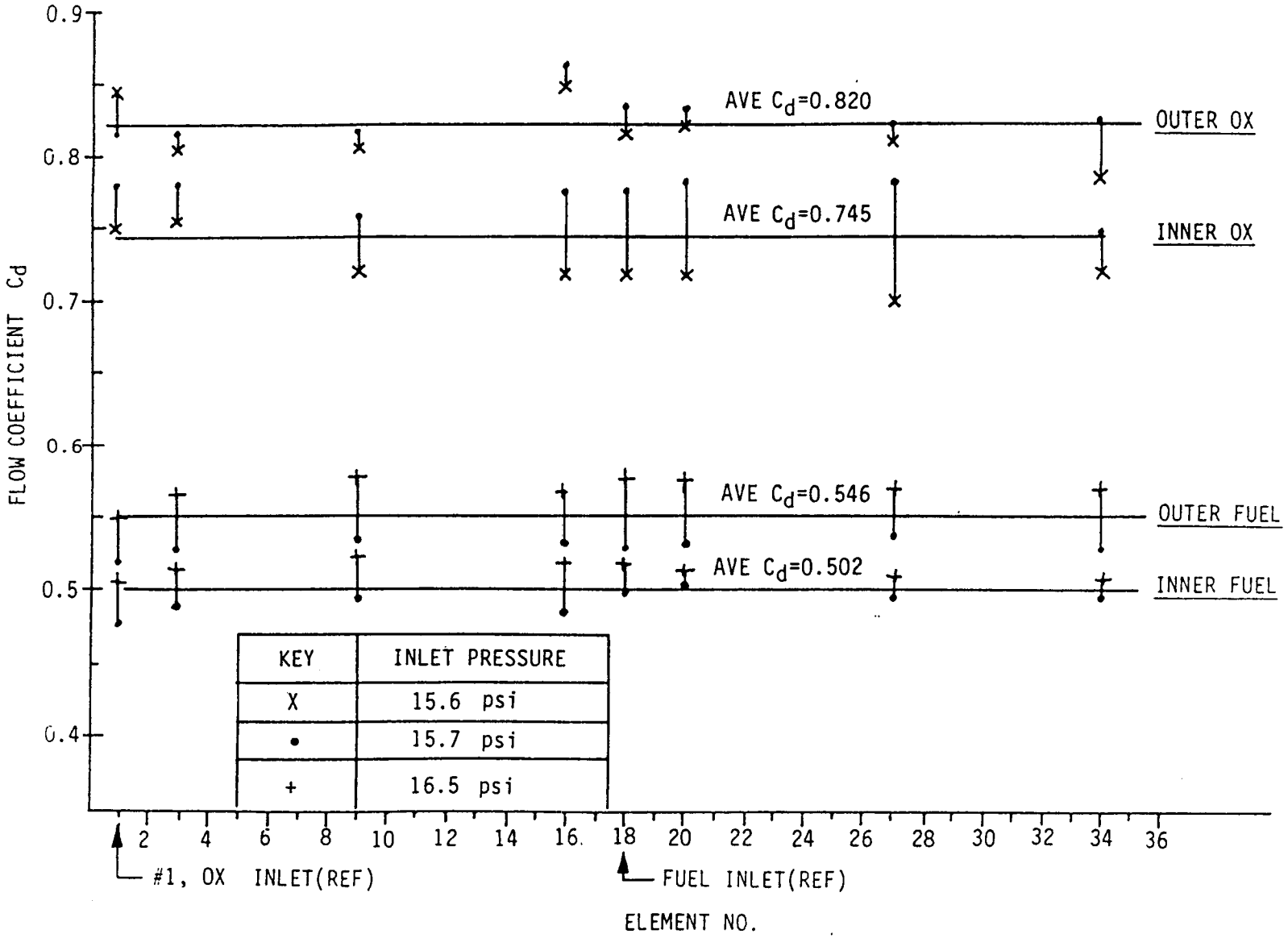

Figure 1.1.3-1. Injector Cold Flow (GN_2) Results

distribution for the two rows of injector elements expressed as a discharge coefficient, Cd. The area used to calculate Cd is the minimum cross-sectional area of the element circuit. Calculation of Cd is based on the flow equation for a perfect gas under isentropic flow conditions and takes the form of:

$$\dot{w} = CdA^* \, Pin \sqrt{\frac{(2*K)}{(k-1)(RT)} * \left[\frac{Pout}{Pin}\right]^{(2/k)} - \left[\frac{Pout}{Pin}\right]^{(k+1/k)}}$$

where:
- w = flowrate (lbm/sec)
- C_dA = discharge coefficient *Area (in^2)
- P in = Pressure, inlet (psia)
- P out = Pressure, outlet (psia)
- k = specific heat ratio
- T = temperature, inlet (°R)
- R = specific gas constant

Of special interest in evaluating the Cd term for the injector elements is to ensure consistency of the results from element to element. Inconsistencies can indicate non-uniformity in the flow distribution. This is of special concern near the propellent inlet lines. Results of the data showed only slightly higher than average flow in the circuit under the inlet lines (Figure 1.1.3-1). Individual flow distribution was within +/- 5 % of the average. A comparison Table of the results of the single element cold flow, full assembly cold flow, and hot fire test for tank head idle mode (35 Pc) operation is provided in Table 1.1.3-I.

1.1.4 Design Modifications

Based on temperature data obtained from the first set of low Pc hot firings, a modification was made to the injector. High temperatures and fluxes were recorded at the front end of the centerbody. Since heat flux increases with chamber pressure, the presence of high heat fluxes at the low Pc (less than 500 psia) tests led to the prediction of heat fluxes levels higher than the heat sink hardware is designed to withstand at the higher Pc tests. Hydrogen film cooling from the face of the injector was selected for cooling of the centerbody. This decision was based on 1) hydrogen film cooling would directly assist cooling of the hot area and 2) the injector fuel velocity would be reduced as a result of the the hydrogen

TABLE 1.1.3-I

SUMMARY OF OTV INJECTOR FLOW DATA

	Oxidizer Circuit C_DA (in^2)	Fuel Circuit C_DA (in^2)
Design Values	0.1551	0.1101
GN2 Cold Flow (through individual elements)	0.1523	0.1232
GO2/GH2 Cold Flow ($\dot{w}_o$ = .028 lb/sec, $\dot{w}_f$ = .0058 lb/sec)	0.1499	0.1266*

Hot Fire Test at 35 psia

#	P_C	MR	$\Delta P_O/P_C$	$\Delta P_f/P_C$	w_o	w_f	C*	C_DA_{ox}	C_DA_f
114	35.1	3.98	.162	.236	.092	.023	7110	0.1403	0.1354*
119	35.2	3.06	.161	.125	.090	.030	6833	0.1291	0.1402*
120	33.5	5.02	.149	.167	.103	.021	6293	0.1479	0.1321*

*Includes resonator cavity bleed holes.

Key

P_c	Chamber Pressure (psia)
w_o	Oxidizer Flowrate (lbm/sec)
w_f	Fuel Flowrate (lbm/sec)
MR	Mixture Ratio (O/F)
$\Delta P_O/Pc$	Ratio of Injector Oxidizer Side ΔP to Pc
$\Delta P_f/Pc$	Ratio of Injector Side Fuel ΔP to PC
ΔP	Pressure Drop (psia)
C*	Characteristic Exhaust Velocity

and 2) the injector fuel velocity would be reduced as a result of the the hydrogen bleed-off. The reduction in injector fuel velocity would lower the heating effect and thus reduce the peak heat flux associated with differential propellant velocity mixing.

The injector was modified by drilling 36 holes (one per element) of 0.015 inch diameter. The holes were EDM'd through the platelet stack from the chamber side into the inner fuel manifold ring. This ring is identified on Figure 1.1.2-2. Addition of these holes allowed GH_2 coolant to impinge on the centerbody in the area where the fluxes were the highest. The addition of these film cooling holes increased the amount of film cooling from a nominal 6% to 9.5%.

At the same time, the test data were used as a basis for optimizing the resonator bleed hole diameters. These bleed holes provide for hydrogen cooling of the resonator cavities as well as providing some cooling to the outer chamber. This optimization involved increasing the hole diameter from 0.015 to 0.020 inches and replacing the screws used to hold the resonator blocks.

The cold flow tests were repeated to establish the new fuel CdA values. There was a slight increase in the CdA values, which did not affect of the previously calculated pressures. The fuel CdA term increased by 22% and the oxidizer CdA term increased by 12.8%.

1.2 Heat Sink Chamber and Throat Hardware

1.2.1 Design

Thrust chamber activities included the detailed design and fabrication of a heat sink chamber with provision for a GH_2 cooled throat section. The heat sink chamber and cooled nozzle, illustrated in Figure 1.2.1-1, were designed and built to accommodate testing of the injector. The chamber was designed to accept interchangeable throat sections. Two throat sections were designed and built: a LH2 cooled throat (Figure 1.2.1-2) and a heat sink throat (Figure 1.2.1-3). The heat sink throat hardware was designed to facilitate a series of low chamber pressure tests (Pc = 100 to 600 psia). It extended to an exit area ratio of 4:1. The regenerative cooled throat was designed to facilitate a series of high chamber

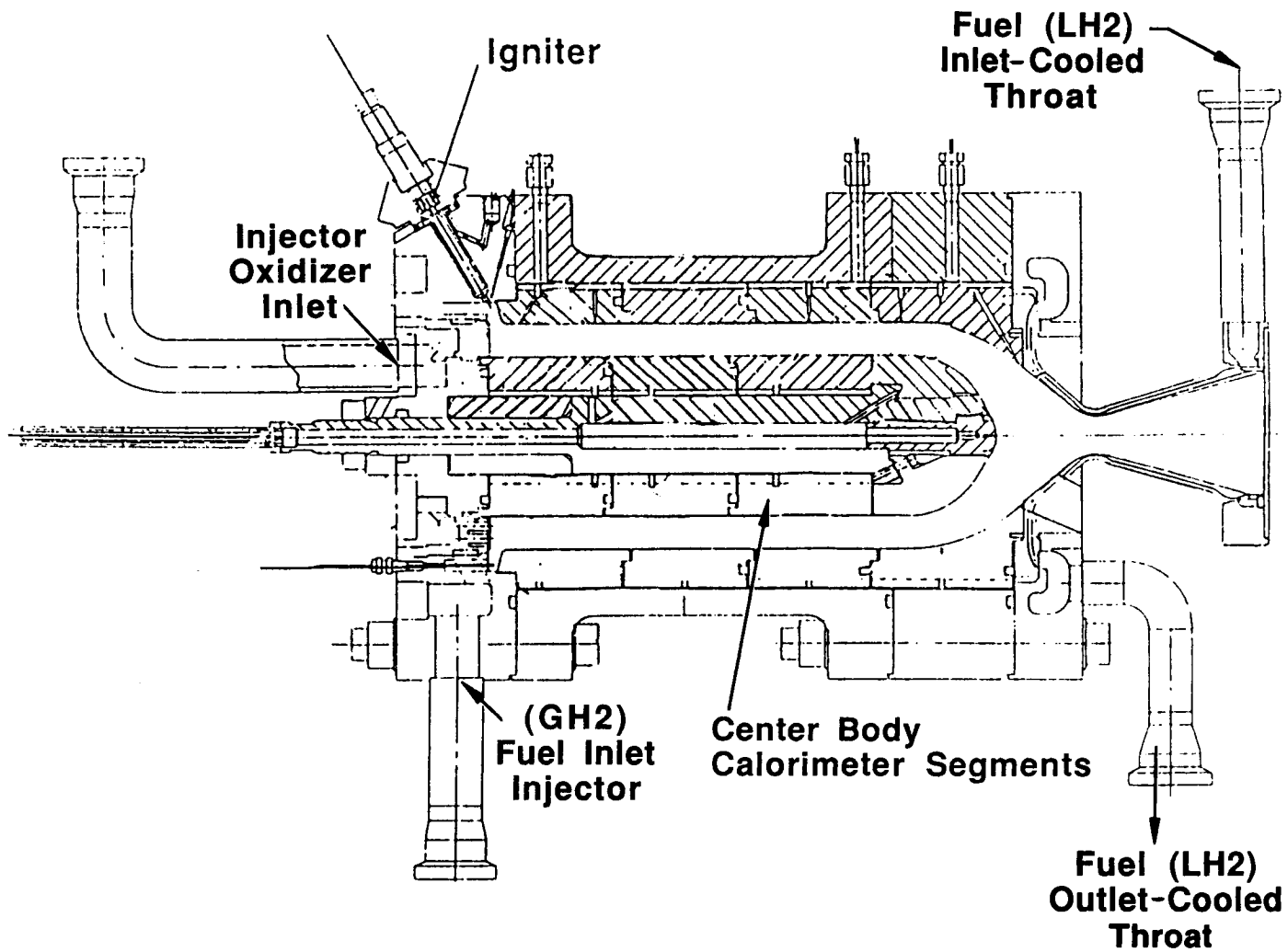

Figure 1.2.1-1. Heat Sink Chamber with LH_2 Cooled Throat

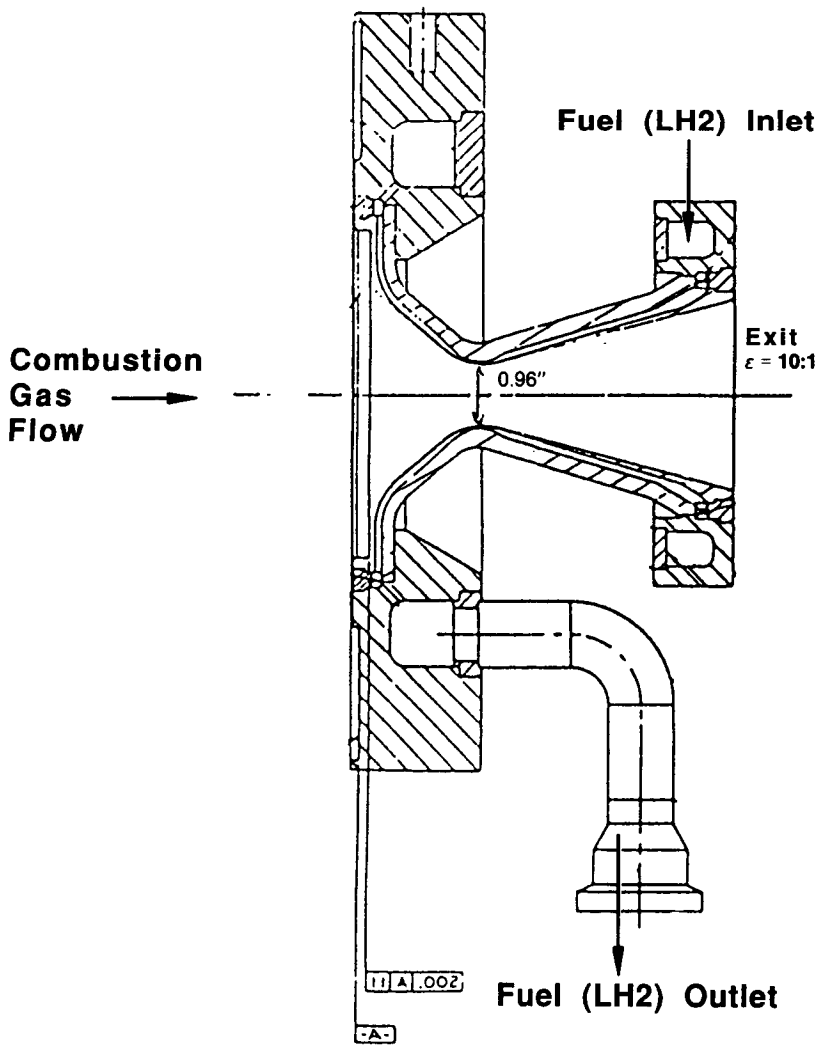

LH2 Cooled Throat:

- Replaces Heat-Sink Throat
- Increases Operation Limits up to 2000 psia Chamber Pressure
- Expected Throat Flux 100 BTU/In^2 Sec
- Design Features
  1. 0.010" Wide Cooling Channels
  2. High Strength EF NiCo Closeout

Figure 1.2.1-2. LH_2 Cooled Throat

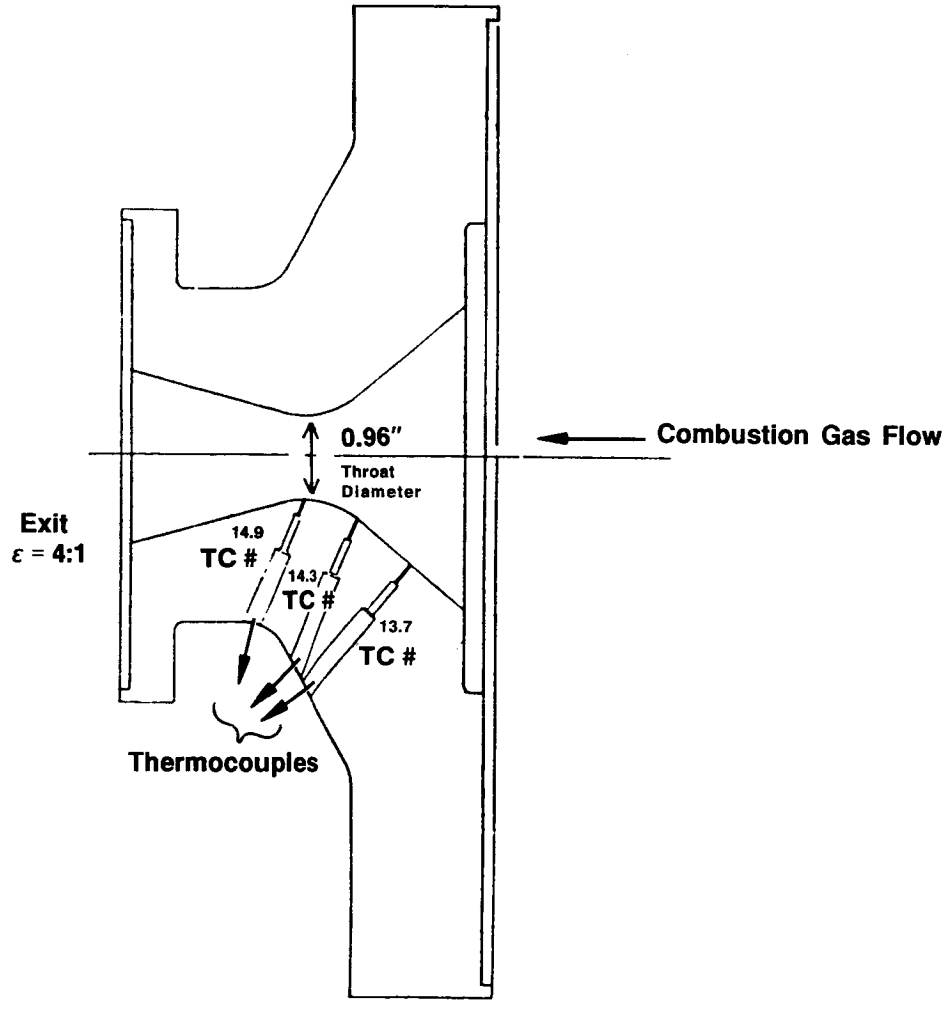

Figure 1.2.1-3. Heat Sink Throat

pressure tests (Pc = 1000 to 2000). It extends to an exit area ratio of 10:1. Details of the cooled throat design and fabrication are discussed in Section 1.4.

The heat sink chamber assembly is shown in Figure 1.2.1-4. A segmented design was chosen for the heat sink chamber and centerbody to allow variation of the chamber length. A view of the chamber ID is shown in Figure 1.2.1-5, looking from the injector end toward the throat. The four large slots in the copper contain tabular rails which align the four outer calorimeter segments, prevent them from contacting the steel housing and accommodate radial thermal expansion.

The heat sink chamber assembly was designed to adjust to the following geometry changes at a minimum cost in terms of extra hardware and buildup between tests.

1) Chamber and Centerbody length (L')
2) Shape of Centerbody nose
3) Resonator cavity depth

The lengths of the pressure housing and the centerbody steel support shaft were sized to accommodate the longest anticipated chamber length. The resonator cavities were sized for the maximum expected depth with provision to use filler blocks for any tests at shorter depths or multiple mode tuning.

The 10 inch long heat sink chamber barrel section was capable of 1.5 seconds of operation at a heat flux of 10 Btu/sec in^2. This was the expected flux for chamber pressures of 2000 psi. Surface temperatures were expected to be below 1500 degrees F during firing. The actual test duration was dependent on operation within the above described limits, and was controlled by high temperature kills using thermocouples in the chamber and centerbody. Installation of two thermocouples in each ring allowed for repeatability of data.

Local heat fluxes were calculated from the transient response of the gas-side surface thermocouples. This was accomplished with a one-dimensional finite difference solution of the transient radial conduction equation

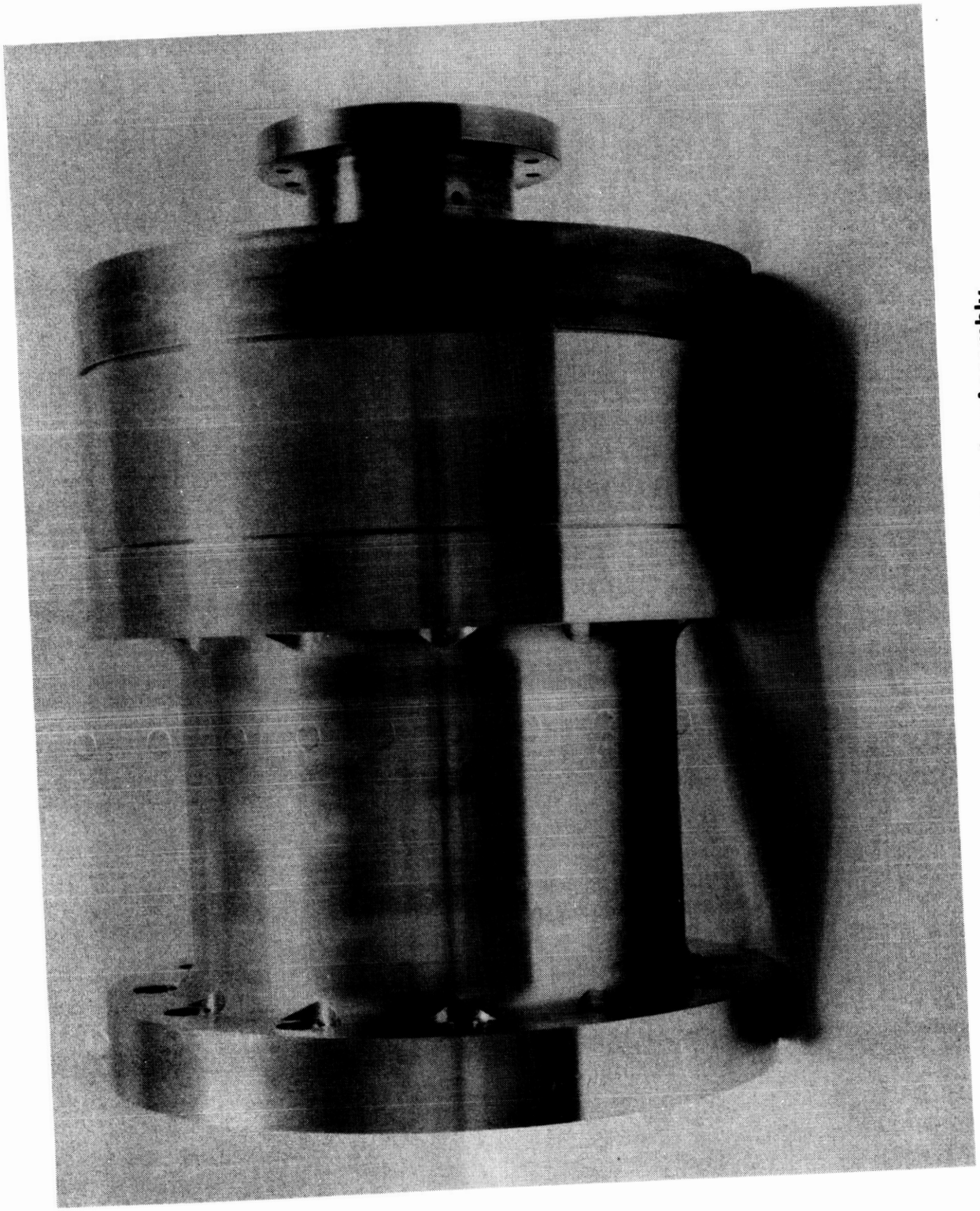

Figure 1.2.1-4. Heat Sink Chamber Assembly

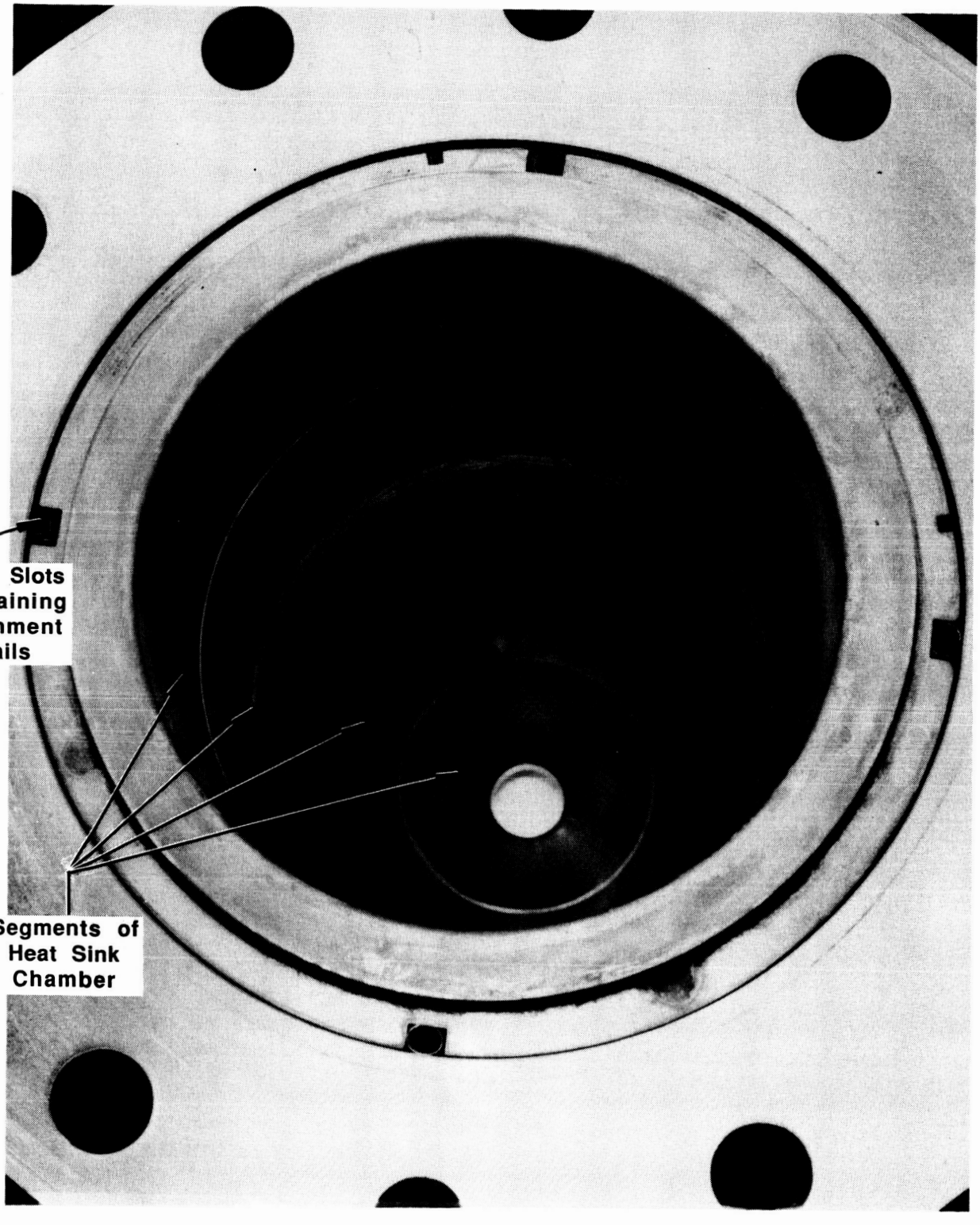

Figure 1.2.1-5. Interior of Heat Sink Chamber

using the thermocouple transient as a boundary condition. Such an analysis defines the heat flux required to provide a surface energy balance as a function of time. A linear fit of the resultant heat flux vs surface temperature characteristic was defined in order to compare all data at the same wall temperature.

1.2.2 Fabrication

An overview of the heat sink components before assembly is shown in Figure 1.2.2-1. The outer pressure housing, fabricated from CRES 304, was designed to accommodate a 4000 psi proof test. A segmented chamber liner, fabricated from OFHC copper, slides into the steel pressure housing. The copper segments are insulated to prevent contact with each other, the housing, and the support shaft. Ports were machined for gas side thermocouples, which were brazed into place and machined flush with the chamber ID.

After the parts were fabricated, a test fit-up of all parts was conducted to enable a dimensional inspection of the critical features. Discrepancies were corrected by relieving portions of the face on the various calorimeter segments. One thermocouple hole in the calorimeter segment immediately upstream of the throat was found to be oversized. This was corrected by plugging the hole with an 0.062" diameter copper bar brazed in place. A new thermocouple hole (0.02" diameter) was then added slightly downstream of the plug.

A photograph of the heat sink chamber and throat during a hot fire test is shown in Figure 1.2.2-2.

1.2.3 Instrumentation

The thermocouples were brazed into place on the gas side heat sink chamber wall. Chromel-Alumel thermocouples were used at various axial distances as illustrated in Figure 1.2.3-1. Each axial location contained two thermocouples, separated radially by 90 degrees. All thermocouples were checked to ensure no open circuitry in the wiring, prior to the start of the hot fire testing. Prior to each hot fire test series, a calibration was made of the thermocouples and other instrumentation to ensure functionality within the desired range of operation.

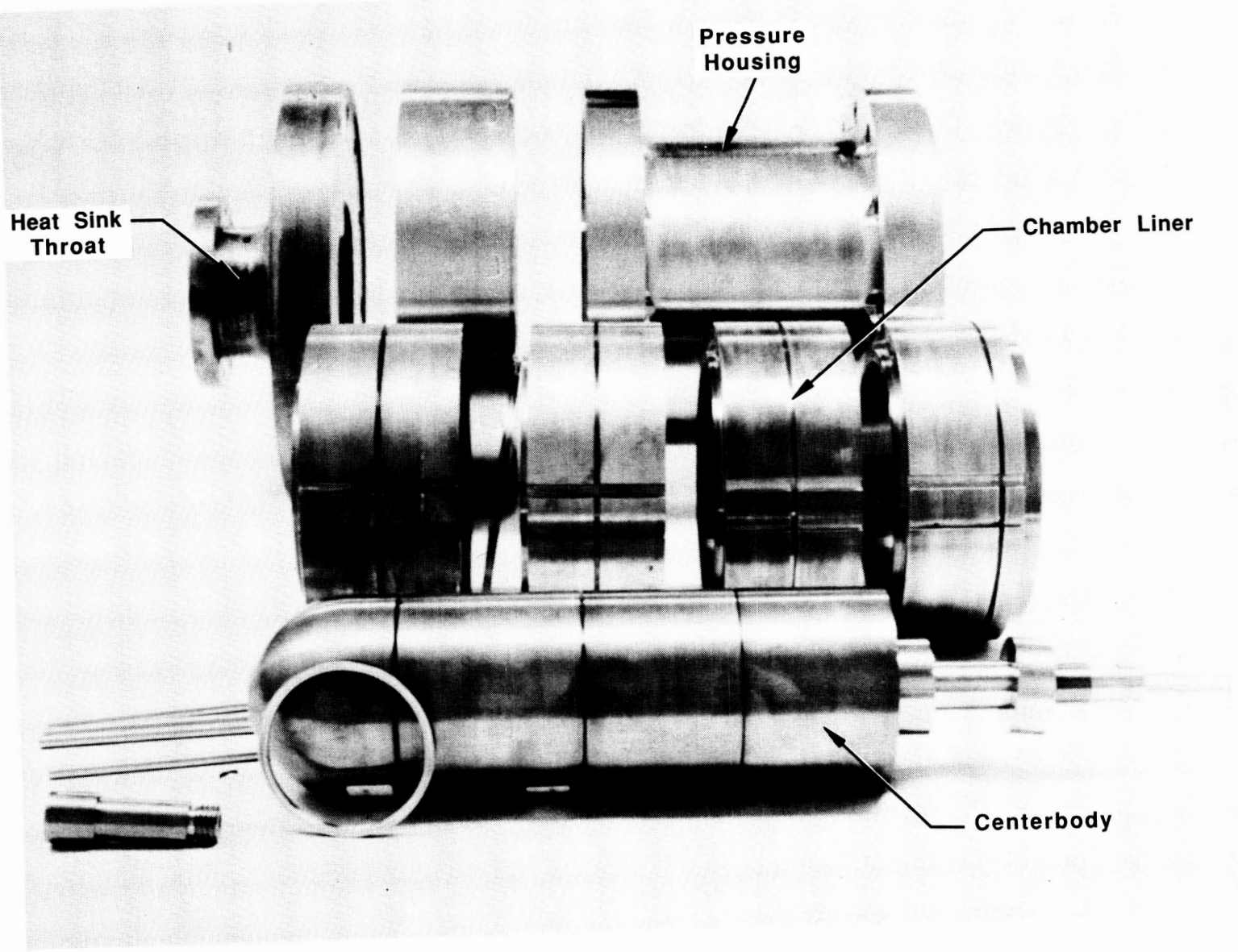

Figure 1.2.2-1. TCA Heat Sink Hardware

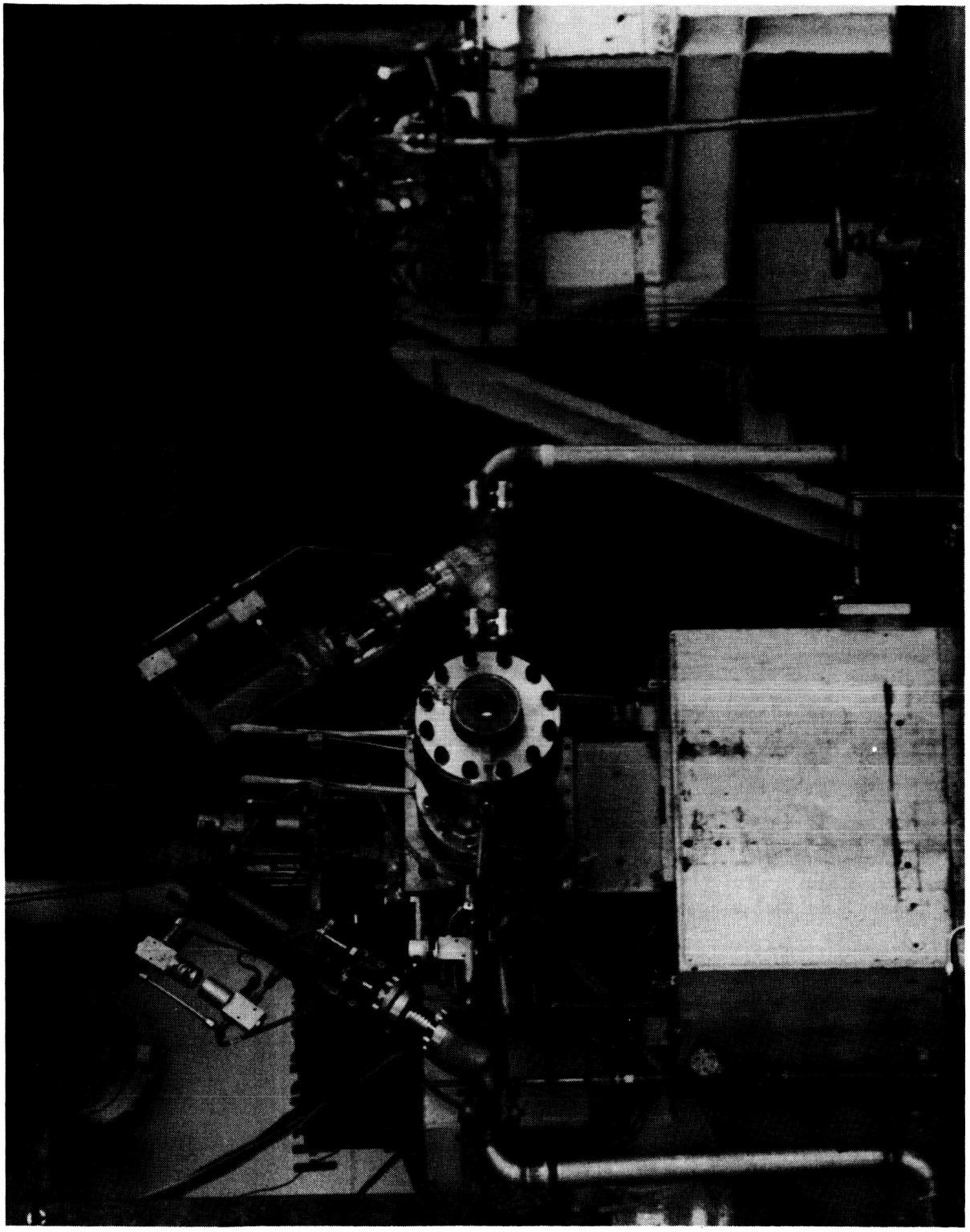

Figure 1.2.2-2. Heat Sink Chamber & Throat During Hot Fire Test

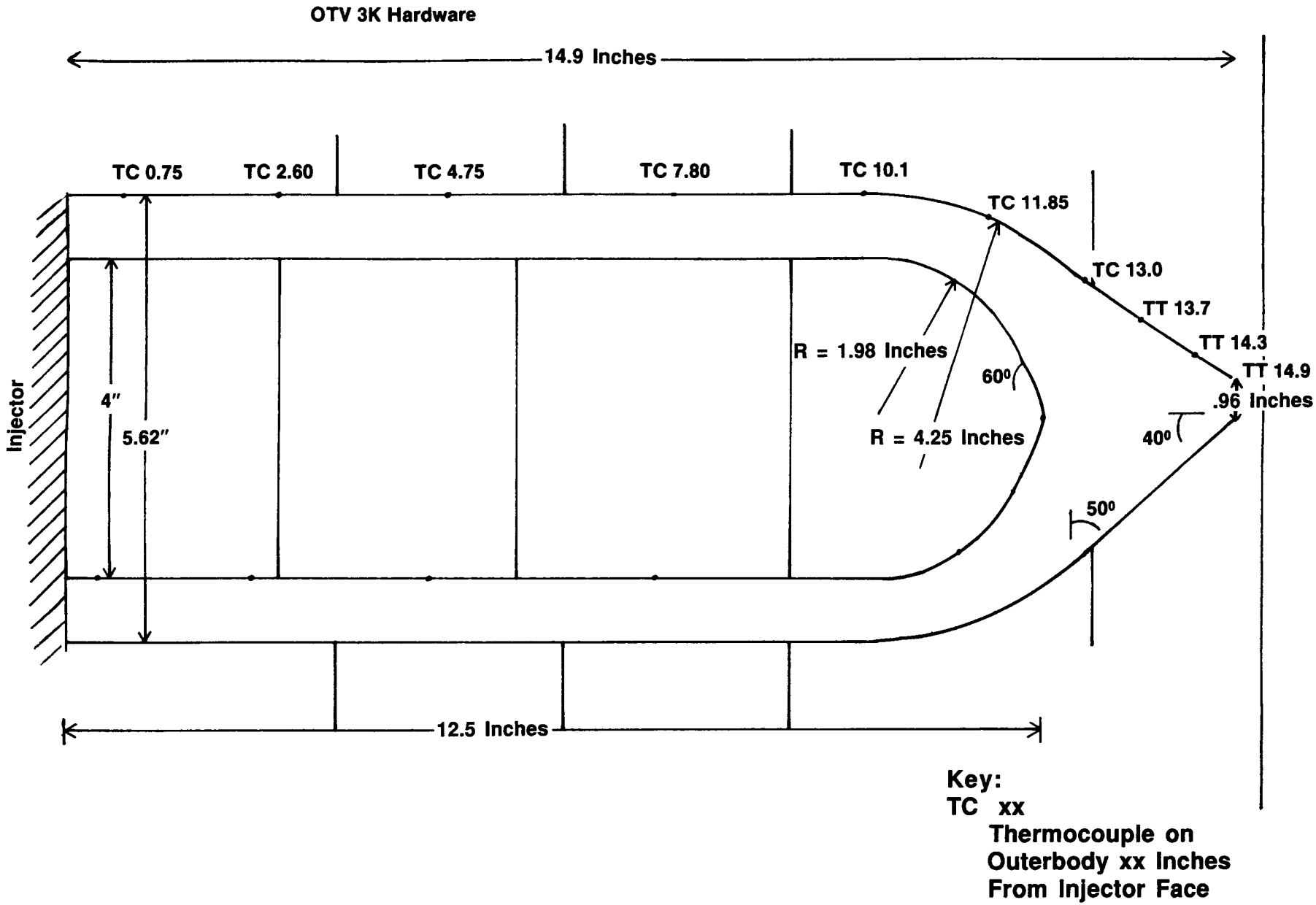

Figure 1.2.3-1. Outerbody Thermocouple (TC) Locations

After an initial set of tests was run, modifications were made to the injector and resonator cavities to increase film cooling to the heat sink centerbody and chamber, respectively. Checkout testing of the thermocouples was repeated. Table 1.2.3-I lists the operational thermocouples.

1.3 Heat Sink Centerbody

1.3.1 Design

The heat sink centerbody design is illustrated by Figure 1.3.1-1. The centerbody is comprised of copper rings with a blunt tip surrounding a steel shaft. Thermocouples are located on the gas side wall of the centerbody.

The heat sink centerbody was also sized for 1.5 seconds of operation at a heat flux of 10 Btu/sec in^2, the expected heat flux at a chamber pressure of 2000 psi. The thickness of the segments would likewise result in soakout temperatures of 500 degrees F following a test with surface temperatures below 1500 degrees F during firing. As noted previously, test kills were established based on thermocouple readings in this range.

1.3.2 Fabrication

The centerbody segments were made from OFHC copper. The support shaft is made from CRES 304. Although it would have been possible to test the centerbody with a variety of tip configurations, no other tip configurations were fabricated. The blunt tip demonstrated satisfactory performance during testing.

Figure 1.3.2-1 shows the five separate calorimeter segments that comprise the chamber centerbody and the support structure through which the thermocouple leads are routed.

The nose view of the centerbody is shown in Figure 1.3.2-2. The gap between the hemispherical nose segment and the first cylindrical segment is a result of the assembly not being clamped when the photograph was taken. The centerbody was made of OFHC copper and used Chromel-Alumel thermocouples.

TABLE 1.2.3-I

HEAT SINK CHAMBER THERMOCOUPLE LOCATION

Outerbody Thermocouples		Throat Calorimeter Thermocouples	
TC	0.75*-0°**	TT	13.7*-0°**
TC	0.75-90°	TT	13.7-90°
TC	2.60-0°	TT	14.3-0°
TC	2.60-90°	TT	14.3-90°
TC	4.75-0°	TT	14.9-0°***
TC	4.75-90°	TT	14.9-90°
TC	7.80-0°		
TC	7.80-90°		
TC	10.10-0°		
TT	14.9-90°		
TC	10.10-90°		
TC	11.85-0°		
TC	11.85-90°		
TC	13.0-0°		
TC	13.0-90°		

Key: TC - Thermocouple located in outer body wall

TT - Thermocouple located in the throat

* Distance from Injector Face (inches)
** Angular Location from Top Dead Center (Degrees)
*** Inoperable Thermocouple

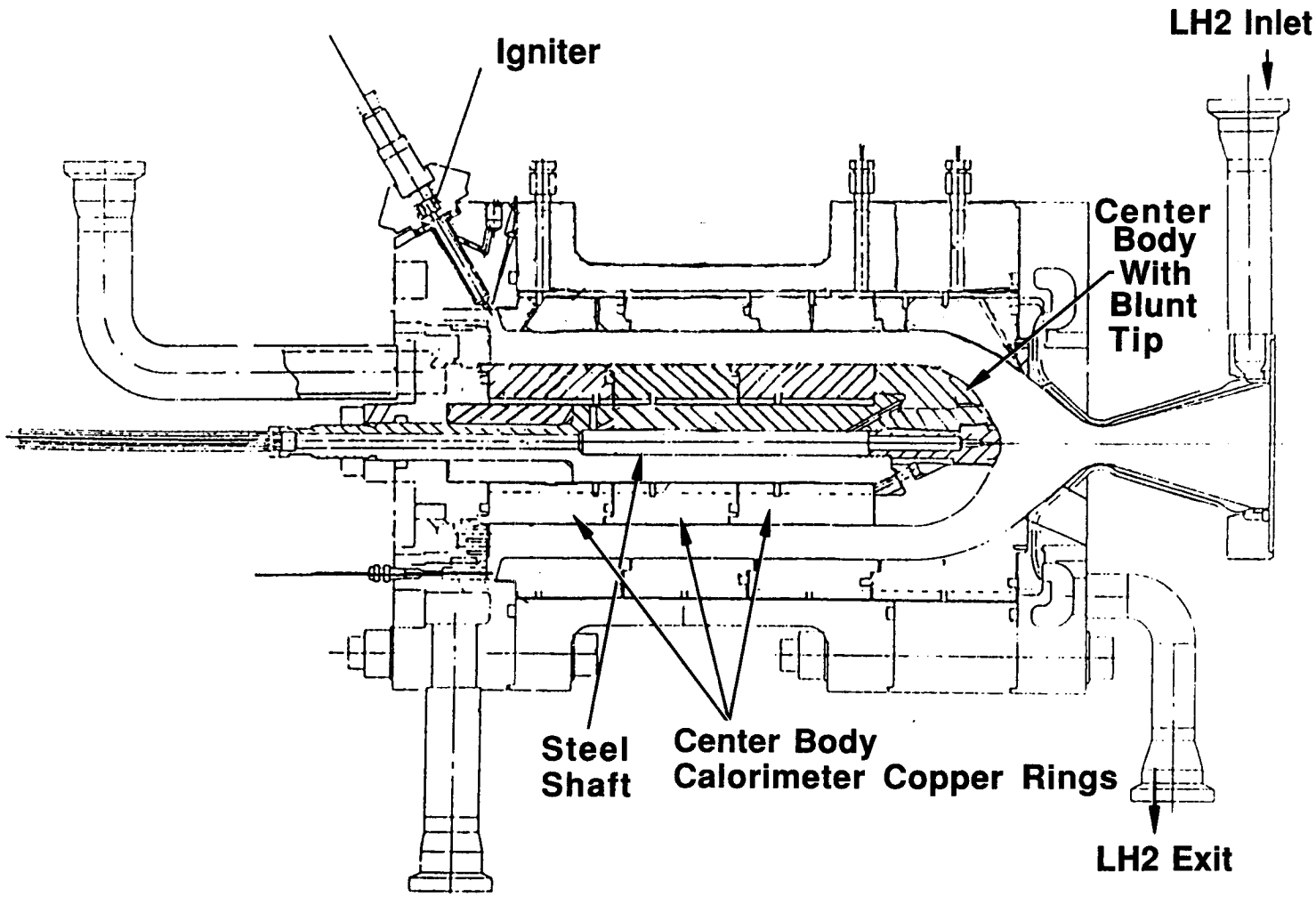

Figure 1.3.1-1. Heat Sink Chamber with Cooled Throat

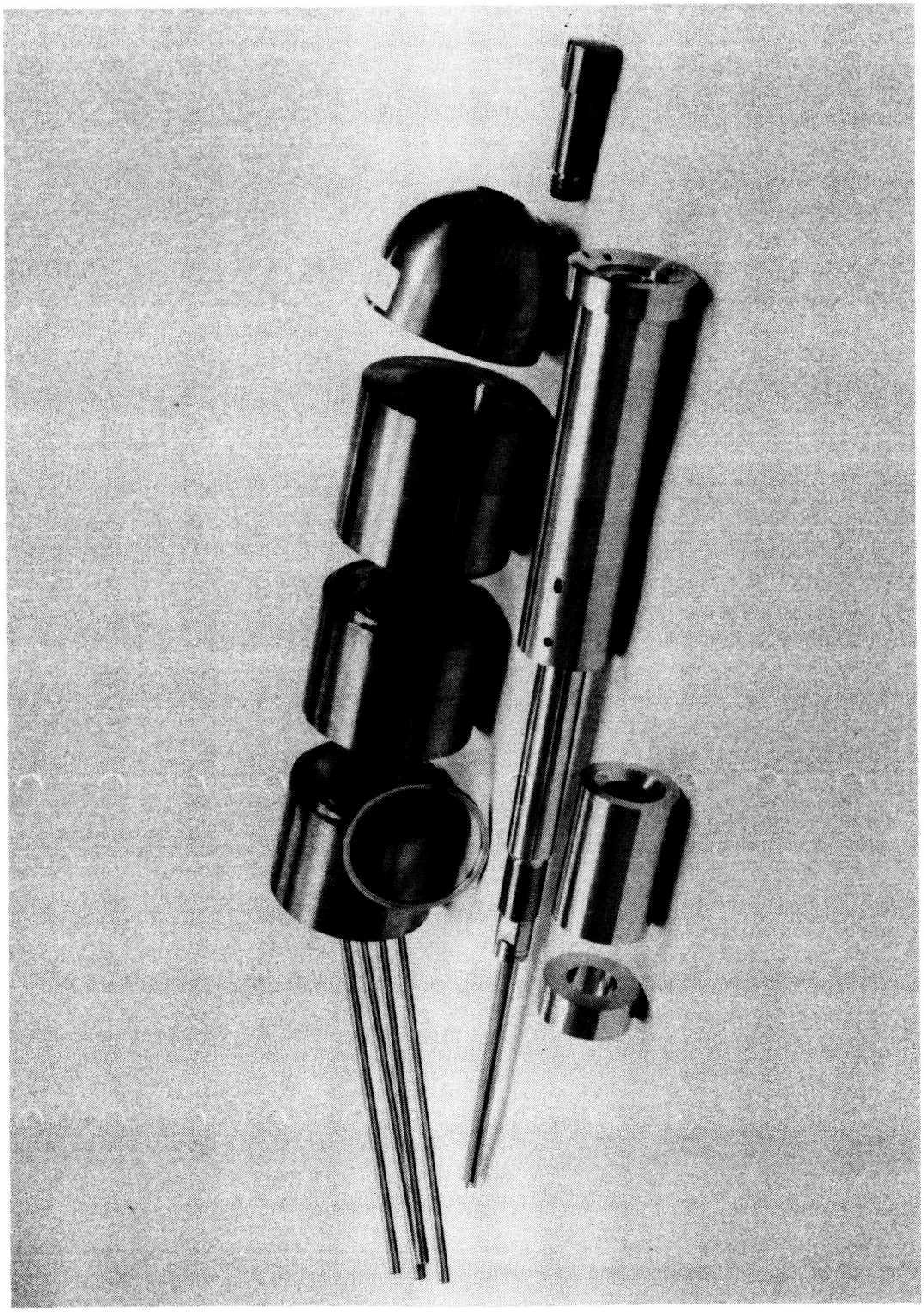

Figure 1.3.2-1. Heat Sink Centerbody Components

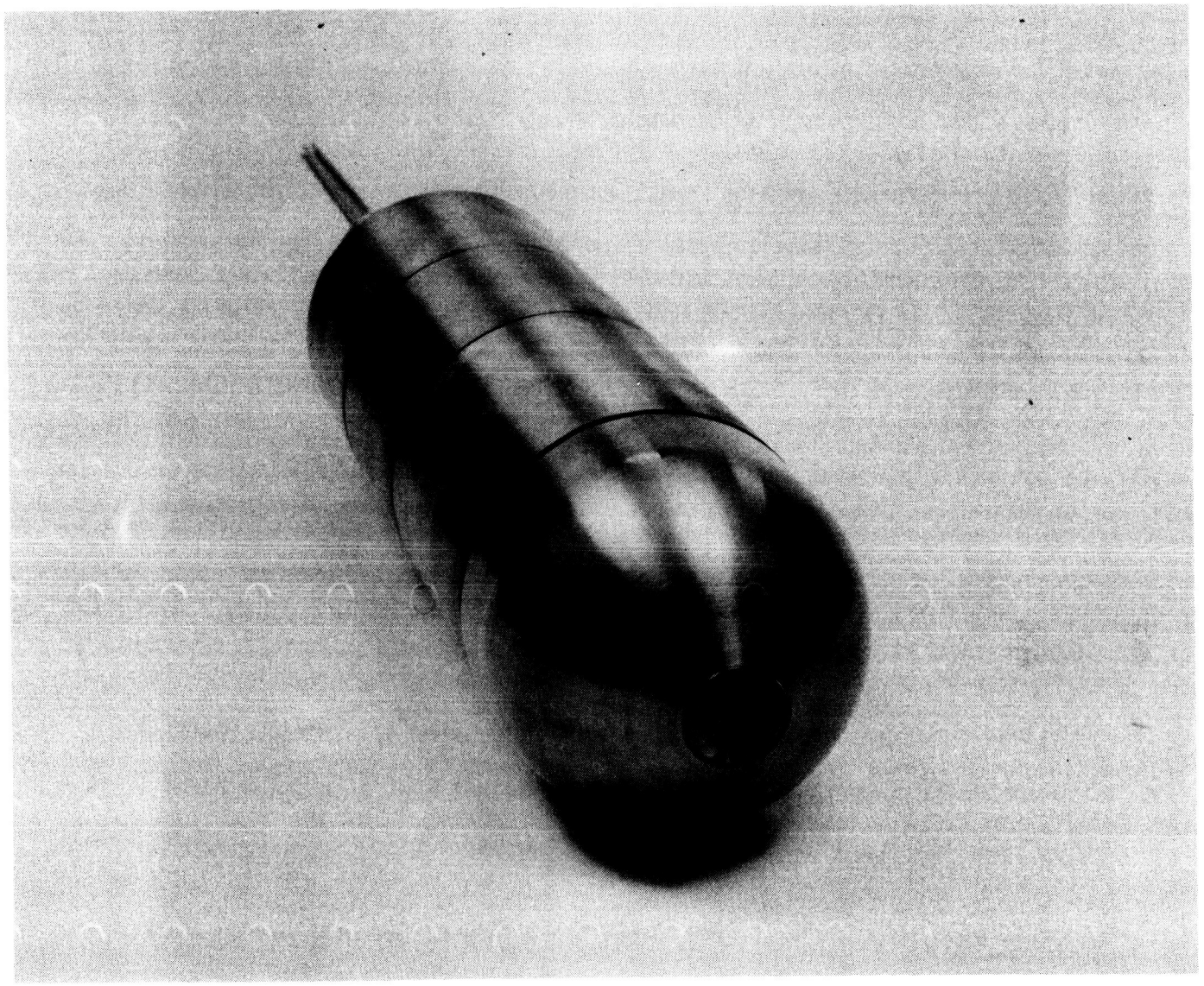

Figure 1.3.2-2. Nose View of Centerbody

1.3.3 Instrumentation

Chromel-Alumel thermocouples were brazed into place on the gas side heat sink chamber wall. Locations of the thermocouples are illustrated by Figure 1.3.3-1. Each axial location contains two thermocouples, separated radially by 90 degrees. All thermocouples were then checked for continuity. A series (Series 3) of low pressure performance, stability and heat transfer testing were conducted. After this set of tests, modifications were made to the injector and resonator cavity to increase film cooling to the heat sink centerbody and chamber, respectively. Checkout testing of the thermocouples was repeated. Table 1.3.3-I lists the operational thermocouples. To minimize risk to the heat sink hardware and functioning thermocouples, no repair was attempted for the non-functioning thermocouples. An additional braze cycle would have been necessary to replace the thermocouples which could cause the first braze alloy to reflow dislodging the functioning thermocouples

Figure 1.3.3-2 is a photograph of the centerbody mounted on the injector in the test bay prior to testing.

1.4 LH_2 Cooled Throat

1.4.1 Design

Design of a cooled throat section for the heat sink hardware was undertaken to demonstrate adequate cooling for a 500 cycle, 20 hour life chamber. Specification levels were for localized heat fluxes of 100 Btu/sec in^2 at the throat with average heat fluxes of 10 Btu/sec in^2 in the barrel and nozzle. To meet the high cycle life requirements for the thrust chamber, two concepts were approached: 1) advanced cooling, and 2) ductile thermal barriers.

Investigation of advanced cooling for the chamber was directed at increasing the low cycle fatigue life by keeping the wall temperature differential low. The second approach was directed at the use of high temperature gas side liners as thermal barriers.

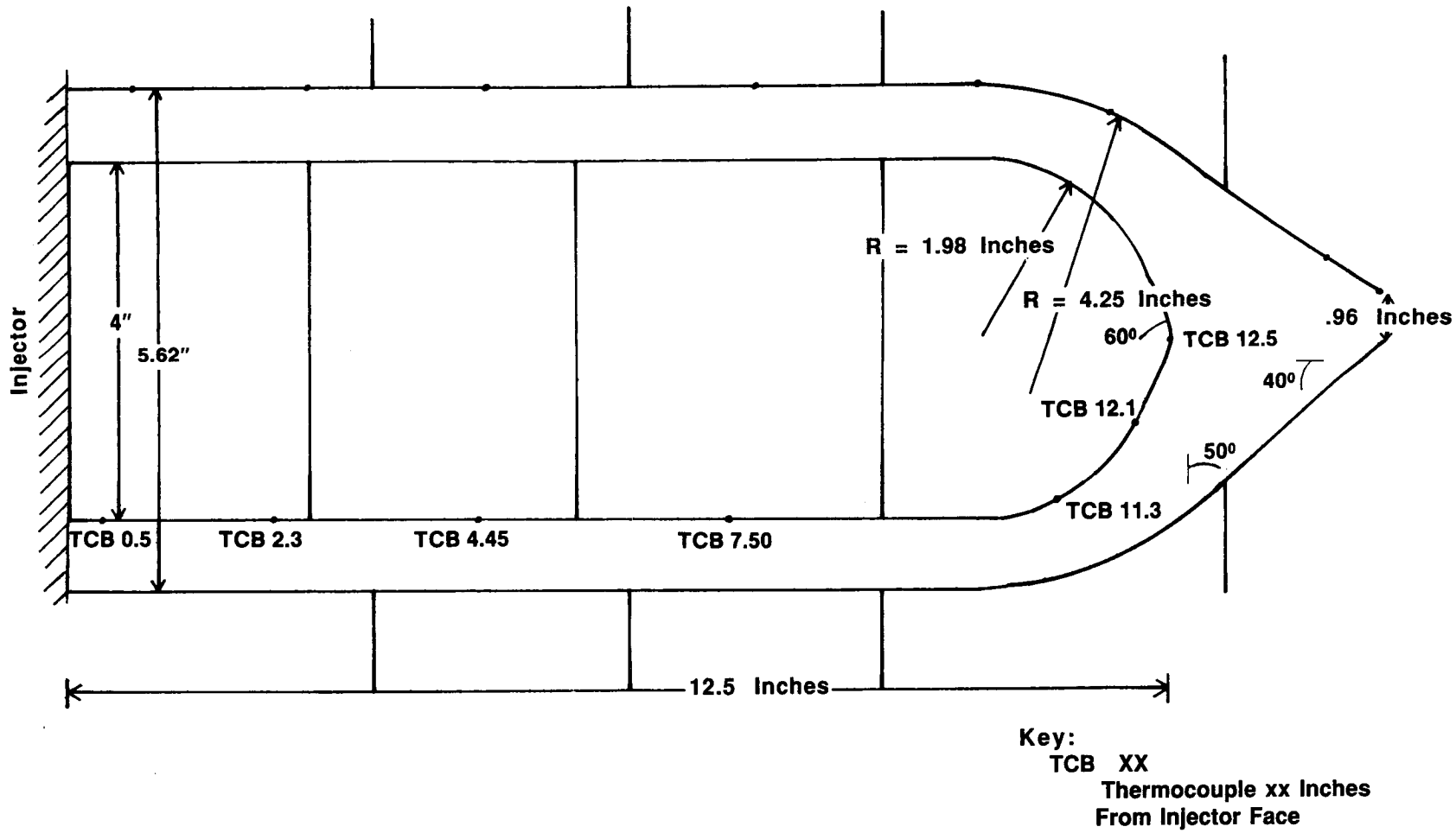

Figure 1.3.3-1. Centerbody Thermocouple (TCB) Locations

TABLE 1.3.3-I

HEAT SINK CENTERBODY THERMOCOUPLE LOCATIONS

Centerbody Thermocouples

TCB	0.5*-90°**
TCB	0.5-0°***
TCB	2.3-90°
TCB	2.3-0°***
TCB	4.45-90°
TCB	4.35-0°
TCB	7.5-0°
TCB	11.2-90°***
TCB	11.2-0°
TCB	12.1-90°
TCB	12.1-0°***
TCB	12.5-90°
TCB	12.5-90°

Key:

TCB- Thermocouple located in centerbody wall

* Linear Location from Injector Face (inches)
** Angular Location from Top Dead Center (Degrees)
*** Inoperable Thermocouple

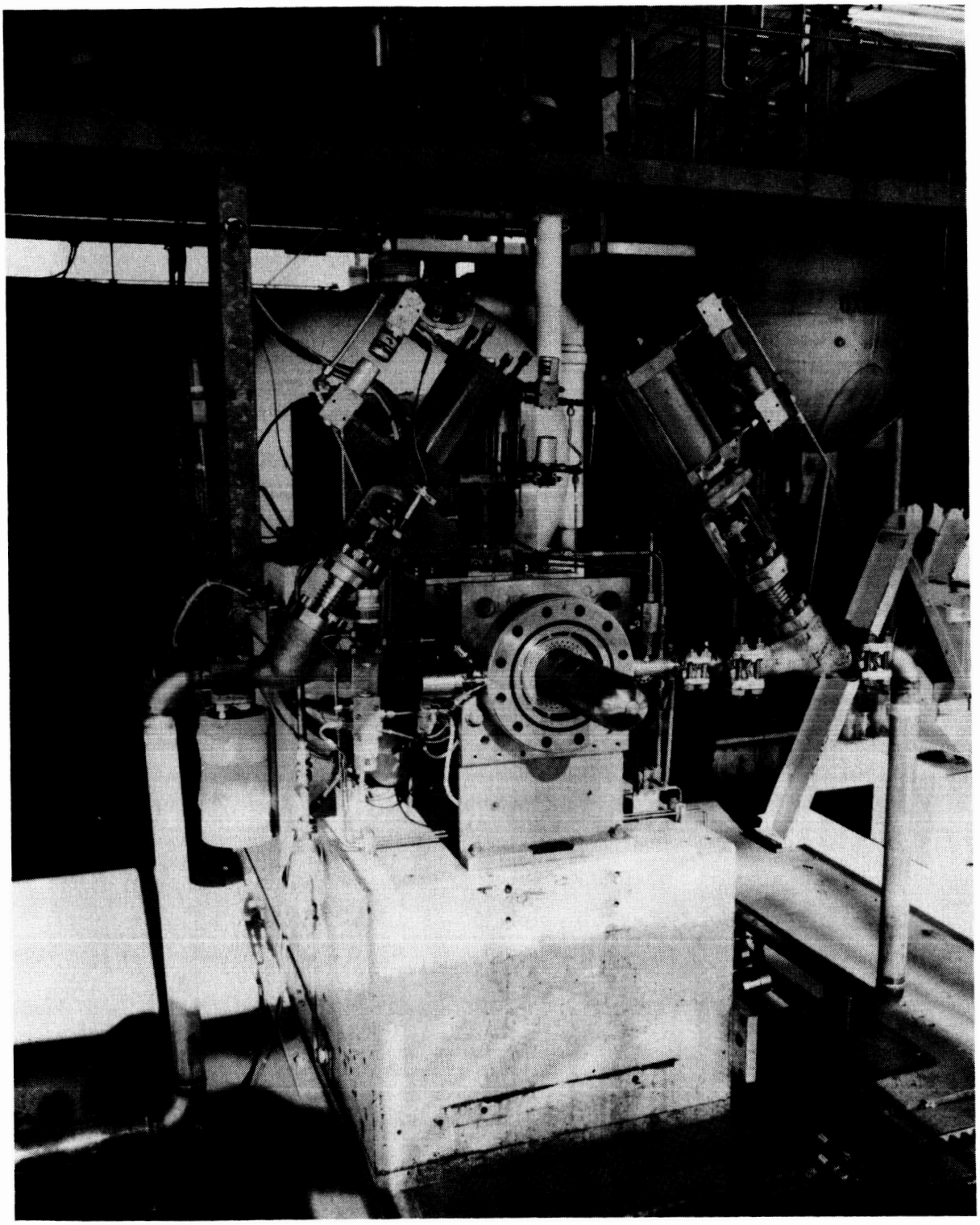

Figure 1.3.3-2. Injector & Centerbody on Test Stand

Materials investigated for potential gas side liner materials included:

1) Platinum plated directly on Copper
2) Copper plated on Platinum
3) Rhenium plated Copper
4) Copper plated Rhenium
5) Copper Aluminide Conversion Coatings

Specimens were fabricated from the above materials and subjected to heat cycling in a 1200 to 1400 degree F environment for up to 144 hours. Metallurgical studies to evaluate the specimens were conducted. Results of these tests are listed in Table 1.4.1-I.

Analytical studies indicated that a factor contributing to an increase in cycle life was the minimization of the temperature gradient across the thrust chamber walls. Gas side wall temperature is limited by the material used. This decrease in temperature corresponds to a decrease in strain rate by the relationship of:

$$\% \text{ strain} = 2*(\text{alpha})*(\text{delta T}).$$

where:

alpha = thermal coefficient of expansion
delta T = temperature differential

In order to minimize this delta T, the geometries illustrated in Table 1.4.1-II were analyzed. Case #6 was selected as being the easiest to fabricate. Further refinement of the geometry from case #6 was undertaken to increase the cycle life from a predicted 480 cycles to over 500 cycles as shown in Table 1.4.1-III. Case #6B was pursued for the fabrication study.

Results of stress and thermal analysis indicated extended low cycle fatigue life could be obtained by a combination of very thin channels with a very thin closure. The closure thickness required was approximately 0.02". Conventional EF Ni closures required a thickness of approximately 0.03 to 0.05" to withstand the pressure differential. A NiCo alloy was identified as having a higher

TABLE 1.4.1-I

HIGH TEMPERATURE LINERS FOR REGENERATIVELY COOLED CHAMBER THROATS

Process	Materials	Progress/Status	Potential
Electroformed Copper over Metallic Foils	EF Cu/Rhenium	Copper did not bond.	-
	EF Cu/Iridium	Inconsistent bond results, second sample recommended.	-
	EF Cu/Platinum	Good bond, need to run bend test.	Inside-out fabricated chamber with gas side Pt chemical barrier.
Brush Plated Coating over Cu Substrate	BP Platinum/ZrCu	• BP Pt adherent but thin, only 60 μ in.	Pt chemical barrier
	BP Rhenium/ZrCu	• BP Re brittle deposit, many cracks normal to Cu surface, although still semi-adherent. • Heat cycling degrades bond.	-
Surface Diffusion Intermetallic Formation	Cu/Aluminide	Cu/Al intermetallic zone .002 in. thick covered with ultrathin Al_2O_3 layer potentially self healing - very oxidation resistant, survived 1400°F 6 days air. Exploration of self-healing characteristics recommended.	Excellent oxidation barrier.

TABLE 1.4.1-II

CHAMBER LIFE VS. COOLANT CHANNEL CONFIGURATION AND QUANTITY

CASE NO.	GEOMETRY	NO. OF CHANNELS	V_c - FPS	MACH NO.	T_{wg} MAX, °F	ΔT - °F	STRAIN ZrCu, %	nf	$n_f/4$	STRAIN EFNi, %	STRESS EFNi, PSI	REQUIRED CLOSEOUT THICKNESS
1 (BASELINE)	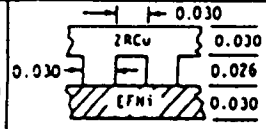	53	1038	0.23	917	971	1.78	512	128	0.20	62,755	0.031
1A	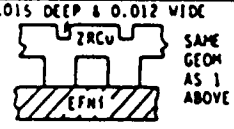	53	1038	0.23	917	971	1.92	440	110	0.19	60,530	0.030
1B	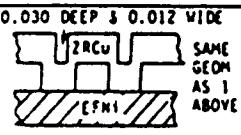	53	1038	0.23	917	971	0.74	4000	1000	0.19	59,074	0.030
3	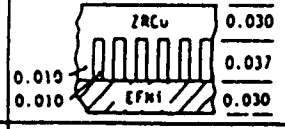	160	725	0.16	772	974	1.52	760	190	0.22	71,256	0.034
3A	SAME GEOMETRY AS 3 ABOVE WITH HEATED BACKSIDE T_g = 5000F, h_g = 0.05	160	725	0.16	774	721	1.11	1560	390	0.25	79,370	0.040
3B	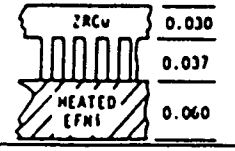	160	725	0.16	773	685	1.14	1480	370	0.30	61,350	0.060
6	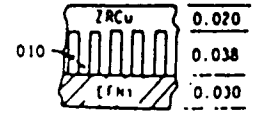	157	727	0.16	609	811	1.02	1920	480	0.22	69,392	0.033

Table 1.4.1-III
Chamber Life Variation with Outer Wall Configuration

CASE NO.	GEOMETRY	NO. OF CHANNELS	V_c - FPS	MACH NO.	T_{wg} MAX, °F	ΔT - °F	STRAIN ZrCu, %	nf	$n_f/4$	STRAIN EFNi, %	STRESS EFNi, PSI	REQUIRED CLOSEOUT THICKNESS
6A	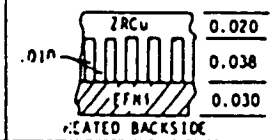 HEATED BACKSIDE	157	727	0.16	613	560	0.81	3280	820	0.25	76,898	0.039
6B	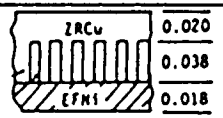 THIN CLOSE OUT	157	727	0.16	609	811	0.94	2320	580	0.24	78,313	0.023
6C	SAME GEOMETRY AS 6B ABOVE WITH EFNi PLASTIC	157	727	0.16	609	811	0.91	2480	620	0.33	63,968	0.019
6D	SAME GEOMETRY AS 6B ABOVE WITH EDCu CLOSEOUT	157	727	0.16	609	811	0.59	ZRCu/6800 /700/EDCu	ZRCu 1700 /175/EDCu	STRAIN EDCu 1.12	EDCu 42,013	0.030
6E	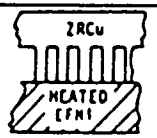	157	727	0.16	611	522	0.822	3232	808	0.24	76,950	0.060
6F	SAME GEOMETRY AS 6E ABOVE WITH EFNi PLASTIC	157	727	0.16	611	522	0.82	3240	810	0.29	66,206	0.060

Table 1.4.1-III
Chamber Life Variation with Outer Wall Configuration (Cont)

Key:	
Vc	Coolant Velocity (fps)
Twg Max	Maximum Gas Side Wall Temperature (°F)
ΔT	Temperature Drop Across Gas Side Wall and Closeout Wall
Strain ZrCu	Thermal Strain in ZrCu Liner (%)
n_f	Number of Cycles to Failure
Strain EFNi	Thermal Strain in EF Nickel Closeout (%)
Stress EFNi	Stress in EF Nickel Closeout (psi)

strength than the Ni alloy, as illustrated in Figure 1.4.1-1, and could be electrodeposited.

A series of fabrication studies, discussed in Section 1.4.3, verified the plating parameters of the higher strength NiCo alloy, and subsequent welding and machining operations. Also demonstrated was the tooling, manufacturing and quality control parameters for the smaller cooling channels, smaller lands, and thinner walls. Table 1.4.1-IV summarizes the technology demonstrated prior to fabrication of the cooled throat hardware.

1.4.2 Fabrication

1.4.2.1 Chamber Material

Two NAS-Z Copper forgings were initially obtained for the fabrication of the cooled throat. NAS-Z was preferable to ZrCu because of the better mechanical properties. After receiving, each forging was analyzed to characterize the grain structure and determine the phase composition. Examination of the photomicrographs of the 2 forgings revealed significantly different grain structures. Additional analysis of the composition indicated no silver present in forging #1. Subsequently, forging #1 was determined to be ZrCu and therefore not suitable for the cooled throat fabrication. A third forging was ordered to replace forging #1. Results of the inspection are listed below.

Forging #1: (SN 1) ZrCu
Large grain size and improper composition

Forging #2: (SN 2) NAS-Z
Acceptable

Forging #3: (SN 3) NAS-Z
Some grain irregularity or small flaws.

Based on the results of the inspection, forging #2 was selected as the primary billet for the fabrication of the fireable cooled throat section.

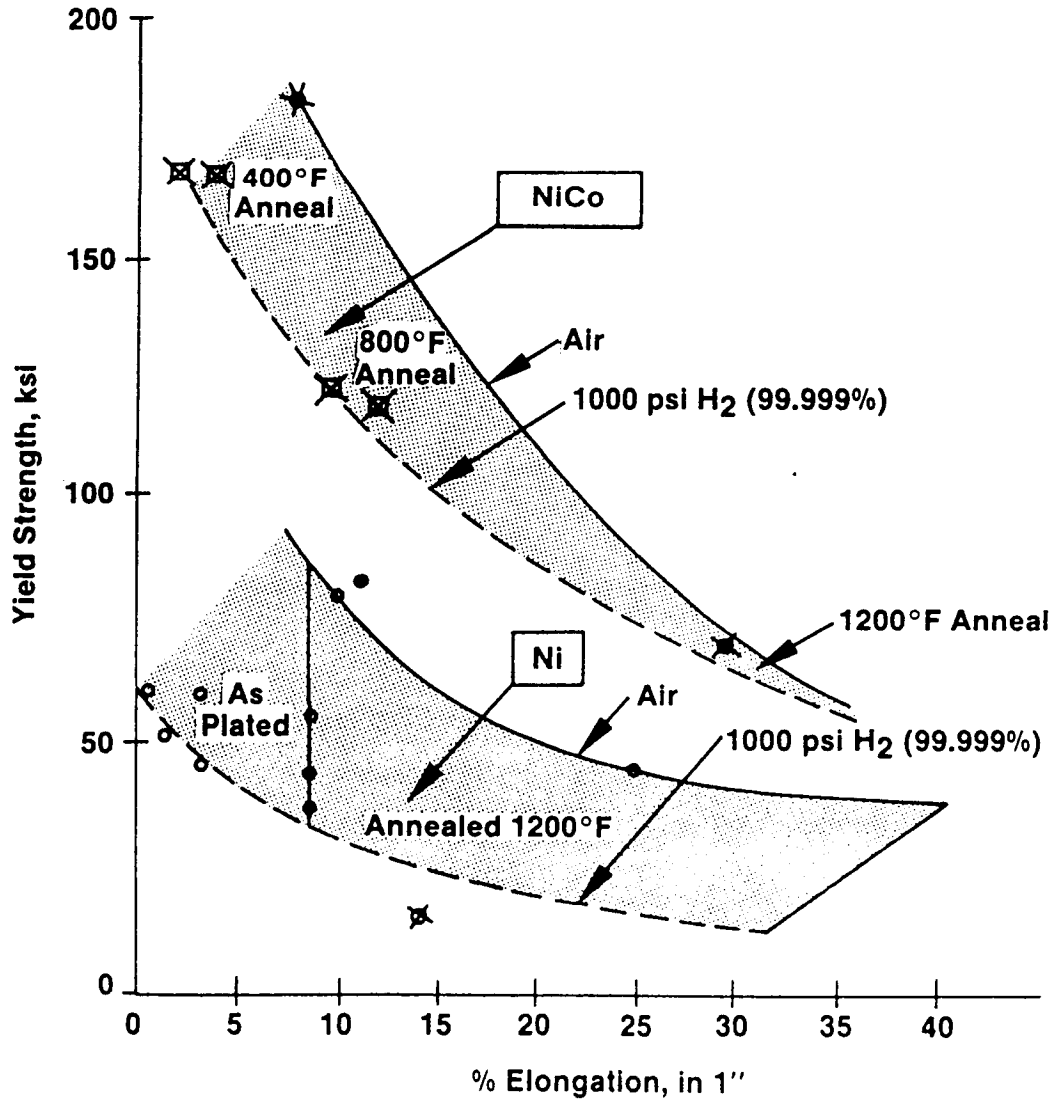

Figure 1.4.1-1. Yield Strength & % Elongation of EF Ni & EF Ni Alloys

TABLE 1.4.1-IV

DEMONSTRATED TECHNOLOGY

1. Machining high aspect ratio 0.01" cooling channels.

2. Maintaining 0.011" wide channel ribs.

3. Holding a gas-side wall of 0.020" to within +0.003"/-0.0005".

4. Electrodeposition of a high strength NiCo alloy closure.

5. Generation of the channel-to-manifold flow path by electrodeposition rather than machining.

6. Welding a manifold closure to the electrodeposited structure.

7. Inspection of the NAS-Z copper forging for defects and inspection of the Ni alloy-to-copper bond on 0.011" thick ribs.

Forging #3 was selected for the machining demonstration tests including chamber contouring and full channel slotting.

1.4.2.2 Slotted Throat Liner

Using methods developed under an Aerojet IR&D program, the machining of 0.010" wide "mini" channels was optimized. The test sample, SN 3, shown in Figure 1.4.2.2-1, contains 80 channels machined in 4 groups of 20 each. Machining parameters were varied slightly in the four groups to determine the optimum fabrication parameters. Slotting parameters and cutter material were evaluated and recorded during SN 3 processing. Cordax inspection was performed at all stages of contouring to verify dimensions before proceeding to the slotting operations.

An NC tape was programmed for the proof machining of the SN 3 chamber. After the slots were completed, Cordax inspection of the SN 3 liner indicated that all channel depths were too deep, resulting in an unacceptable undersized wall condition. Although the variation from channel to channel was within tolerances, all the channels were cut slightly deep. For machining of SN 2, special precautions were undertaken in order to maintain the critical wall thickness, especially in the throat region. To ensure proper dimensions, manual adjustments were made to the numerically controlled program tape after preliminary slots were cut. For machining of SN3, no manual adjustments had been made to the NC tape.

A special tool, shown in Figure 1.4.2.2-2, was fabricated to check the depth of the slots while SN 2 liner remained in the mill. When machining the slots on SN 2, shallow cuts were made initially and the depth measured and recorded. Figure 1.4.2.2-3 is a photograph of SN 2 liner being machined. Calculations were made from the inspection data to determine exactly where the arbor should be located in order to cut the correct slot depth. In this manner, manual adjustments to the NC tape correctly identified the variation required to obtain acceptable slot depths and wall thickness.

A closeup of the liner channels for SN 2 is shown in Figure 1.4.2.2-4. A cross sectional photograph of these thin channels is shown in Figure 1.4.2.2-5.

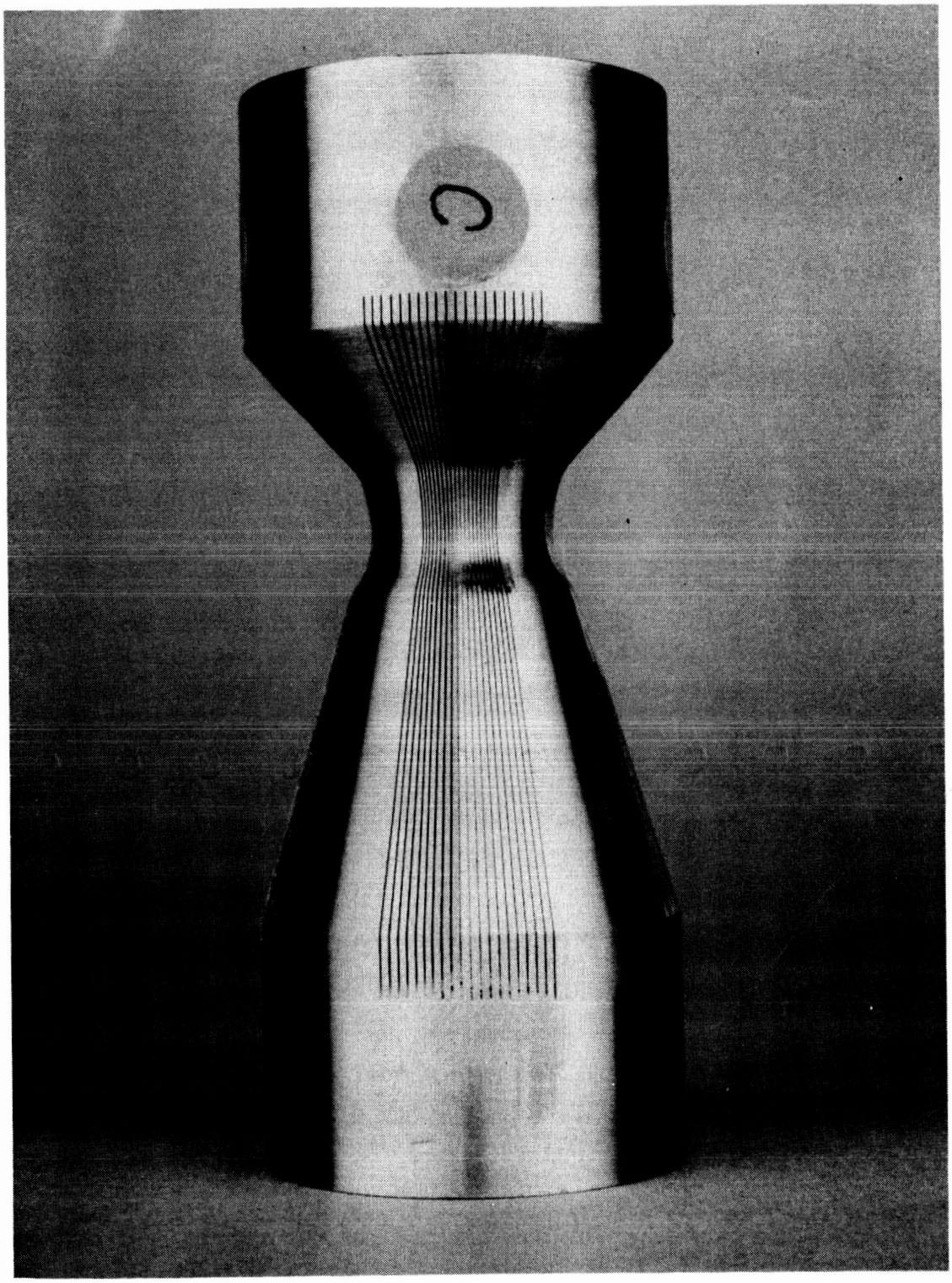

Figure 1.4.2.2-1. LH_2 Cooled Throat Section

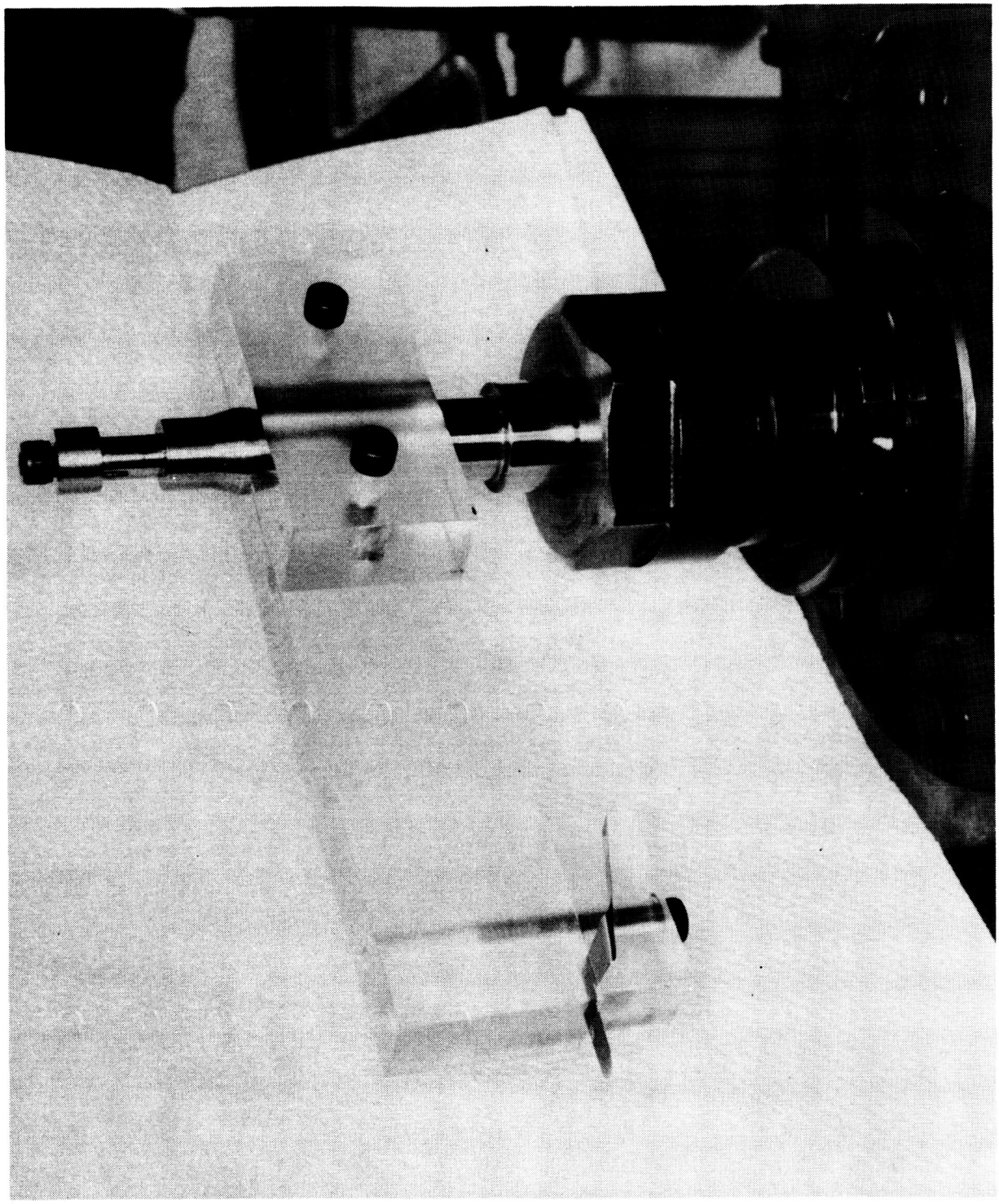

Figure 1.4.2.2-2. Tooling to Measure Slot Depth

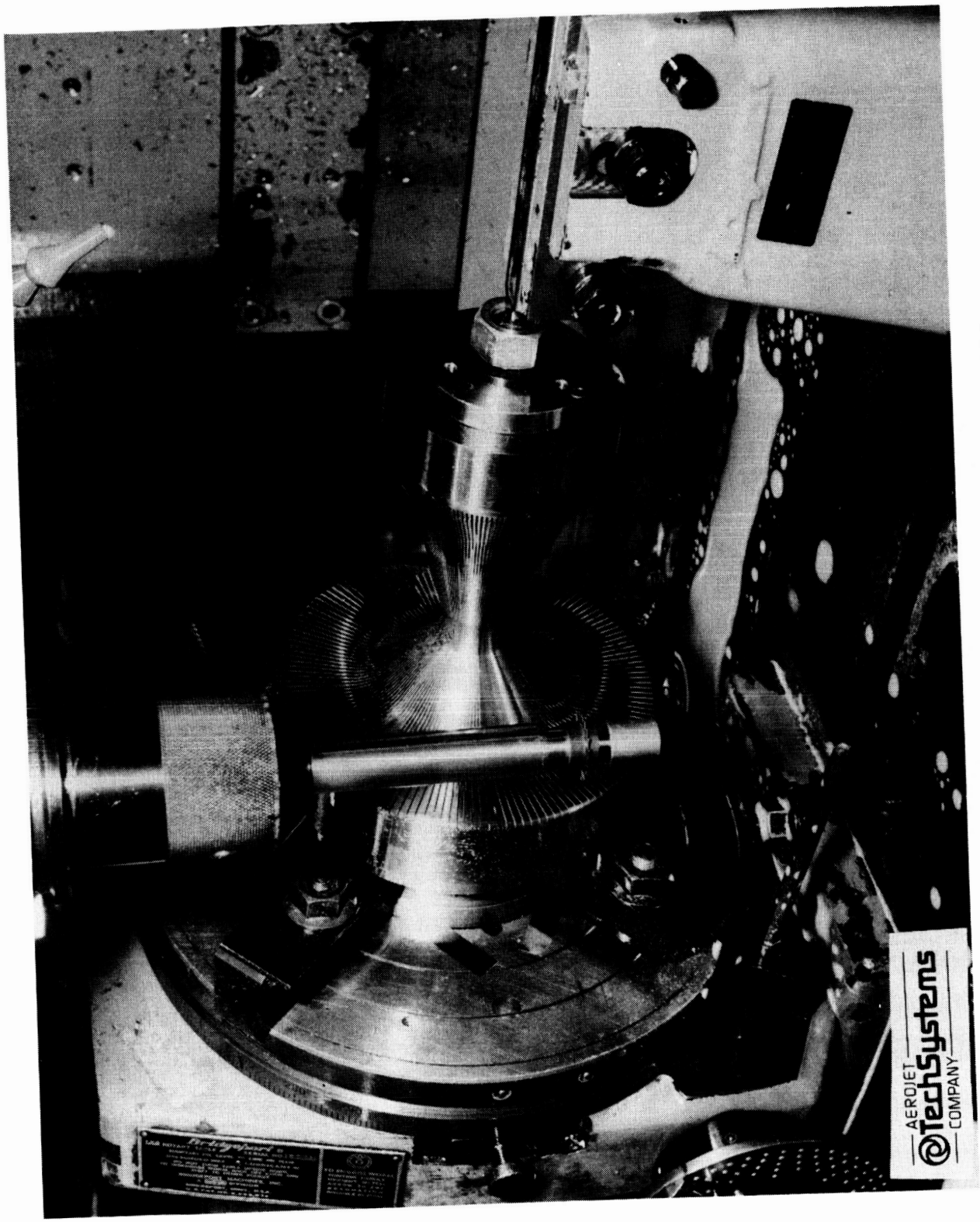

Figure 1.4.2.2-3. Machining of SN_2 Throat Liner

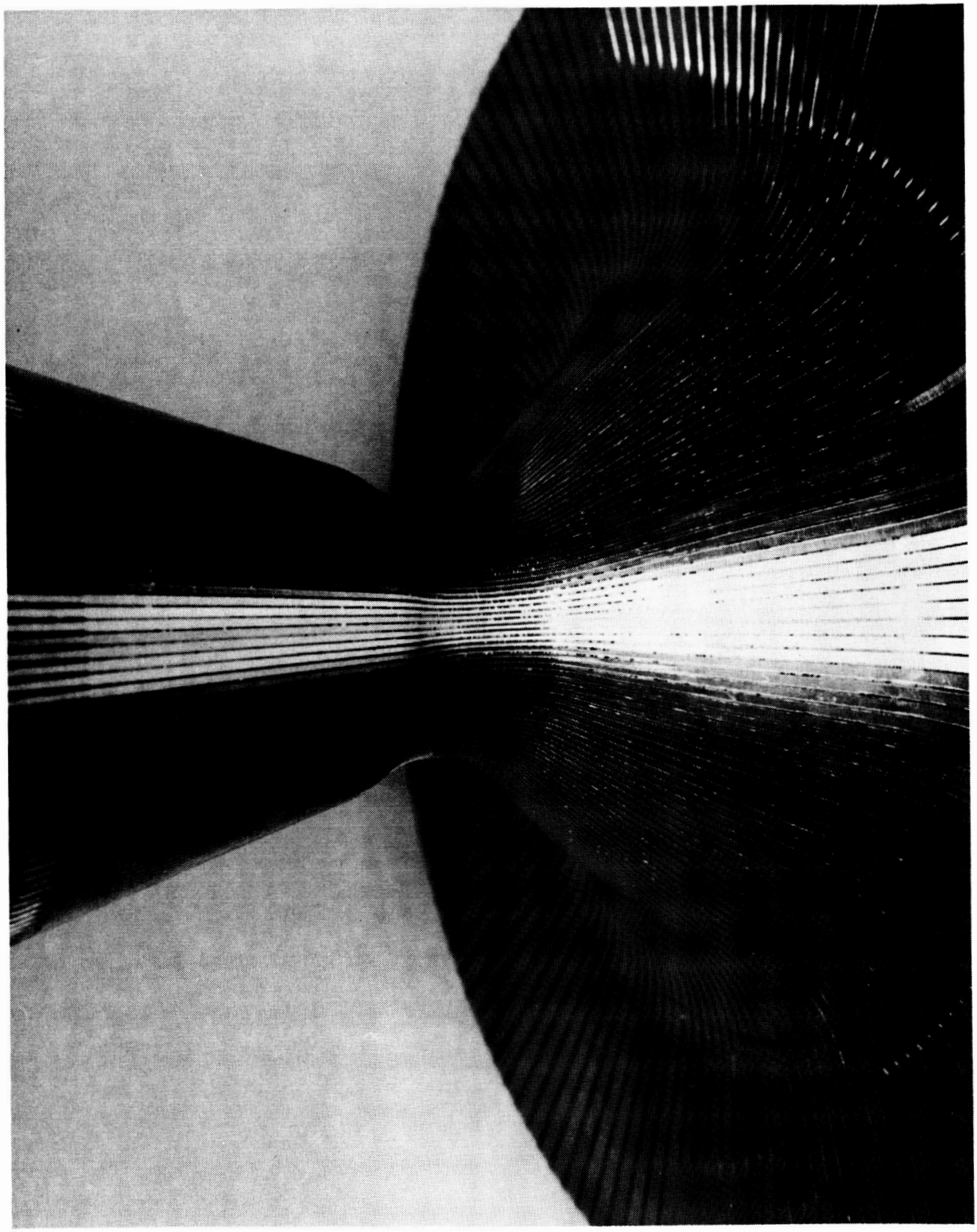

Figure 1.4.2.2-4. Closeup of Throat Cooling Channels

ORIGINAL PAGE IS
OF POOR QUALITY

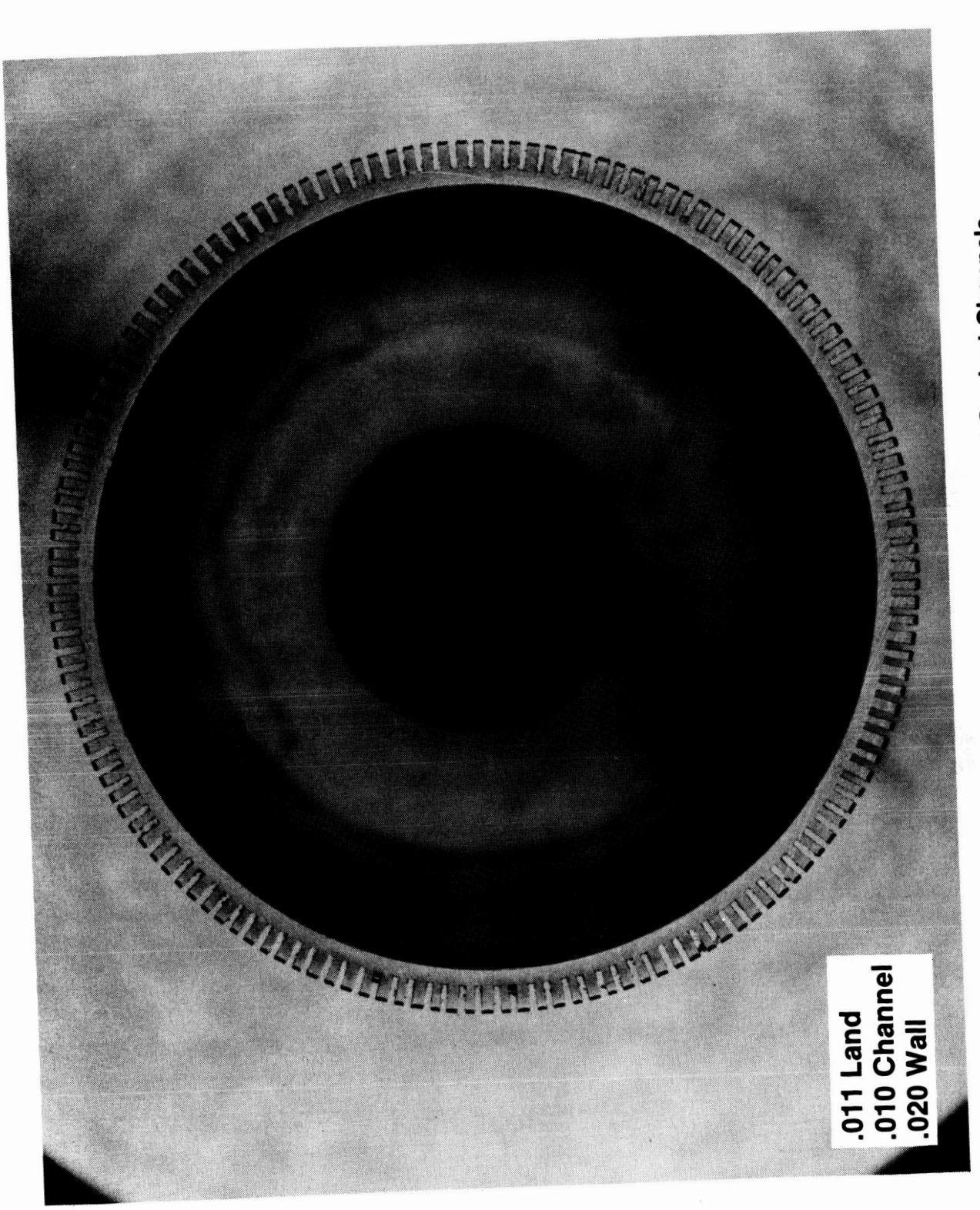

Figure 1.4.2.2-5. X-Sectional View of Coolant Channels

1.4.2.3 Closure

After the throat liner was completed, the channels were filled with a conducting wax. Because of the width of the "mini" channels (0.01"), there was concern as to the removal of the wax in terms of viscosity effects and the presence of filler materials. Verification of the wax removal method is discussed in Section 1.4.3.1.

After the channels were filled with wax, the liner was shipped to the plating company for electro-deposition of a NiCo closeout. NiCo was selected for its high strength properties to accommodate the thin closeout required for high cycle life. Stress analysis indicated that a wall thickness of 0.02" at the throat was required to obtain a cycle life of 500. The pressures in the channel would require a conventional Nickel closure to be on the order of 0.05" thick, thereby increasing the temperature gradient across the wall and subsequently decreasing cycle life. The NiCo alloy was chosen because of its high strength properties and its ability to be electro-deposited. Figure 1.4.2.3-1 shows the throat hardware after the electro-plating process.

Based on the final selection of the wax, the removal process for SN 2 chamber was refined. The steps followed are listed below:

1) Soak in hot mineral oil (200 deg F)

2) Shake ultrasonically while still in mineral oil

3) Insert wire (0.008" diameter) down individual channels to check for residual wax or particles.

4) Resoak in hot mineral oil if necessary. Purge individual channels with GN_2 during mineral oil soak if necessary.

5) Perchloroethylene degrease with flow manifold tool.

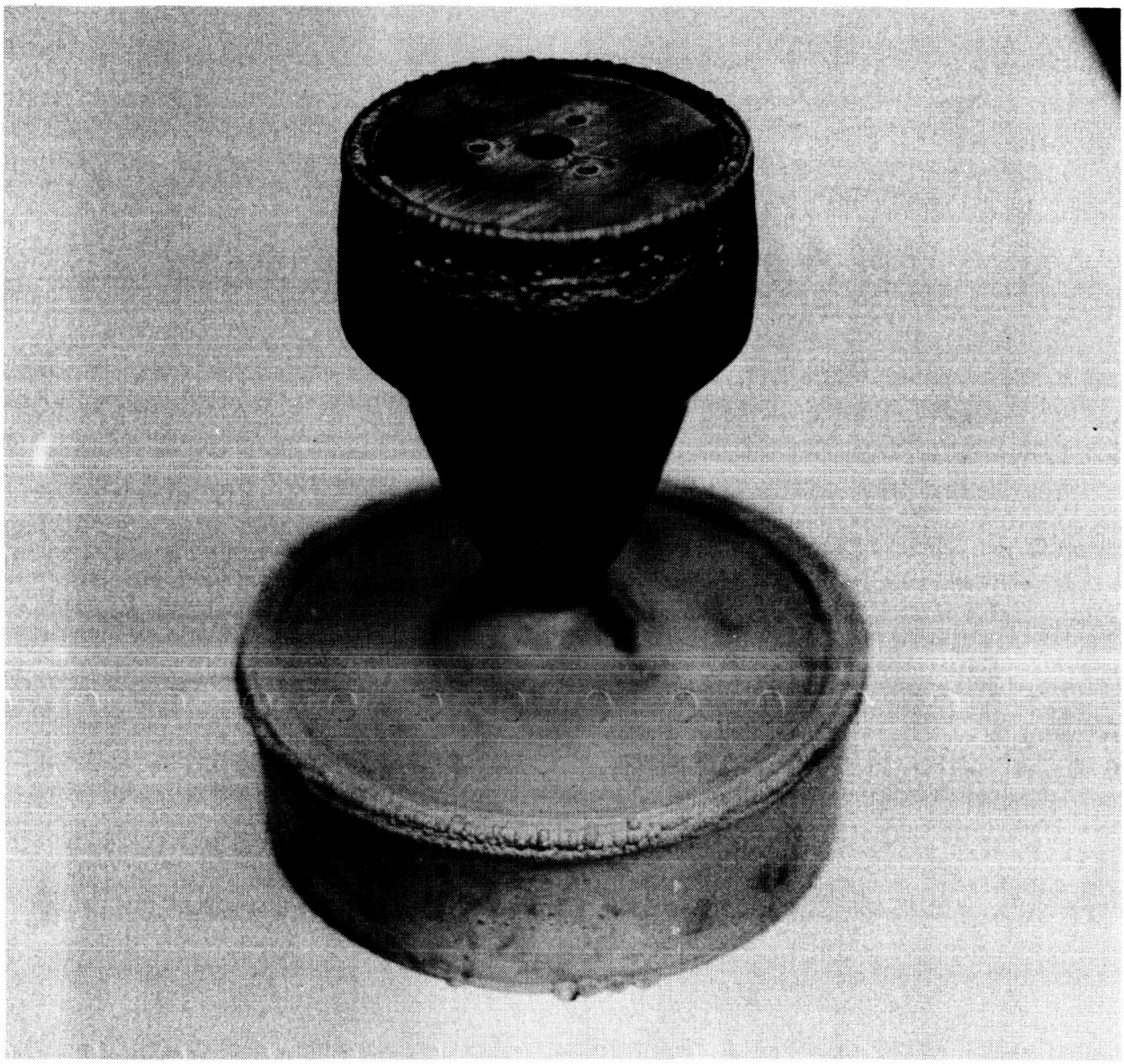

Figure 1.4.2.3-1. SN/2 LH_2 Cooled Throat after Electroforming

6) Water flow and pressure drop test with flow manifold tool.

After the electro-deposition of the NiCo closure, the outer contour of the hardware was machined to the required closeout thickness and to expose the ends of the channels for communication with the manifolds. Figure 1.4.2.3-2 is a photograph of the machined throat hardware.

1.4.2.4 Manifolds

Figure 1.4.2.4-1 illustrates the forward and aft manifold attachment to the regen-cooled throat. The manifolds were attached and welded, first the forward manifold followed by the aft manifold. Both welds involved 0.2" deep penetrations between the EF NiCo chamber closeout and the 304L CRES manifold. Nickel 200 closure rings were match machined to the above welded assembly. The Nickel rings are used to seal the stainless steel manifold to the copper substrate since stainless is not weldable to copper. The channels were covered with aluminum tape during the machining operation to prevent chips from entering the channels.

After machining and cleaning, the aft Nickel 200 ring was assembled and welded with the inlet filter and shims in place. Next the stainless closure was welded to seal the backside of the forward manifold. After completion of the EB welds, dye penetrant inspection verified weld integrity.

The final fabrication steps of the cooled throat hardware included:

1) Final internal machining

2) TIG welding of the inlet pipes and exit pipes to the manifold

3) Final degreasing and bagging.

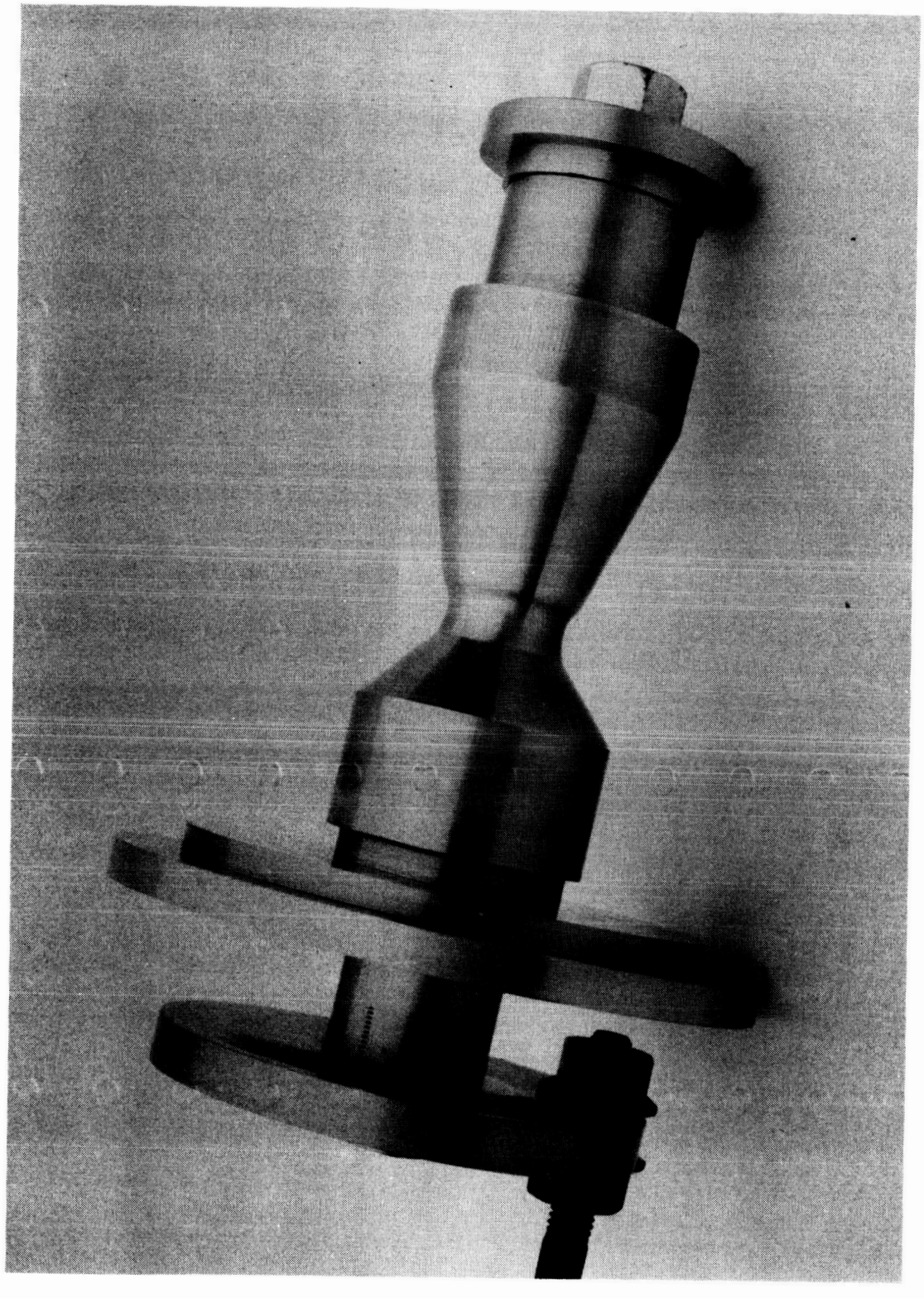

Figure 1.4.2.3-2. SN_2 LH_2 Cooled Throat after Machining

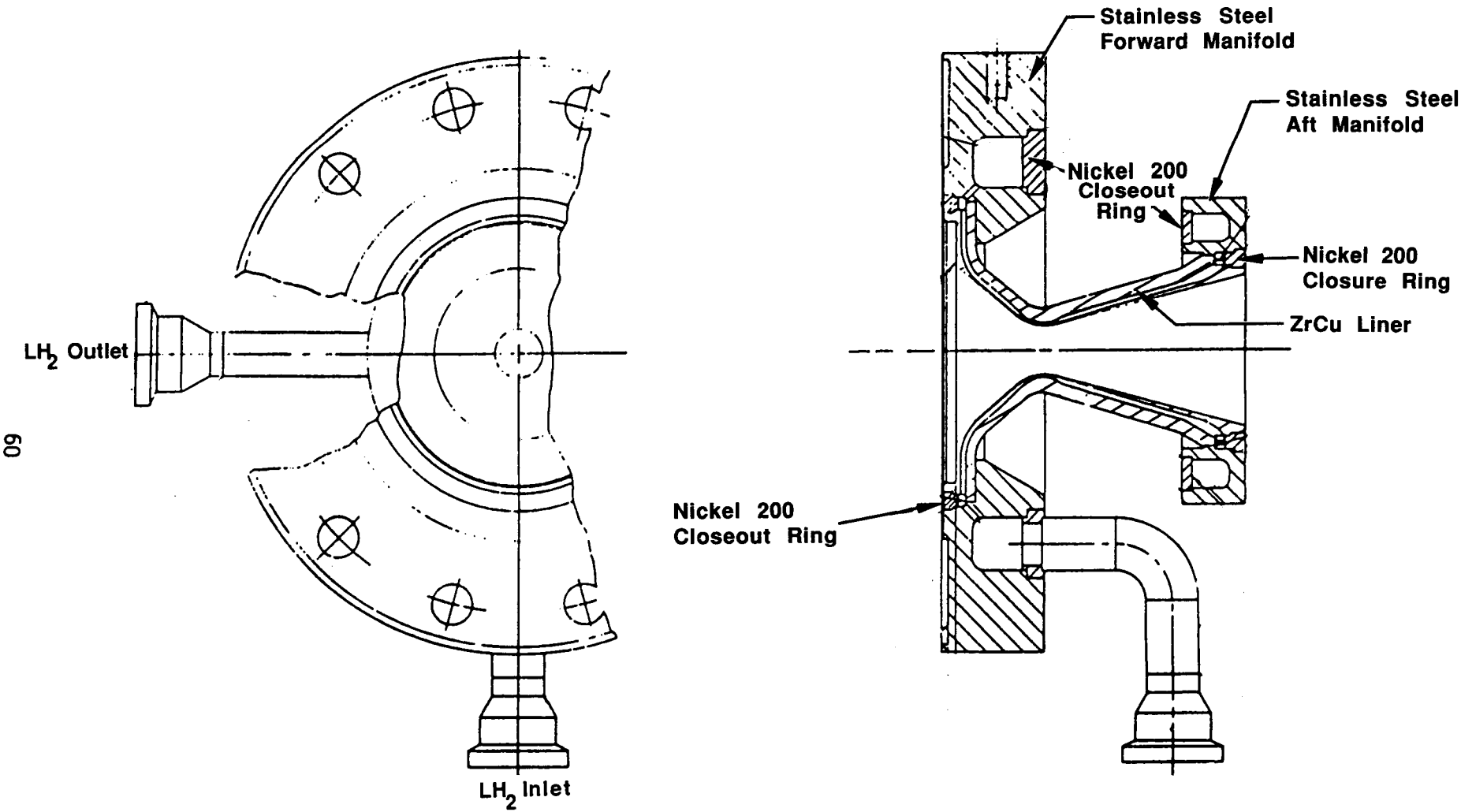

Figure 1.4.2.4-1. Manifold Assembly

The cooled throat hardware is shown prior to welding in Figure 1.4.2.4-2 and as a completed assembly in Figure 1.4.2.4-3.

1.4.3 Fabrication Verification Studies

1.4.3.1 Wax Removal

After verification of the slot cutting parameters, the tool proof (SN 3) chamber was used for the wax removal tests. Wax removal from the 0.01" wide channels was anticipated to be more difficult than with the typically larger regenerative channels that are 0.03" wide. Based on these studies, the properties of the wax for both deposition of the NiCo and subsequent removal from the thin channels could be evaluated. Three different types of waxes were selected.

1) Rigidax Blue (calcium carbonate filled and lined with silver powder).

2) Microcrystalline wax (no filler and lined with silver power).

3) Aerojet proprietary graphite filled wax.

Each wax was used to fill 1/3 of the slots in the first "tool proof" liner. This liner is referred to as the "tool proof" because it was a test article intended to proof the fixturing and methodology developed for fabrication of the LH2 cooled throat hardware. A closeout of 0.065" thickness EF NiCo followed. Figure 1.4.3.1-1 shows the "tool proof" liner in the as-deposited condition. After this initial plating, a one inch long axial crack was observed originating below the aft end. Although the crack didn't affect processing of the tool proof chamber, it was unacceptable for a fireable chamber. A failure analysis, discussed further in Section 1.4.3.2.2, was undertaken to identify the cause of the crack.

The channels were exposed by machining the EF NiCo from the aft "bump". Removal of the wax from the channels was accomplished by placing the chamber in a 250 degree F oven overnight, immersion in MEK (Methyl Ethyl Ketone) solvent, and additional oven cycling. Insertion of a 0.009" wire into the channels verified

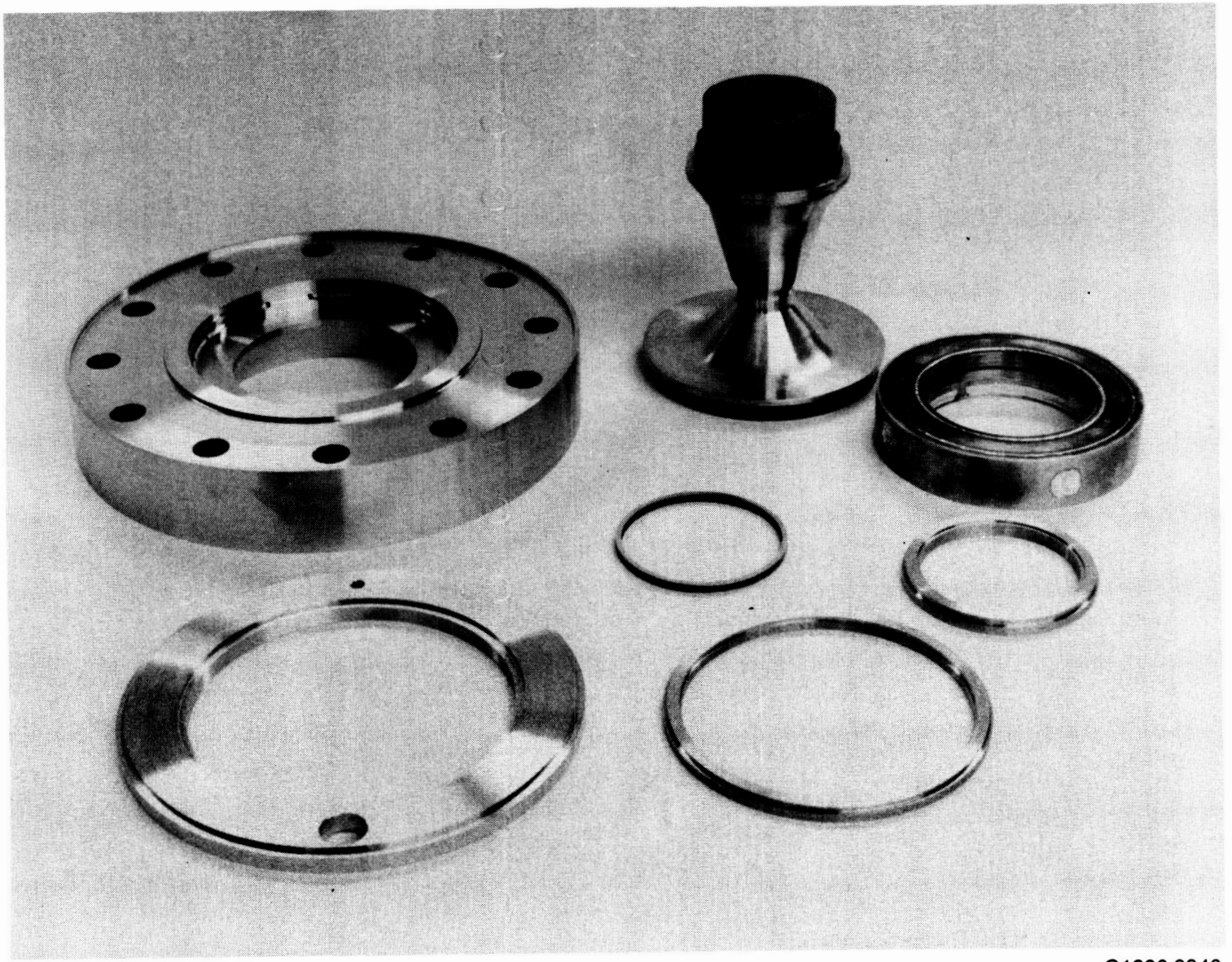

C1286 3946

Figure 1.4.2.4-2. LH_2 Cooled Throat Hardware Prior to Assembly & Weld

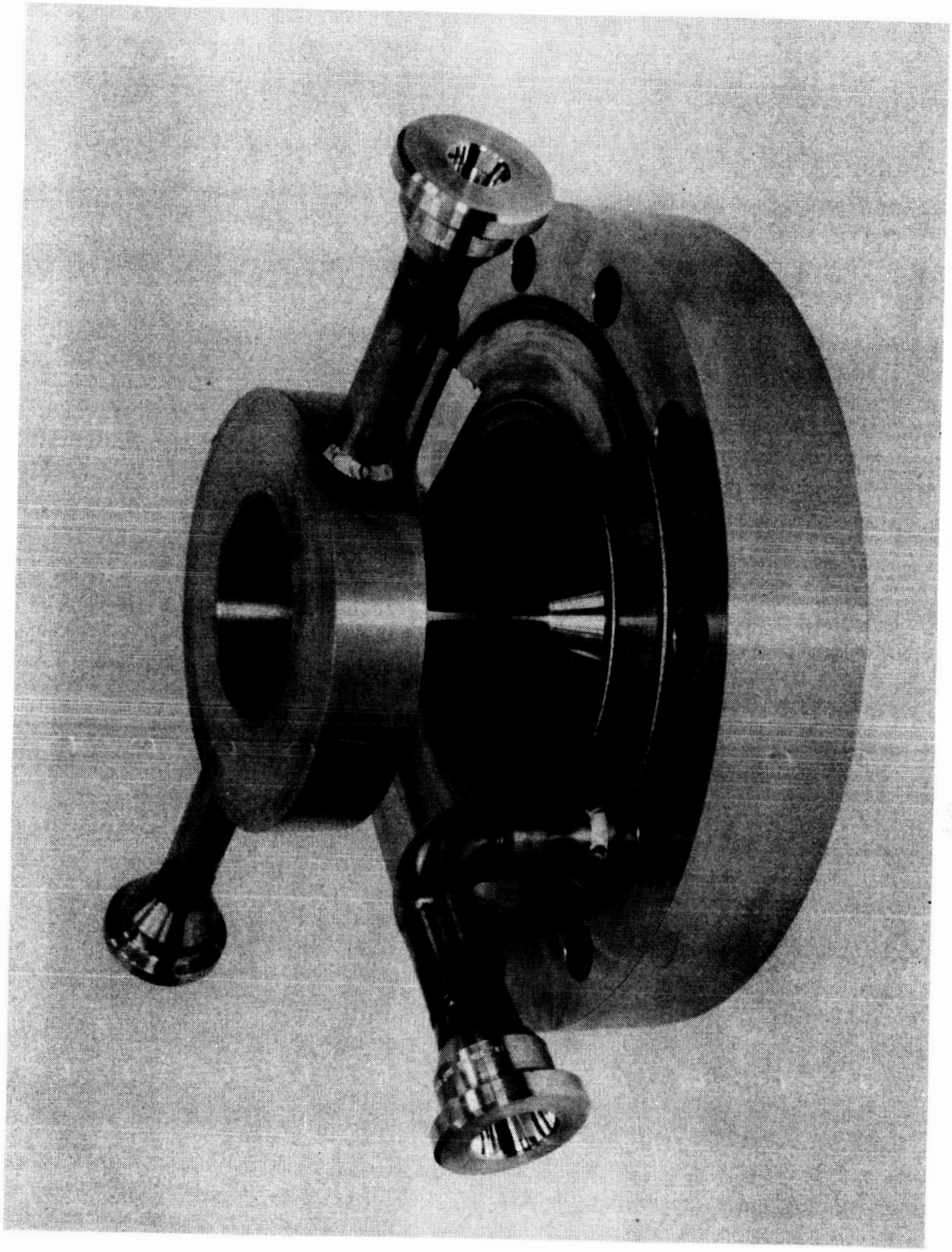

Figure 1.4.2.4-3. LH_2 Cooled Throat Assembly

Figure 1.4.3.1-1. SN_3 Tool Proof Liner after Electrodeposition

that a reasonable number of channels had been cleared of wax. Of the three waxes, the microcrystalline wax appeared to flow the easiest. This was attributed to higher viscosities and the presence of filler materials in the other two waxes. Although the microcrystalline wax-filled channels flowed the easiest, the presence of residual closeout material inside the channel area was suspected due to the wax shrinkage characteristics. Cold flow tests were next performed to indicate if there was any systematic deposition of NiCo inside the channel.

After the cold flow tests, discussed in Section 1.4.5, the chamber was sectioned at the throat to examine the closeout and the bonds at the substrate interface. Photomicrographs of the interfaces for the three waxes are shown in Figure 1.4.3.1-2. The photomicrographs indicate random abnormal plating directly over several of the channels in each of the three groups. Nodule formation above the discrepant channels was attributed to the rough surface condition of the wax. This rough surface was attributed to the use of three different waxes on the same part rather than the wax, since difficulty was experienced in obtaining a smooth finish. Since this plating rough surface condition has not been experienced on chambers with one wax and smooth finish, the rough condition was not expected to occur on the actual test hardware fabricated.

Based on the relative removal characteristics and the photomicrographs, Rigidax was selected for processing the SN 2 cooled throat.

1.4.3.2 Plating Studies

1.4.3.2.1 Electroformed Channel to Manifold Flow Path

Normally the channel to manifold flow path is machined through the electroformed closure, which is time consuming. A method to generate this channel to manifold flow path by electroforming explored the use of a non-conducting filler material placed in the channel at the coolant entrance and exit. A punch and die assembly, shown in Figure 1.4.3.2.1-1, was designed and fabricated to produce 300 plastic blanks approximately 0.01" thick. These strips were inserted into the cooling channels of the throat section prior to the electroforming operation as illustrated by Figure 1.4.3.2.1-2. This figure shows the assembly with teflon sheet tabs inserted and the final electroformed Nickel deposited to a depth of

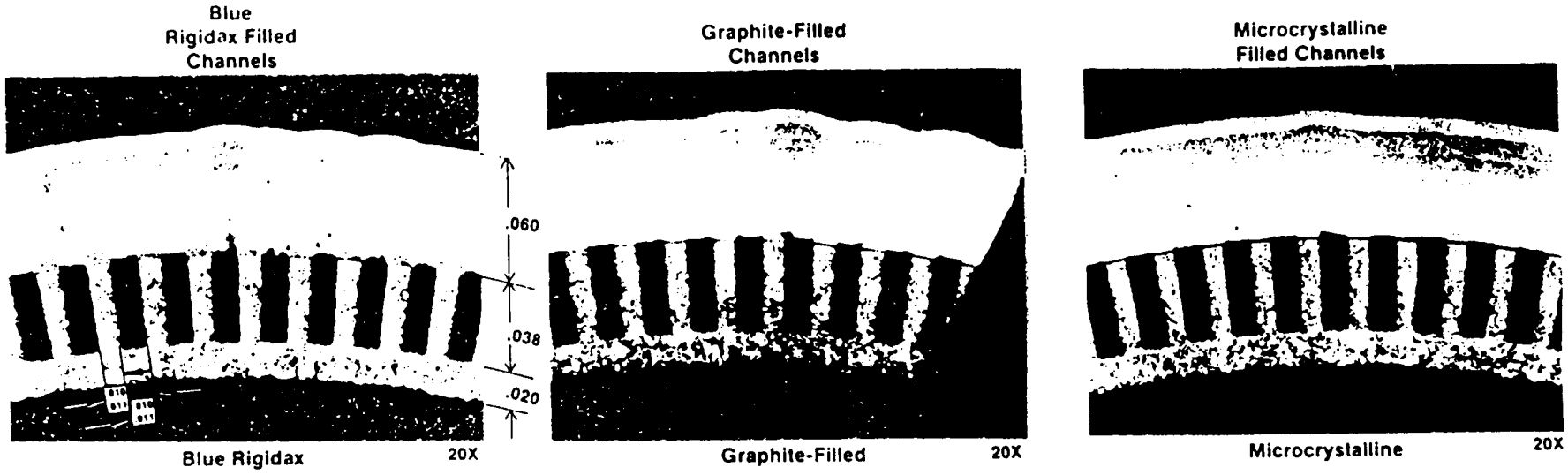

The micrographs indicate random abnormal plating directly over several of the channels in each of the three groups. The apparent nodule formation above the discrepant channels is due to the rough surface condition of the wax. The rough surface is attributed to the difficulty in obtaining smooth finishes with three different waxes on the same part. Smooth finishes without nodules have been demonstrated on chambers with only one wax (Blue Rigidax). Based on the removal characteristics and also on the above photomicrographs, Blue Rigidax has been selected for processing the cooled throat fireable unit S/N-02.

Throat Photomicrographs S/N-03 Chamber

Note:
All Units are in Inches

Figure 1.4.3.1-2. SN_3 Throat Photomicrographs

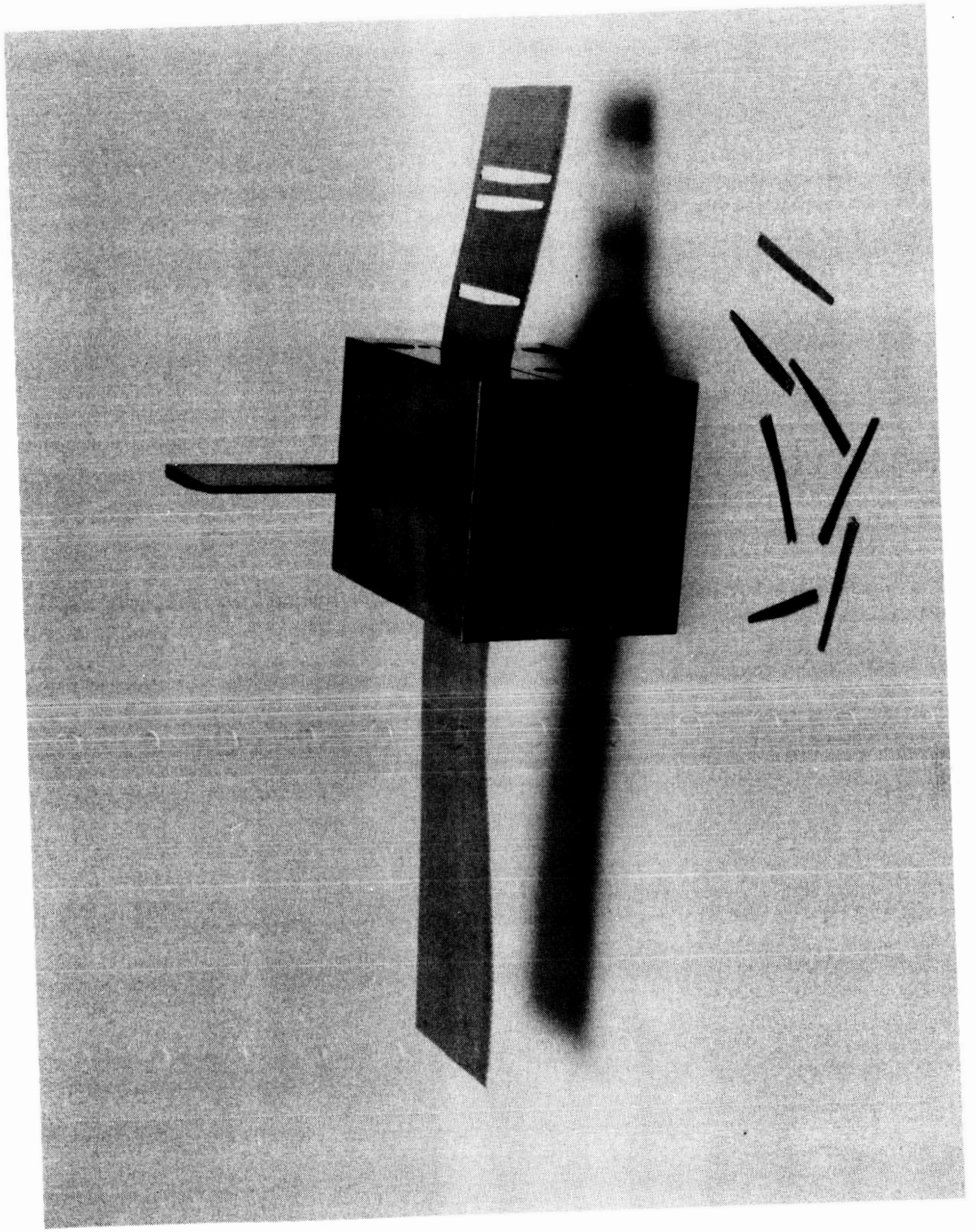

Figure 1.4.3.2.1-1. Punch/Die Assembly

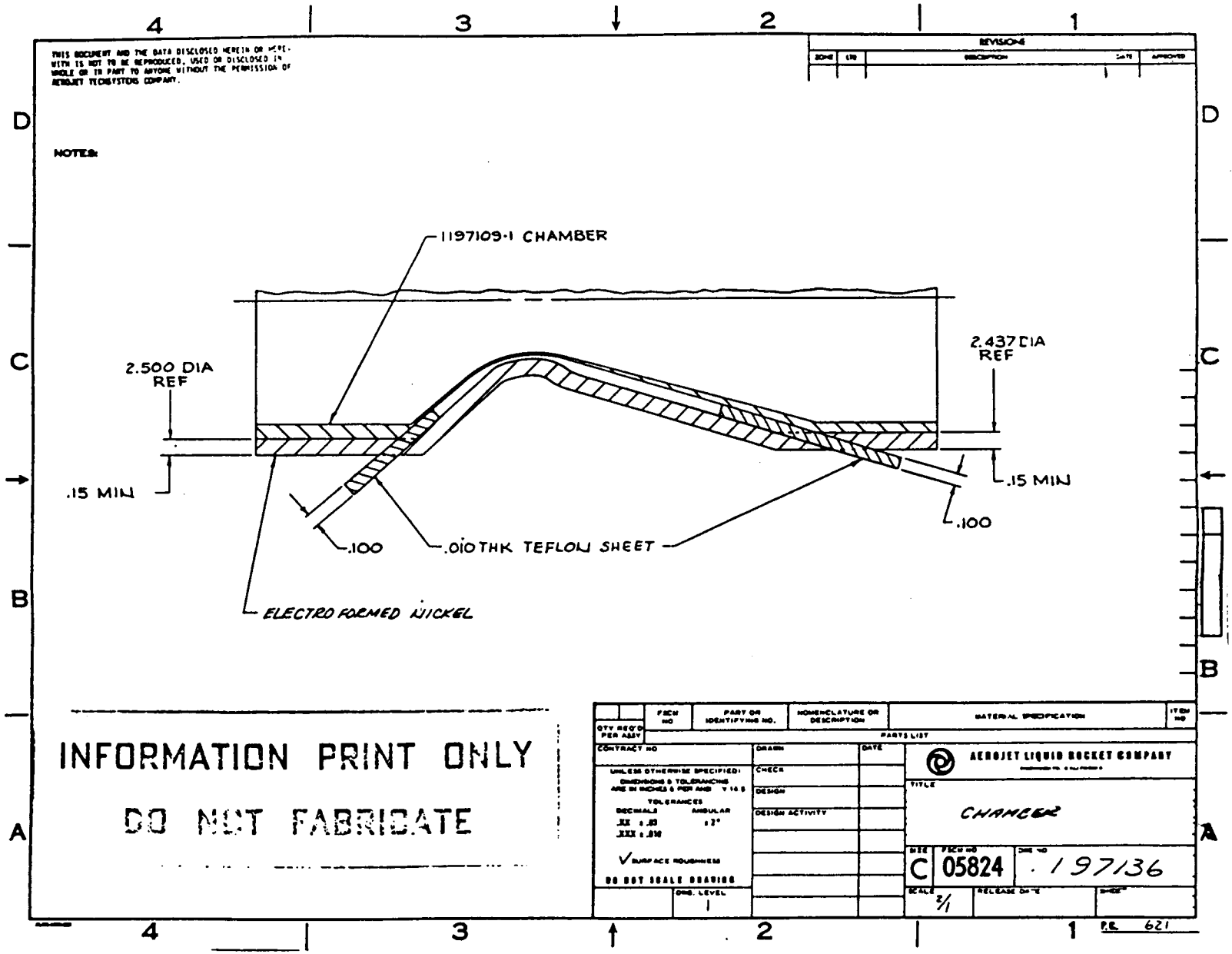

Figure 1.4.3.2.1-2. Test Chamber Electroforming Setup

0.15" The teflon strips are inserted into the chamber coolant channel prior to the electroformed closeout. Figure 1.4.3.2.1-2 illustrates the teflon strips after the EF closeout and prior to their removal. After removal, the inlet and outlet portions of the coolant channel would be exposed. This method was intended to provide inlet and exit cooling manifolds that would be internally reinforced with electroformed NiCo.

Unfortunately, difficulties were encountered in forming the channel to manifold flow path during the electroforming process. Removal of the insert filler material proved to be difficult. Trial with Teflon strips, instead of the plastic, was tried with limited success. Figure 1.4.3.2.1-3 shows the chamber following the plating of the NiCo alloy with the filler strips extended. Although the plating (approximately 0.2" thick) was satisfactorily deposited between the strips as shown in Figure 1.4.3.2.1-4, the alignment of the channels after removal of the filler strips was unacceptable for the intended purpose.

1.4.3.2.2 EF NiCo Closure Crack Analysis

The as-deposited condition of SN 3 chamber is shown in Figure 1.4.3.2.2-1. As shown in this figure, a crack was noted in the as-deposited EF NiCo closeout on the tool proof chamber SN 3. The crack originated in the EF NiCo plating next to the aft aluminum mandrel. The chamber was dye-penetrant inspected and no additional lengthwise cracks were found, although more radial cracks were noted originating from the aft mandrel. The chamber was next machined in the "bump" area to expose the channels for wax removal. During the machining and subsequent oven exposure, the crack propagated axially down the length of the chamber.

Several hypotheses were formulated as to the cause of the crack. The preplate stress level of the electroforming bath was 17 ksi tensile as measured with a spiral contractometer. Presence of a high residual tensile stress level in the deposit could contribute to a crack. The stress level of the bath following the plating was 12 ksi. Since the ductility of the EF NiCo is low, this level of stress would not be expected to cause the formation of cracks.

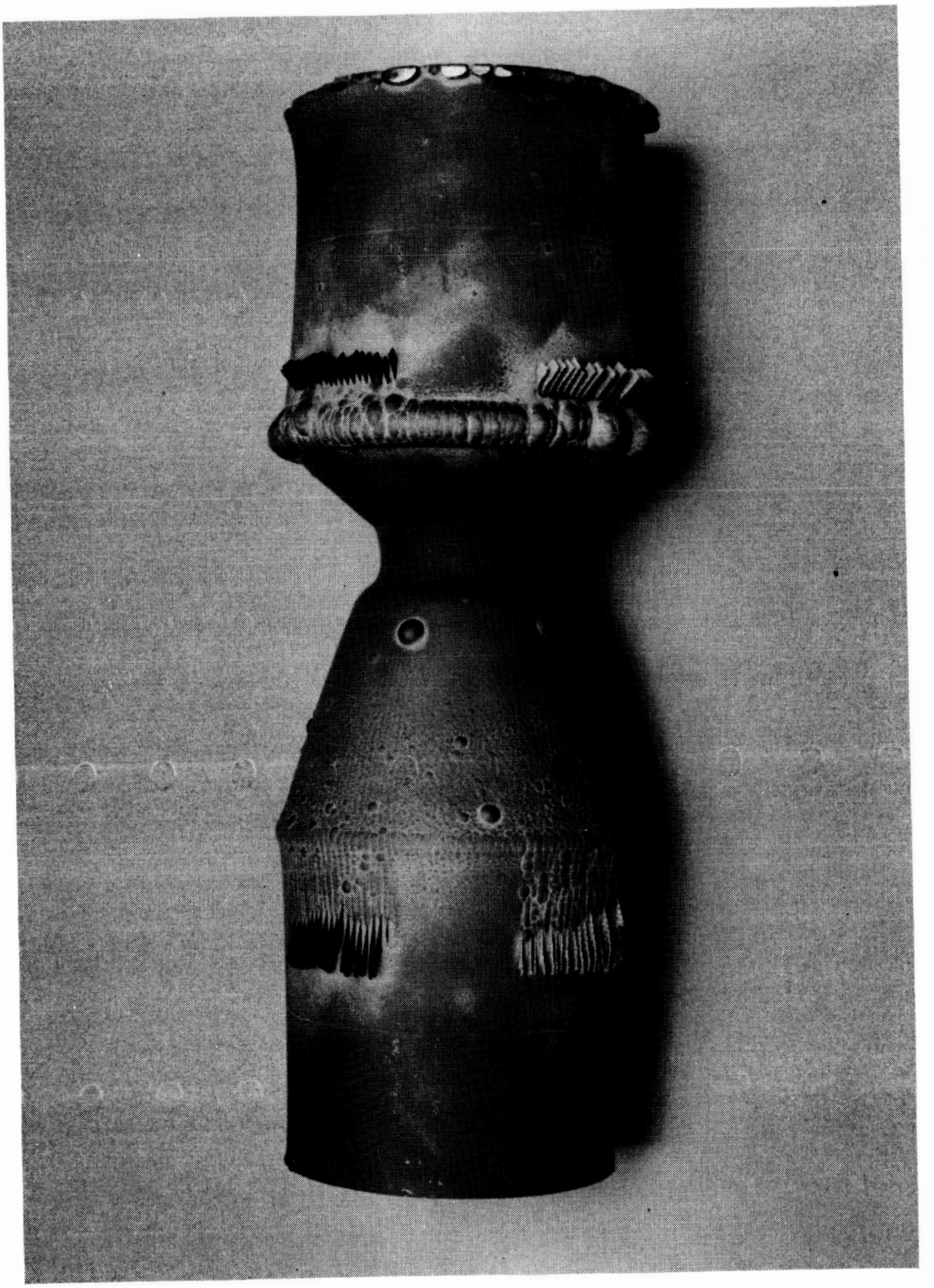

Figure 1.4.3.2.1-3. Test Chamber after Electroforming

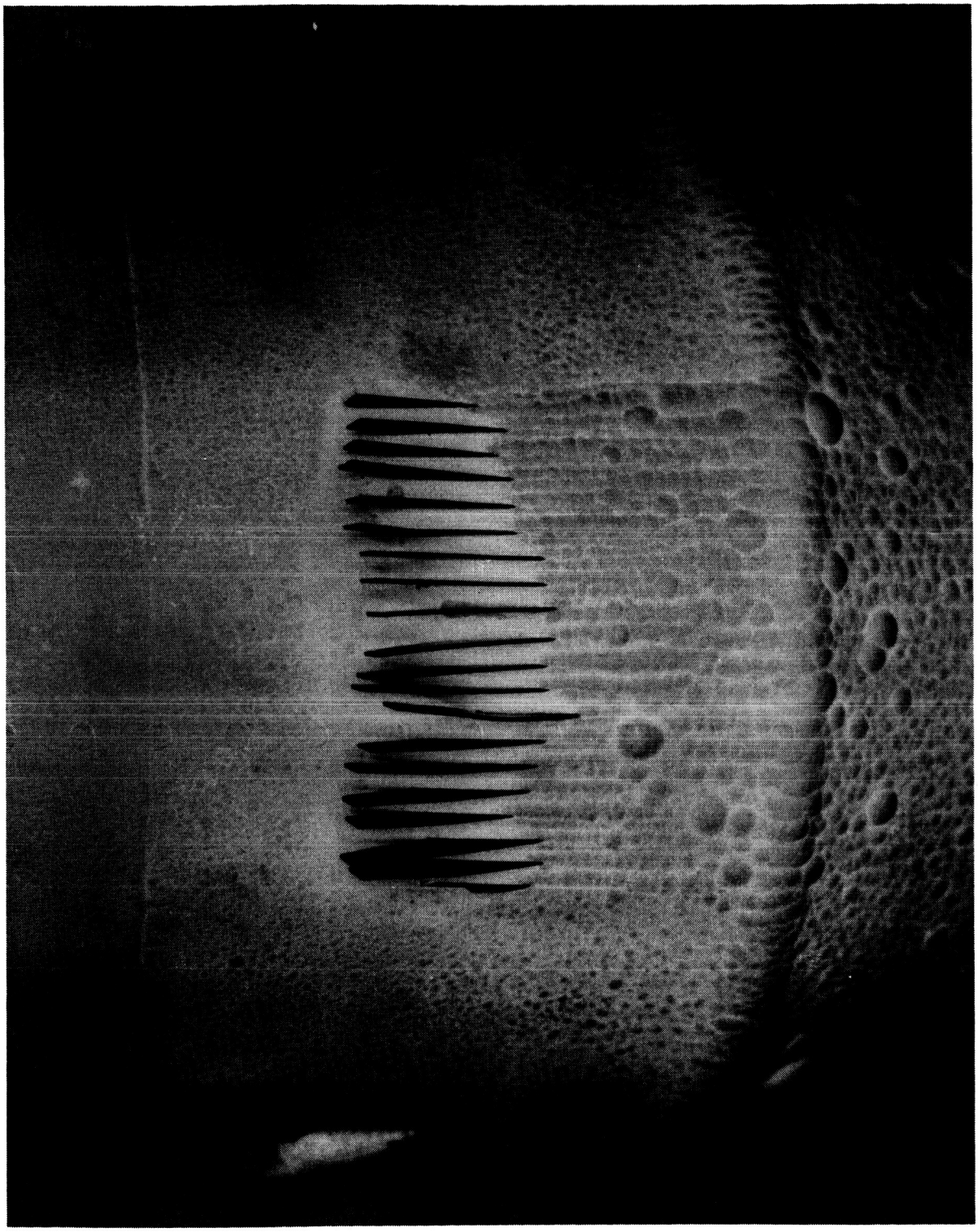

Figure 1.4.3.2.1-4. Irregularity of Flow Channel Alignment

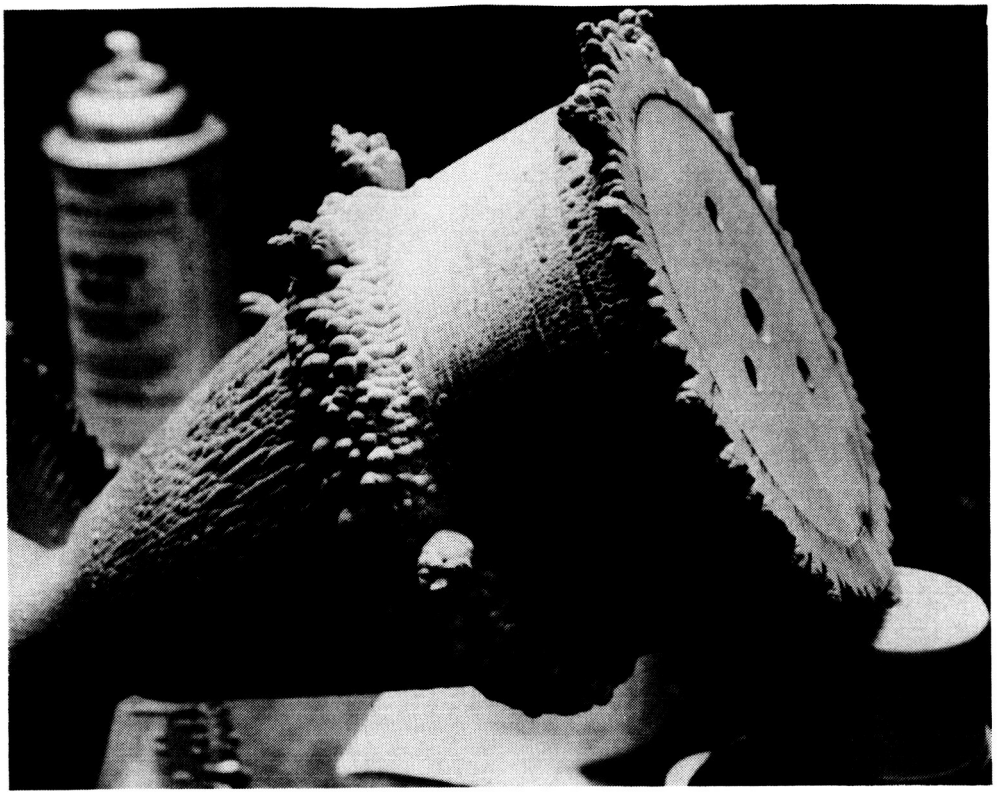

C0186 268

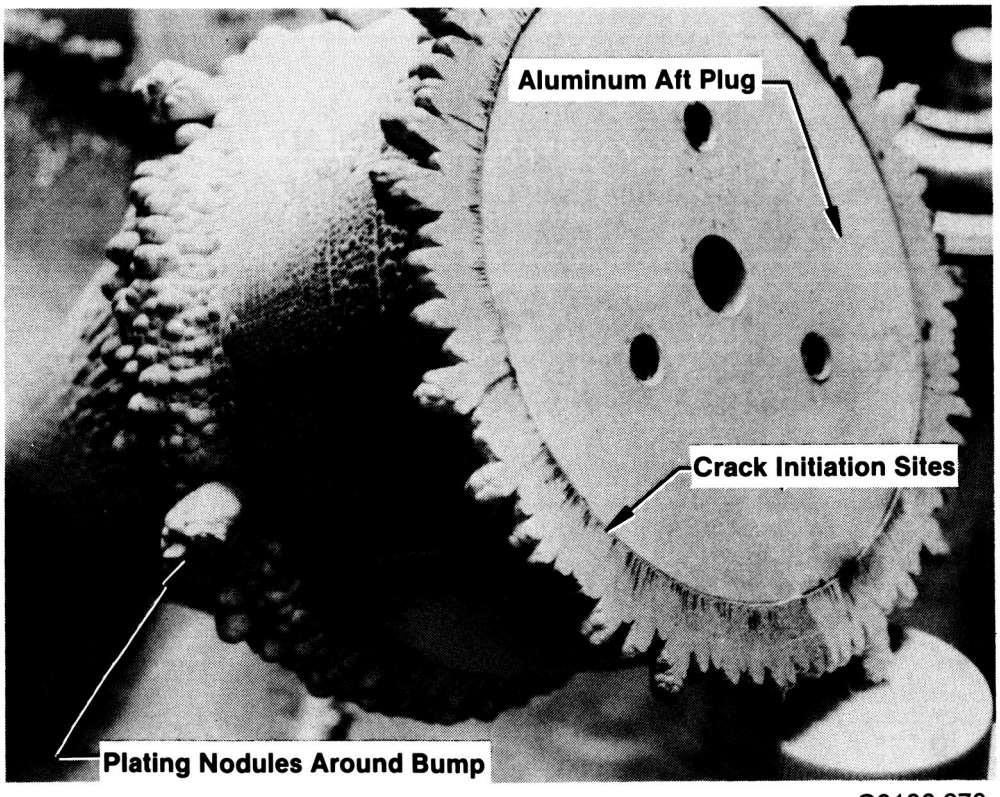

C0186 270

Figure 1.4.3.2.2-1. SN_3 Tool Proof Liner - Aft End Crack

Nodule formation was noted to be significantly higher on the aft end where the crack formed compared to the forward end of the chamber which displayed virtually no nodule formation. Although nodules occur along corners and edges, severe formation can lead to unwanted stress concentration areas. Shielding of the cathode (chamber) in the plating tank limits the nodule formation in a particular area by directing the electrolyte flow. Further reduction of the nodules is possible by a refined plating bath and smoother geometries. The chamber design was modified to smooth the "bump" area.

Numerous areas of crack initiation or void sites were noted in the plating over the end plugs. The copper is activated to accept the EF NiCo, whereas the aluminum used for the plugs is not specifically activated. It was theorized that the void areas were due to the plugs not being made of copper and therefore not activated for NiCo plating.

Sulfur contamination is known to cause intergranular brittleness. Improper refinement of the plating bath can result in the deposit containing a higher than desired sulfur content. The sulfur migrates to the grain boundaries and results in brittleness.

In order to evaluate the later hypothesis, scanning electron microscope (SEM) and microprobe analysis were preformed to determine the sulfur content near the failure area and to determine the crack characteristics. The failure surface had a high sulfur concentration with some aluminum contamination at the corner where the crack appeared to originate. Propagation of the crack occured at about 45 degrees from the axis of the chamber. Both brittle and ductile areas were found on the surface. No sulfur was detected below or underneath the failure area.

Results of the EF NiCo failure were discussed with an alloy plating specialist, Mr Glenn Malone with Bell Aerospace-Textron in Buffalo, N.Y. Mr Malone was concerned with the cleanliness control of the tanks and bath filtration, and expected the crack to be due to sulfur deposition in the areas of high current density. Recommendations were made which included modifying the shielding/end plates to avoid areas with high current density, lowering the average current density from 20 to 16 amps/square foot, and increasing the bath temperature

from 115 degrees F to 120 degrees F. In addition, a sulfuric acid activation solution was recommended to replace the phosphoric acid solution.

With the concurrence in the hypotheses and recommendations by Mr Malone, the modifications were discussed with the electroformer. Following incorporation of the modifications, a new sample in the form of a flat plate was plated and analyzed to verify the changes. Bend tests were preformed on a thin section and showed excellent ductility. A tensile test in the as-deposited condition verified the mechanical properties listed below.

Ultimate Strength	197 ksi
Yield Strength	139 ksi
% Elongation	5.5 %
Youngs Modulus	27.5 Msi

Next a full size demonstration chamber was prepared for qualification of the plating. Chamber SN 1 was contoured (with no channel slots) and sent to the electroformer for plating preparations. OFHC copper plugs were substituted for the aluminum end plugs and used on the aft end where the crack occurred on SN 3. Due to the unavailability of a large diameter copper stock material for the forward plug, a stainless plug was fabricated. Copper was used for the SN2 chamber end plugs. The O-ring location on the end plugs was changed to avoid internal chamber leakage. A 0.10" thick closeout was applied to verify plating quality. Figure 1.4.3.2.2-2 shows the as-deposited SN 1 forging. No cracks were detected during the dye penetrant inspection. As a result of this successful verification of plating quality, SN 2 chamber was authorized for plating. Based on the plating studies with SN 3 and SN 1, SN2 chamber channels were filled with Blue Rigidax wax and then plated with 0.20" thick EF NiCo closeout. SN 2 is shown in Figure 1.4.3.2.2-3 after electroforming. Nodule formation was reduced and no cracks were noted.

Figure 1.4.3.2.2-2. Electroformed SN_1 Forging

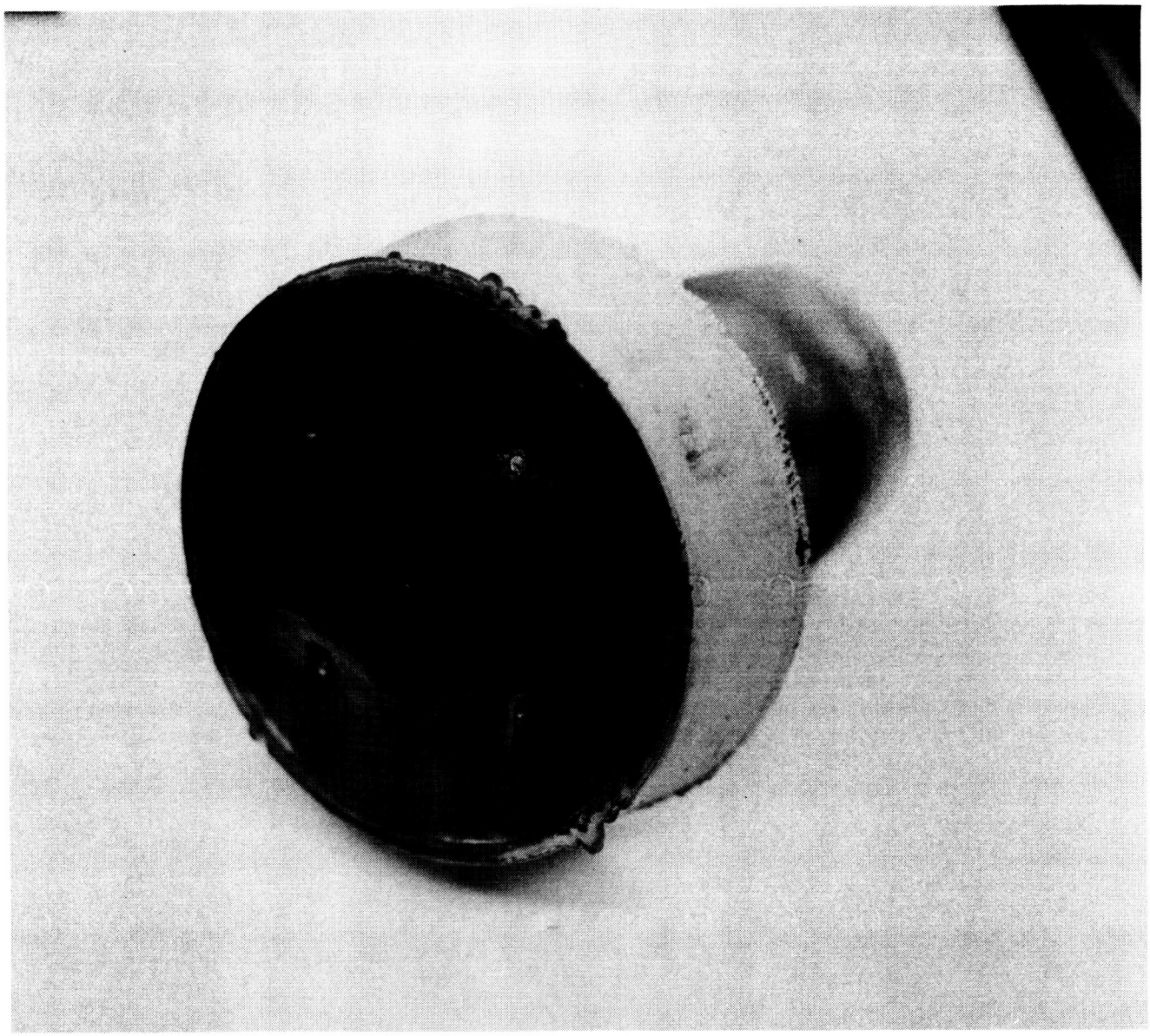

Figure 1.4.3.2.2-3. SN_2 Liner after Electroforming Closeout

1.4.3.3 Welding Studies:

Objectives of the welding studies included:

1) Demonstration of the weldability of the EF NiCo closure.

2) Evaluation of bond strength in the heat effected zone after welding.

3) Definition of a suitable weld configuration schedule.

Three 0.4" wide rings were machined off the extended test material zone on one end of the chamber as shown in Figure 1.4.3.3-1. These rings were utilized in the initial weldability experiments on the electrodeposited

Electroplate NiCo closure on pilot chamber
containing 80 slots .010 in. wide

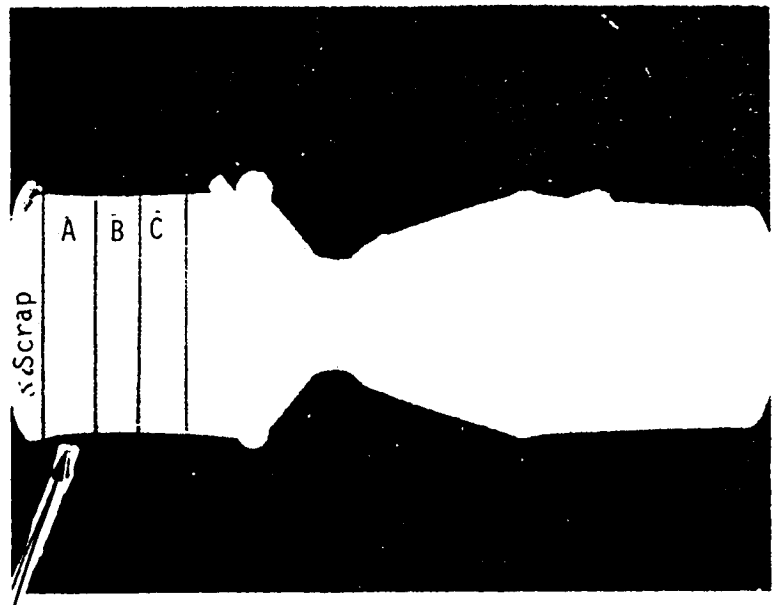

Three (3 ea.) test rings cut
from forward plug

Anneal Parameters:

A.) 800°F ½ HR

B.) 800°F 1 HR

C.) 600°F 1 HR

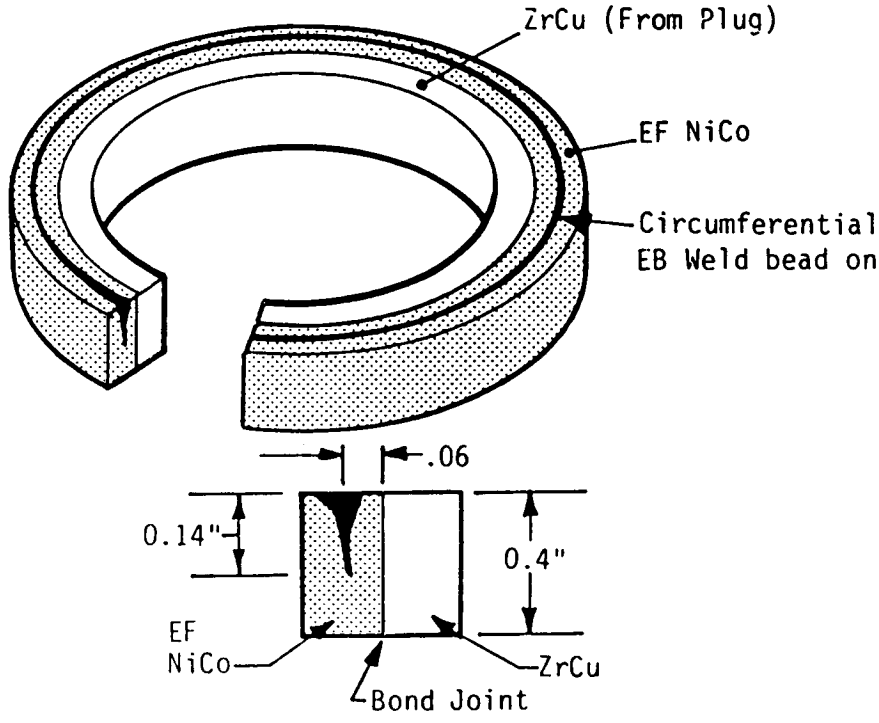

Figure 1.4.3.3-1. Weld Test Rings

NiCo. Each of the three sections was subjected to a slightly different anneal cycle to assess the weldability, ductility, and susceptibility to hydrogen embrittlement. The anneal cycles were as follows:

Test specimen #1: 600 degrees F for 60 minutes
Test specimen #2: 800 degrees F for 30 minutes
Test specimen #3: 800 degrees F for 60 minutes

Electron beam (EB) welds were made within each of the three electrodeposited NiCo rings. No weld cracks were visible in any of the three samples, which indicated that the material was weldable and not sensitive to the pre-weld anneal cycle.

Although the anneal cycle reduces the yield strength, it also significantly increases the ductility. The strength can be related to the material hardness based on previous calibration work conducted as a separate ATC IR&D program.

Using the three samples, welds were then made within 0.06" of the NiCo-Cu interface. Experimental results showed disbonding in the heat affected zones in each specimen. Further investigations were undertaken to explore the mechanisms by which the disbonding occurred. This included determining the required temperature for disbonding of NiCo-Cu and defining the actual mechanism for separation.

Specimens remote from the heat effected zone were tested for bond shear strength. The parts failed in the copper at shear levels equal to those for ZrCu in a nearly hard condition, indicating a strong bond between the substrate and the plating.

Further tests were performed on flat specimens to determine the bond strength of EF NiCo to NAS-Z copper substrate. Six lap shear specimens were machined with three samples prepared from two disks. The two disks were subjected to different plating methods, the first was plated with 0.1" EF NiCo and the second was first plated with 0.01" EF CU followed by the 0.1" EF NiCo plating.

Tests indicated plate bond strength capability in excess of 21 ksi shear strength. Specimens displayed either excellent bond or no bond. The effect of anneal and the EF Cu underplating on the bond strength was inconclusive.

The effect of the EB weld on the electrodeposited alloy was indicated by hardness profiles taken of the sample. The low hardness measurements at the weld indicate a very ductile material. Most of the high tensile strength present in the deposited material is lost at the weld. Therefore, the design of the weld affected zone for the chamber utilized the mechanical properties of the NiCo as that of fully annealed Ni.

The NiCo alloy hardness and grain structure at the copper separation zone suggested thermally induced mechanical stresses were responsible rather than melting or overheating at the NiCo-Cu interface. Results of bend tests performed on typical electrodeposited NiCo-Cu samples, shown in Figure 1.4.3.3-2, revealed no disbonding. Although no difficulties were encountered in the NiCo-Cu welds, weldability of NiCo to Ni was also studied. Additional design data obtained from the pilot chamber samples include:

1) NiCo interface tensile bond strength.
2) Minimum tensile strength of Ni to NiCo EB Weld
3) Minimum tensile strength of Ni to 304L EB Weld

As a result of the weld feasibility studies, the cooled chamber manifold attachment underwent several design iterations. These design changes were made to create a support structure capable of sustaining an internal proof pressure of 3000 psi, a channel proof pressure of 7500 psi, and an operating life approaching 500 cycles. Special attention was paid to the EB welds to avoid the previous problems with the NiCo to Cu disbonds.

One of the more difficult welds was the 0.2" deep circumferential EB weld between the EF NiCo closeout and the 304L CRES which forms the inlet manifold. Two modifications which made the weld successful were increasing the thickness of the EF NiCo from 0.07" to 0.17" and making the

EF NiCo Following Modifications

- **Eliminated Contamination**
- **Lowered Current Density**
- **Increased Bath Temperature**

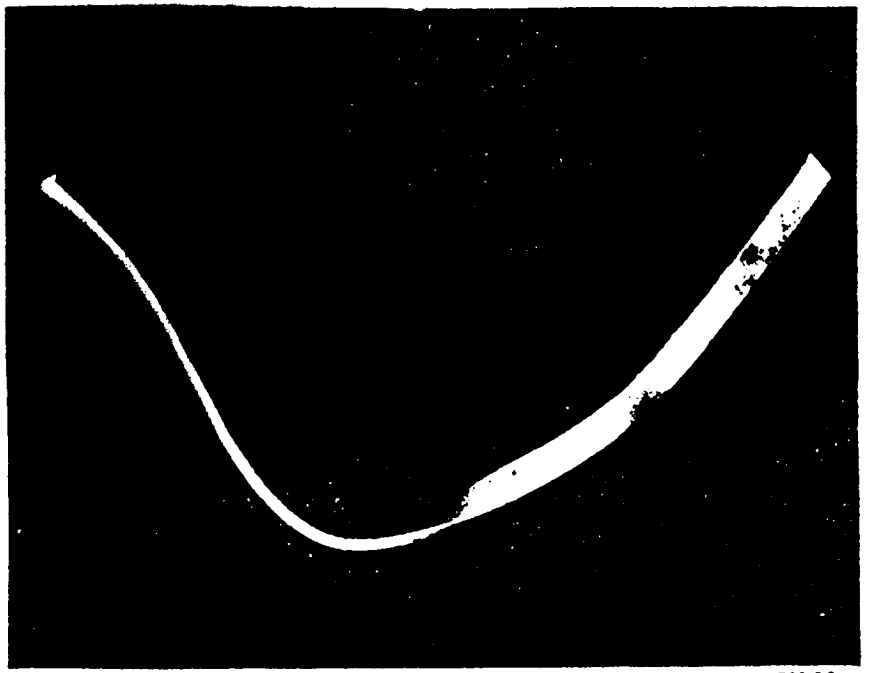

~ 1.5X Mag

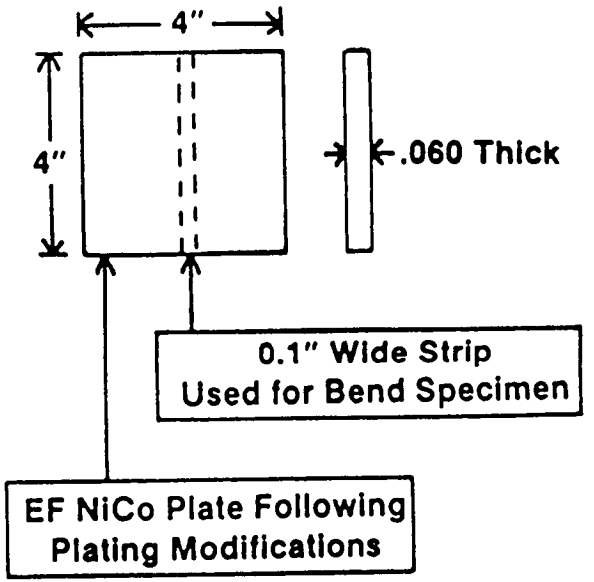

EF NiCo Bend Specimen Shows Good Ductility

Mechanical Property Testing
(As-deposited, RT)

UTS	=	**197 ksi**
YS	=	**137 ksi**
% Elong	=	**5.5%**
Modulus	=	**25.8 x 10^3 ksi**
Hardness	=	**R_C 40**

Figure 1.4.3.3-2. EF NiCo Bond Sample

specimen heat sink more closely resemble the heat sink available in the full scale chamber.

1.4.4 Proof Tests

Proof tests of the EF NiCo closeout were planned to test the integrity of the EF NiCo to NAS-Z Cu bonds. A 7500 psi hydrostatic proof test was performed on the tool proof liner (SN 3). The critical area is in the throat region where the lands are only 0.011" wide.

An electroformed closeout seals the forward end of the chamber while the aft end is connected to a manifold. Hydrostatic proof tests with 7500 psi water were performed for two minutes with no visible deformation. After successful completion of the 7500 psi proof test, a room temperature gaseous H_2 proof test was performed for two minutes to check for hydrogen embrittlement. Again no deformation was observed.

The pilot chamber was then subjected to five cryogenic liquid nitrogen dip cycles to simulate filling of the channels with cryogenic liquid hydrogen cooling. The chamber was proof tested with 7500 psi gaseous hydrogen, again with no visible deformation. The pilot chamber was next sectioned to examine the bonds in the throat region. Metallurgical examination of the EF NiCo - Cu joint indicated sound bonds existed. Since the proof test with gaseous hydrogen at room temperature was not detrimental to the bond, regenerative cooling with cryogenic hydrogen was not considered a risk since hydrogen embrittlement effects have been shown to be more pronounced at room temperature.

1.4.5 Flow Tests

To facilitate the cold flow tests, two aluminum manifolds were fabricated and assembled. One manifold was designed to pressurize all channels to check for channel-to-channel flow uniformity and the other to direct pressure to single channels. Both manifolds were alternately used to assure visual flow uniformity. Figure 1.4.5-1 shows the aluminum manifold attached to the cooled throat. Visual results of the water flow tests are shown in Figure 1.4.5-2 and 1.4.5-3. Figure 1.4.5-4 is a plot of the cold flow Kw values for the cooled throat. Values for Kw are documented for later reference. Since Kw is calculated from

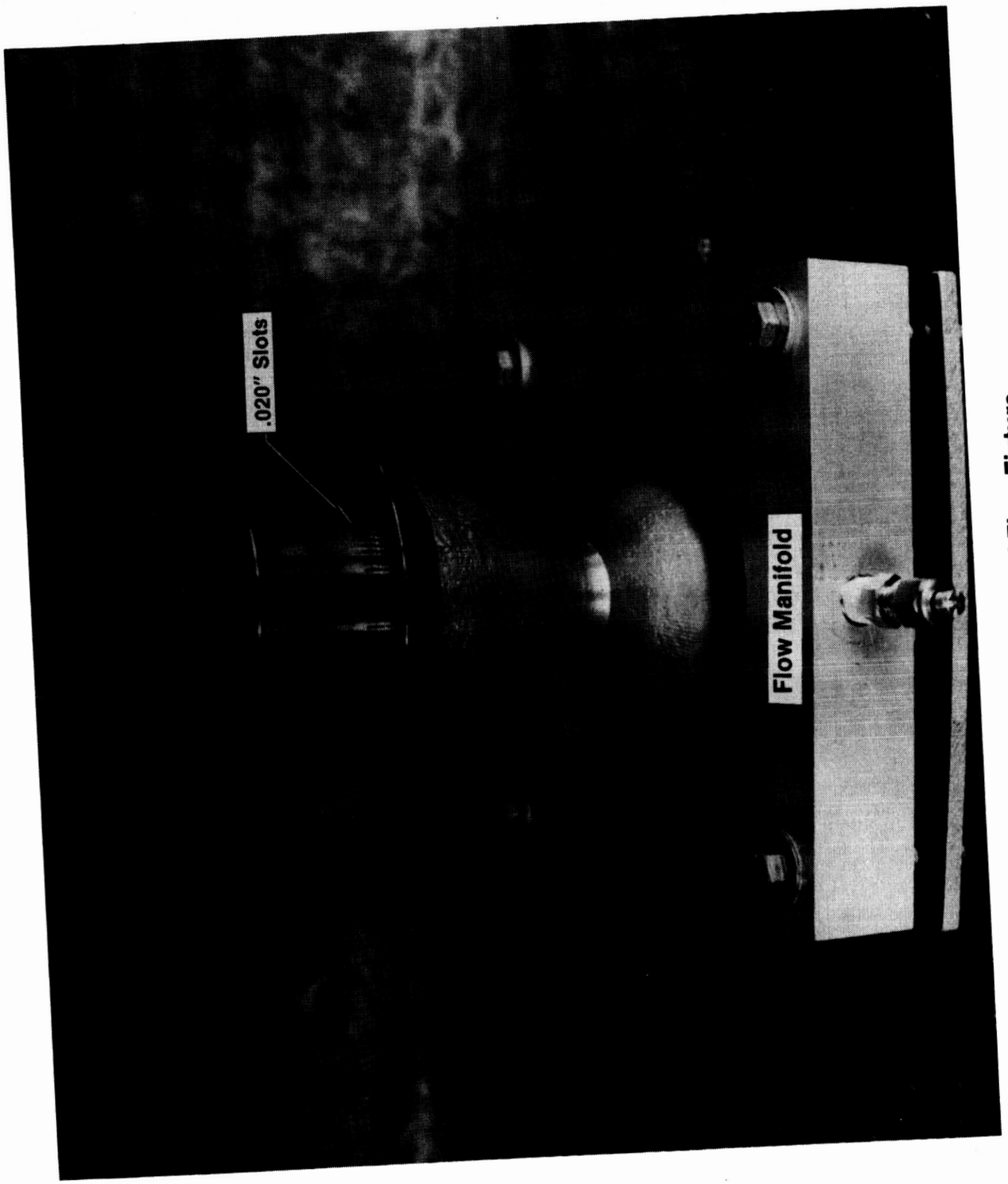

Figure 1.4.5-1. Cold Flow Fixture

Figure 1.4.5-2. LH_2 Cooled Throat Cold Flow Testing

C-2

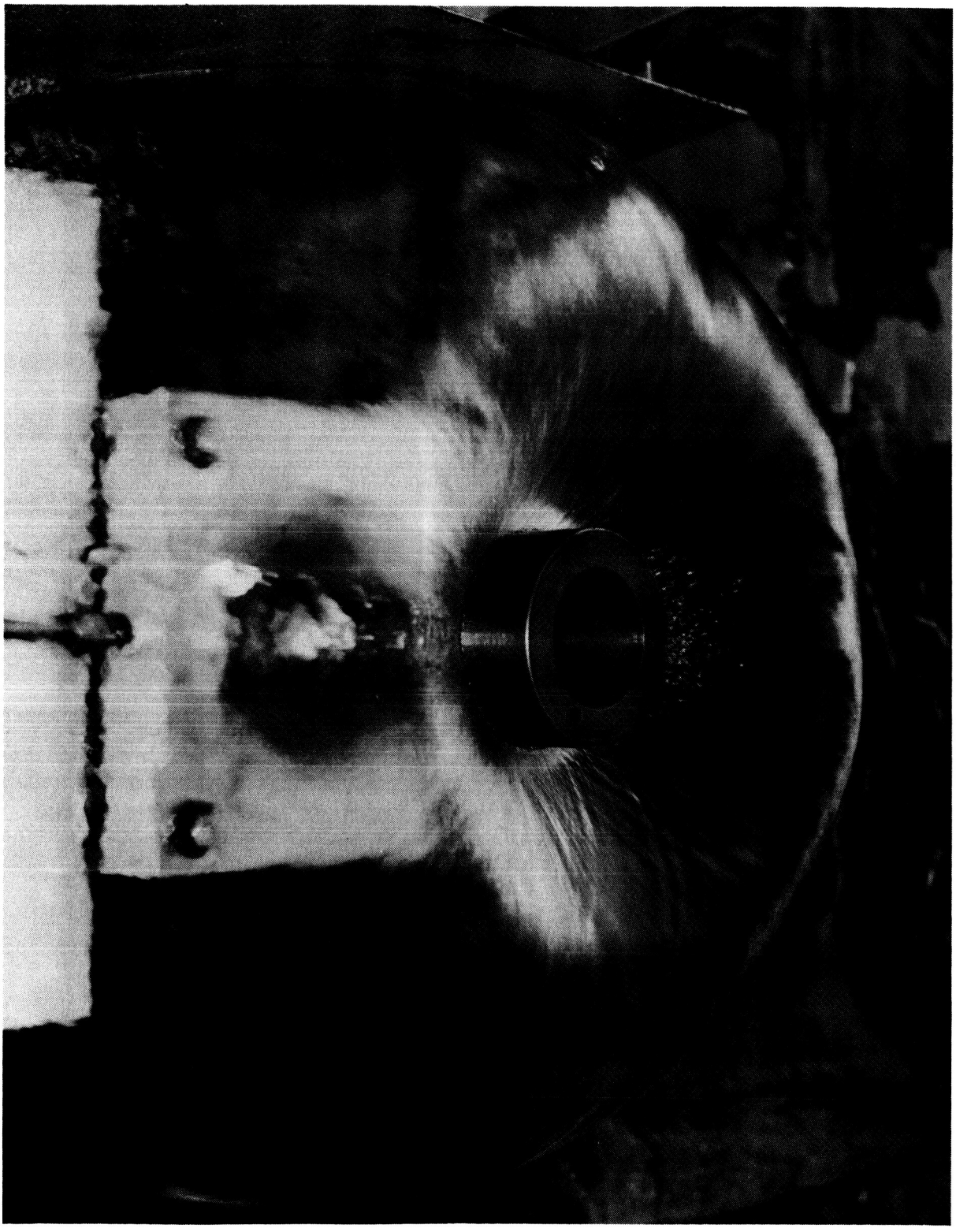

Figure 1.4.5-3. LH_2 Cooled Throat Cold Flow Testing

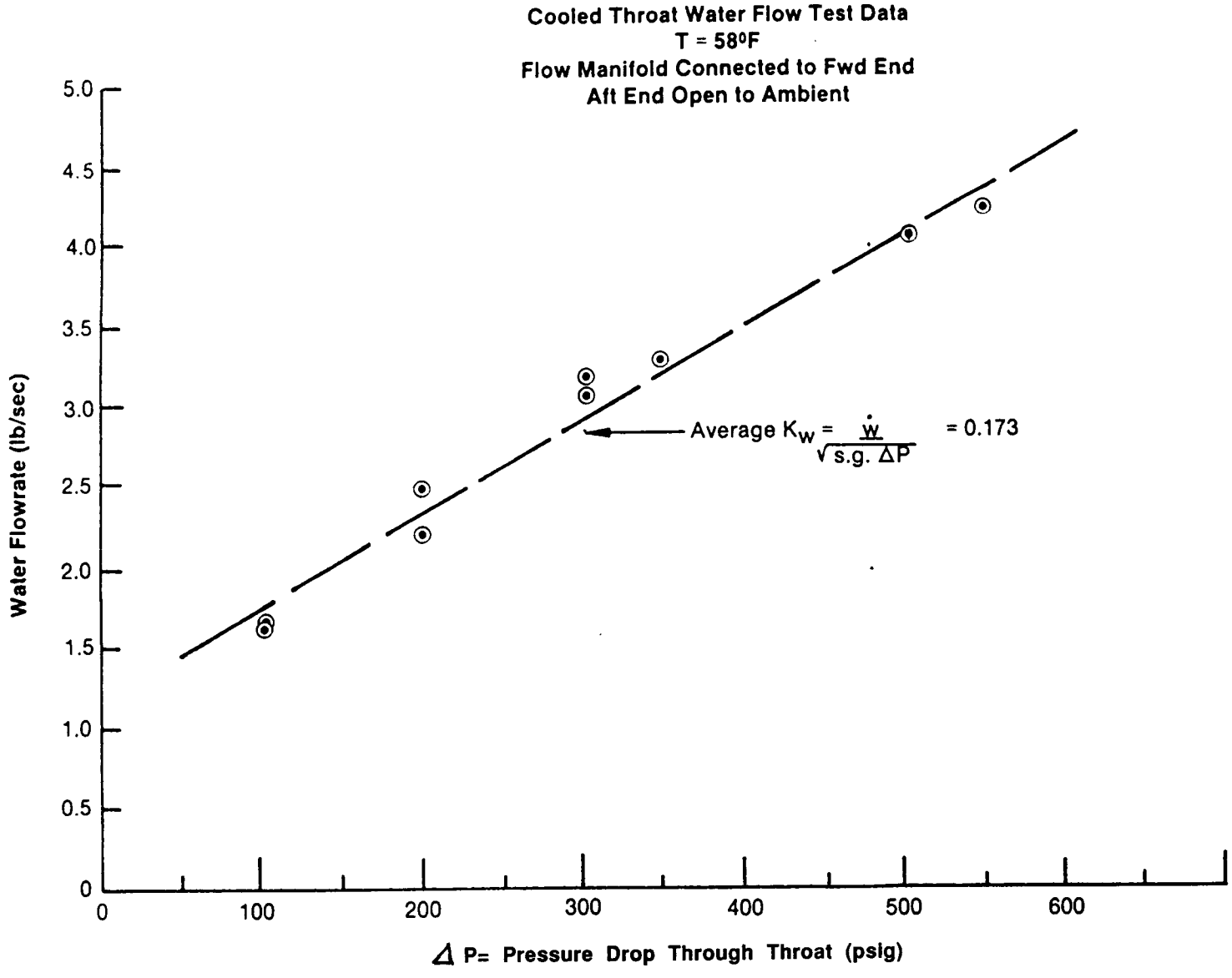

Figure 1.4.5-4. LH_2 Cooled Throat Water Flow Test Data

know pressure drops and flowrates, any restrictions due to debris is event during subsequent cold flow Kw checks.

Based on the visual inspection of the flow uniformity, the absence of restrictions in the coolant channels was verified. After the water flow tests were complete, the cooled throat was cleaned, bagged and transported to the EB weld facility. Weld samples verified the weld parameters and penetrations before the actual welds were performed.

To facilitate the cold flow tests, a manifold is attached to the forward end to allow warm perchlorethelene to flow through the channels for final wax removal. Water is used in the actual flow tests. Relative flow from each group of channels provides visual information on any potential channel blockage.

Prior to installing the cooled throat hardware on the test stand, a freon flow check of the channels was used to verify the cleanliness level. The effluent was filtered and inspected under 10X magnification for particle presence.

After the injector was mounted on the test stand, a final series of proof/leak tests was performed. A proof plate was designed and fabricated for assembly to the cooled throat front end manifold. Leak tests were performed with GN_2 at 250, 500, and 1000 psig.

1.5 Filter

1.5.1 Design

A filter was designed as part of the secondary coolant inlet manifold for the throat section (Figure 1.5.1-1). This was included as a safeguard against potential clogging of the throat channels during operation. A downstream plenum was included to redistribute coolant behind any blocked portion of the filter. Structural analysis indicated a filter size of approximately 0.15" to 0.20" wide by 0.030" thick. Pressure drops were expected to be less than 500 psi across the filter during startup transients. Slow entry of the coolant into the manifold is desired to avoid a large pressure drop during fill. The actual pressure drop across the filter during operation was expected to be less than 100 psi.

1.5.2 Fabrication

The filter was fabricated using Aerojet photoetch platelet technology. Individual 347 CRES platelet rings (0.040" wide x 0.009" thick) were depth etched to form radial channels. A sample platelet is shown in Figure 1.5.2-1. Inspection of the channel widths was made using a stereomicroscope. After inspection the platelets were stacked and bonded.

Approximately 28 Stainless Steel platelets were bonded to form an annular ring with approximately 20,000 each 0.008" diameter filtering holes. A closeup of the filter is shown in Figure 1.5.2-2. Burrs were present on the filter holes and a deburring operation was attempted. However due to the size and number of channels, success of the deburring was limited. Next water was flowed through the manifold at approximately 200 psia to remove any loose burrs.

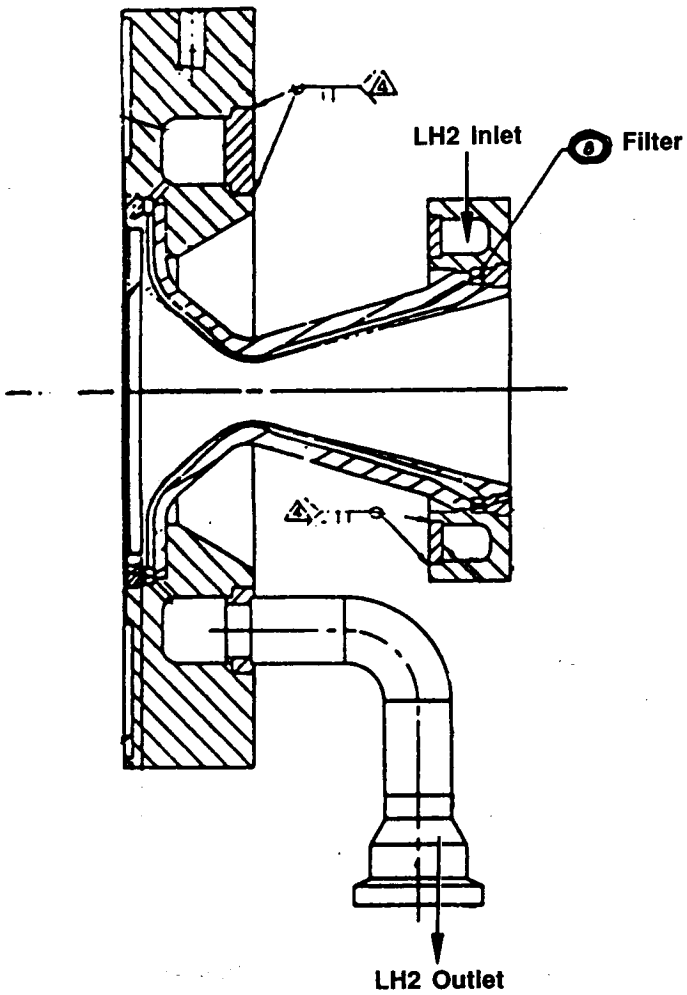

Cooled Nozzle Assembly
P/N 1197112

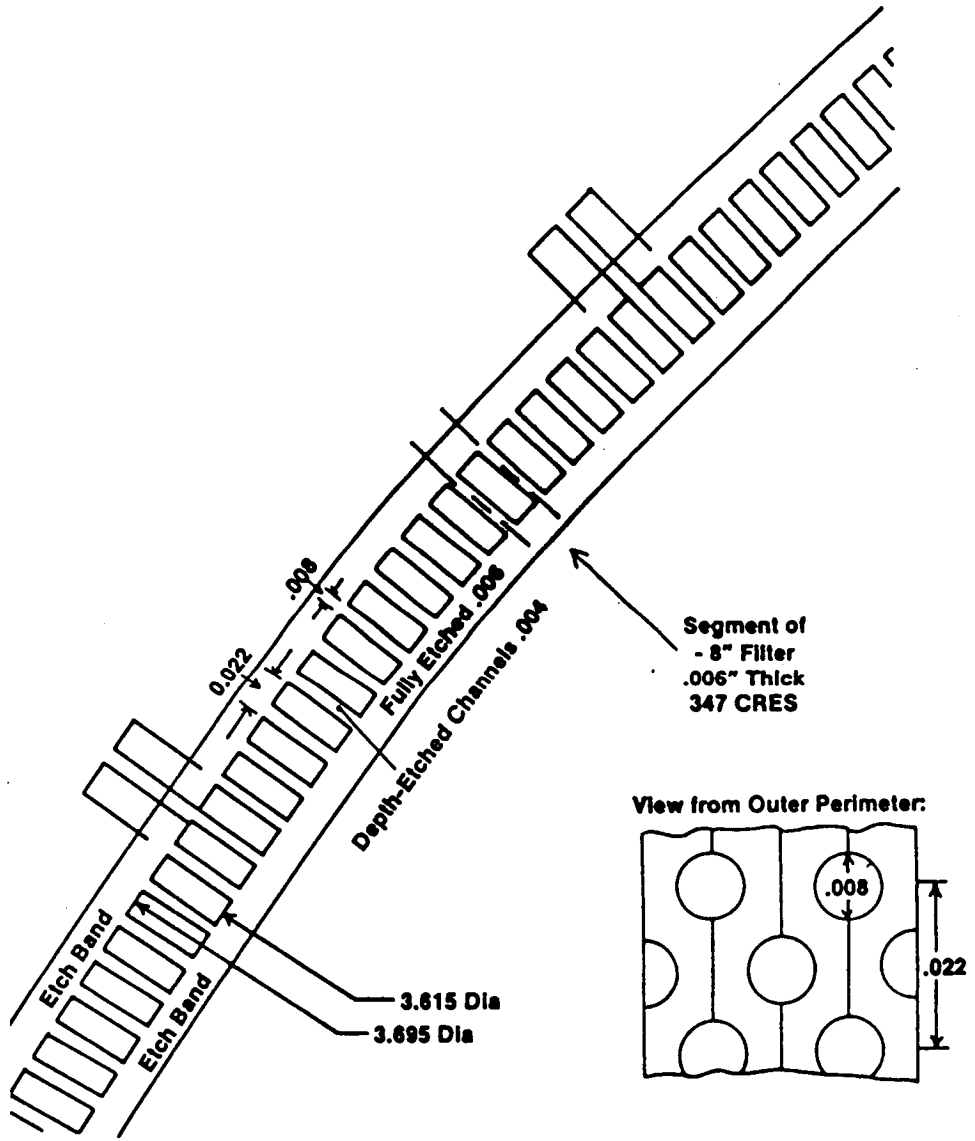

-8 Filter Detail

Note:
All Dimensions
Are in Inches

Figure 1.5.1-1. Manifold Filter

Figure 1.5.2-1. Filter Platelet

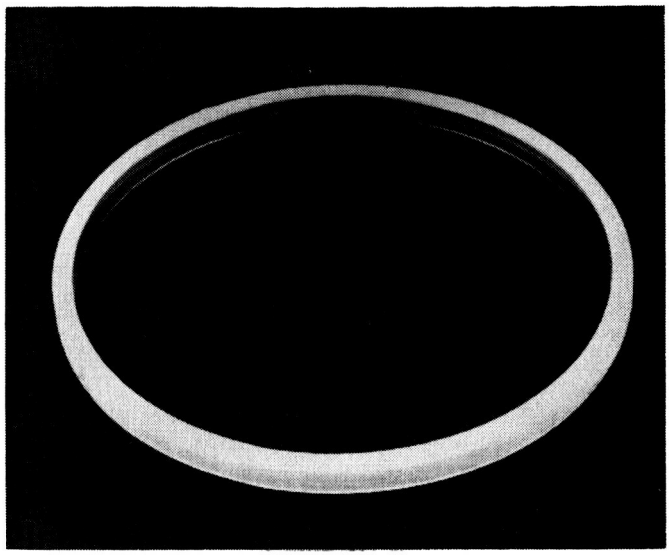

CRES 347

Manifold Filter

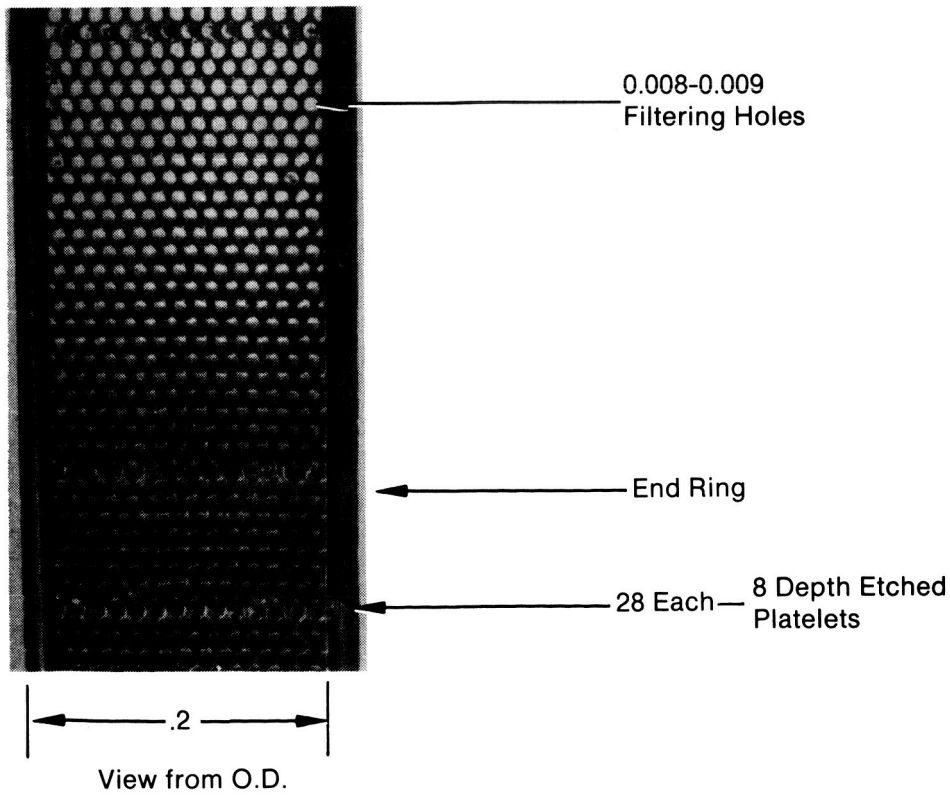

Figure 1.5.2-2. Closeup of Manifold Filter Screen

2.0 Hot Fire Test Facility

2.1 Description

The tests described in this report were conducted at ATC's Rocket Development Laboratory (Test Area A). The OTV Thrust Chamber Assembly (TCA) hardware was installed in Test Bay 6 (Figure 2.1-1) which has provisions for handling gaseous and cryogenic propellants. The run tanks available include a 150 gal, 5500 psig liquid hydrogen tank, a 58 cubic foot gaseous hydrogen cascade, and a 50 gal, 5500 psig liquid oxygen tank. The test area converts liquid oxygen to gaseous oxygen which is then stored in a 50 cubic foot, 6000 psig tank.

The test bay is connected to the laboratories central control and instrumentation system which provides automatic computer control of test functions and high speed data acquisition with on-line data reduction.

2.1.1 Heat Sink Chamber & Throat Test Setup

A schematic of the test stand used in testing of the injector with the heat sink chamber and throat is shown in Figure 2.1.1-1. Flow regulators are used to set and adjust flowrates of the gaseous hydrogen and oxygen propellants. Sonic venturis are located upstream of the regulators for calculation of the flowrates. Augmentation circuits provide the fuel and oxidizer flow to the igniter.

Figure 2.1.1-2 is a photograph of the actual test stand with the heat sink hardware prior to testing.

2.1.2 Modifications to Test Setup for Heat Sink Chamber & LH_2 Cooled Throat Tests

Facility definition and modification was undertaken for the high pressure tests with the heat sink chamber, centerbody and the cooled throat. A schematic of the facility for the high PC tests is shown in Figure 2.1.2-1.

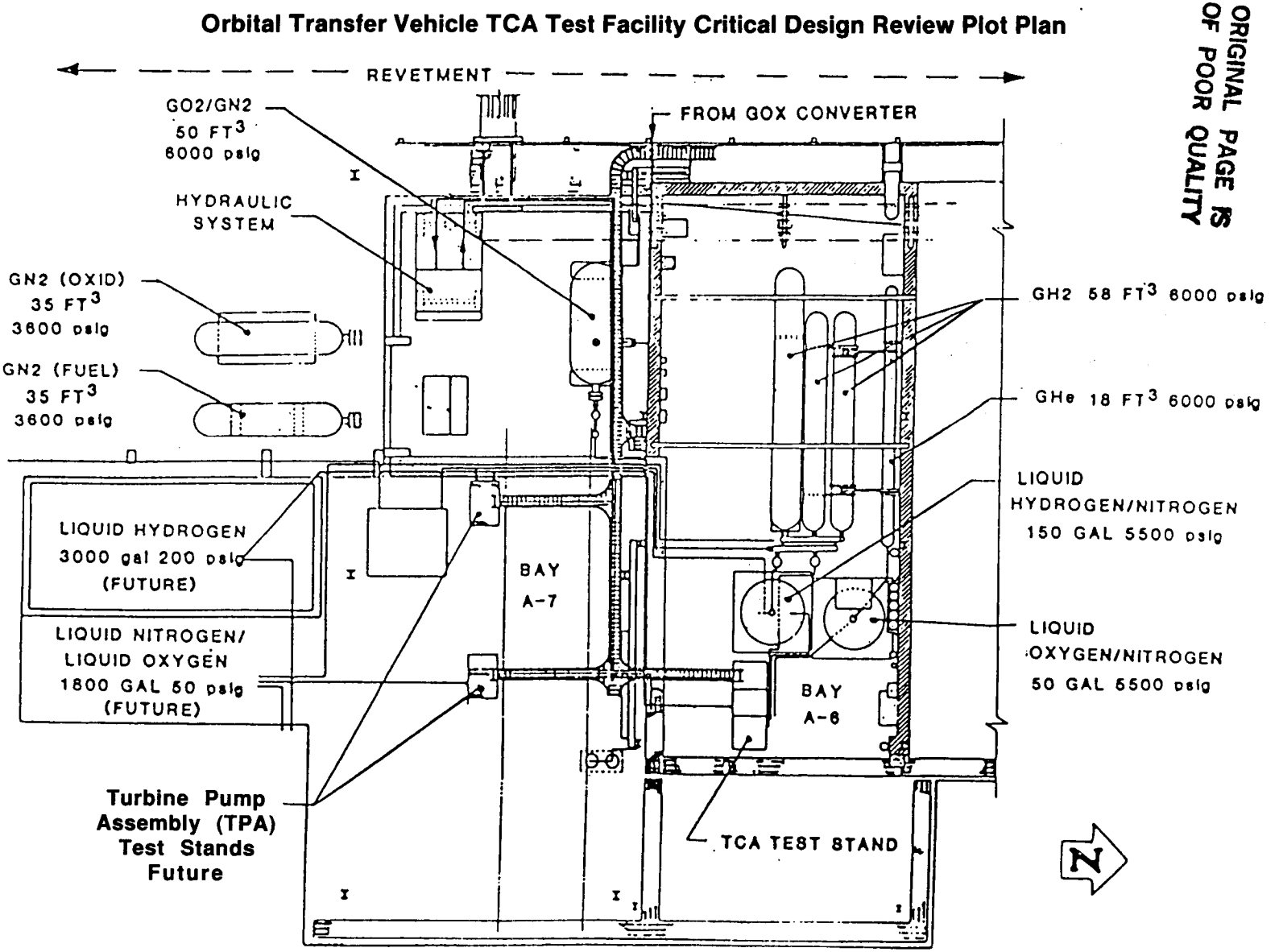

Figure 2.1-1. OTV TCA Test Facility

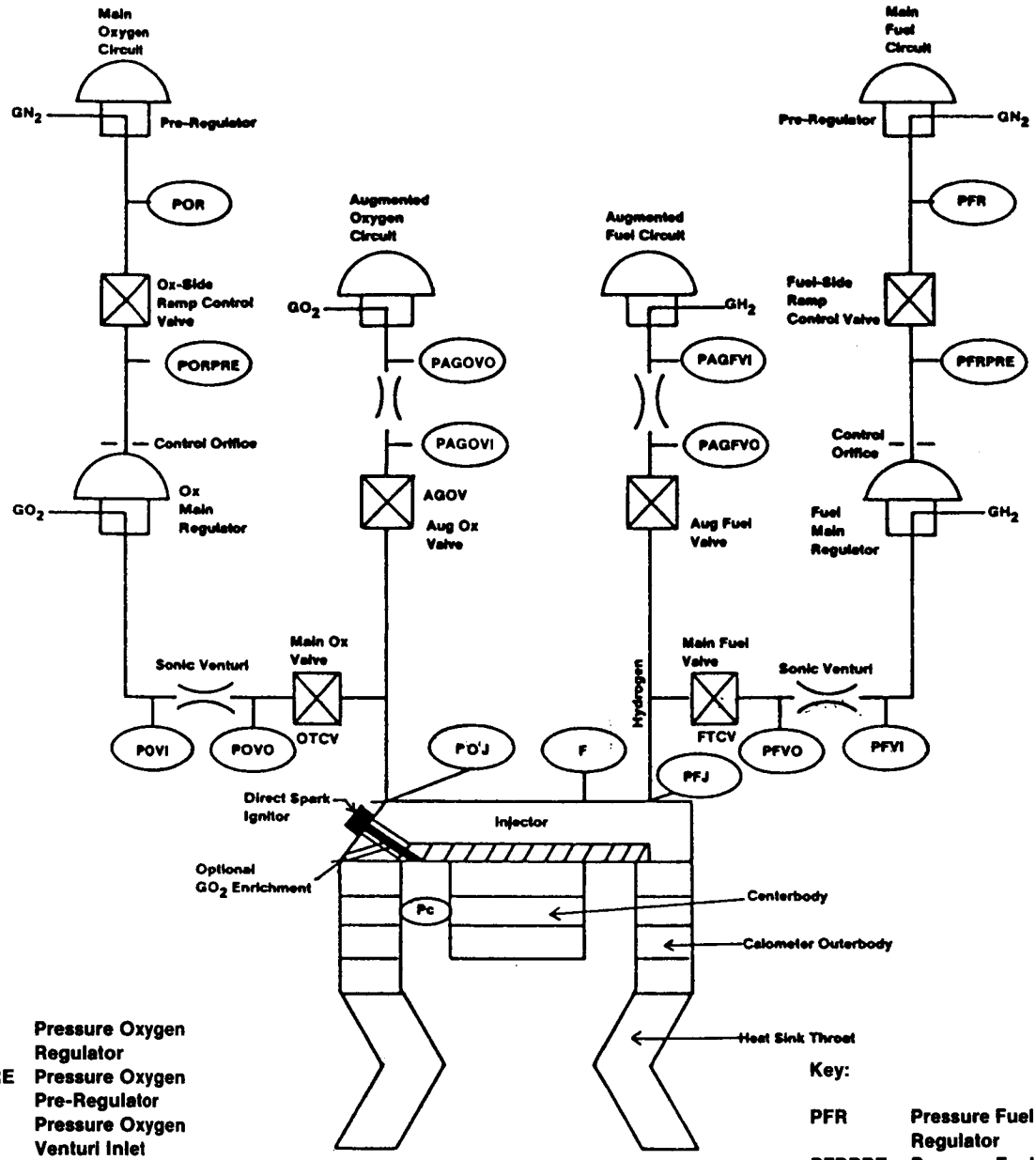

Key:

POR	Pressure Oxygen Regulator
PORPRE	Pressure Oxygen Pre-Regulator
POVI	Pressure Oxygen Venturi Inlet
POVO	Pressure Oxygen Venturi Outlet
PAGOVI	Pressure Aug. Ox. Valve Venturi Inlet
PAGOVO	Pressure Aug. Ox Valve Venturi Outlet
AGOV	Aug. Oxygen Valve Injector
OTCV	Ox. Thrust Chamber Valve
Pc	Chamber Pressure
F	Thrust

Key:

PFR	Pressure Fuel Regulator
PFRPRE	Pressure Fuel Pre-Regulator
PFVI	Pressure Fuel Venturi Inlet
PFVO	Pressure Fuel Venturi Outlet
PAGFVI	Pressure Aug. Fuel Valve Venturi Inlet
PAGFVO	Pressure Aug. Fuel Valve Venturi Outlet
FTCV	Fuel Thrust Chamber Valve
PFJ	Injector Fuel Pressure

Figure 2.1.1-1. Heat Sink Test Assembly Schematic

ORIGINAL PAGE IS
OF POOR QUALITY

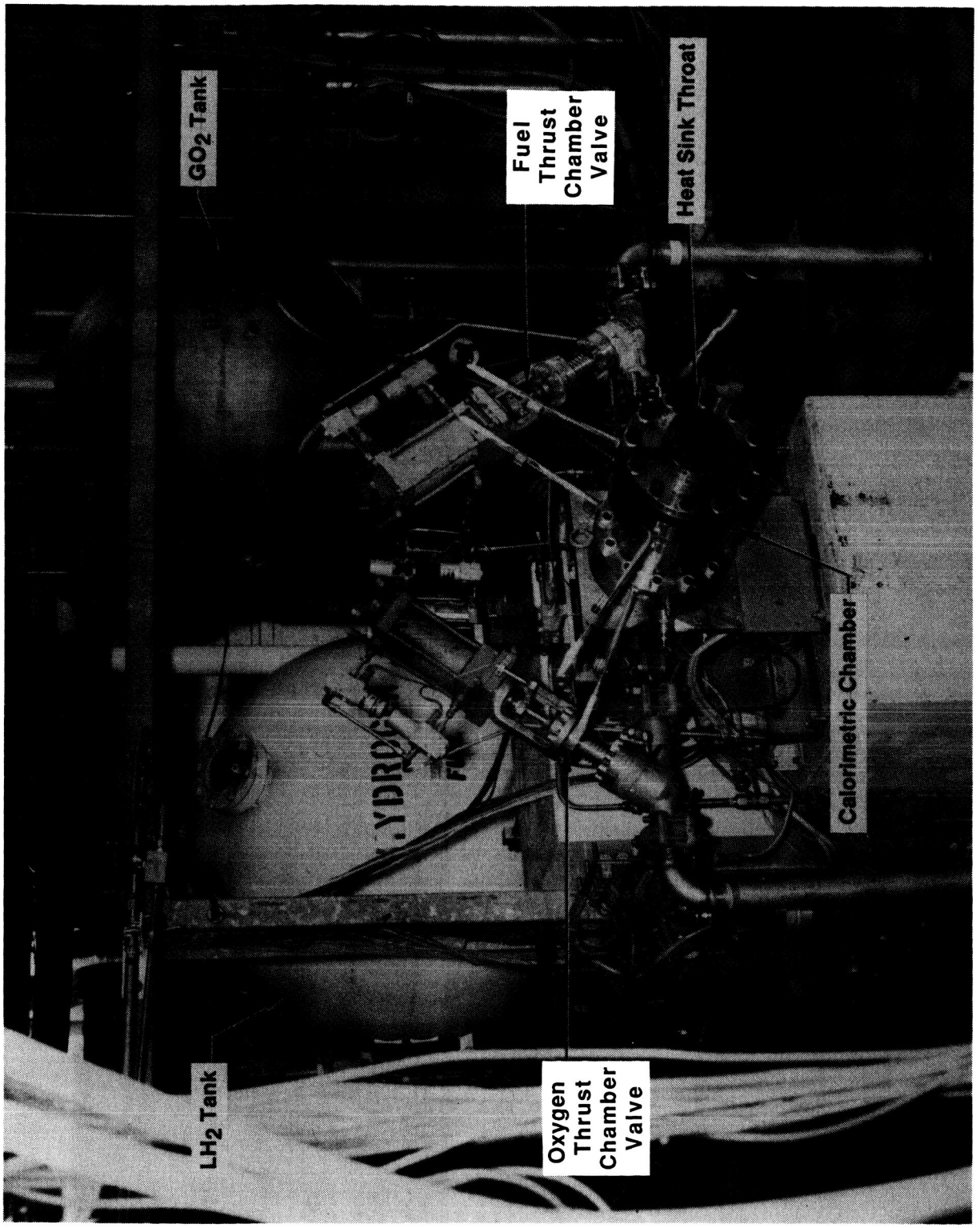

Figure 2.1.1-2. Test Stand Setup for Low PC Test Series

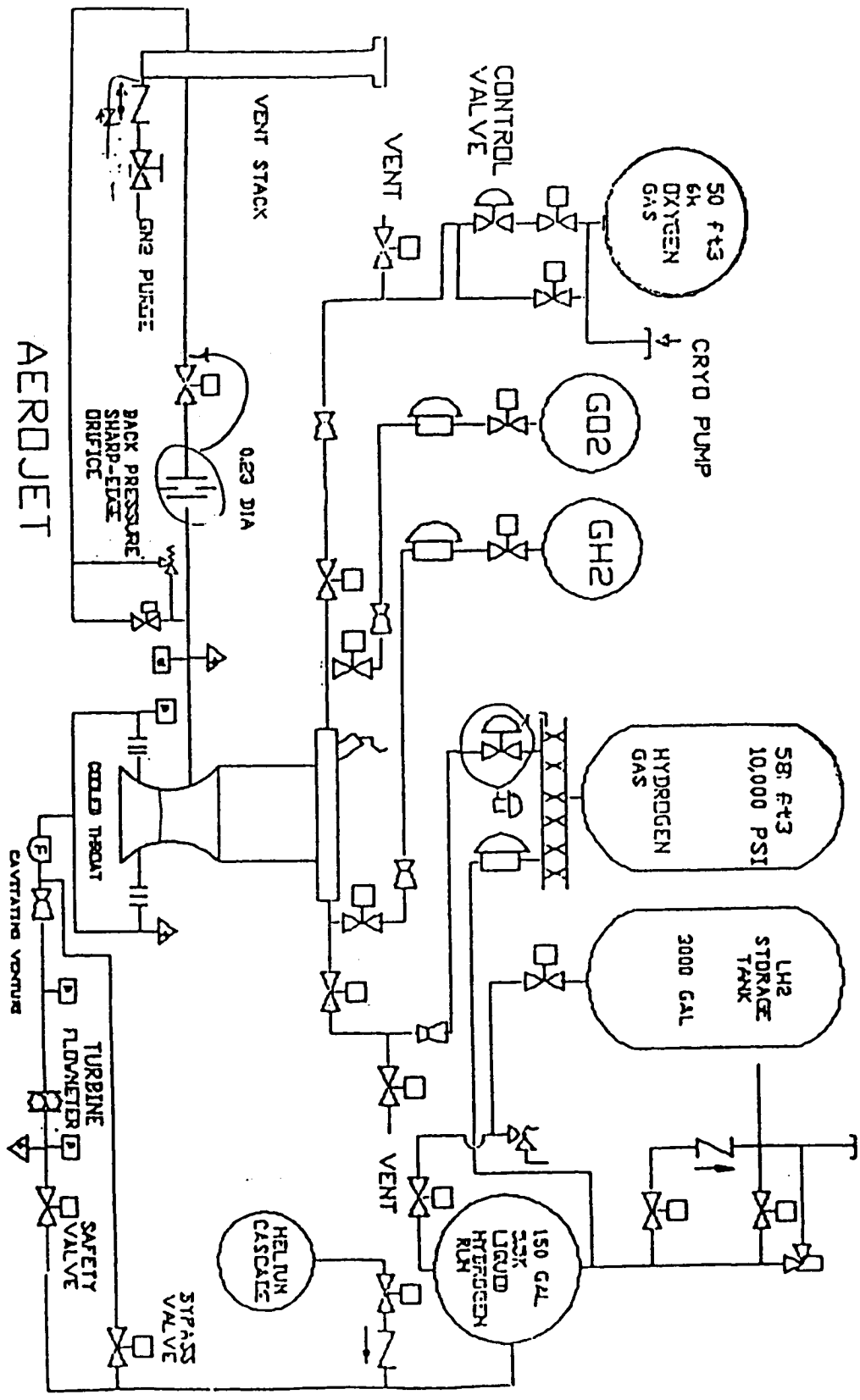

Figure 2.1.2-1. Test Facility Schematic

During the low pressure test series, regulators were used to control the sonic venturi upstream pressures. The response times of these regulators were slower than desired, because orifices were required upstream of the regulator dome to limit the dome pressurization rate to assure proper regulation. To increase the valve response time for the high pressure test series, control valves replaced the regulators in the gaseous O_2 and H_2 inlet lines. On the gaseous oxygen line, space was available for the control valve to be directly substituted for the regulator. However, on the fuel side, space limitations caused the control valve to be placed in the line about a foot upstream of the sonic venturi, as shown in Figure 2.1.2-2.

The fuel & oxygen augmentation circuit used for obtaining ignition remained unchanged from that used in the low PC test series.

The addition of a liquid hydrogen circuit was made to supply LH_2 to the cooled throat section. Flow control of the high pressure LH_2 was a major concern. Because of this, flowrates and inlet pressures into the cooled throat were adjusted prior to each new test to demonstrate cooling at the proper levels. A turbine flowmeter was placed downstream of the venturi to enable the flowrates to be accurately measured. Cavitating venturis and a back pressure orifice control the LH_2 inlet pressures and flowrates. Figure 2.1.2-3 shows the cooled throat test stand and inlet LH_2 lines. The LH_2 exit line is shown in Figure 2.1.2-4.

2.2 Instrumentation

A list of the instrumentation used in the OTV 3K TCA test program is presented in Table 2.2-I. Locations of the pressure transducers are noted on Figures 2.1.1-1 and 2.1.2-1. Changes of the pressure transducers between the low and the high chamber pressure set of tests are noted on Table 2.2-I by an asterisk.

Additional instrumentation added to monitor the cooled throat parameters are listed on Table 2.2-II.

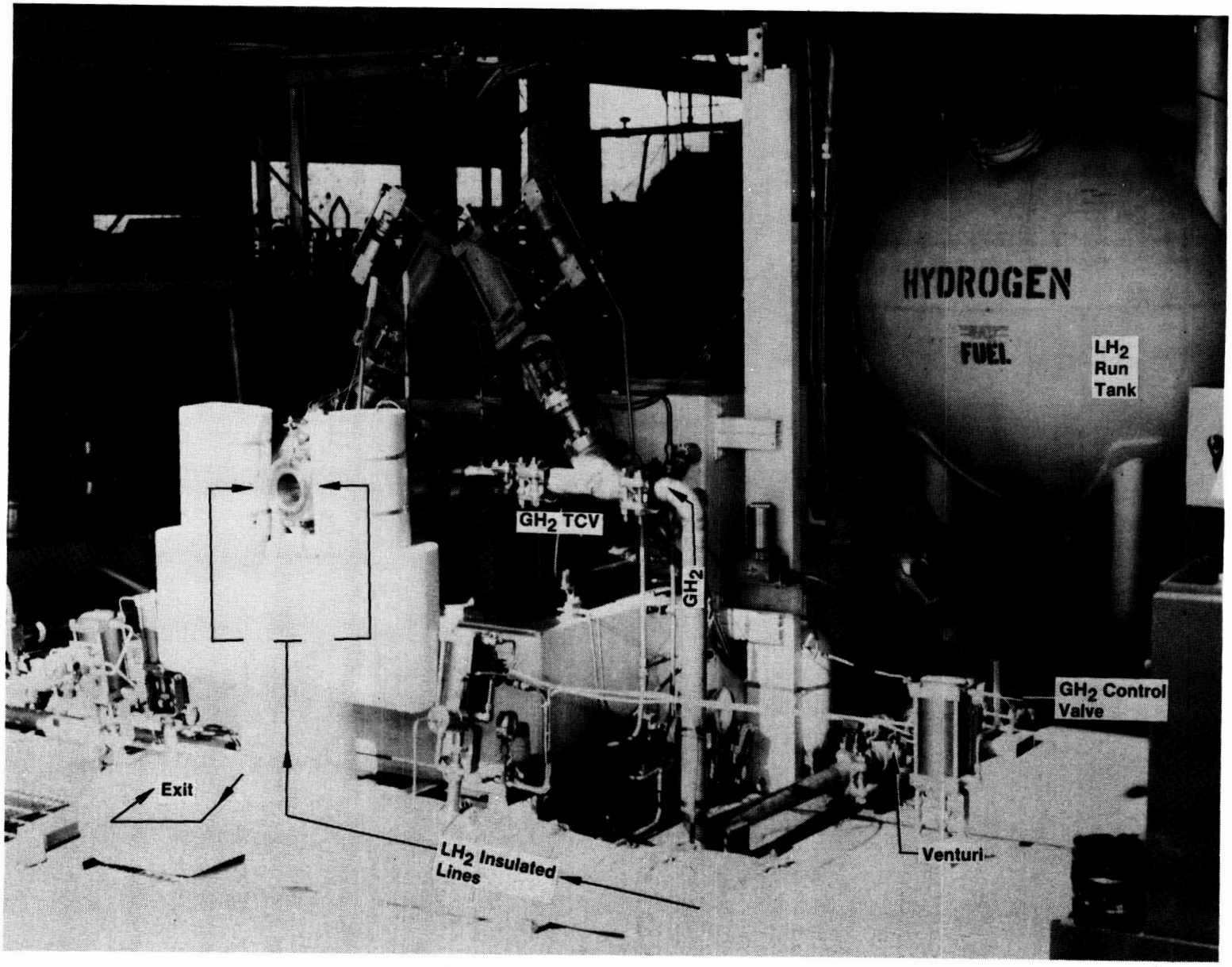

Figure 2.1.2-2. OTV LH_2 Cooled Throat Test Stand

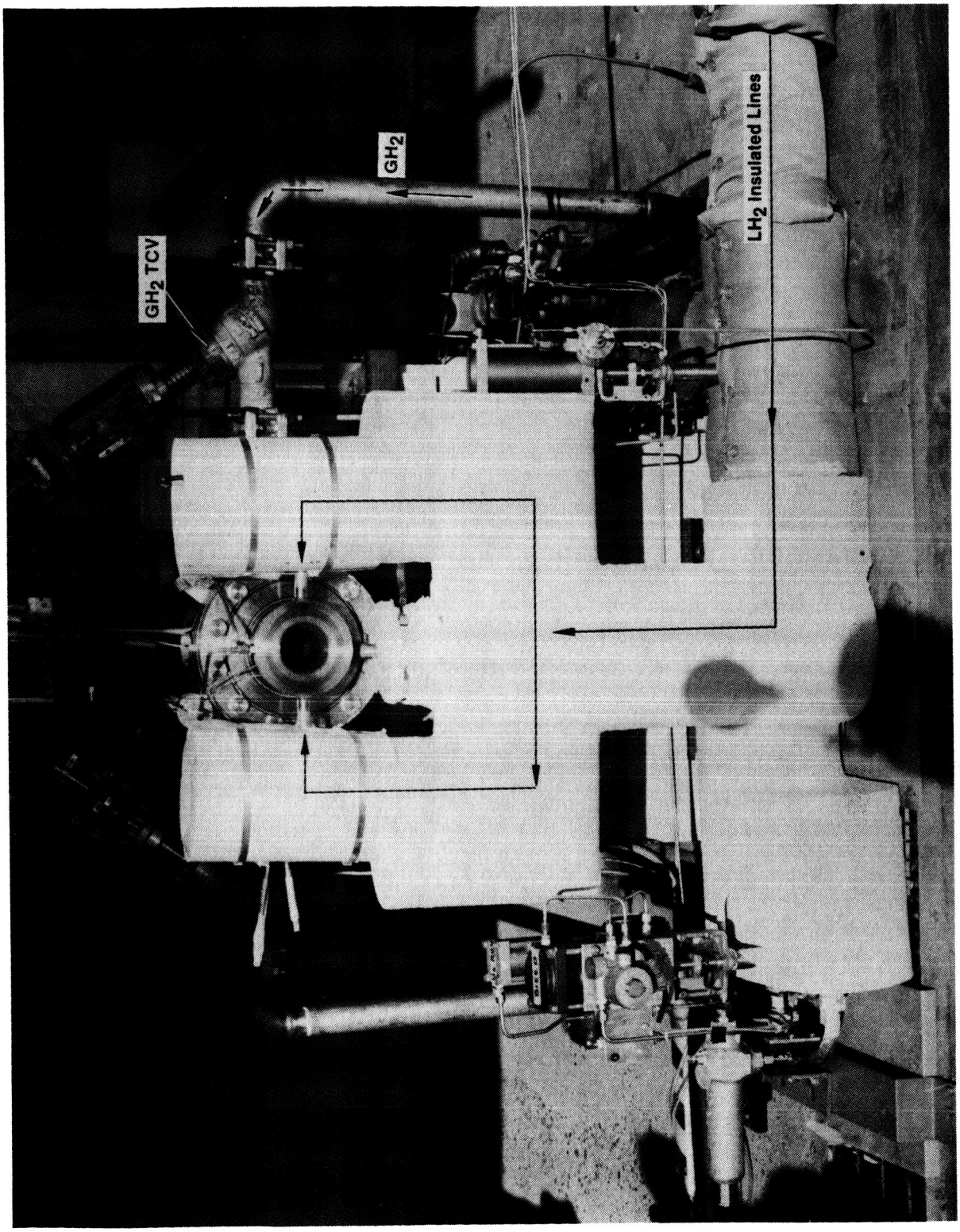

Figure 2.1.2-3. LH_2 Cooled Throat Test Stand - View of LH_2 Inlet Line

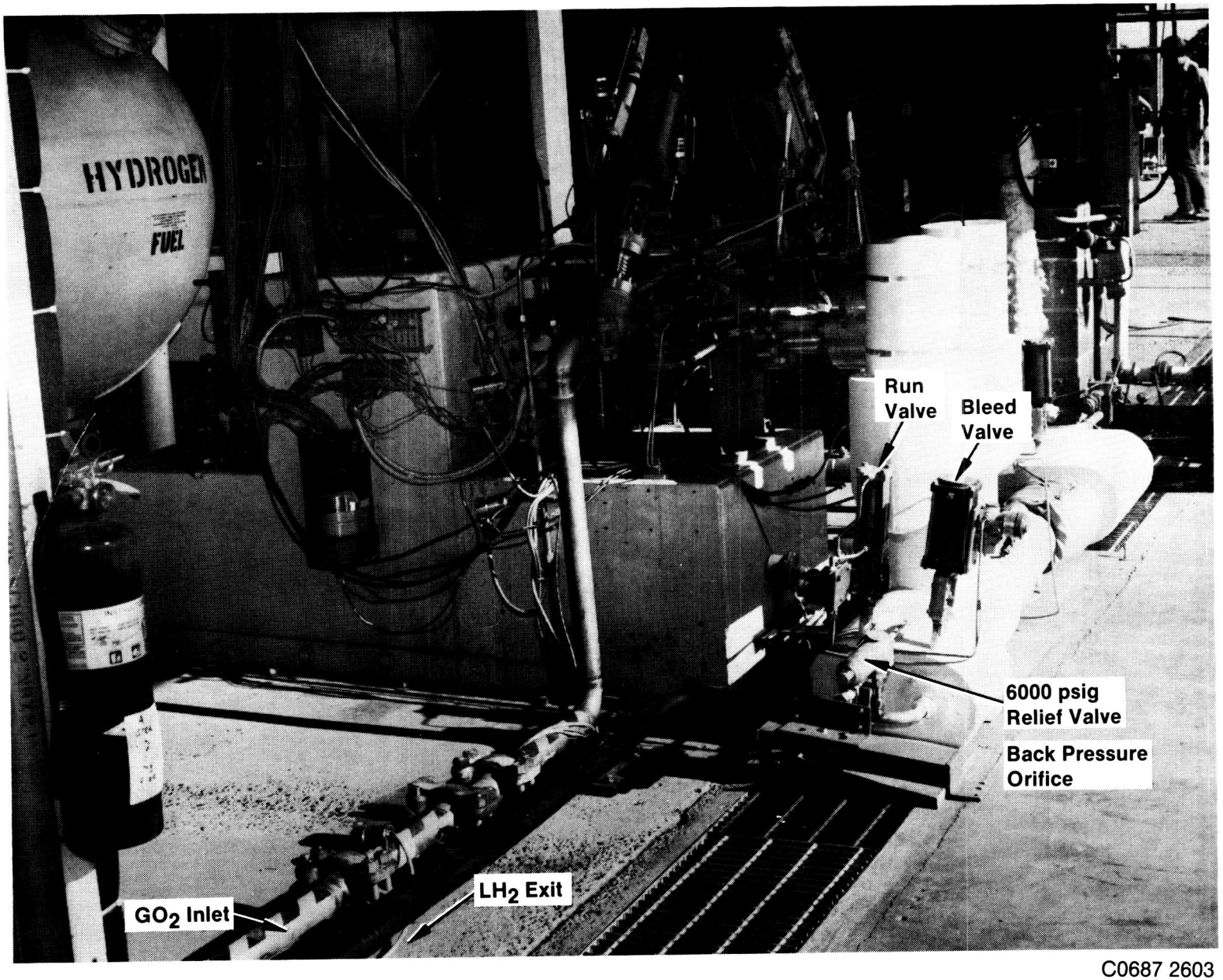

Figure 2.1.2-4. LH_2 Cooled Throat Test Stand - View of LH_2 Exit Line

TABLE 2.2-I
INSTRUMENTATION LIST

	Function	Type	Range
FA, FB	Thrust	Dual Bridge SG	200-2000 lbF
Pc	Chamber Pressure	SG Tabor	1000*, 2000
P_{oj}	Ox Manifold Pressure	SG Tabor	1000*, 2500
P_{fj}	Fuel Manifold Pressure	SG Tabor	1000*, 2500
P_oFM (1&2)	O_2 Venturi Inlet Pressure	SG Tabor	TBD
PFFM (1&2)	H_2 Venturi Inlet Pressure	SG Tabor	TBD
POV	Pressure Ox Valve Inlet		1000*, 2500
PfV	Pressure Fuel Valve Inlet		1000*, 2500
PHm	Pressure LH_2 to Cooled Throat		5000 psi
P H_2	Cooled Throat Pressure Drop		500 psi
PcHf (3)	High-Frequency Chamber Press	Kistler He Bleed	
PoT	O_2 Supply Pressure	SG Tabor	4500 psi
PfT	H_2 Supply Pressure	SG Tabor	4500 psi
EOV	Ox Pilot Valve Voltage		28 V
EFV	Fuel Pilot Valve Voltage		28 V
LVO	LOX Valve Position Indicator		0-1 in.
LVF	Fuel Valve Position Indicator		0-1 in.
S	Spark Plug Discharge Voltage		TBD
E OVI	O_2 Igniter Valve Voltage		28 V
E FVI	H_2 Igniter Valve Voltage		28 V
TCR (1&2)	Resonator Cavity Temp	Pt-Rh (B or R) dia 0.062 in.	3000•F
TofM (1&2)	Ox Venturi Inlet Temp	C/A (K)	70 ±±0•F
TfFM (1&2)	Fuel Venturi Inlet Temp	C/A (K)	70 ±±†0•F
T_F (1&2)	Flange Temp at Resonator	C/A (K)	0-2000•F

*Low-pressure test series.

TABLE 2.2-I (cont.)

Thermocouples:

Designation	Function	Type	Range
TCB 0.5*, 0° & 90°**	Centerbody Calorimeter Segment I	Chromel/Alumel (C/A) Type K (k)	0-2000°F
TCB 2.3, 0° & 90°	Centerbody Calorimeter Segment I	C/A (K)	
TCB 4.45, 0° & 90°	Centerbody Calorimeter Segment II	C/A (K)	
TCB 7.5, 0° & 90°	Centerbody Calorimeter Segment III	C/A (K)	
TCB 11.3, 0° & 90°	Centerbody Nose Section	C/A (K)	
TCB 12.1, 0° & 90°	Centerbody Nose Section	C/A (K)	
TCB 12.5, 0°	Centerbody Tip	C/A (K)	
TC 0.75, 0°, 90°	Chamber Calorimeter I	C/A (K)	0-2000°F
TC 2.60, 0°, 90°	Chamber Calorimeter II	C/A (K)	
TC 4.75, 0°, 90°	Chamber Calorimeter II	C/A (K)	
TC 7.80, 0°, 90°	Chamber Calorimeter III	C/A (K)	
TC 10.10, 0°, 90°	Convergent Nozzle	C/A (K)	
TC 11.85, 0°, 90°	Convergent Nozzle	C/A (K)	

TABLE 2.2-I (cont.)

Thermocouples:

Designation	Function	Type	Range
TC 13.0, 0°, 90°	Convergent Nozzle	C/A (K)	
TT 13.70, 0°, 90°	Throat Calorimeter	C/A (K)	0-2000°F
TT 14.3 0°, 90°	Throat Calorimeter	C/A (K)	
TT 14.9, 0°, 90°	Throat Calorimeter	C/A (K)	

* Axial distance from injector face, in.,
** angular locations, deg.

TABLE 2.2-II

OTV HIGH PRESSURE COOLED THROAT INSTRUMENTATION
MODIFICATIONS FROM LOW Pc TEST SERIES

WLHF	LH_2 Coolant Flow Rate	0-1 lbm/sec
PLHG	LH_2 Coolant Flowmeter Pressure	1000-5500 psia
TLHF	LH_2 Coolant Flowmeter Temp (RTD)	30-120 R
TLHI	LH_2 Coolant Inlet Temp (RTD)	30-120 R
TLHO1	LH_2 Coolant Outlet Temp (RTD)	30-300 R
TLHO2	LH_2 Coolant Outlet Temp (Type T TC)	30-300 R
PLHI	LH_2 Coolant Inlet Manifold Pressure	1000-5500 psia
PLHO	LH_2 Coolant Outlet Manifold Pressure	1000-5500 psia
TCT 1&2	Cooled Throat OD Temp (CR/AL TC) 0 and 90	100-1000 F
TCT 3&4	Cooled Throat OD Temp (CR/AL) 0 and 90	100-1000 F
TCT 5&6	Cooled Throat OD Temp (CR/AL)	100-1000 F

TCA Testing

3.0 Test Description

3.1 Test Plan

The TCA test program was configured to supply data to support the design verification as follows:

1) Low Pressure Ignition
   a) Direct Spark
   b) Oxidizer Rich Torch
2) Chamber Thermal Characteristics
   a) Total heat load to centerbody
   b) Total heat load to outer chamber
   c) Local heat flux at selected stations
   d) Injector face cooling
   e) Resonator cavity cooling
3) TCA Performance
   a) C* combustion efficiency
   b) Thrust based energy release efficiency

To accomplish these objectives three hot fire test series (#2 - 4) were planned for the 3K OTV Thrust Chamber Assembly as described below.

Series 2: Low pressure ignition tests

Series 3: Low pressure stability, performance, and thermal characteristics.

Series 4: High pressure stability, performance, and thermal characteristics.

Cold flow testing of the injector was studied under Series 1 and is discussed in Section 1.1.3. These cold flow tests verified non-blockage of the

propellant passages, established the Kw and CdA coefficients for the injector, and provided valve response times.

Series 2 through 4 involved hot fire testing of the injector. Series 2 was designed as a set of low pressure tests for ignition verification at tank head start modes. Series 3 investigated the stability, performance, and thermal characteristics at low chamber pressure firings. Series 4 investigated the stability, performance, and thermal characteristics at high chamber pressure firings. The throat section was changed between test series 3 & 4 from a heat sink throat to an LH_2 cooled throat.

3.2 Test Summary

3.2.1 Conduct of Tests

3.2.1.1 Low Pressure Direct Ignition

Direct ignition involves a spark discharge within the combustion chamber without augmentation of oxidizer, and is theoretically the simplest approach to ignition. The igniter port is located in the resonator cavity of the injector, as described in Section 4.1. Historically, the direct ignition approach has not always been successful due to the dependency on the mixture ratio in the spark gap zone. Augmentation of GO_2 in the spark zone is available in the event of poor ignition reliability. In the event oxidizer augmentation would be required, a separate valve or check valve is necessary to terminate the O_2 flow following ignition. The response time of the power supply has been recorded as 10 ms. Actuation of the spark is timed to coincide with simultaneous propellant flow into the manifolds. The augmentation circuit, which simulates tank head ignition at 30 psig, is used for all start transients. Nominal mixture ratio during the tank head start is 5.0. Assuming augmentation venturi sizes of 0.079 inches for the oxygen and 0.070 inches for the fuel, the upstream venturi pressures are set by regulators to 870 psia and 880 psia, respectively, for the oxidizer and fuel.

3.2.1.2 Combustion Stability

To define stable operation, three Kistler pressure transducers are located on the back of the injector. These pressure transducers

monitor the pressure in 3 of the 12 resonator cavities. In the event of combustion instability developing, resonator cavity tuning blocks can be sized, fabricated, and installed. Each cavity has two threaded holes to retain the tuning blocks. In addition, threaded holes are used to provide and control GH_2 bleed to the cavities. The main function of the bleed is for active cavity cooling. Control of the bleed flow is obtained by sizing the bleed flow holes in the screws.

3.2.1.3 Performance and Hydraulics

Thrust and pressure based Isp and C* data were obtained on all tests. NBS traceable critical flow nozzles with upstream temperature and pressure measurements were utilized in the flow rate calculations. Pressure, pressure drop, and calculated injector CdA information were generated for each test.

3.2.1.4 Thermal Characteristics

Local heat flux data for cooling system design and the engine cycle power balance were generated for each test condition. The transient response of each thermocouple during the test was used to compute local heat flux values as described in Section 1.2.

3.2.1.5 LH_2 Cooled Throat

The LH_2 cooled throat underwent proof and leak testing prior to hot fire testing. A proof fixture was assembled to the cooled throat front end manifold for the leak/proof test. The leak test was performed at 250, 500, and 1000 psig with GN_2. Internal proof test at 3000 psig on the cooled throat was performed simultaneously with a hydrostatic channel proof at 7500 psig for a duration of 5 minutes. The plate was then reversed and bolted to the calorimetric hardware without the throat for similar proof and leak testing.

Prior to flow of LH_2 though the cooled throat, the following sequence of operations was followed to ensure complete evacuation of air or moisture from the cooled throat channels.

1) Three hours prior to test, initiate a warm GHe purge.

2) One hour prior to test, initiate a low pressure LH_2 trickle from the storage tank.

3) Once the inlet temperature to the cooled throat reaches 150 R, the hardware will be considered properly chilled down for the test. The low pressure LH_2 bleed will be continued until the test is ready to commence. Five seconds prior to the test, the high pressure LH_2 will be activated.

Figure 3.2.1.5-1 displays the preferred pre-test purge and start sequence showing the individual valve actuations. This sequence was slightly adjusted based on the cold flow results which measured actual valve response times.

3.2.1.6 Instrumentation Shutdown Parameters

The following test conditions were cause for automatic termination of a test.

TCB 0.5 -90	> 1300 F
TCB 2.3 -90	> 1300 F
TCB 4.45-90	> 1300 F
TC 0.75-90	> 1300 F
TT-OD	> 400 F

Coolant temperature rise across the cooled throat channels < 300 F

3.3 Test Plan

The low chamber pressure test series plan is outlined in Table 3.3-I. Tests were to be conducted over a range of chamber pressures of 200 to

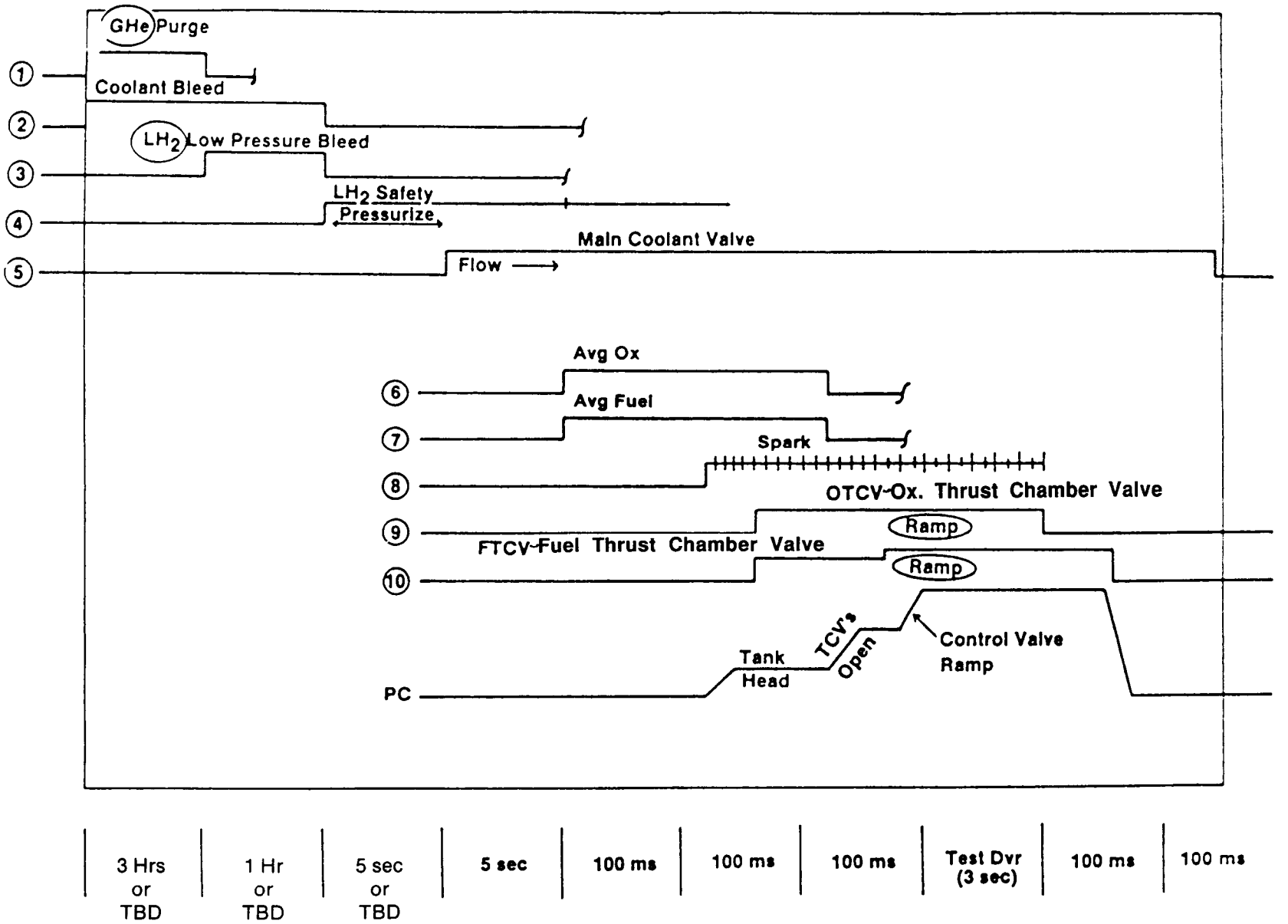

Figure 3.2.1.5-1. OTV Cooled Throat Suggested Pre-Test Purge & Start Sequence

TABLE 3.3-I

OTV HEAT SINK CHAMBER TEST
PROPOSED LOW PRESSURE TEST SERIES

Test No.	Pc psia	MR	$\dot{w}_o$ (lbm/sec)	$\dot{w}_o$ (lbm/sec)	POJ (psia)	PFJ (psia)	POVI (psia)	PFVI (psia)	Du sec
1	200	4	.47	.12	281	230	293	386	5
2	400	4	.94	.23	437	455	586	740	5
3	400	6	1.06	.18	448	432	661	579	5
4	400	8	1.19	.15	460	422	742	483	5
5	500	6	1.33	.23	560	540	826	724	5
6	600	4	1.41	.35	655	685	879	1127	5
7	600	5	1.50	.30	663	661	935	966	5
8	600	6	1.59	.26	672	648	991	837	5
9	600	7	1.68	.24	683	639	1047	772	5
10	600	8	1.77	.22	689	632	1103	708	5

Key:

Pc - Chamber Pressure

$\dot{w}_o$ - Ox Flow Rate

$\dot{w}_f$ - Fuel Flow Rate
POJ - Pressure Ox Injector Manifold
PFJ - Pressure Fuel Injector Manifold
POVI - Pressure Ox Inlet Venturi
PFVI - Pressure Fuel Venturi Inlet
Dur - Test Duration

600 psi with mixture ratio distributions from 4 to 8. Test durations were expected to be on the order of 5 seconds.

Table 3.3-II outlines the high chamber pressure cooled throat test matrix. Tests were to be conducted at 4 different chamber pressures from 500 to 2000 psia with mixture ratios in the range of 5 to 7. These ranges were selected as representative of the overall expected operating range of the OTV engine.

4.0 Data Evaluation

The operating range of the actual tests is illustrated in Figure 4.0-1. Operation was demonstrated over a range of mixture ratios from 4.2 to 7.6.

Summaries of the test results are listed in Tables 4.0-1 to 4.0-III.

Notes from the low and high chamber pressure tests are listed in Tables 4.0-IV and 4.0-V respectively.

4.1 Low Pressure Ignition

Three possible start modes are envisioned for the OTV engine:

1) Tank head start - 5 to 20 psia supply
2) Electric motor driven boost pumps - 40 psi supply
3) Stored gas bottles - 500 to 1000 psi supply

Previous H_2/O_2 engines utilized an injector face center mounted oxidizer rich torch/spark ignition system. This design has proven highly successful in a wide range of applications at pressures up to 2000 psia. Specifications for operation of the OTV in a tank head start mode required verification of the ignition system at low pressures.

Two igniter concepts were evaluated for the OTV design, torch (Section 4.1.1) and direct (Section 4.1.2) ignition. An igniter port was located in the resonator cavity of the OTV injector, as shown in Figure 4.1-1. This port can be

Table 3.3-II
OTV High Pressure Cooled Throat Test Matrix

MAIN INJECTOR CIRCUIT

TEST NO.	Pc psia	MR	Wo lbm/sec	Wf lbm/sec	POJ psia #1	PFJ psia #2	POVI psia #3	PFVI psia #4
1	1000	6	2.647	0.441	1078	1045	1620	1869
2	1500	6	3.951	0.659	1603	1566	2417	2792
3	2000	6	5.247	0.875	2131	2088	3210	3708
4	2000	5	4.975	0.995	2118	2114	3044	4216
5	2000	7	5.535	0.791	2146	2072	3387	3352
6	1500	5	3.740	0.748	1593	1586	2288	3169
7	1500	7	4.172	0.596	1614	1554	2553	2525
8	1000	5	2.501	0.500	1070	1057	1530	2119
9	1000	7	2.799	0.400	1085	1037	1713	1695
10	500	5	1.255	0.251	546	529	768	1064
11	500	6	1.332	0.222	549	523	815	941
12	500	7	1.410	0.201	554	519	863	852

AUGMENTATION CIRCUIT MR=5

PAGOVI psia #5	PAGFVI psia #6	Wo lbf/sec	Wf lbf/sec
870	880	0.101	0.02

LH2 COOLANT CIRCUIT

TEST NO.	LH2 Wf lbm/sec	ThrtDelP psia #8	PCTO psia #9	PCTI psia	Tin R	Tout R	PCVI psia #10	PBPO psia #11	VENTURI RATIO #12
1	0.366	203	1940	2143	100	330	2824	1904	0.76
2	0.547	223	2860	3083	100	323	4299	2815	0.72
3	0.726	228	3740	3968	100	315	4498	3690	0.88
4	0.826	275	4160	4435	100	304	5117	4124	0.87
5	0.657	208	3470	3678	100	331	4070	3423	0.90
6	0.621	240	3170	3410	100	310	4880	3131	0.70
7	0.495	203	2660	2863	100	343	3854	2625	0.74
8	0.415	202	2140	2342	100	314	3202	2106	0.73
9	0.332	188	1840	2028	100	358	2500	1799	0.81
10	0.208	200	1000	1200	100	259	1489	959	0.81
11	0.184	200	900	1100	100	270	1299	866	0.85
12	0.167	200	830	1030	100	274	1172	792	0.88

Key:

Pc	Chamber Pressure
MR	Mixture Ratio (O/F)
$\dot{\omega}_O$	Ox Flow Rate
$\dot{\omega}_F$	Fuel Flow Rate
POJ	Pressure Ox Injector Manifold
PFJ	Pressure Fuel Injector Manifold
POVI	Pressure Ox Venturi Inlet
PFVI	Pressure Fuel Venturi Outlet
PAGOVI	Pressure Aug. Ox Valve Venturi Inlet
PAGFVI	Pressure Aug. Fuel Valve Venturi Inlet
$LH_2\dot{\omega}_F$	LH_2 Flow Rate
PCTP	Pressure Cooled Throat Outlet
PCTI	Pressure Cooled Throat Inlet
T_{in}	Temp. Cooled Throat Inlet
T_{out}	Temp. Cooled Throat Outlet
PCVI	Pressure Cooled Throat Venturi Inlet
PCVO	Pressure Cooled Throat Venturi Outlet

NOTES:

#1 - injector ox circuit CdA = function of Wo
#2 - injector fuel circuit CdA = 0.1647 in2
#3 - main ox venturi CdA = 0.0661 in2, dia = 0.290 in
#4 - main fuel venturi CdA = 0.0387 in2, dia = 0.224 in
#5 - augmentation ox venturi CdA = 0.0049 in2, dia = 0.079 in
#6 - augmentation fuel venturi CdA = 0.00385 in2, dia = 0.070 in
#7 - cooled throat ideal pressures based in power balance
#8 - throat delta P including channels, filter, and manifolds
#9 - real throat pressures based on back pressure orifice
#10 - coolant venturi (test 1-9, CdA = 0.0085 in2, dia =0.105), (test 10-13, CdA = 0.011, dia = 0.119)
#11 - coolant back pressure orifice CdA = 0.0249 in2, dia = 0.230 in
#12 - recovery of coolant venturi (Pinrl/PCVI)

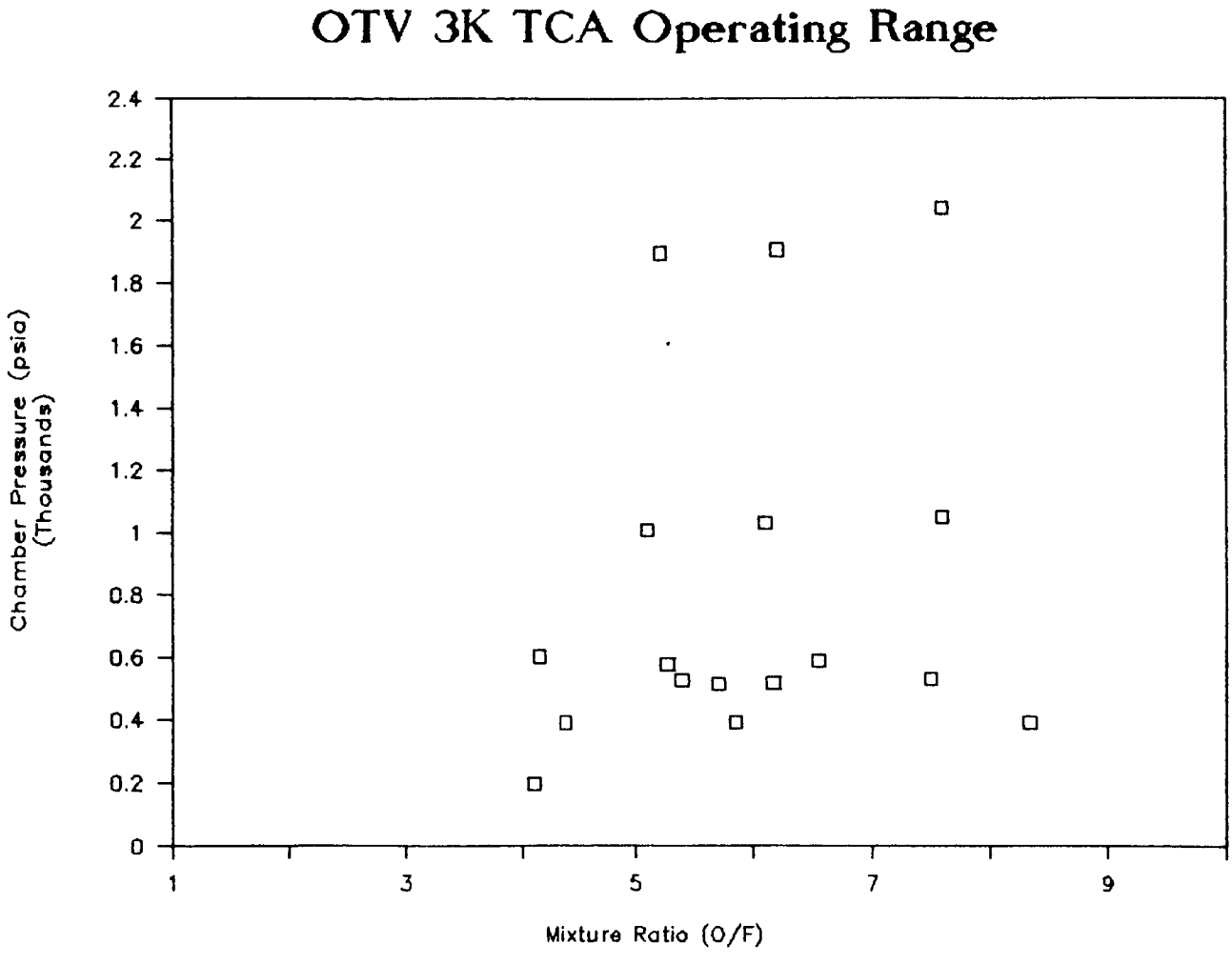

Figure 4.0-1 Demonstrated Operating Range

Table 4.0-I
TCA Hot Fire Test Summary
(Before Injector Modification)

Test No.	Date	Pc (psia)	POJ (psia)	PFJ (psia)	POJ-Pc (%)	PFJ-Pc (%)	MR	Isp_{vac} (sec) $\varepsilon = 4.0$	Dur (sec)	C* (ft/sec)
121	6/28/85	85	100	98	16	16	3.9	359	1.2	7,186
122	6/28/85	106	123	117	16	10	5.4	346	4.0	7,082
123	6/28/85	105	124	112	18	7	7.7	336	4.0	6,573
124	6/28/85	99	117	107	18	8	7.6	356	4.0	6,626
125	7/10/85	184	209	210	14	14	4.0	335	2.2	7,316
126	7/10/85	187	212	203	13	9	5.7	334	2.4	7,068
127	7/10/85	187	216	199	16	6	7.6	326	4.4	6,807
128	7/10/85	180	213	190	18	6	9.2	312	4.2	6,378
129	7/10/85	181	211	230	17	27	3.0	281	1.1	5,716
130	7/11/85	359	403	406	12	13	4.1	340	2.1	7,327
131	7/11/85	271	305	300	13	11	4.7	349	2.8	7,450
133	7/11/85	287	325	309	13	8	6.1	346	4.0	7,338
134	7/11/85	287	329	303	15	6	7.8	328	4.4	6,893
135	7/11/85	316	355	353	12	12	4.3	349	2.5	7,414

Key:

Pc	**Chamber Pressure**
POJ	**Pressure Ox. Manifold Injector**
PFJ	**Pressure Fuel Manifold Injector**
POJ-Pc	**% Pressure Drop Oxygen Circuit**
PFJ-Pc	**% Pressure Drop Fuel Circuit**
MR	**Mixture Ratio (O/F)**
Isp	**Specific Impulse**
Dur	**Test Duration**
C*	**Characteristic Exhaust Velocity**

Table 4.0-II
OTV Hot Fire Test Reduced Data
(Modified Injector)

Test No. 2459-120-A6-	F_{vac} (lbs)	Isp_{vac} Meas (sec)	C*[1] Meas (ft/sec)	Pc (psia)	MR	Dur (sec)	POJ (psia)	PFJ (psia)	$\frac{\Delta POJ-Pc}{Pc}$ %	$\frac{PFJ-Pc}{Pc}$ %	$\dot{\omega}_t$ lb/sec	Heat Flux Average Btu/in^2-sec
140	227	362	7537	197	4.1	5.0	218	215	10	9	.6275	2.00
144	442	365	7707	390	4.4	4.6	427	419	9	7	1.2113	2.88
145	449	368	7656	391	5.84	5.0	430	408	10	5	1.2219	3.56
146	452	327	6802	393	8.3[2]	5.0	440	404	12	3[3]	1.3837	3.34
147	584	356	7552	517	6.16	4.5	568	540	10	5	1.6391	3.82
149	681	361	7864	620	4.13	3.2	676	673	9	9	1.8877	3.79
150	640	338	7488	588	5.23	2.6	642	625	9	6	1.8812	3.69
151	667	334	7214	601	6.51	2.6	659	628	10	5	1.9955	3.55
154	589	339	7314	530	7.49[2]	3.5	584	548	10	3[3]	1.7365	3.90
155	571	363	8005	526	5.4	4.2	572	553	9	5	1.5740	3.31

[1]Not corrected for thermal effects.
[2]Fuel venturi possibly not sonic, questionable $\dot{\omega}_f$ and MR.
[3]Low ΔP through injector fuel circuit due to cooling hole modifications larger C_dA → smaller ΔP.

Key:

F	Thrust
Isp	Specific Impulse
C*	Characteristic Exhaust Velocity
Pc	Chamber Pressure
MR	Mixture Ratio (O/F)
Dur	Test Duration
POJ	Pressure Ox Manifold Injector
PFJ	Pressure Fuel Manifold Injector
$\frac{POJ-Pc}{Pc}$	% Pressure Drop Injector Ox Circuit
$\frac{PFJ-Pc}{Pc}$	% Pressure Drop Injector Fuel Circuit
$\dot{\omega}_t$	Total Flow Rate

Table 4.0-III
OTV 3K TCA Cooled Throat Hot Fire Test Summary

OTV 3K TCA
COOLED THROAT
HOT FIRE TEST SUMMARY

TEST NO.	POVI (psia)	POJ (psia)	TOVI (F)	PFVI (psia)	PFJ (psia)	TFVI (F)	DURATION (sec)	F VAC (lbf)	PC (psia)	$\dot{W}o$ (lbm/s)	$\dot{W}f$ (lbm/s)	MR	INJ CdA-ox (in**2)	INJ CdA-fuel (in**2)	POJ-Pc / Pc	PFJ-Pc / Pc	ISP (VAC)	CSTAR (VAC)
108	1624	1150	101	1931	1134	91	1.60	1239	1046	2.637	0.579	4.6	0.1568	0.1595	9.94%	8.41%	385	7569
109	1534	1129	102	2148	1135	83	1.60	1201	1018	2.480	0.647	3.8	0.1482	0.1505	10.90%	11.49%	384	7576
110	1739	1174	95	1654	1128	88	1.60	1305	1056	2.862	0.497	5.8	0.1640	0.1662	11.17%	6.82%	389	7316
111	828	576	97	1023	571	96	1.80	620	513	1.321	0.306	4.3	0.1539	0.1558	12.28%	11.31%	381	7338
113	3225	2120	126	3745	2093	71	1.10	2263	1989	5.074	1.110	4.6	0.1744	0.1839	6.59%	5.23%	366	7485
114	3055	2118	127	4183	2134	59	1.00	2464	1966	4.879	1.255	3.9	0.1616	0.1701	7.73%	8.55%	402	7459
115	3483	2275	115	3329	2190	61	1.13	2464	2104	5.589	1.005	5.6	0.1751	0.1840	8.13%	4.09%	374	7426

COOLANT CIRCUIT

TEST NO.	PLHRT (psia)	PLHFMI (psia)	TFM (F)	PCTI (psia)	TCTI (F)	PCTO (psia)	FMLH (lbm/sec)	LH2 DENSITY (lbm/ft3)	TCTO (F)	WLH2 (lbm/s)	WLH2 desired	THROAT DEL P	THROAT DEL T	ENTHALPY IN (btu/lbm)	ENTHALPY OUT (btu/lbm)	HEAT LOAD (btu/sec)
108	2771	2809	-345	1701	-324	1453	5.900	2.250	-54	0.337	0.481	248	270	253	1321	513
109	3275	3311	-355	1956	-325	1682	6.286	2.490	-85	0.398	0.537	274	240	246	1201	513
110	2488	2522	-342	1594	-314	1356	5.676	1.980	16	0.302	0.413	238	330	291	1584	533
111	1421	1450	-319	740	-276	610	5.057	0.760	-36	0.155	0.254	130	240	500	1385	225
113	4735	4651	-350	2550	-323	2168	7.180	2.890	-78	0.505	0.921	382	245	253	1232	902
114	4910	4826	-331	2381	-304	2018	7.330	2.450	-81	0.478	1.042	363	223	322	1220	935
115	4132	4181	-365	2662	-340	2280	7.020	3.330	-47	0.502	0.834	382	293	195	1355	968

Key:

- **Injector CdA-Ox** – Area Discharge Coefficient Ox Inlet
- **Injector CdA-Fuel** – Fuel Area Discharge Coefficient Fuel Inlet
- **$\frac{POJ-Pc}{Pc}$** – % Pressure Drop Oxidizer Circuit
- **$\frac{PFJ-Pc}{Pc}$** – % Pressure Drop Fuel Circuit
- **Isp** – Specific Impulse
- **C*** – Characteristic Exhaust Velocity
- **POVI** – Pressure Ox. Venturi Inlet
- **POJ** – Pressure Ox Manifold Injector
- **TOVI** – Temp. Ox Venturi Inlet
- **PFVI** – Pressure Fuel Venturi Inlet
- **PFJ** – Pressure Fuel Manifold Injector
- **TFVI** – Temp. Fuel Venturi Inlet
- **F** – Thrust
- **Pc** – Chamber Pressure
- **$\dot{\omega}_o$** – Ox Flowrate
- **$\dot{\omega}_f$** – Fuel Flowrate
- **MR** – Mixture Ratio (O/F)
- **PLHRT** – LH_2 Run Tank Pressure
- **PLHFMI** – LH_2 Flowmeter Inlet Pressure
- **TFM** – Temp. Flowmeter
- **PCTI** – Pressure Cooled Throat Inlet
- **PCTO** – Pressure Cooled Throat Outlet
- **TCTI** – Temp. Cooled Throat Inlet
- **FMLH** – Flowmeter Liquid Hydrogen (Calibrated for Water)
- **TCTO** – Temp. Cooled Throat Outlet
- **$\dot{\omega}LH_2$** – Flowrate Liquid Hydrogen

Table 4.0-IV
OTV Hot Fire Test Comments

Test No. 2459-120-A6-	F (lbf)	Pc (psia)	MR	Dur (sec)	Comments
-137	-	28.0	5	1.0	Ignition test - direct igniter
-138	-	28.9	5	1.0	Ignition test - direct igniter
-140	166	190	4	5.0	Full ignition test
-144	389	389	4	4.6	1300°F kill on centerbody, still steady state
-145	395	390	6	5.0	Full duration test
-146	399	393	8	5.0	Full duration test
-147	525	516	6	4.5	1300°F kill on centerbody, still steady state
-149	618	626	4	3.5	1500°F kill on throat, still steady state
-150	599	598	5	2.6	1500°F kill on throat, barely steady state
-151	615	611	6	2.6	1600°F kill on throat, barely steady state
-154	529	532	7	3.5	1600°F kill on throat, steady state
-155	512	527	5	4.2	1300°F kill on throat, steady state

Key:

F	**Thrust**
Pc	**Chamber Pressure**
MR	**Mixture Ratio**
Dur	**Test Duration**

TABLE 4.0-V

LH_2 COOLED THROAT HOT FIRE TEST COMMENTS

Test	Date	Pc	MR	Comments
-108	7/15/87	1000	6	Temp kill increased to 1500 deg F for following tests
-109	7/15/87	1000	5	Throat measures 0.965" dia
-110	7/15/87	1000	7	Exhaust appears green at shutdown
-111	7/15/87	500	6	90 deg TC's on OB went overscale, some green in exhaust
-112	7/21/87	2000	6	Short igniter light, reset
-113	7/22/87	2000	6	No green in exhaust
-114	7/22/87	2000	5	Kill on TCBO.5 @ 1650 F
-115	7/22/87	2000	7	Kill on TCBO.5 @ 1600 F, green toward shutdown
-116	7/22/87	1500	6	Insufficient GH_2 to pressurize LH_2 tank

Key:

Pc - Chamber Pressure (psia)
MR - Mixture Ratio (Ox/Fuel)

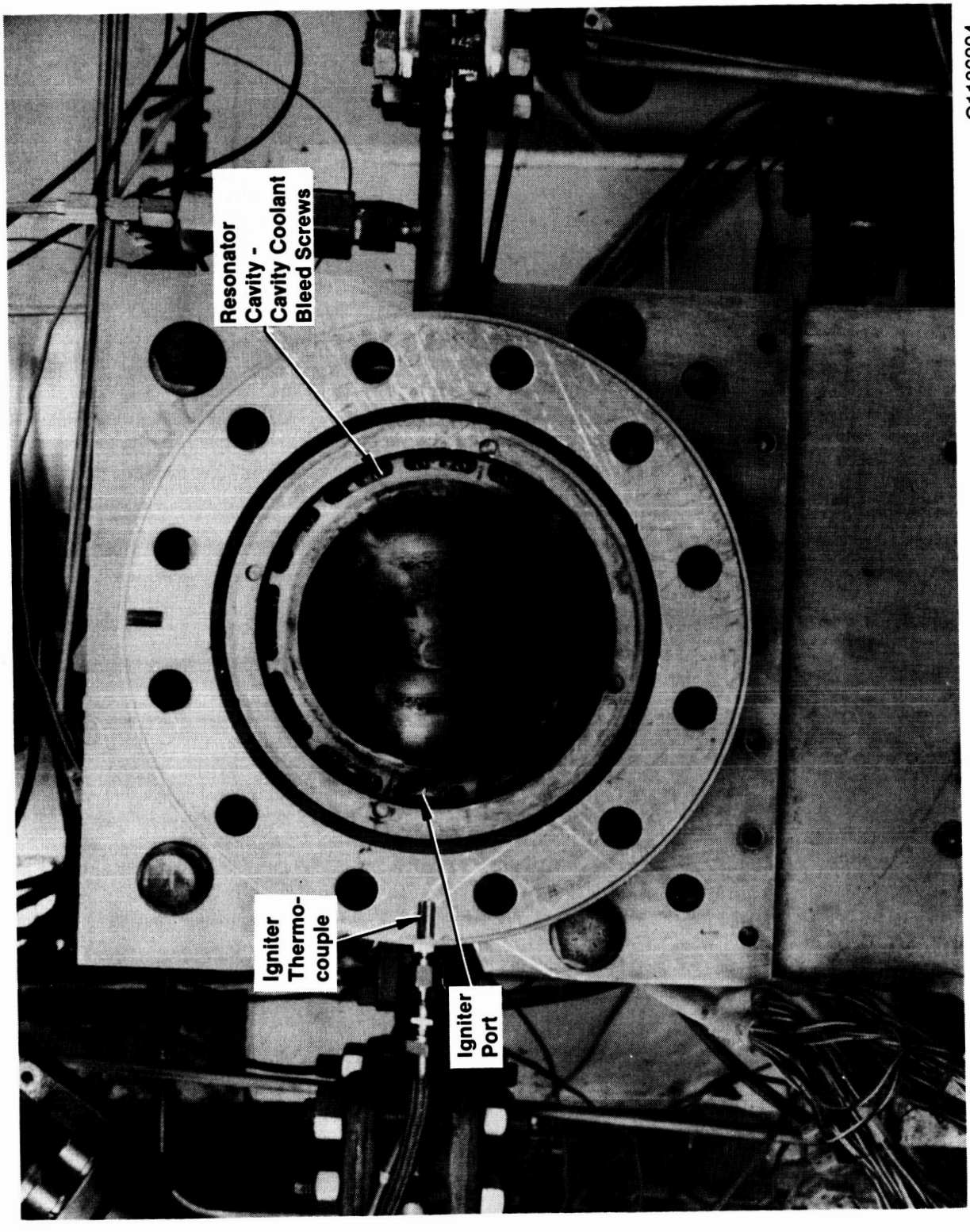

Figure 4.1-1. Injector Following Igniter Checkout Tests

fitted with a long electrode spark plug (direct ignition) or a more traditional torch igniter having its own propellant supply.

Provisions were made within the igniter housing to enable operation of either a torch or a direct igniter. The two designs are illustrated in Figure 4.1-2. For the torch ignition, valves were used to flow propellants to the electrode to initiate ignition. For the direct igniter scheme, these flow paths were not used. Critical dimensions of the igniter include spark gap, chamber diameter, cold flow pressures, and cooling flow distribution. These dimensions were selected based on ATC ignition and cooling models and supporting analysis. The initial test plan for the igniter is outlined in Figure 4.1-3.

4.1.1 Oxidizer Rich Torch Ignition

A photograph of the torch ignition hardware is shown in Figure 4.1.1-1. Gaseous hydrogen and oxygen ports are provided in the igniter housing. Flow paths within the igniter assembly are formed by channels machined onto the surfaces of washers and cylinders. The flow paths deliver the propellants to the spark electrode tip where they are ignited and propagate as a flame down the oxidizer rich cylinder to ignite the elements. This is a simplification of an ATC design liquid propellant igniter which utilized platelets to distribute the propellants to the tip of the electrode. Modifications to the aviation engine spark plug included removal of the ground, shortening of the electrode, and recessing of the ceramic insulation. Nominal test parameters are listed in Table 4.1.1-I.

Figure 4.1.1-2 shows the igniter housing mounted on the test stand. The configuration used for testing the torch igniter is shown schematically in Figure 4.1.1-3. Each nominal test series contained 1 cold pulse (valves actuated but no spark) followed by 9 hot pulses (valves and spark actuated) with a 10 second delay between each pulse. Ignition was determined by the igniter chamber pressure rise in comparison to the first cold pulse and by visual observation of the flame. Visual inspection of the igniter port and injector face was performed after each test series. A total of 76 hot pulses, 100% successful, was recorded during testing.

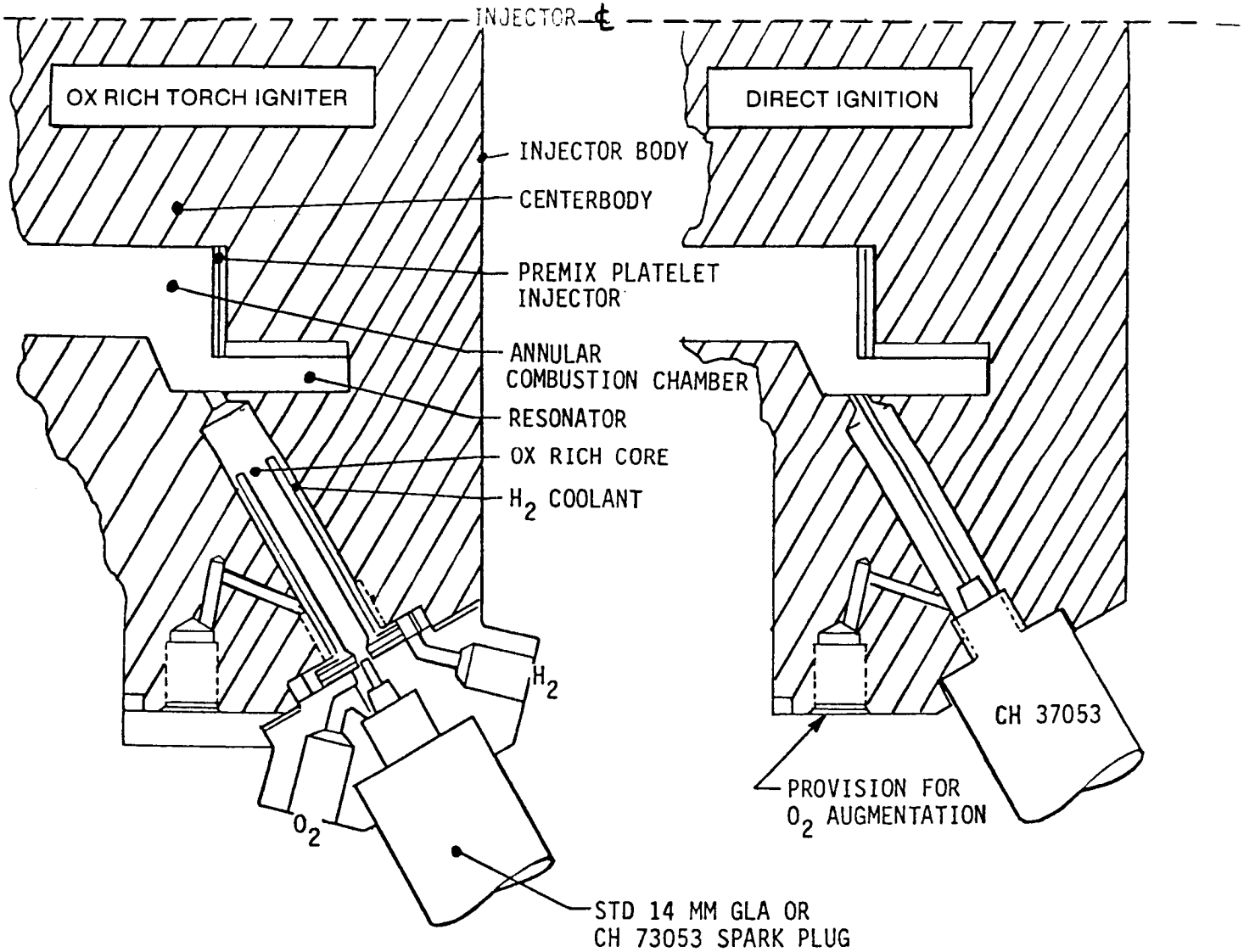

Figure 4.1-2. Torch & Direct Igniter Concepts

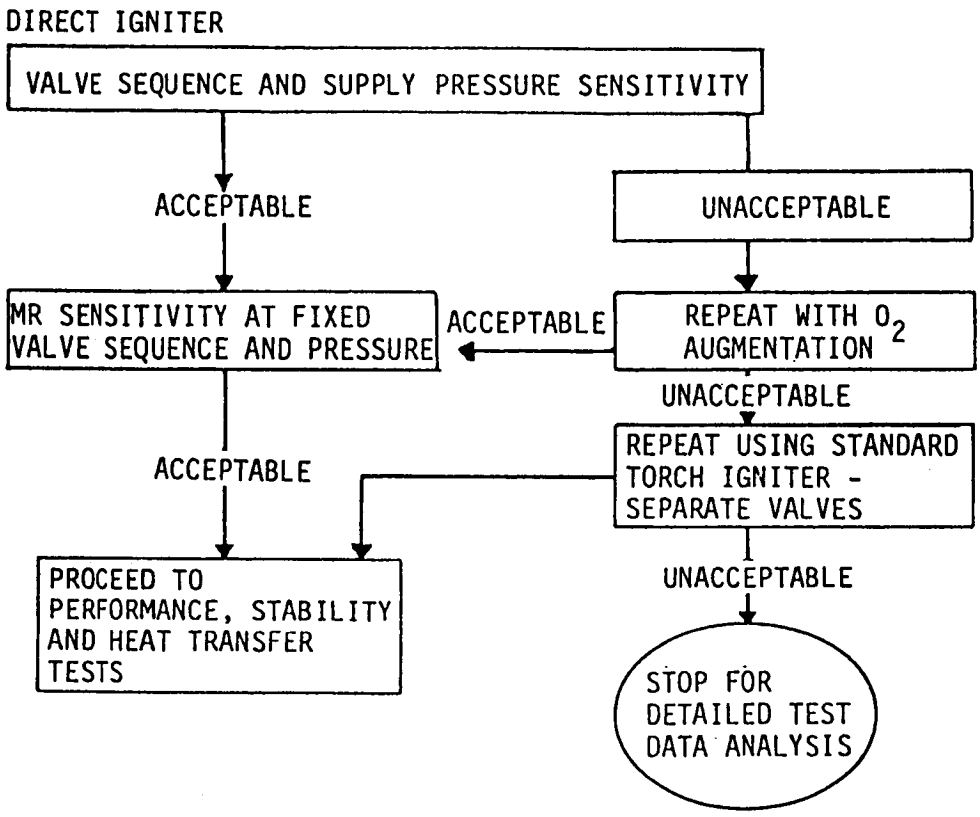

Igniter Test Logic

Figure 4.1-3. Igniter Test Logic

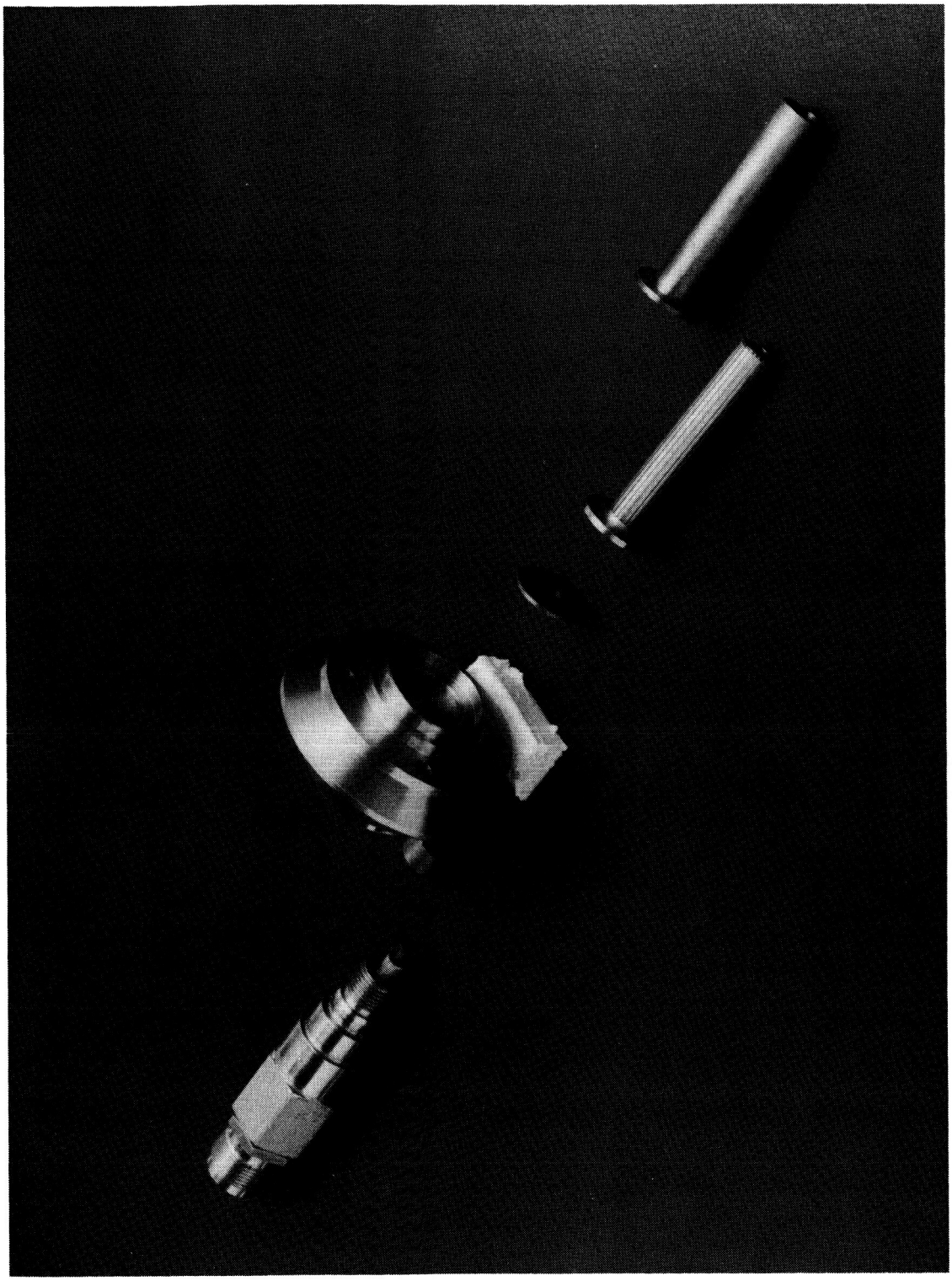

Figure 4.1.1-1. Disassembled Torch Igniter

TABLE 4.1.1-I

OTV TORCH IGNITER
NOMINAL TEST PARAMETERS

Spark Rate (sparks/second)	300
Spark Power Supply (millijoules)	10
Spark Response Time (sec)	0.015
Oxidizer Valve Response Time (sec)	0.030
Fuel Valve Response Time (sec)	0.040
Pulse Duration (sec)	0.2-0.3
Overall Mixture Ratio Test Range	3.6 ± 1.0
Core Mixture Ratio Estimated	26 to 46
Test Sequence Range	21.1 - 25.4
Oxidizer Lead = .010 and .030 sec Fuel Lead = .010 and .030 sec	

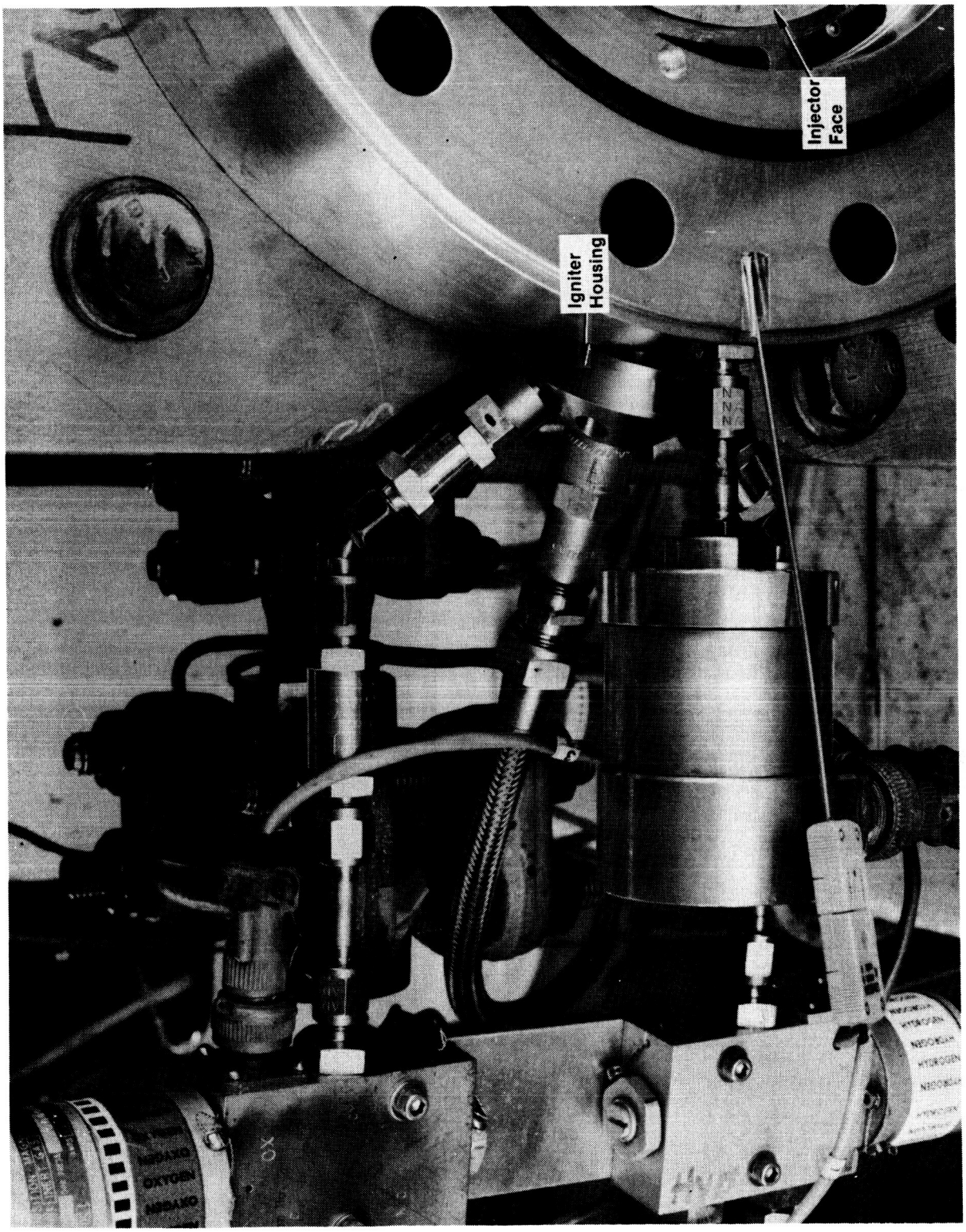

Figure 4.1.1-2. Preassembled Torch Igniter Hardware

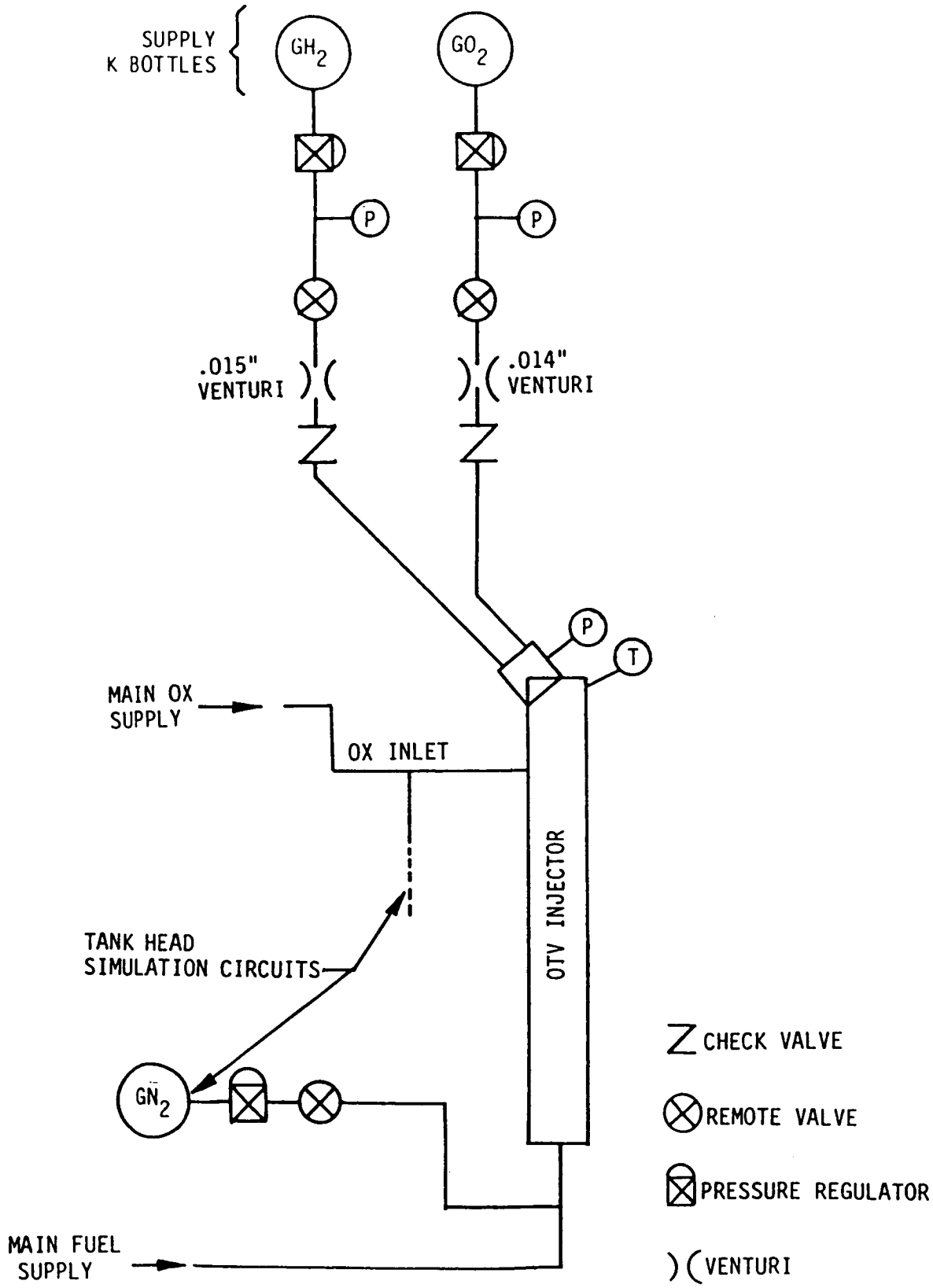

Figure 4.1.1-3. Test Configuration for OTV Torch Igniter

These tests were conducted over the following range of mixture ratios and valve sequences.

MR overall	2.6 to 4.6
MR core	26 to 46
Supply Pressure	21 to 25 psia
Valve sequence	Ox lead 0 to 0.03 seconds
	Fuel lead 0 to 0.03 seconds

Next a series of 20 low pressure (25 to 35 psia) tests was conducted using the torch igniter. The objective was to characterize the injector/annular combustion chamber under tank head idle mode operating conditions. The test parameters included valve sequencing and igniter sequencing. Table 4.1.1-II and 4.1.1-III provide a complete listing of the test conditions, valve sequencing and overpressures. These tests range from 1 to approximately 10 seconds in duration.

The igniter test series was conducted by activating the oxidizer rich core torch igniter ahead of the main injector flow. The igniter lead time was reduced in 0.010 second increments until the igniter was activated after main propellant flow was established. As indicated previously, all tests resulted in an acceptable start transient, however, the simultaneous sequence used in tests #109 and 110 was found to be best. Figure 4.1.1-4 shows the Pc trace on the various sequences.

Test #114 employed the same simultaneous sequence as #109, but resulted in a start which resembled a delayed igniter. Repeat tests #115 and 116 suggested that the igniter was not receiving full propellant flow. This was subsequently traced to a faulty igniter O_2 valve. Tests #117 through #120 were conducted by activating only the spark system, i.e., no flow to the torch igniter. Successful direct ignition was attained on all four tests. Test #119 of Figure 4.1.1-5 shows a typical direct ignition start.

The tests demonstrated the torch igniter to be insensitive to potential operational variables. Figure 4.1.1-6 displays a sample oscillograph trace of 1 hot pulse with simultaneous spark and valve electrical actuation. A

TABLE 4.1.1-II

OTV TORCH IGNITER TEST SUMMARY

Test No. (2459-120-A6-)	Valve Sequence	MR	Duration (sec)	P_c (psia)	$\dot{w}_o$ (lbm/sec)	POJ (psia)	$\dot{w}_f$ (lbm/sec)	PFJ (psia)		Comments
008	Simultaneous	3.47	0.30	22.1	.0025	670	.00072	711	Valve Sequencing Sensitivity Test at Nominal MR	1 cold, 3 hot; burned hole through Al protective face plate, manual shutdown.
009	Simultaneous	3.47	0.20	21.9	.0025	669	.00072	712		1 cold, 1 hot; shorter pulse, removed Al plate, looked good.
010	Simultaneous	3.47	0.20	21.9	.0025	669	.00072	712		1 cold, 9 hot, looked good.
011	.010 oxidizer lead	3.47	0.20	21.9	.0025	669	.00072	713		1 cold, 9 hot, looked good.
012	.010 fuel lead	3.47	0.20	21.9	.0025	667	.00072	713		1 cold, 9 hot; looked good.
013	.030 fuel lead	3.47	0.23	21.9	.0025	666	.00072	714		1 cold, 9 hot; looked good.
014	.030 oxidizer lead	3.47	0.23	21.9	.0025	664	.00072	713		1 cold, 9 hot; visible heat wave looked good.
015	Simultaneous	4.67	0.23	21.1	.0028	737	.0006	593	MR Sensitivity Test	1 cold, 5 hot; manual shutdown suspicious hot area, but still looked good.
016	Simultaneous	4.67	0.23	21.1	.0028	737	.0006	593		1 cold, 4 more hot; looked good.
017	Simultaneous	2.61	0.23	23.1	.0024	643	.00092	909		1 cold, 9 hot; looked like plume moved away from injector face.
018	Simultaneous	3.59	0.23	25.4	.0033	877	.00092	903	Higher P_c	1 cold, 9 hot; higher flow at nominal MR, looked good.

*Refers to potential heat marks on injector edge in line with igniter plume.

Key:

MR	Mixture Ratio (O/F)
Pc	Chamber Pressure
$\dot{\omega}_o$	Ox Flowrate
$\dot{\omega}_f$	Fuel Flowrate
POJ	Pressure Ox Manifold, Injector
PFJ	Pressure Fuel Manifold, Injector

TABLE 4.1.1-III

OTV HOT FIRE TEST SUMMARY
AUGMENTATION CIRCUIT/TORCH IGNITER

JUNE 6-7, 1985

Test No.	MR	P_c (psia)	POJ (psia)	PFJ (psia)	P_cIGN (psia)	$\frac{\Delta P_O}{P_c}$ %	$\frac{\Delta P_F}{P_c}$ %	DUR (sec)	Aug Valve Sequence (Ox & Fuel) (sec)	Aug Valve Sequence to Ign Ox (sec)	P_c Transient Comments
101	4.04	28	33	32-33	30	15.2	15.2	0.50	simultaneous	.030 aug delay	slight P_c spike
102	4.03	28	33	33	29	17.8	17.8	0.50	simultaneous	.030 aug delay	slight P_c spike
103	4.10	30	35	35	31	16.7	16.7	0.50	simultaneous	.020 aug delay	slight P_c spike
104	4.11	31	36	36	31	16.1	16.1	0.50	simultaneous	.020 aug delay	slight P_c spike
105-106	4.00	29	35	35	31	20.7	20.7	0.50	simultaneous	.010 aug delay	smooth
107-108	4.01	30	36	36	32	20.0	20.0	0.50	simultaneous	simultaneous	smooth
109-110	4.11	31	36.5	36.5	32	17.7	17.7	0.50	simultaneous	.010 aug lead	very smooth P_c
111	4.06	32	37	37	32	15.6	15.6	2.00	simultaneous	.020 aug lead	slight P_c spike
112	4.00	32	37	38	32	15.6	18.8	2.00	.020 ox lead	.010 aug ox lead	slight P_c spike
113	4.04	32	37	38	33	15.6	18.8	2.00	.020 fuel lead	.010 aug ox delay	slight P_c spike
114	3.98	33	39	39	33	18.2	18.2	5.00	simultaneous	.010 aug lead	slight P_c spike
115	4.15	32	37	37	32	15.6	15.6	1.00	simultaneous	.010 aug lead	slight P_c spike
116	4.19	32	37	37	32	15.6	15.6	1.00	simultaneous	.010 aug lead	slight P_c spike
117	4.10	32	38	38	31	18.8	18.8	1.00	simultaneous	.010 aug lead	slight P_c spike
118	4.07	32.5	38	38	32	16.9	16.9	1.00	simultaneous	.010 aug lead	slight P_c spike
119	3.04	35	43	43	34	17.1	22.9	9.29	simultaneous	.010 aug lead	slight P_c spike
120	5.01	35	40	40	35	17.1	14.3	5.80	simultaneous	.010 aug lead	slight P_c spike

Key:

MR	**Mixture Ratio (O/F)**
Pc	**Chamber Pressure**
POJ	**Pressure Ox Manifold, Injector**
PFJ	**Pressure Fuel Manifold Injector**
Pcign	**Chamber Pressure at Ignition**
$\frac{\Delta Po}{Pc}$	**% Pressure Drop Ox Manifold Circuit**
$\frac{\Delta Pf}{Pc}$	**% Pressure Drop Fuel Manifold Circuit**
Dur	**Test Duration**

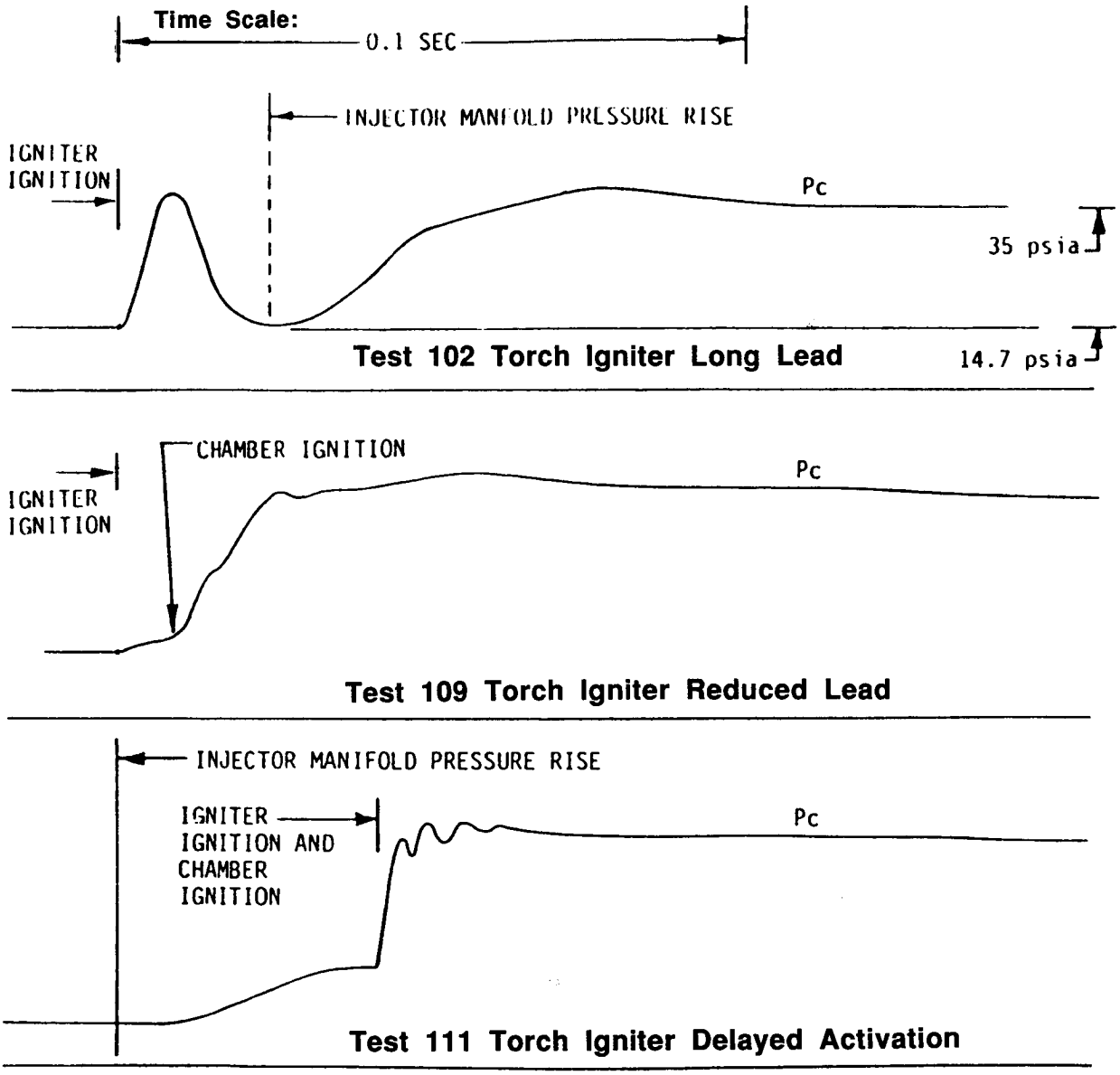

Figure 4.1.1-4. Effect of Igniter Sequence on Ignition

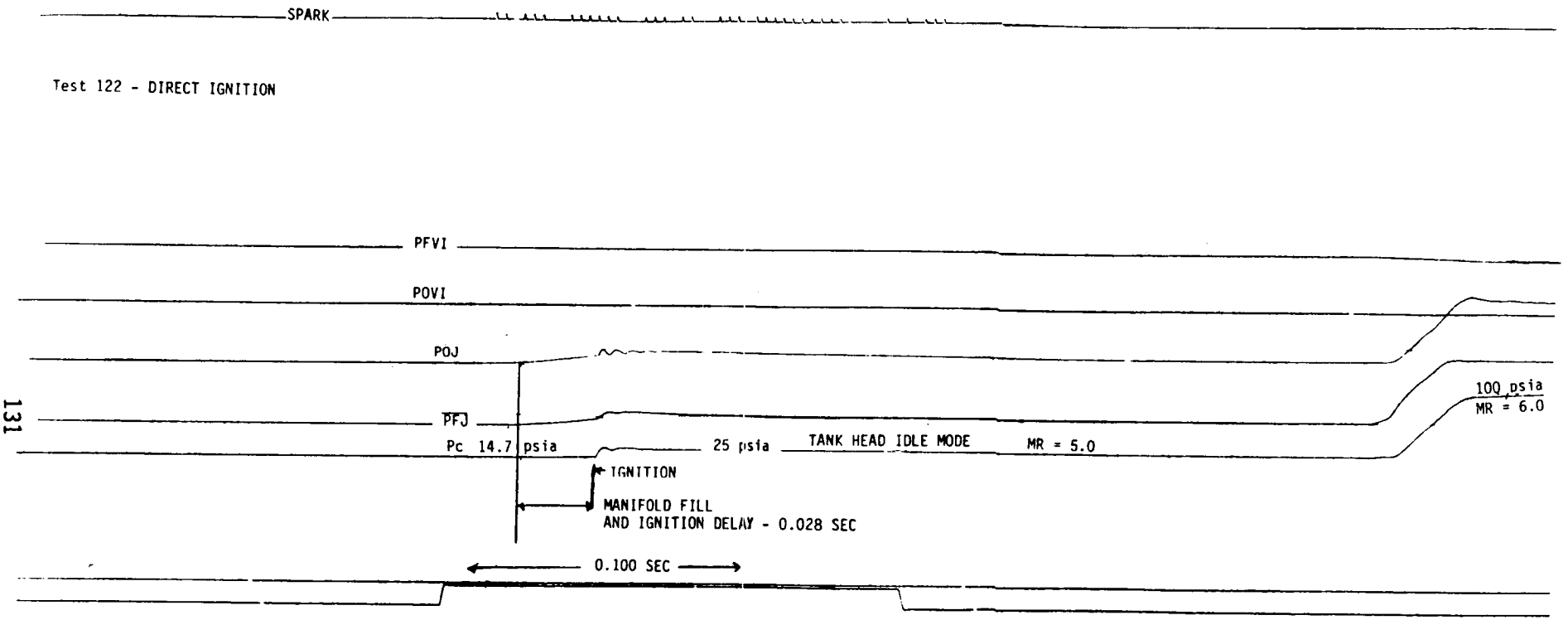

Figure 4.1.1-5. Test #122 Direct Ignition Start

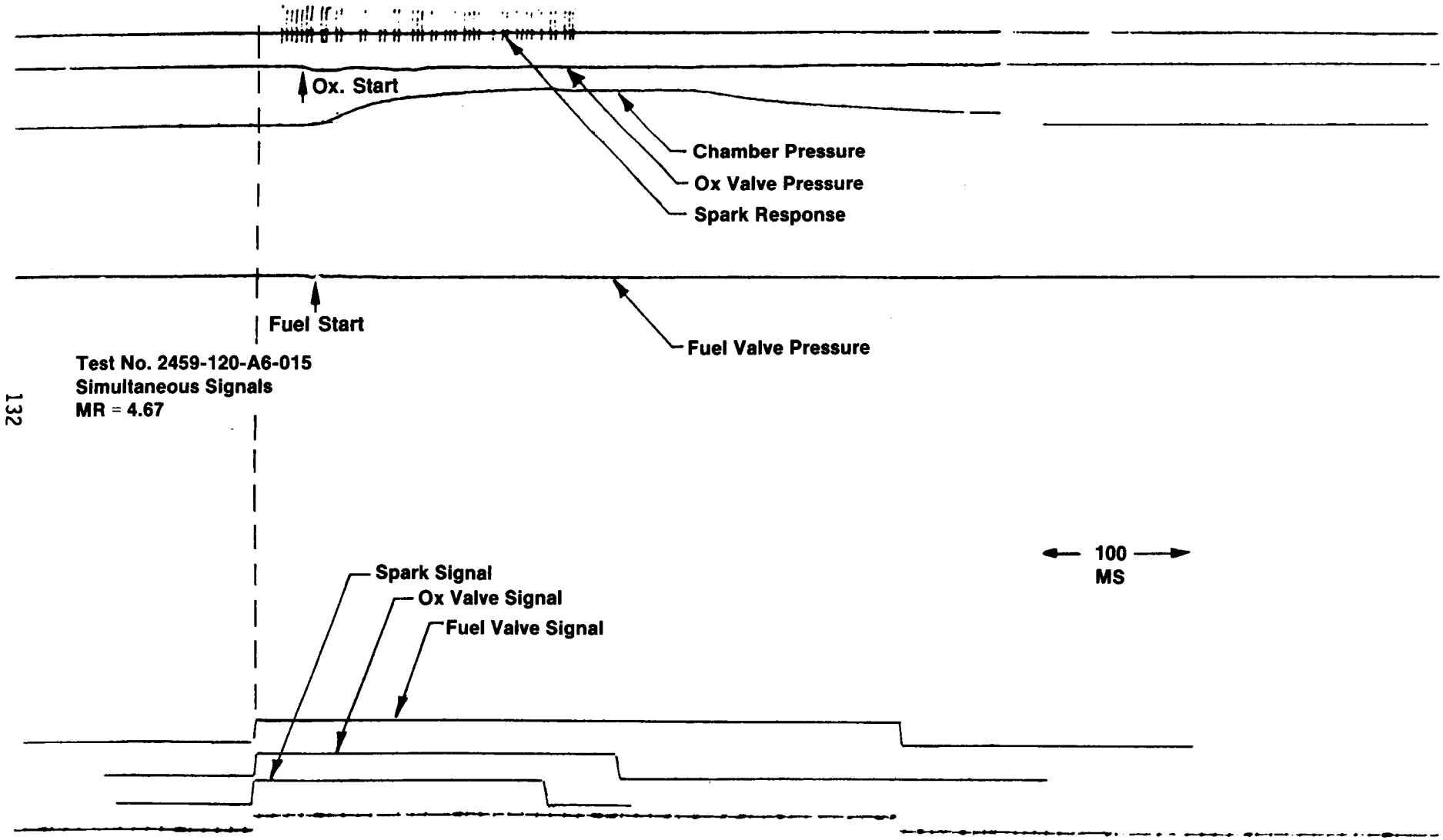

Figure 4.1.1-6. OTV Torch Igniter Test: Pressure Response to Signal Initiation

simultaneous signal to the valves yields a 0.010 second oxidizer lead into the chamber because of the slower response of the fuel valve.

4.1.2 Direct Spark

The use of a direct ignition method is simpler and involves a spark discharge within the combustion chamber. However, this approach is highly dependent on the mixture ratio in the spark gap zone. Therefore, provision was made for GO_2 augmentation in the spark zone if needed for reliability.

Figure 4.1.2-1 is a photograph of the spark plug used as the direct igniter. For this concept the spark plug was not modified. Rather the long electrode extended into the combustion chamber, through the resonator cavity, where the spark triggered the ignition of the gases from the injector elements. The direct igniter is shown mounted on the test chamber in Figure 4.1.2-2. This method eliminated the need to separately plumb fuel and oxidizer to the igniter.

Table 4.1.2-I summarizes the direct igniter tests. Tests #121 through #124 resulted in successful ignition at a tank head idle mode pressure of approximately 25 psia. After approximately 0.3 seconds, the chamber pressure of the TCA was ramped from the tank head idle mode pressure to 100 psia.

Based on the successful results of use of the direct spark ignition concept and to gather additional information on the reliability of the direct igniter during hot fire testing, the direct spark ignitor was used in the series of low and high pressure tests. The test plan for the thrust chamber assembly hot firings are presented in Section 3.3.

4.2 Combustion Stability

4.2.1 Earlier Aerojet work with various GO_2/GH_2 injectors had demonstrated that combustion instability was not a serious problem with this propellant combination when used with gas-gas injector elements (see Table 4.2.1-I). Standard ATC design practice is to provide instability damping despite a benign propellant combination and chamber design. Acoustic cavities were the preferred

Figure 4.1.2-1. Direct Igniter

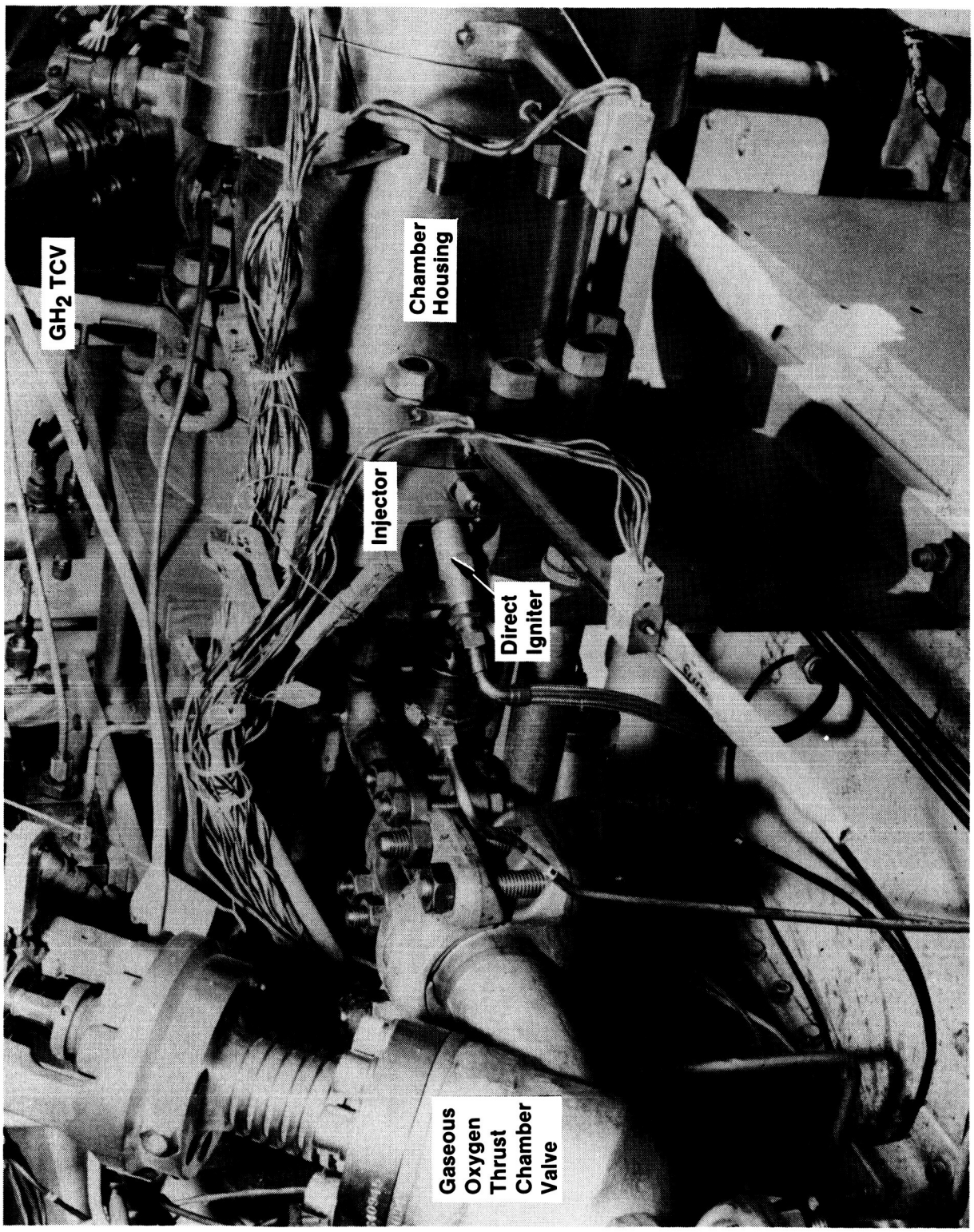

C0687 2601

Figure 4.1.2-2. OTV Test Hardware - View of Direct Igniter

TABLE 4.1.2-I

TCA HOT FIRE TEST SUMMARY
MAIN CIRCUIT/DIRECT IGNITER

Test No.	Date	P_C (psia)	POJ (psia)	PFJ (psia)	$\frac{\Delta P_{OJ}}{Pc}$ (%)	$\frac{\Delta P_{OJ}}{Pc}$ (%)	MR	ISP_{VAC} (sec)	DUR (sec)	C* (ft/sec)
121	6/28/85	85	100	98	16	16	3.5	378	1.2	7,564
122	6/28/85	106	123	117	16	10	5.4	359	4.0	7,340
123	6/28/85	105	124	112	18	7	9.2	346	4.0	6,766
124	6/28/85	99	117	107	18	8	8.8	361	4.0	6,826

Key:

Pc	**Chamber Pressure**
POJ	**Pressure Ox. Manifold Injector**
PFJ	**Pressure Fuel Manifold Injector**
$\frac{\Delta P_{OJ}}{Pc}$	**% Pressure Drop Ox Circuit**
$\frac{\Delta P_f}{Pc}$	**% Pressure Drop Fuel Circuit**
MR	**Mixture Ratio (O/F)**
Isp	**Specific Impulse**
C*	**Characteristic Exhaust Velocity**

TABLE 4.2.1-I

TECHNOLOGY EXPERIENCE H_2/O_2 GAS COMBUSTION

Injector Element Type	Contract	Chamber Length (In)	Number Of Elements	Thrust Per Element	Experimental ERE
O-F-O Triplet	NAS 3-14347	(6)	144	10	100
F-O-F Triplet	NAS 3-14379	(3)	72	20	100
Premix Triplet Sm. Cup	NAS 3-14354	(7.0)	72	20	99.5
Premix Triplet Sm Cup	NAS 3-14354	(5.5)	72	20	98.5
Premix Triplet Deep Cup	NAS 3-14354	(3)	36	41	98.4
Coaxial Shear	NAS 3-14354	(5.5)	42	35	97
Coaxial Swirl	NAS 3-14354	(8.3)	42	35	97
-2 Zones (F-O-F Triplet)	NAS 3-14379	(3)	72	20	96.8
-1 Zones (F-O-F Triplet)	NAS 3-14379	(3)	72	20	96.2
Coaxial Tube	NAS 3-14352	(5)	54	27	96
Tri Slot	NAS 3-14352	(5)	16	94	93

stability device. The cavities were sized based on the chamber mode frequencies derived from chamber parameters and gas properties (see Figure 4.2.1-1). This preliminary design was then used as the starting point for a detailed analysis using the ICASE computer code (Reference 1).

4.2.2 Acoustic Cavity Design

The OTV TCA injector assembly incorporates 12 identical cavities around the outer periphery of the injector (Figure 4.2.2-1). Cavity depth in the assembled condition is 1.25 inches from the bottom to the injector face. Two holes are drilled and tapped in each cavity case to accept screws to mount blocks that can reduce the cavity depth should tuning be necessary. No blocks were used during the test program as tuning was not needed. The screws are center drilled to admit hydrogen into the cavities for necessary cooling. The cavity entrance height was selected as 0.01 inch during the analysis. Actual dimensions are set by the injector-to-chamber assembly tolerances. No adjustment was made to the assembled entrance height of 1.25 inches, but the opening could have been increased had testing proved it was needed.

4.2.3 Pressure Data Collection

Chamber pressure roughness was monitored by three Kistler high frequency pressure transducers. Data were recorded on both the digital data collection system and as an electro-optical signal trace on a strip chart. The strip chart has the advantage of avoiding all signal filtering that could mask the small pressure oscillations characteristic of combustion roughness. The vertical scale, however, is compressed to keep the signal on the strip chart. A better overall chamber pressure profile is generated from the digital data collection. An evaluation of combustion stability requires both. A typical pressure profile is shown in Figure 4.2.3-1. This was test #113, a test to 2000 psia chamber pressure. Total time for the test duration, which extends from Fire Switch to thermal cutoff, was 1.2 seconds. The strip chart trace for the initial start transient is shown in Figure 4.2.3-2. The balance of the signal from Fire Switch (F.S.) +0.040 seconds to cutoff showed a smooth pressure rise with no anomalies.

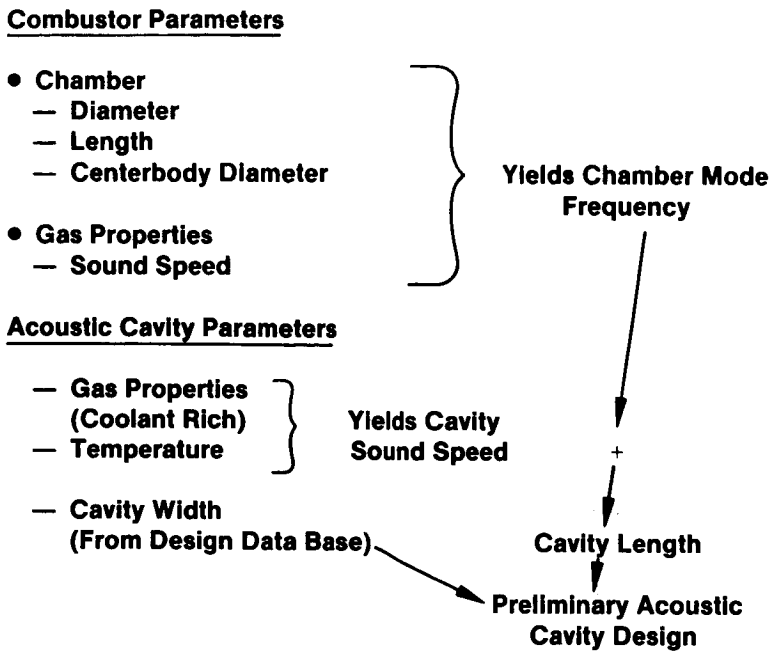

Figure 4.2.1-1. Methodology of Combustion Stability Analysis

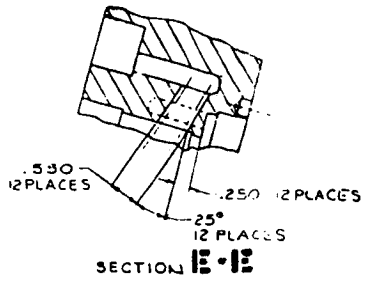

SECTION E-E

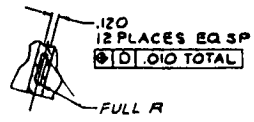

SECTION D-D

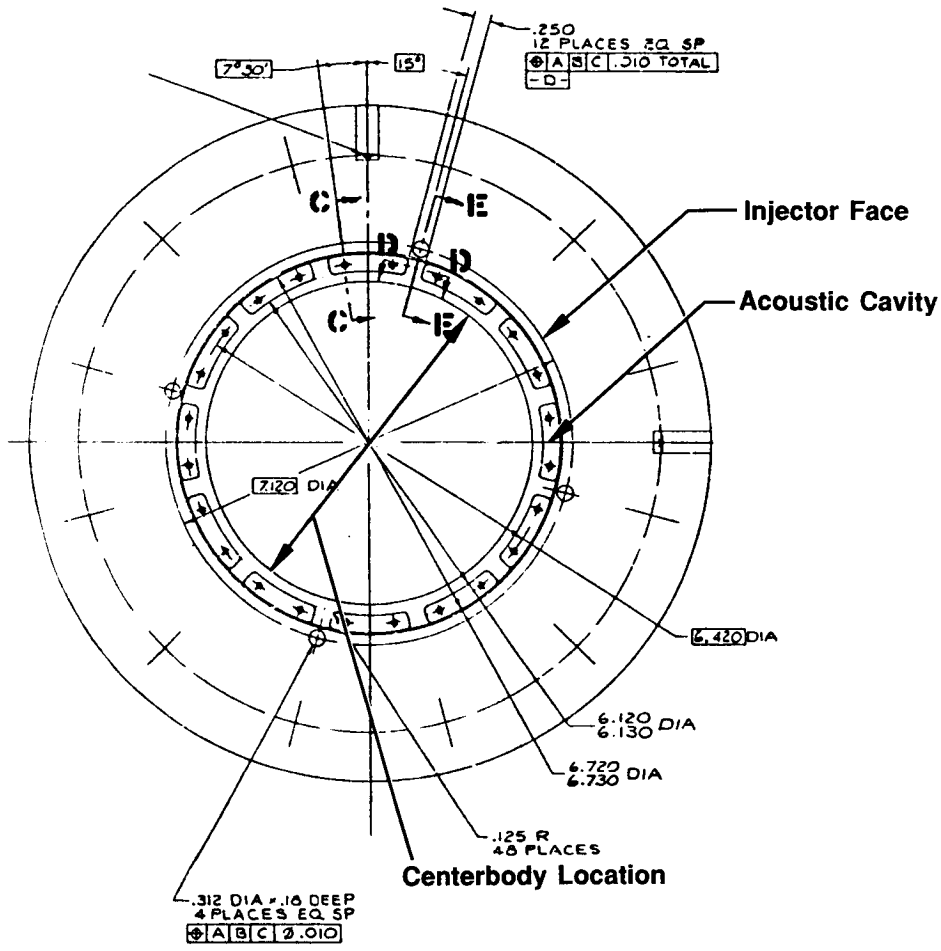

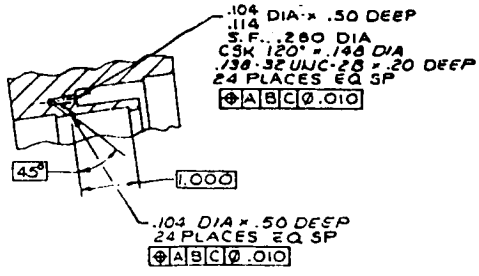

SECTION C-C

Figure 4.2.2-1. OTV 3.0 K TCA Acoustic Cavity Arrangement and Dimensions

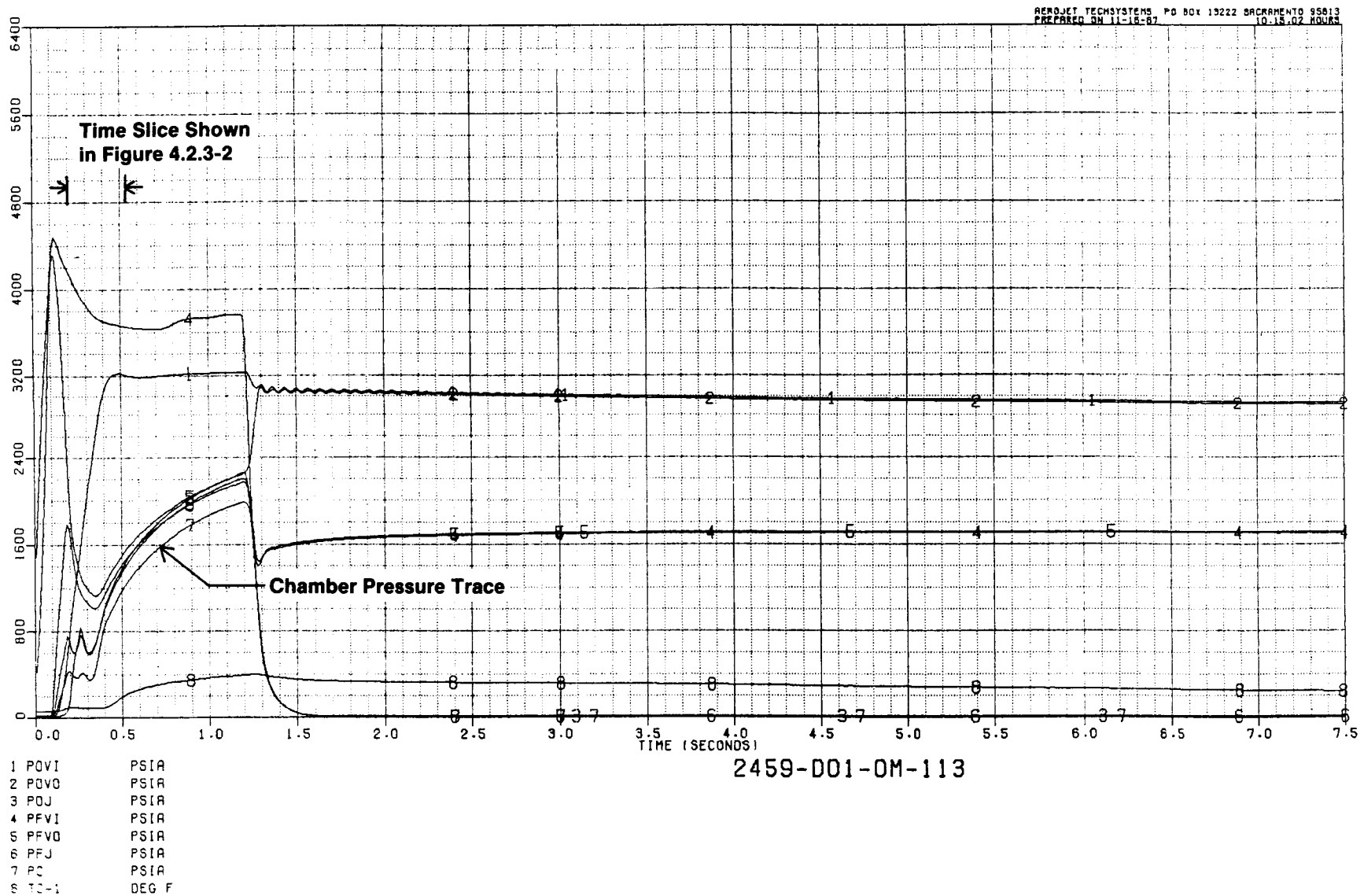

Figure 4.2.3-1. OTV 3.0 K TCA Hot Fire Test #113 - 2000 psia Chamber Pressure

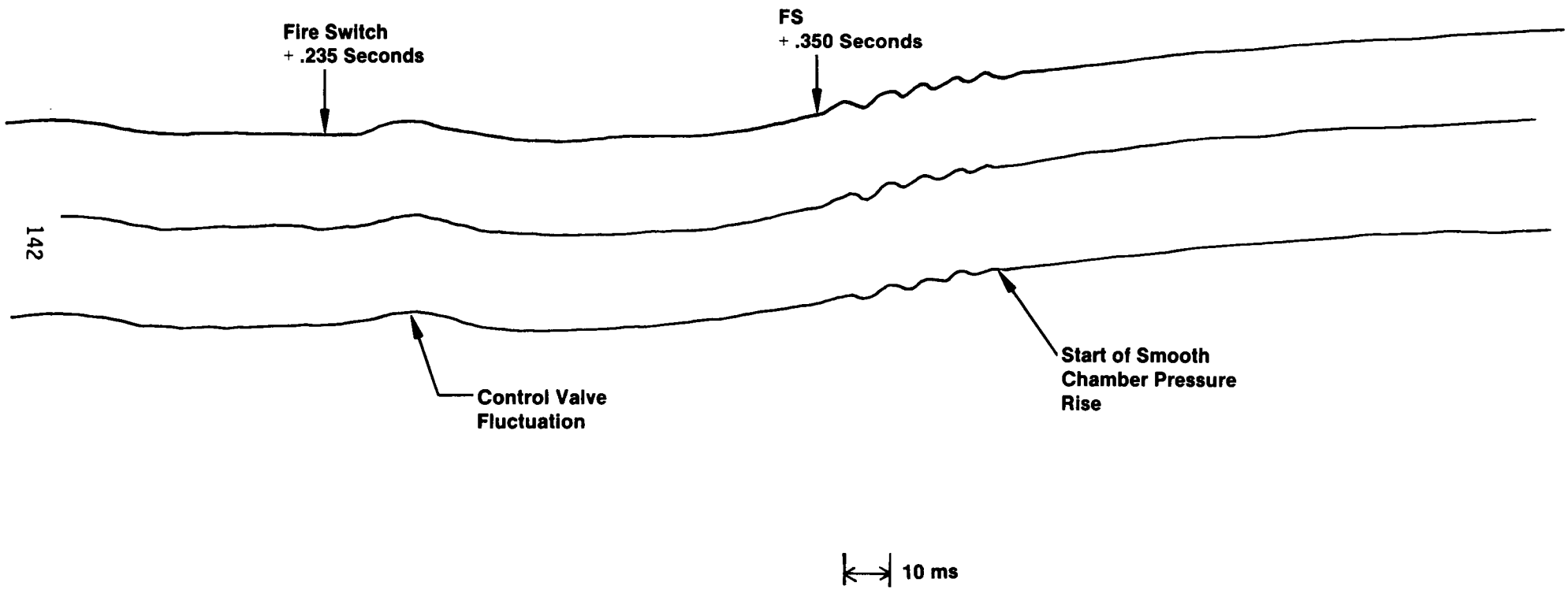

Figure 4.2.3-2. OTV 3.0 K TCA Hot Fire Test #113 - Kistler Hi Frequency Playback Start Transient

4.2.4 Stability Evaluation

Test #113 was atypical in that there was a cyclical pressure oscillation evident during the early start transient. Traces from other tests showed only the fluctuations caused by control valve "hunting" as the system corrected mixture ratio variations during the pressure rise. One such event is marked on Figure 4.2.3-2 at 0.235 seconds. At 0.350 seconds there was an oscillation, evidently combustion related, that damped in 40 mseconds. Peak-to-peak pressure variation is difficult to calculate from the data, but appears to be less than 40 psi. The low frequency (~100 Hz) indicates feed system coupling rather than activation of a chamber instability mode. The rapid damping indicates any such mode as having a narrow pressure range and nonpersistent characteristics. The balance of the pressure rise was very smooth with no evidence of roughness greater than 1/2 of 1 percent (the effective limit of resolution of the data). This was true for all tests.

4.2.5 Conclusions

1) Any start transient pressure oscillations were of low magnitude and quickly damped.

2) Combustion roughness was less than 0.5% from early in the start transient to steady state.

3) For normal start-up there was no evidence of combustion instability.

4) Test durations were too short to evaluate sustained steady state stability.

4.3 Injector Characteristics

The injector element utilized is a modified "I"-triplet premix, as discussed in Section 1.1.1. Two fuel streams impinge upon the oxidizer stream at 90• angles to form an element. Information summarized on the injector includes CdA coefficients and pressure drops for the two propellant circuits. Table 4.3-I

TABLE 4.3-1

INJECTOR CdA COEFFICIENTS
INITIAL VALUES

	Oxidizer	Fuel
Design	0.1550	0.1100
Cold Flow	0.1490	0.1270
Low Pc Hot Fire	0.1390	0.1359

AFTER INJECTOR MODIFICATION

	Oxidizer	Fuel
Design	0.1523	0.1232
Low Pc Hot Fire	0.1700	0.1630
Cold Flow	0.1709	0.1630
High PC Hot Fire	0.1619	0.1520

summarizes the CdA coefficients for the injector fuel and oxidizer circuits and compares the predicted value, cold flow value, and hot fire value before and after the injector modification. Uniformity of these values ensures consistency of the hardware between series of tests and/or test hardware modifications.

Individual circuit pressure drops and CdA values are plotted versus flowrate and mixture ratio in Figure 4.3-1 and -2 for the fuel circuit, and Figure 4.3-3 and -4 for the oxidizer circuit. In Figure 4.3-1, a mixture ratio dependency is observed for the fuel pressure drop. Figure 4.3-2 illustrates the influence of mixture ratio on the CdA term. Less dependency is seen for tests with chamber pressures in the range of 200 to 1000 psia. Increased dependancy of the CdA term to Mixture Ratio at 2000 psia chamber pressure may be due to non-steady state conditions experienced. Due to the short test duration, tests at 2000 Pc did not reach steady state.

The oxygen circuit characteristics appear to be less influenced by either MR or chamber pressure than the fuel circuit as evidenced by Figures 4.3-3 and -4.

Consistencies in the range of values for the pressure drop and CdA data between the low and high chamber pressure test series indicate little injector hydraulic performance variation.

4.4 Chamber Thermal Characteristics

4.4.1 Total Heat Load to Centerbody

Table 4.4.1-I lists the heat flux summary for the centerbody. This data is presented in Figure 4.4.1-1 cross plotted versus axial distance from the injector face. A uniform increase in flux is noted with increasing chamber pressure. The range of mixture ratios (4-8) tested are presented in Figure 4.4.1-1. No discernable effect was noted from the mixture ratio variance. Figures 4.4.1-2 through 4.4.1-5 separate the data into respective mixture ratio ranges.

Results of the low Pc test series were plotted as heat flux versus PC in order to project the flux profiles for the series of high PC tests (Pc = 2000

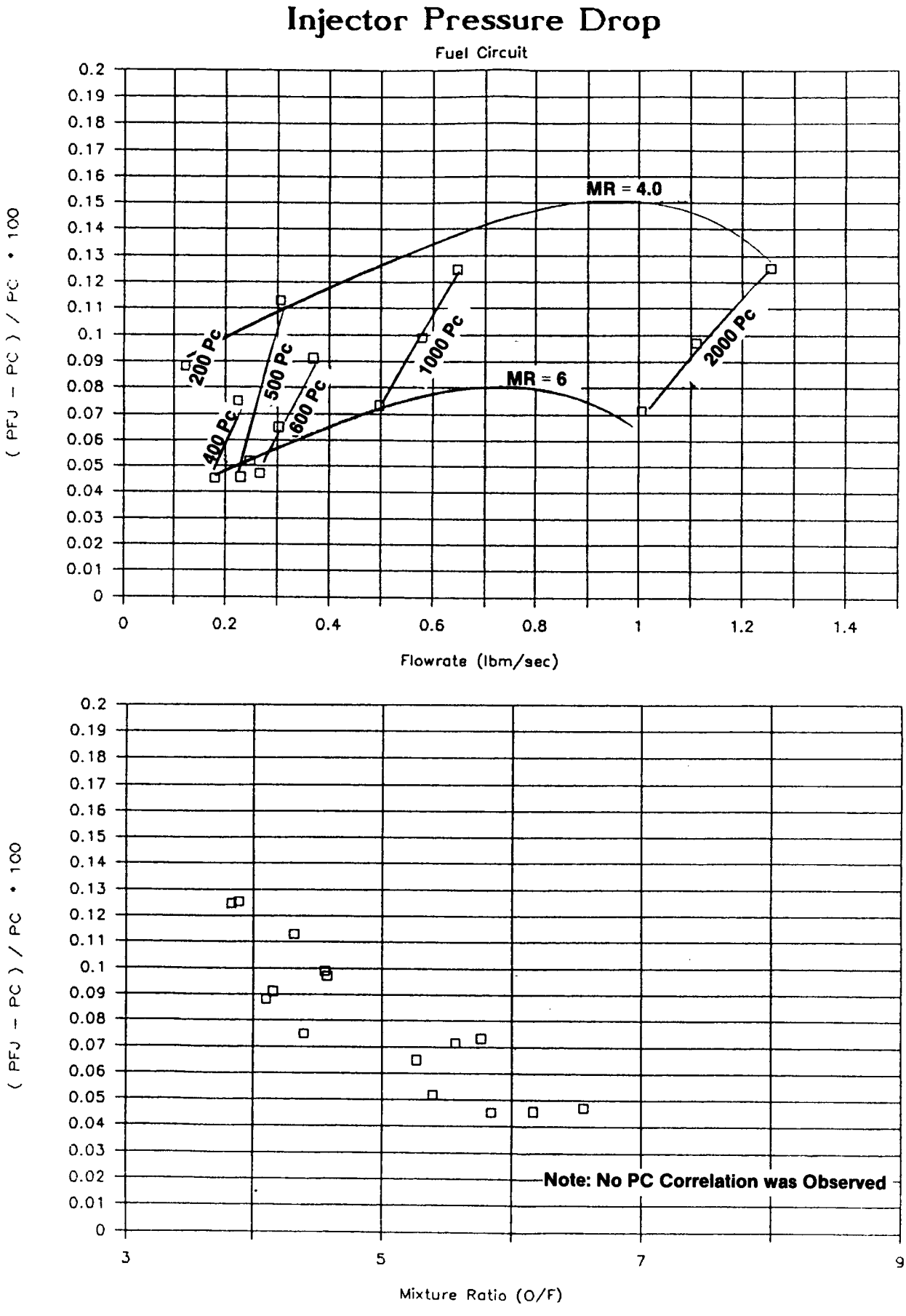

Figure 4.3-1. Injector Pressure Drop - Fuel Circuit

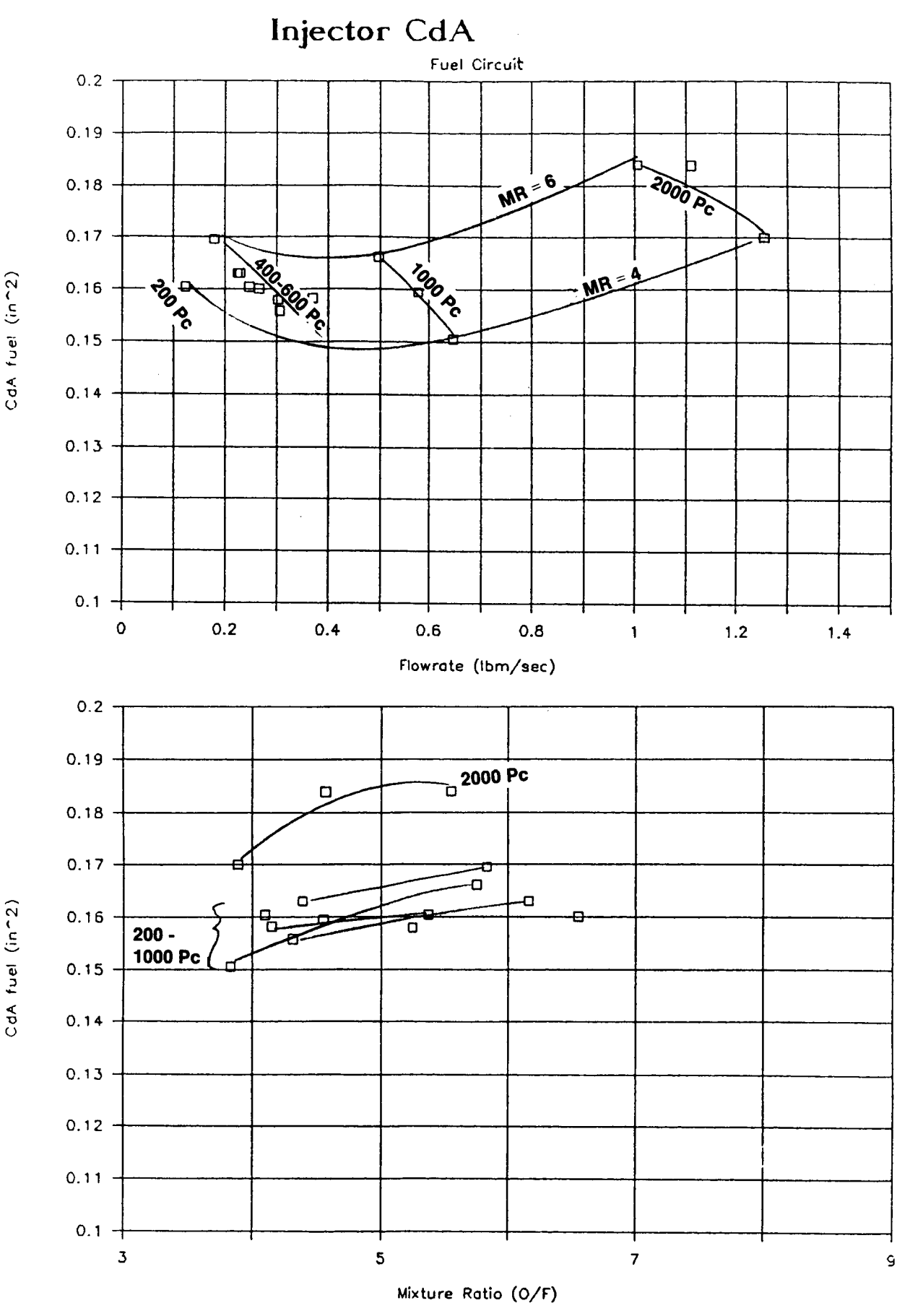

Figure 4.3-2. Injector CdA Coefficient - Fuel Circuit

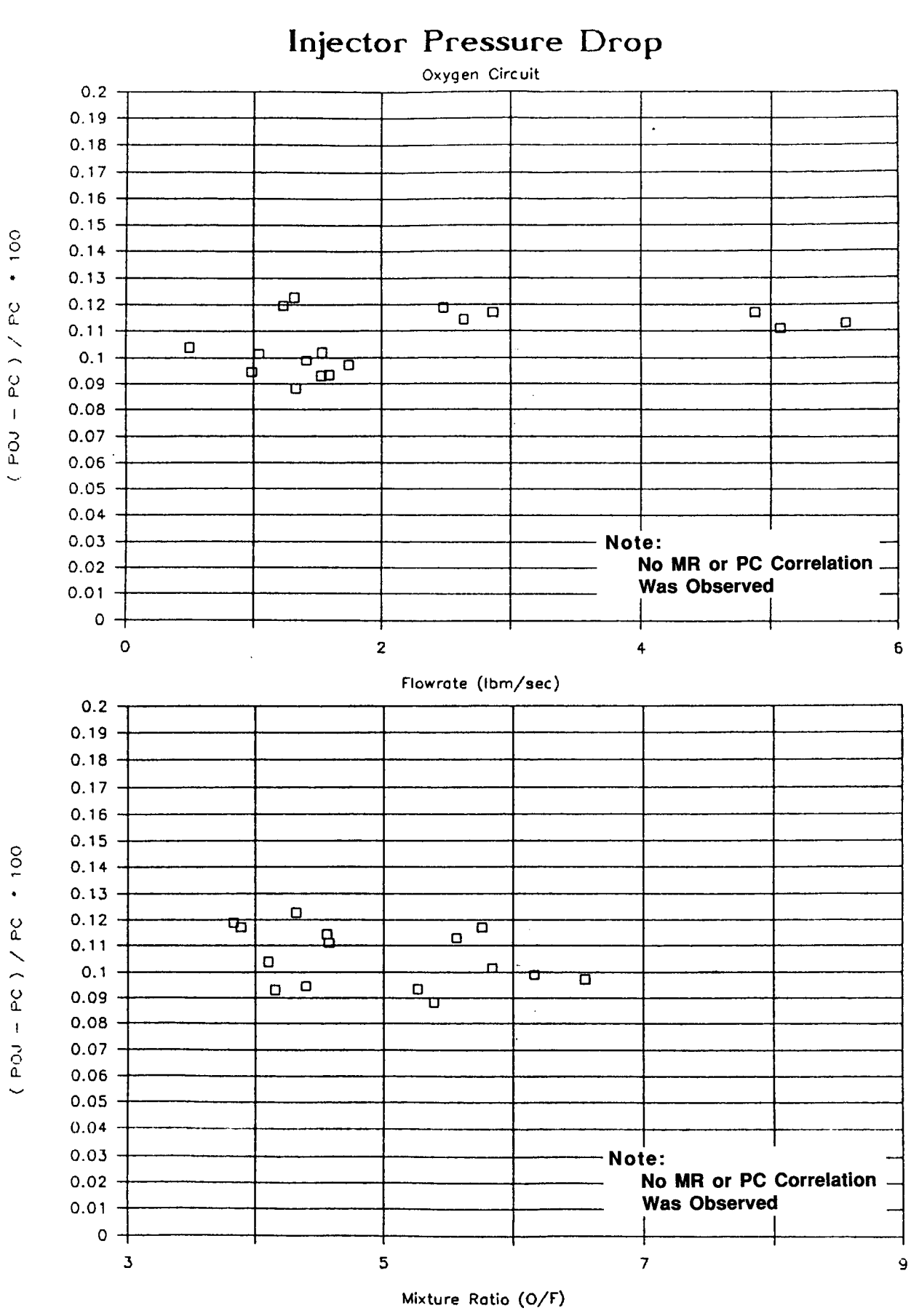

Figure 4.3-3. Injector Pressure Drop - Oxidizer Circuit

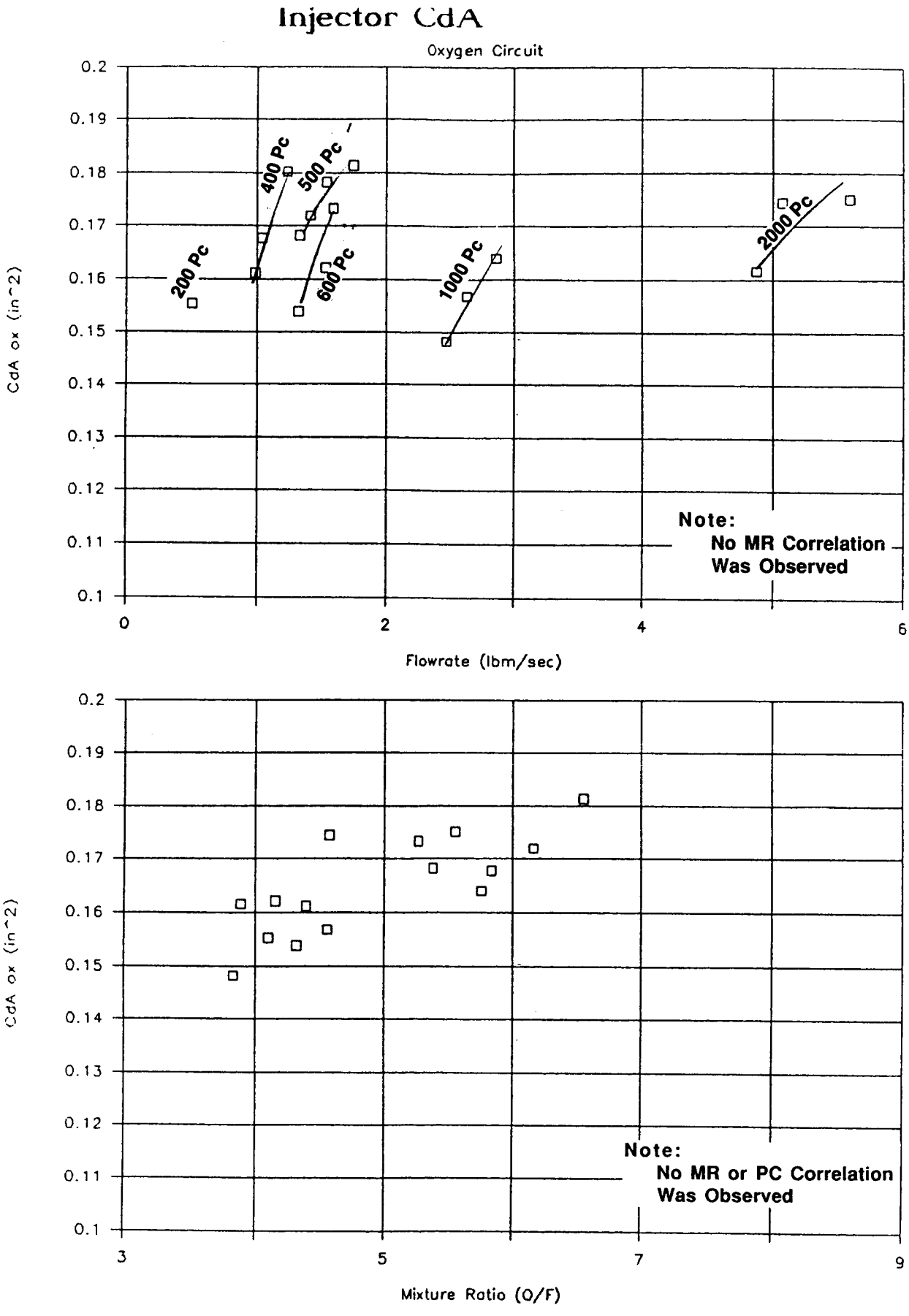

Figure 4.3-4. Injector CdA Coefficient - Oxidizer Circuit

Table 4.4.1-I. OTV Hot Fire Tests - Centerbody Heat Flux

OTV HOT-FIRE TESTS
HEAT FLUX
(Btu/sec in2)

TEST NO.		140	144	145	146	147	149	150	151	154	155	108	109	110	111	113	114	115
MR		4.1	4.4	5.8	8.3	6.2	4.2	5.3	6.5	7.5	5.4	4.6	3.9	5.7	4.3	4.7	4.0	5.9
Pc		197	390	391	400	517	600	570	588	529	526	1032	1009	1051	514	1908	1896	2044
CENTERBODY TCB																		
0.50	90	4.14	5.04	4.60	3.89	4.83	5.99	5.69	5.33	4.97	4.90	13.85	15.59	11.24	7.50	29.66	30.19	34.18
2.30	90	2.98	4.16	4.12	4.35	4.83	5.78	6.64	6.62	5.19	4.94	8.80	7.37	8.79	8.22	---	13.69	15.03
4.50	0	2.09	2.62	3.21	3.38	3.76	3.70	5.23	5.51	4.47	3.71	---	---	---	---	15.76	7.49	14.35
4.50	90	2.11	3.13	3.43	3.32	4.04	3.74	5.45	5.84	4.56	3.94	6.08	6.67	6.12	4.36	10.35	10.20	10.49
7.50	0	2.04	2.79	2.90	2.93	3.47	4.46	5.15	5.49	4.25	3.44	6.29	6.15	5.13	3.46	11.81	11.64	9.79
7.50	90	2.53	3.64	3.34	2.82	3.69	5.32	6.43	5.75	4.83	3.78	9.58	6.34	5.26	5.62	12.28	11.80	10.02
11.30	0	2.01	2.64	2.93	2.72	3.35	---	---	5.49	3.90	---	7.12	6.53	5.26	3.07	12.48	12.09	10.68
12.10	0	1.82	2.74	3.04	2.80	3.76	4.29	5.49	5.65	4.43	3.77	---	---	---	---	---	---	---
12.10	90	1.70	2.76	2.97	2.69	3.06	4.22	4.11	6.22	4.61	3.80	5.59	6.39	5.22	4.16	11.36	11.71	10.00
12.50	0	2.18		2.16	3.11	3.40	3.38	4.85	5.18	5.05	3.21	8.03	6.23	7.77	5.12	14.32	13.54	11.91

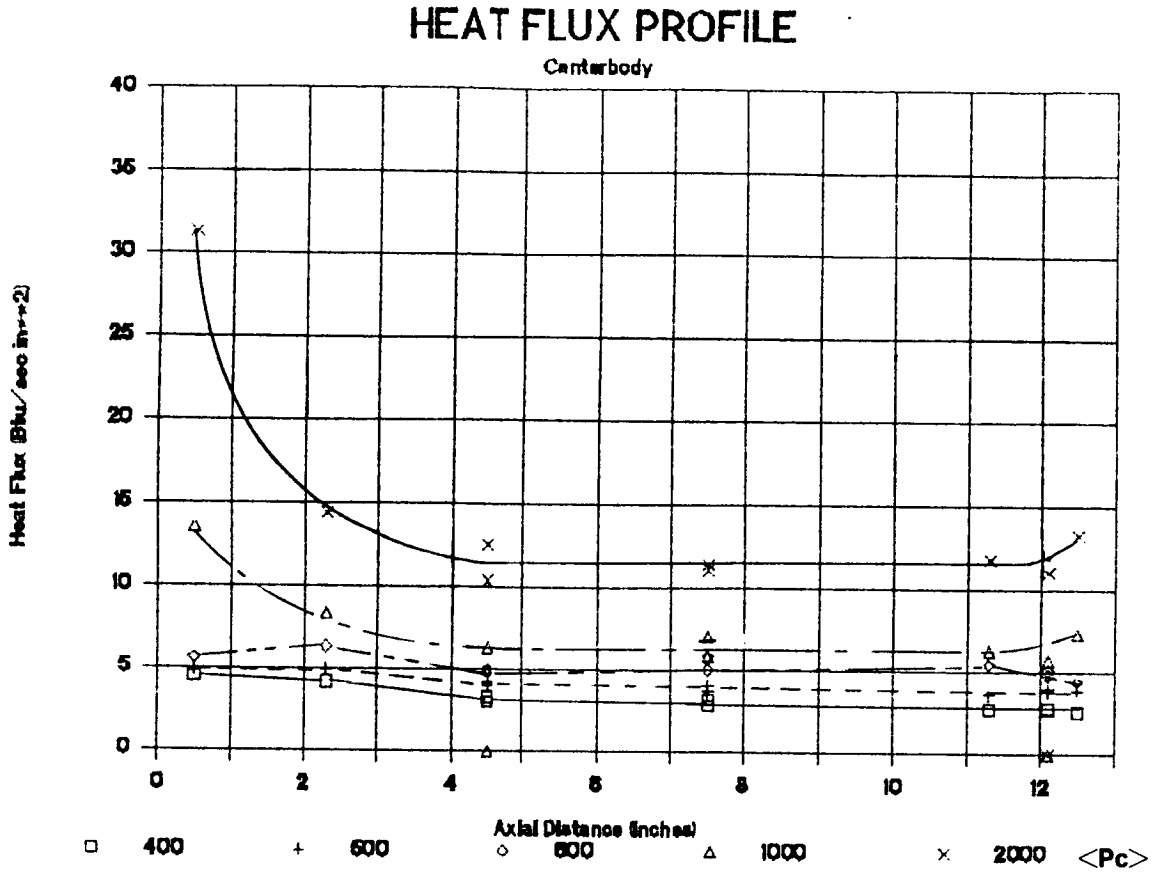

Figure 4.4.1-1. Heat Flux Profile - Centerbody

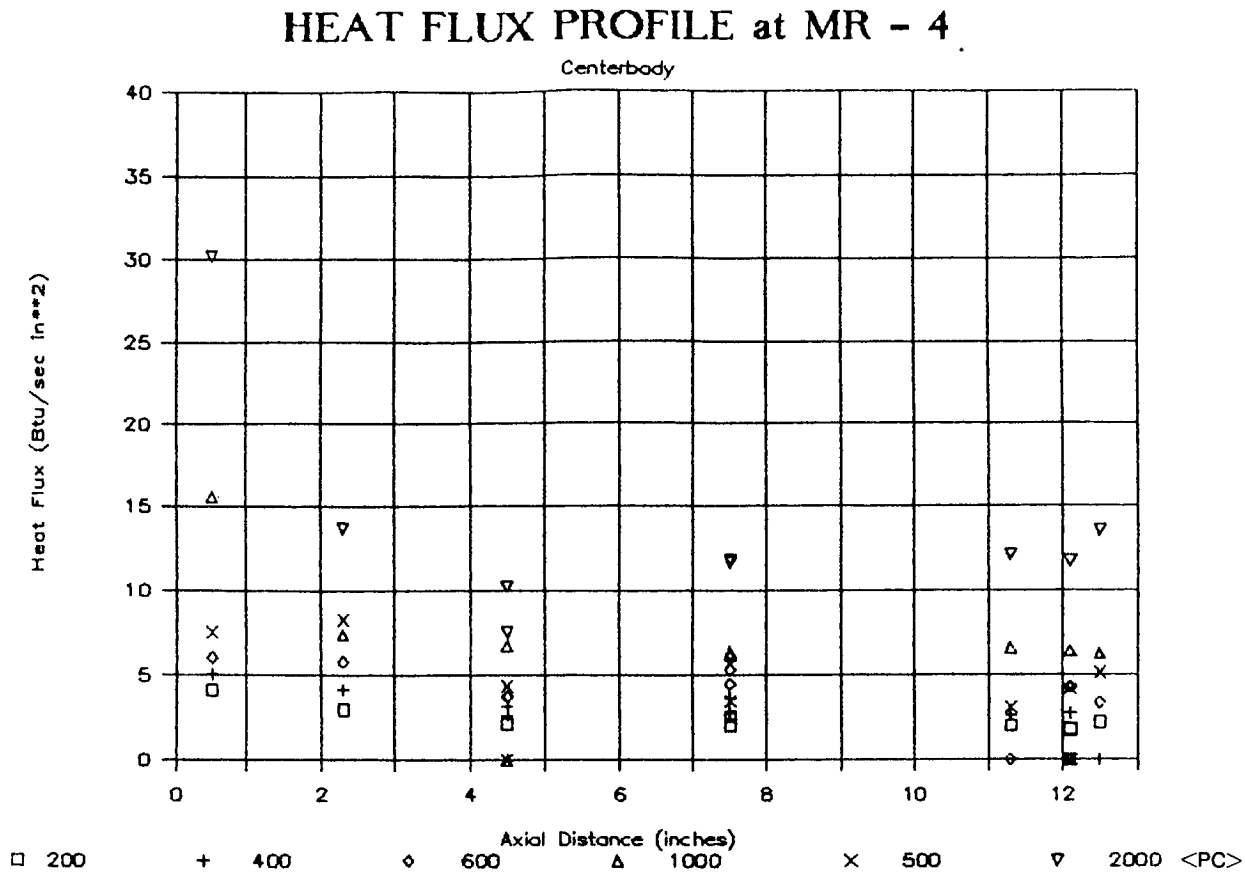

Figure 4.4.1-2. Heat Flux Profile at MR = 4 - Centerbody

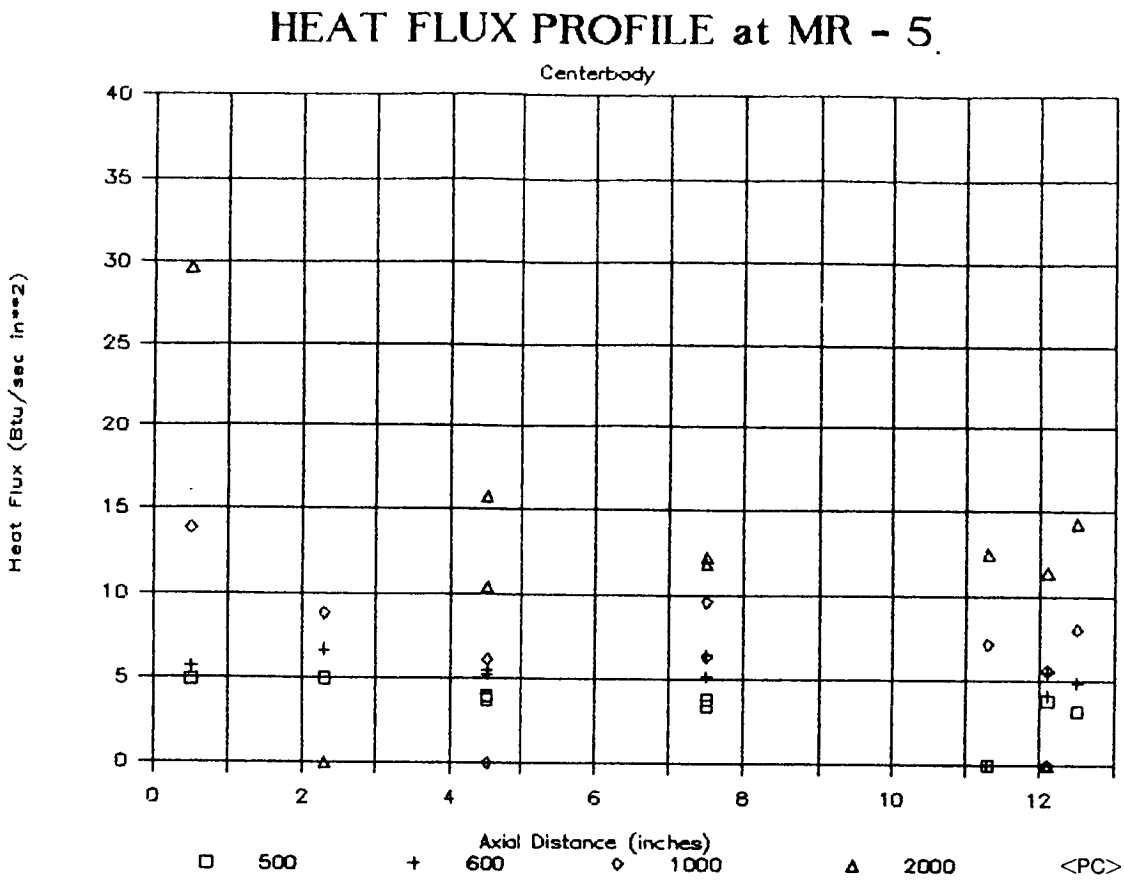

Figure 4.4.1-3. Heat Flux Profile at MR = 5 - Centerbody

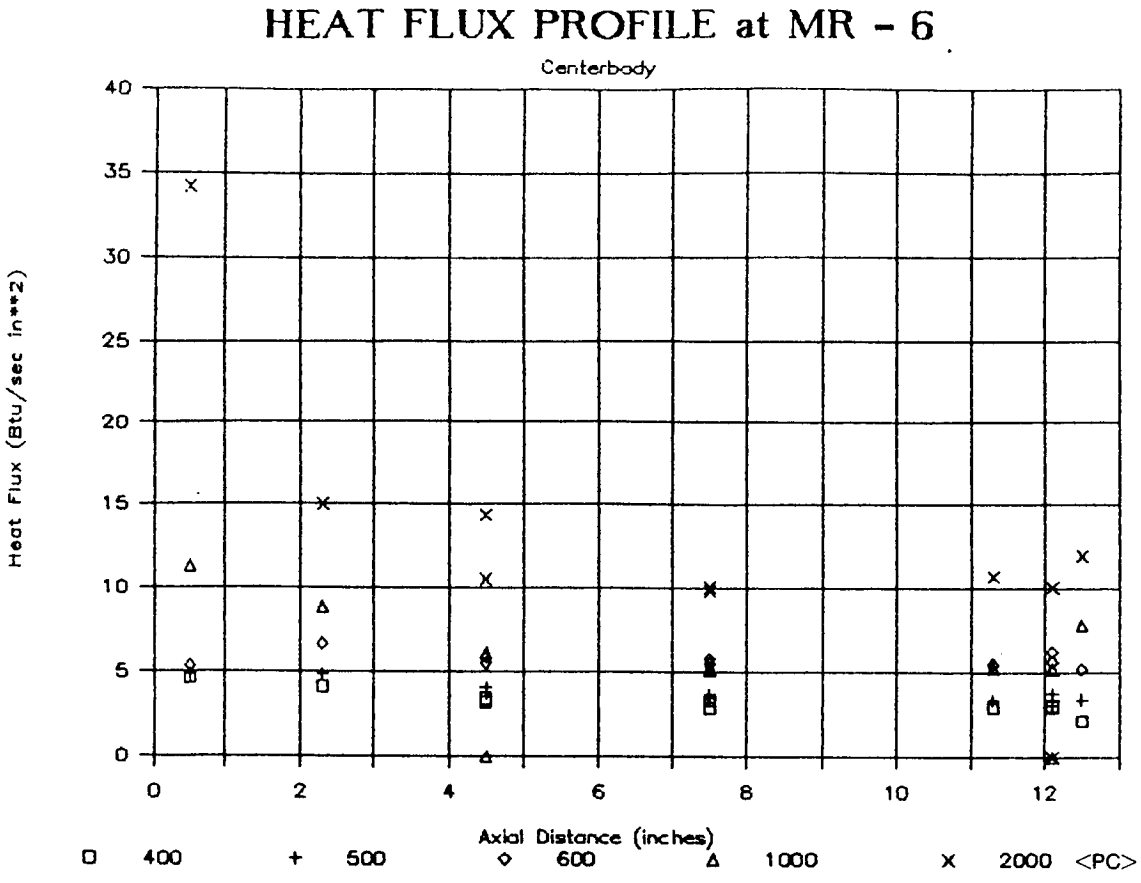

Figure 4.4.1-4. Heat Flux Profile at MR = 6 - Centerbody

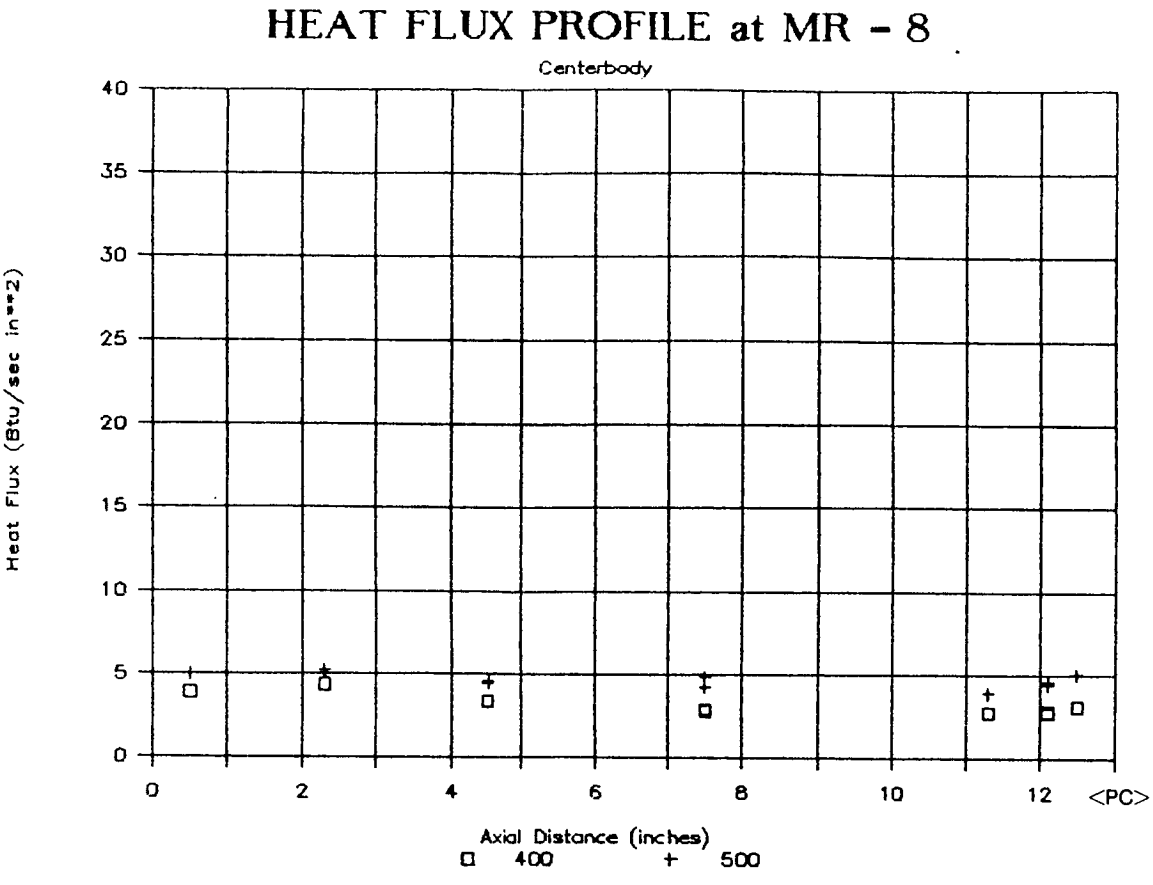

Figure 4.4.1-5. Heat Flux Profile at MR = 8 - Centerbody

to 2400). Figures 4.4.1-6 through 4.4.1-11 present the heat flux data versus Pc at each axial thermocouple location. Based on the centerbody heat flux data at the low pressure tests, the ability to achieve steady state duration tests at higher pressures tests can be evaluated.

Using the relationship of Flux = Pc** 0.8, a line has been drawn to the 0.8 slope on plots 4.4.1-6 through 4.4.1-11. The station nearest the injector face (0.5 inches) exhibited a very high heat flux based on one thermocouple. A visual examination of the centerbody in this area showed the thermocouple still submerged, so the reading was not due to the thermocouple protruding into the hot gas stream. The copper surface in this area was blanched but not visibly melted as would be expected if the high heat flux was general and not localized. There is a possibility of some error in the thermocouple reading, but this seems unlikely. There is also a possibility of a pattern irregularity in one or more injector elements near the thermocouple due to a hydrogen passage flow blockage. This could be verified by a cold flow test of the elements in the area of the thermocouple. Until a cold flow can be performed on the injector to assess element blockage, the consensus is that the high heat flux was real but localized and likely caused by contamination in the hydrogen circuit to one or more elements.

A second, smaller rise in flux is noted on the curved downstream face of the centerbody. There has been some concern expressed as to the presence of a stagnation area at the tip of the centerbody. Construction of the centerbody made provisions for variation of the length and proximity to the throat plane. In case high heat fluxes were encountered, the test plan initially had provision to vary the length to ensure a uniform environment. However, no further testing was conducted to study the environment around the centerbody tip.

With the exception of these two locations where the flux is higher, results of the heat fluxes from the high pressure tests show the predicted heat fluxes to be within 10 to 20% as shown in Table 4.4.1-II.

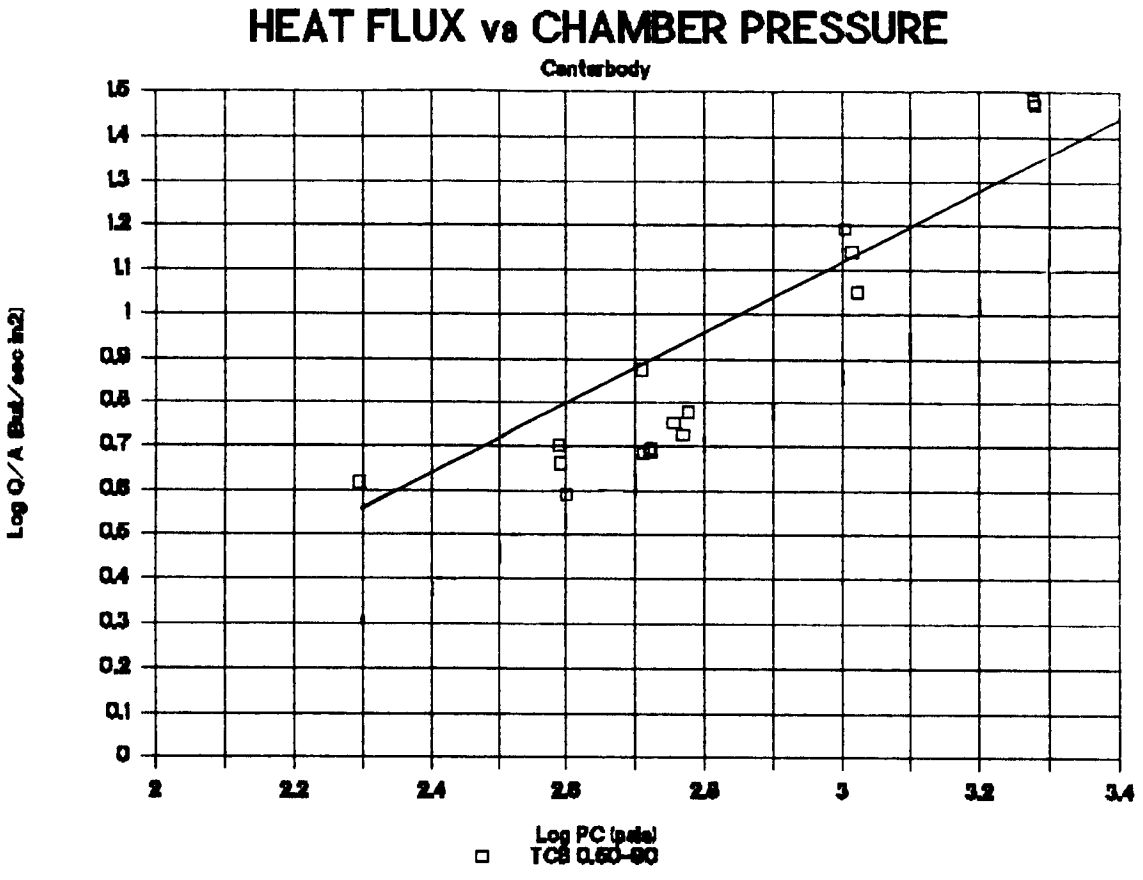

Figure 4.4.1-6. Heat Flux vs. Chamber Pressure at 0.5"

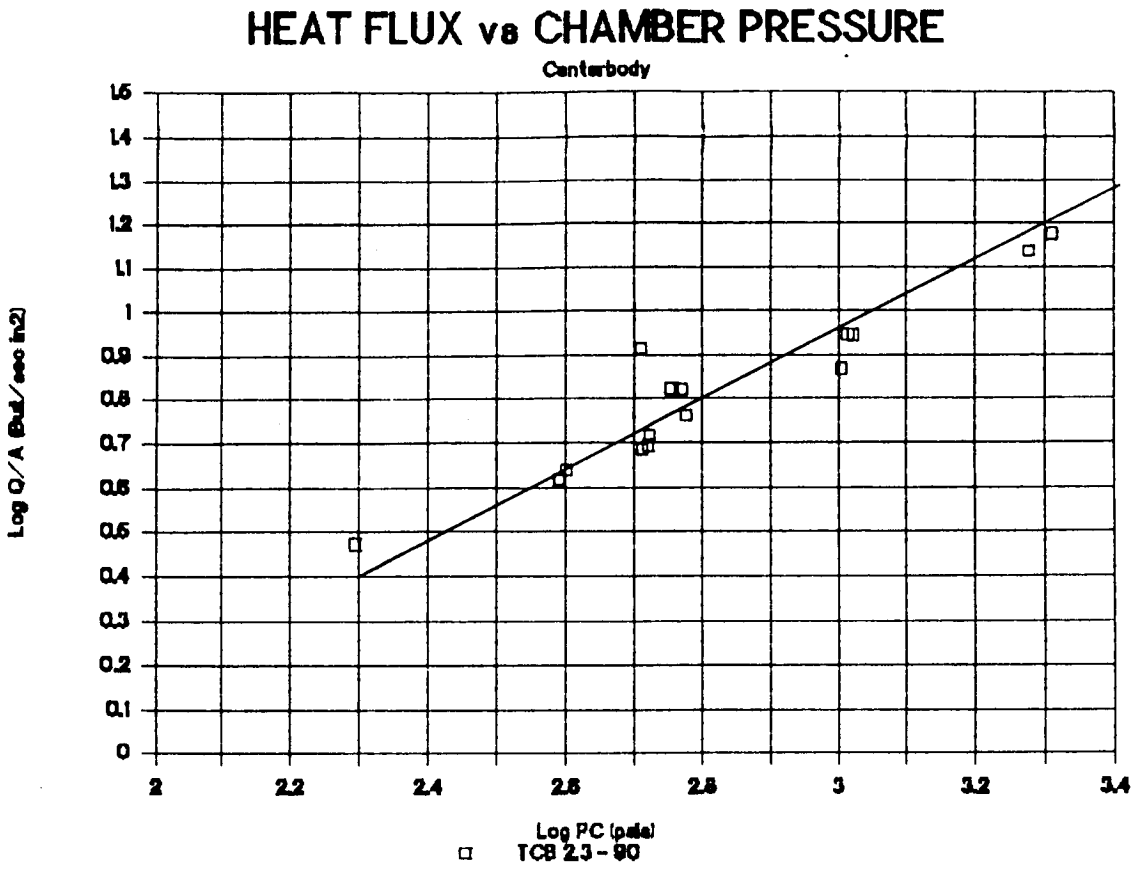

Figure 4.4.1-7. Heat Flux vs. Chamber Pressure at 2.3"

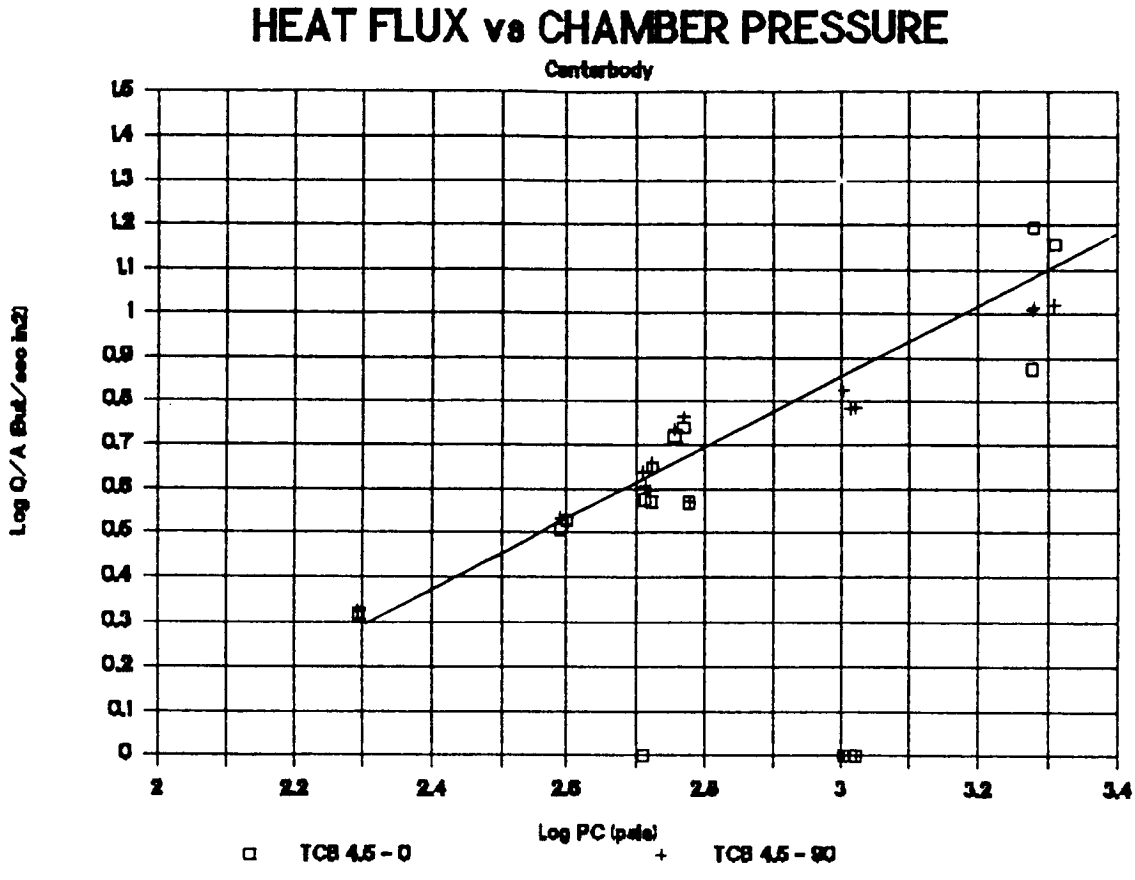

Figure 4.4.1-8. Heat Flux vs. Chamber Pressure at 4.5"

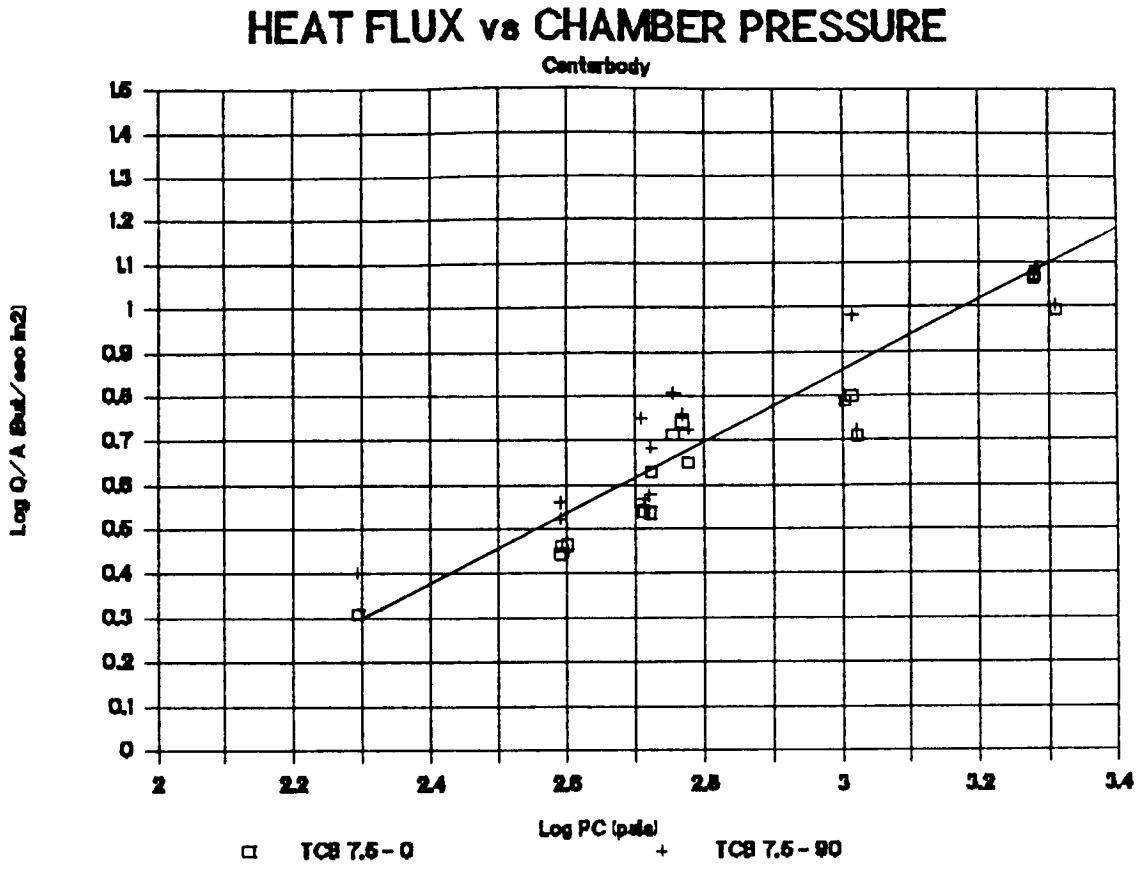

Figure 4.4.1-9. Heat Flux vs. Chamber Pressure at 7.5"

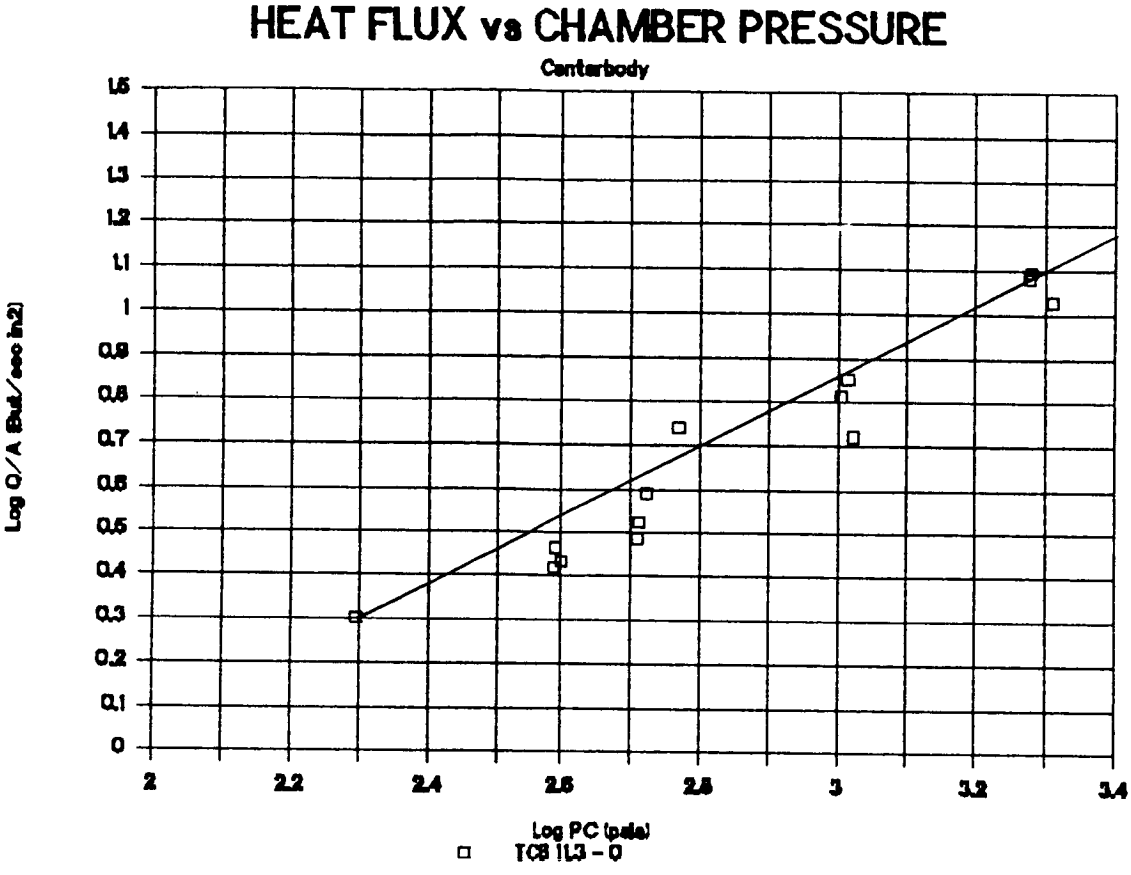

Figure 4.4.1-10. Heat Flux vs. Chamber Pressure at 11.3"

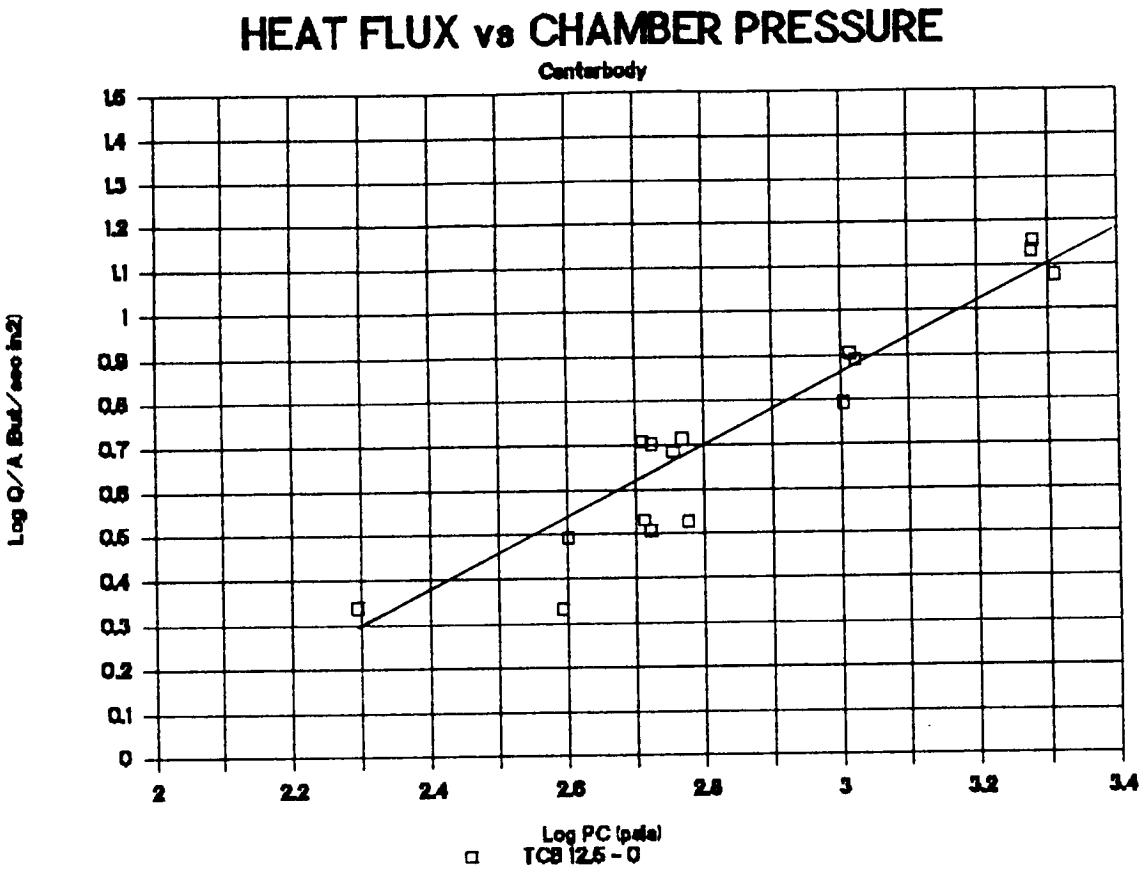

Figure 4.4.1-11. Heat Flux vs. Chamber Pressure at 12.5"

TABLE 4.4.1-II

CENTERBODY HEAT FLUX VALUES

TC Locations	Predicted Fluxes from low PC Tests	Actual Fluxes from High Pc Tests	%Δ
0.5	12.6	31.34	59.8%
2.3	15.8	14.36	-10.0
4.45	10.7	11.44	6.5
7.5	10.0	11.22	10.9
11.3	9.1	11.75	22.6
12.1	8.3	11.02	24.7
12.5	7.9	13.26	40.4

4.4.2 Total Heat Load to Outerbody

Table 4.4.2-I lists the heat flux summary for the outerbody. This data is presented in Figure 4.4.2-1 cross data plotted versus axial distance from the injector face. A uniform increase in flux is noted with increasing chamber pressure. The range of mixture ratios (4-8) tested are presented in Figure 4.4.2-1. No discernable effect was noted from the mixture ratio variance. Figures 4.4.2-2 through 4.4.2-5 separate the data into respective mixture ratio ranges.

Results of the low Pc test series were plotted as heat flux versus Pc in order to project the flux profiles for the series of high Pc tests (Pc = 2000 to 2400). Figures 4.4.2-6 through 4.4.2-15 present the heat flux data versus Pc at each axial thermocouple location. Evaluation of the curves from the low Pc tests also assist in determining if the outerbody configuration is adequate. Based on the outerbody heat flux data at the low pressure tests, the ability to achieve steady state duration tests at higher pressure tests can be evaluated. Using the relationship of Flux $\equiv$ Pc** 0.8, a line has been drawn of the 0.8 slope on plots 4.4.2-6 through 4.4.2-9. The data in Figures 4.4.2-10 through 4.4.2-15 indicate either a different slope or a slope change. In the convergent section this is the result of different boundary layer regimes for three different chamber pressure ranges, as illustrated in Figure 4.4.2-15. At low chamber pressures and Reynolds numbers the boundary layer can undergo a reverse transition from turbulent to laminar due to a significant history of high flow acceleration; in this regime the heat flux should be proportional to Pc 0.5. At intermediate chamber pressures the boundary layer is in the transition regime and heat flux is very sensitive to pressure. At high chamber pressures the boundary layer remains turbulent, but heat fluxes are lower than would be expected with no flow acceleration.

The station nearest the injector face (0.5 inches) exhibited a slightly higher heat flux based on one thermocouple. With the exception of this location where the flux is higher, results of the heat fluxes from the high pressure tests show the predicted heat fluxes to be within 10% as shown in Table 4.4.2-II. Unfortunately many of the thermocouples were inoperative by the time these tests were run.

Table 4.4.2-I. OTV Hot Fire Tests - Outerbody Heat Flux

OTV HOT-FIRE TESTS
HEAT FLUX
(Btu/sec in2)

TEST NO.		140	144	145	146	147	149	150	151	154	155	108	109	110	111	113	114	115
MR		4.1	4.4	5.8	8.3	6.2	4.2	5.3	6.5	7.5	5.4	4.6	3.9	5.7	4.3	4.7	4.0	5.9
Pc		197	390	391	400	517	600	570	588	529	526	1032	1009	1051	514	1908	1896	2044
OUTERBODY TCO																		
0.75	0	3.09	4.22	3.98	3.99	4.74	6.08	6.20	6.19	5.05	4.86	8.70	8.82	8.30	6.44	12.90	13.67	12.82
0.75	90	2.76	4.03	3.74	4.15	4.46	5.79	5.75	5.38	4.95	4.56	8.63	8.99	8.17	6.05	13.10	14.14	12.06
2.60	0	2.62	3.55	3.96	4.35	4.60	4.88	6.25	5.87	5.34	4.14	7.27	7.12	7.88	6.66	12.47	12.17	11.66
2.60	90	2.74	3.77	4.10	4.68	4.82	5.00	6.50	6.03	5.62	4.46	7.43	7.31	7.93	---	---	---	---
4.75	0	2.01	2.97	3.05	4.13	4.41	4.85	4.25	6.07	4.34	3.53	6.89	7.12	7.21	6.21	12.51	11.91	11.39
4.75	90	2.04	2.97	3.35	4.07	4.38	4.89	4.76	5.39	4.96	3.64	6.99	7.04	7.24	5.98	---	---	---
7.80	0	1.43	2.78	2.77	3.76	4.47	4.43	5.39	4.60	4.83	3.37	6.97	6.34	7.55	6.48	---	---	---
7.80	90	1.71	3.06	3.31	3.77	4.54	5.24	5.88	6.23	4.38	3.49	7.98	7.43	7.51	5.79	---	---	---
10.10	0	9.74	5.44	4.32	3.43	4.28	6.74	8.42	7.10	5.91	4.58	8.45	9.52	8.38	9.73	---	---	---
10.10	90	2.45	4.46	4.06	4.07	4.78	6.30	7.52	7.59	5.81	4.86	---	---	---	---	---	---	---
11.85	0	2.14	2.81	3.25	3.76	3.84	4.10	4.99	6.07	4.20	3.71	---	6.05	5.84	5.34	---	---	---
11.85	90	2.03	---	---	---	---	---	---	---	---	---	---	---	---	---	---	---	---
13.00	0	---	1.88	2.58	2.73	3.50	5.83	6.58	6.70	4.47	3.69	---	8.73	7.79	5.71	---	---	---
13.00	90	---	2.96	2.40	3.00	3.83	4.97	6.40	6.19	4.39	3.91	---	8.63	8.27	3.37	---	---	---

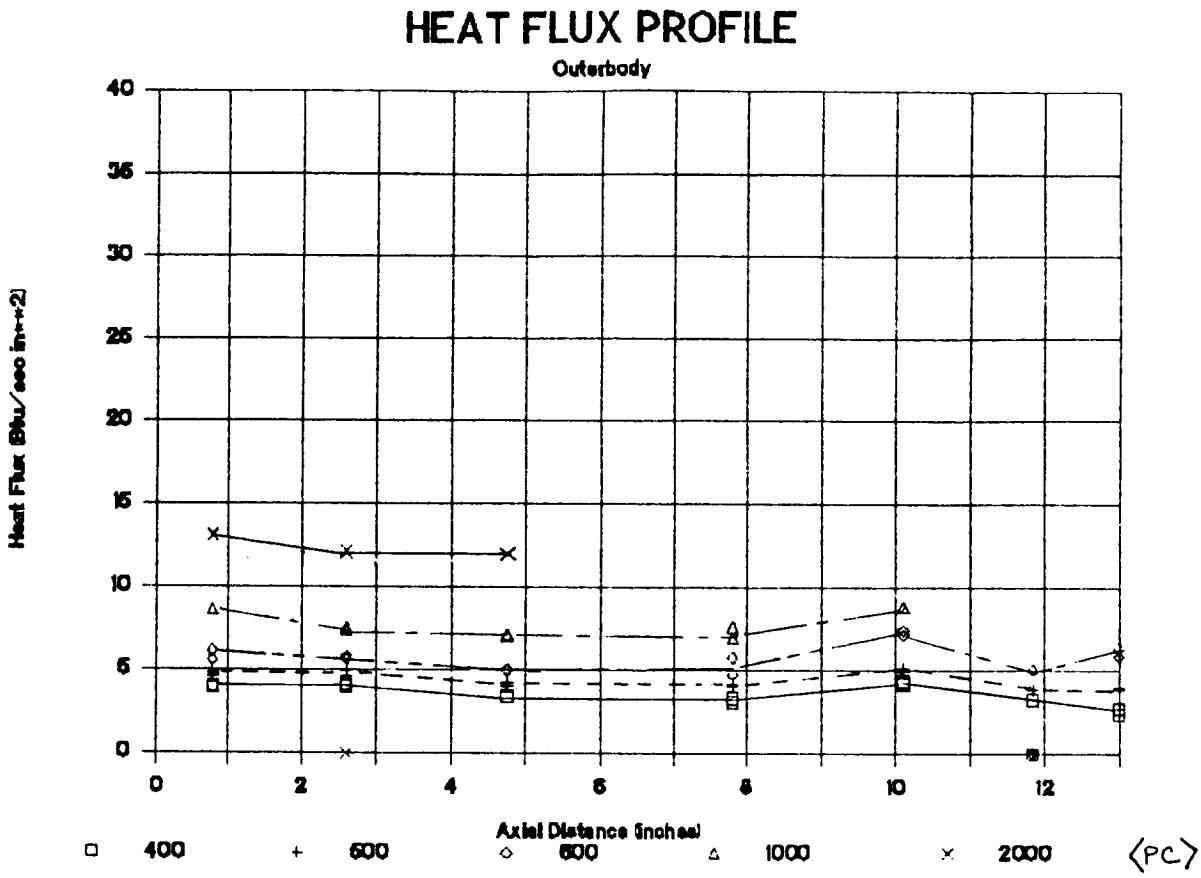

Figure 4.4.2-1. Heat Flux Profile - Outerbody

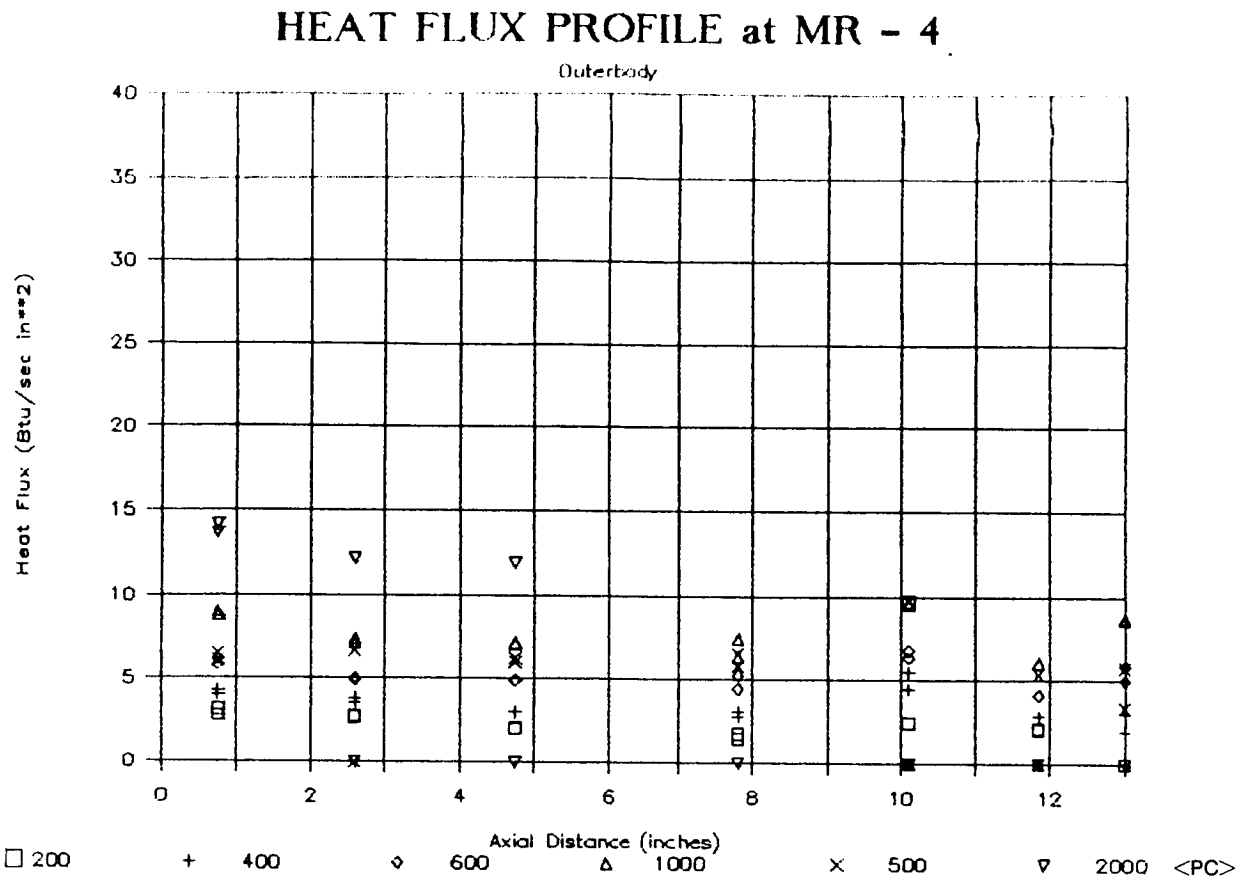

Figure 4.4.2-2. Heat Flux Profile at MR = 4 - Outerbody

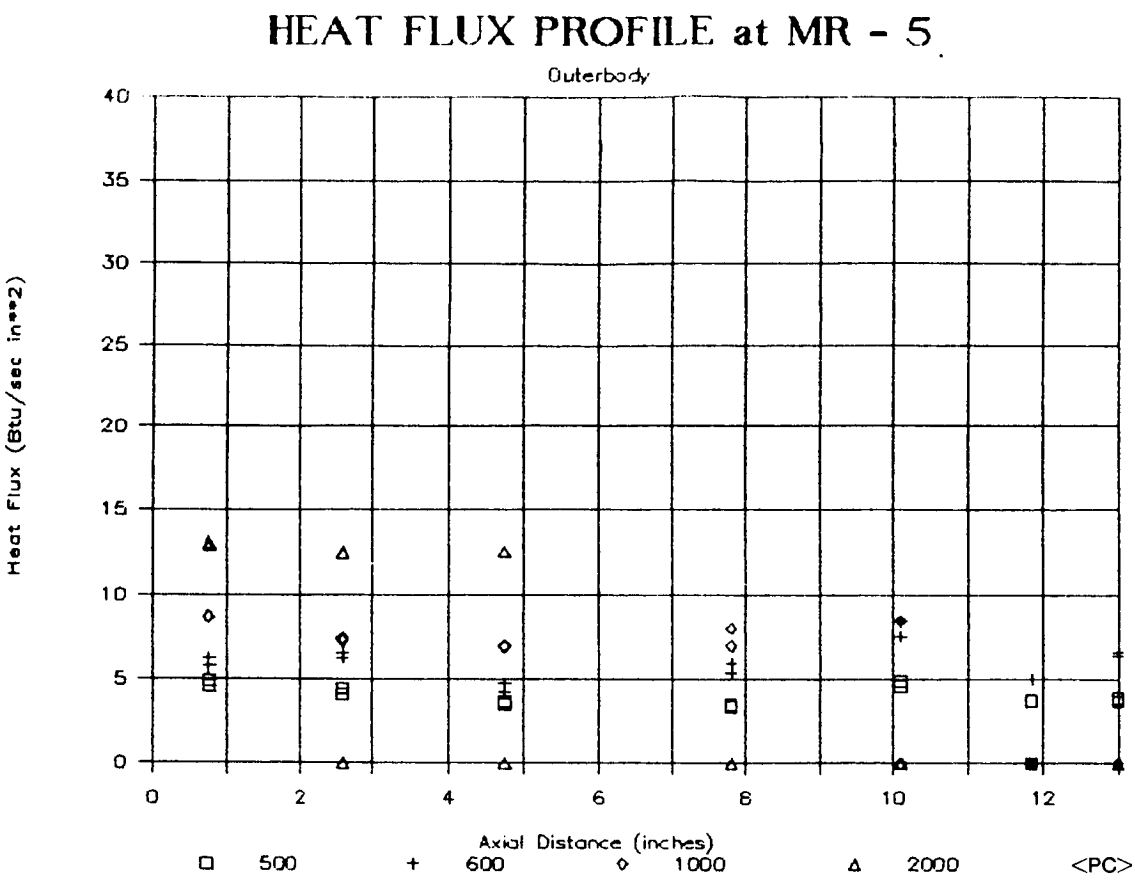

Figure 4.4.2-3. Heat Flux Profile at MR = 5 - Outerbody

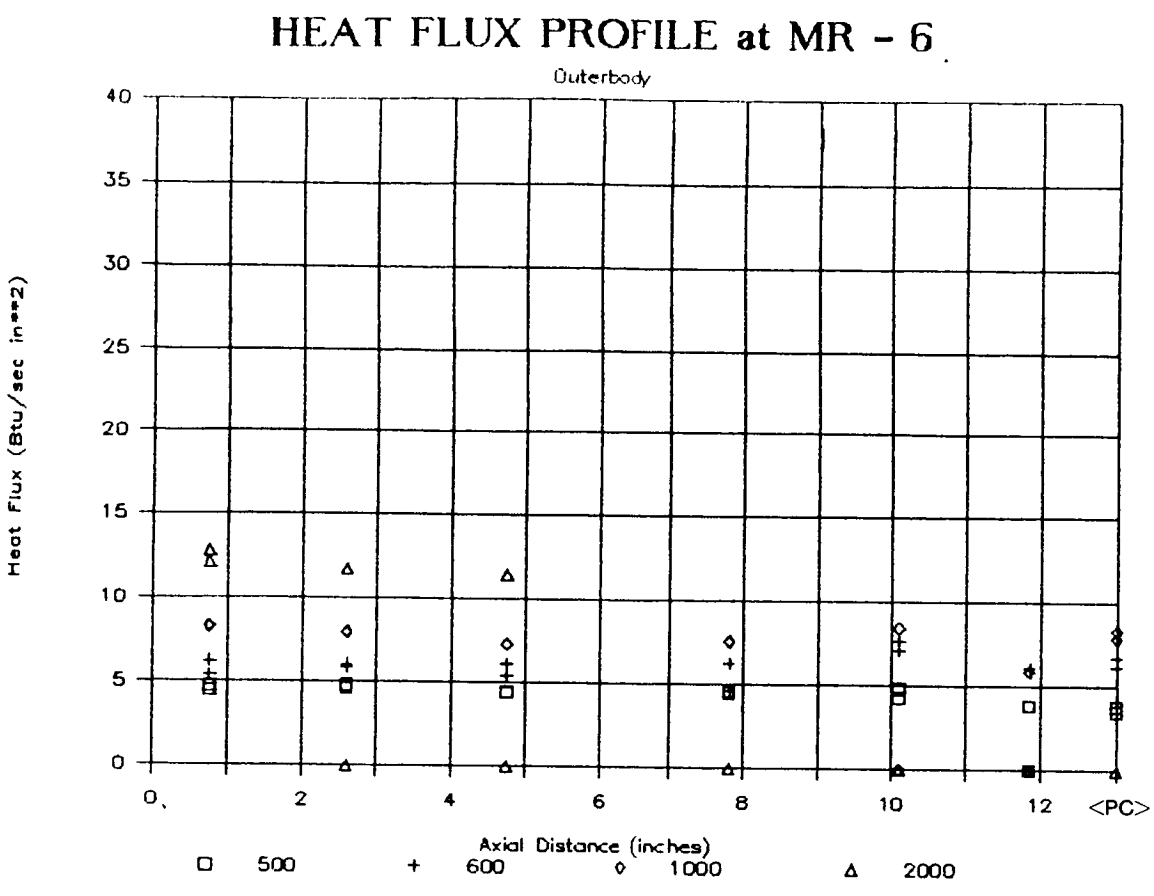

Figure 4.4.2-4. Heat Flux Profile at MR = 6 - Outerbody

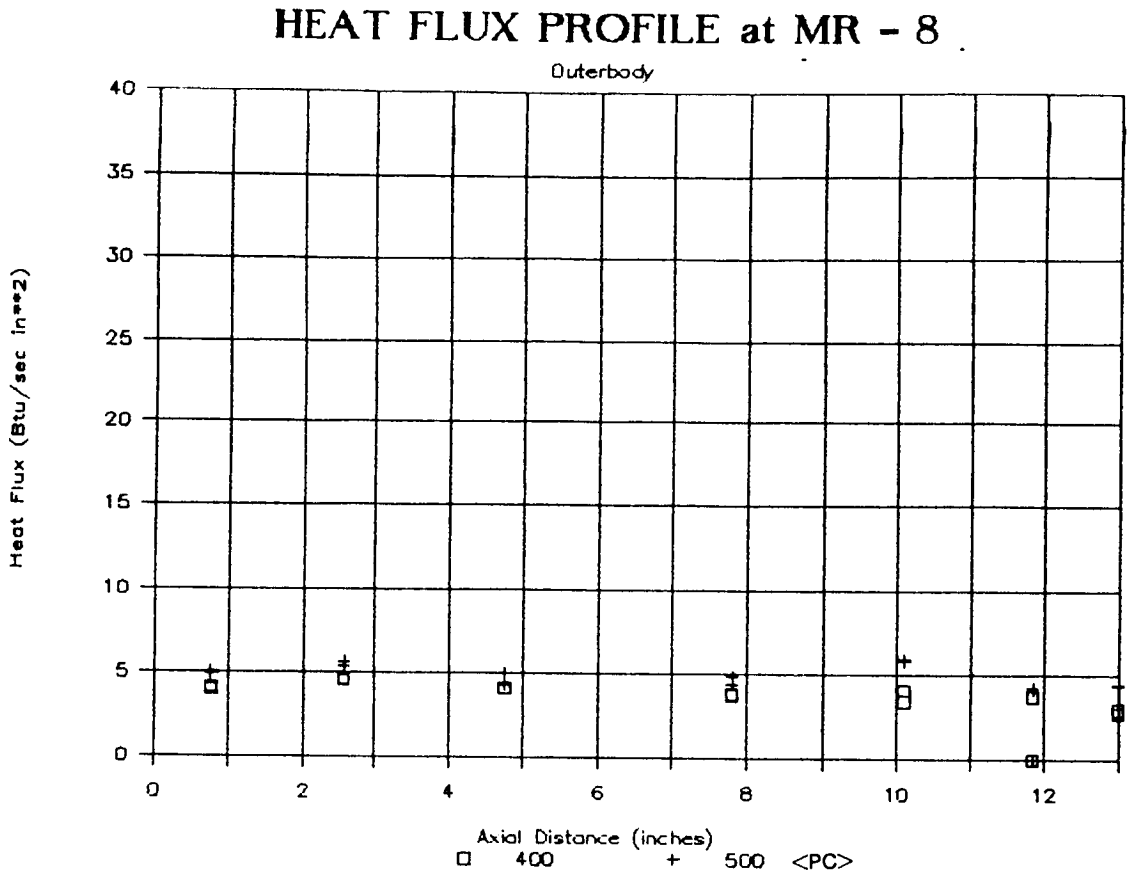

Figure 4.4.2-5. Heat Flux Profile at MR = 8 - Outerbody

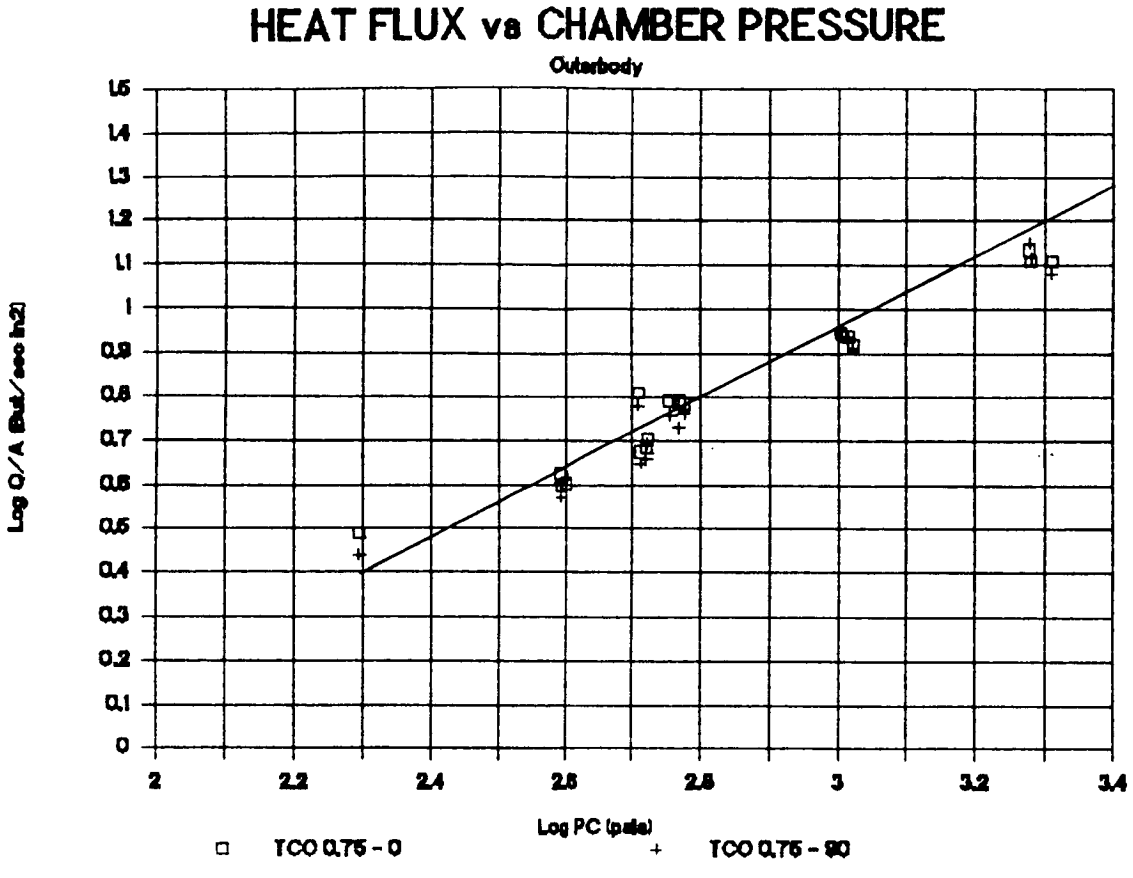

Figure 4.4.2-6. Heat Flux vs. Chamber Pressure at 0.75"

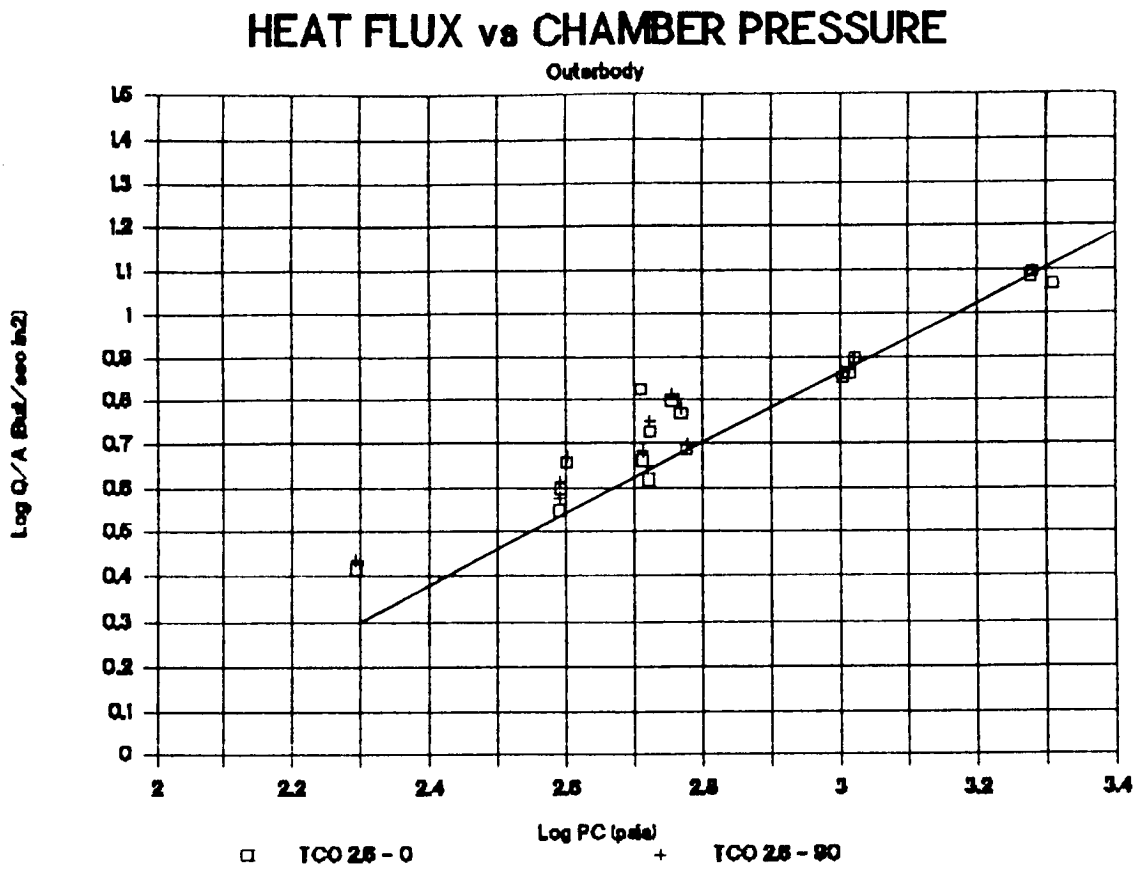

Figure 4.4.2-7. Heat Flux vs. Chamber Pressure at 2.5"

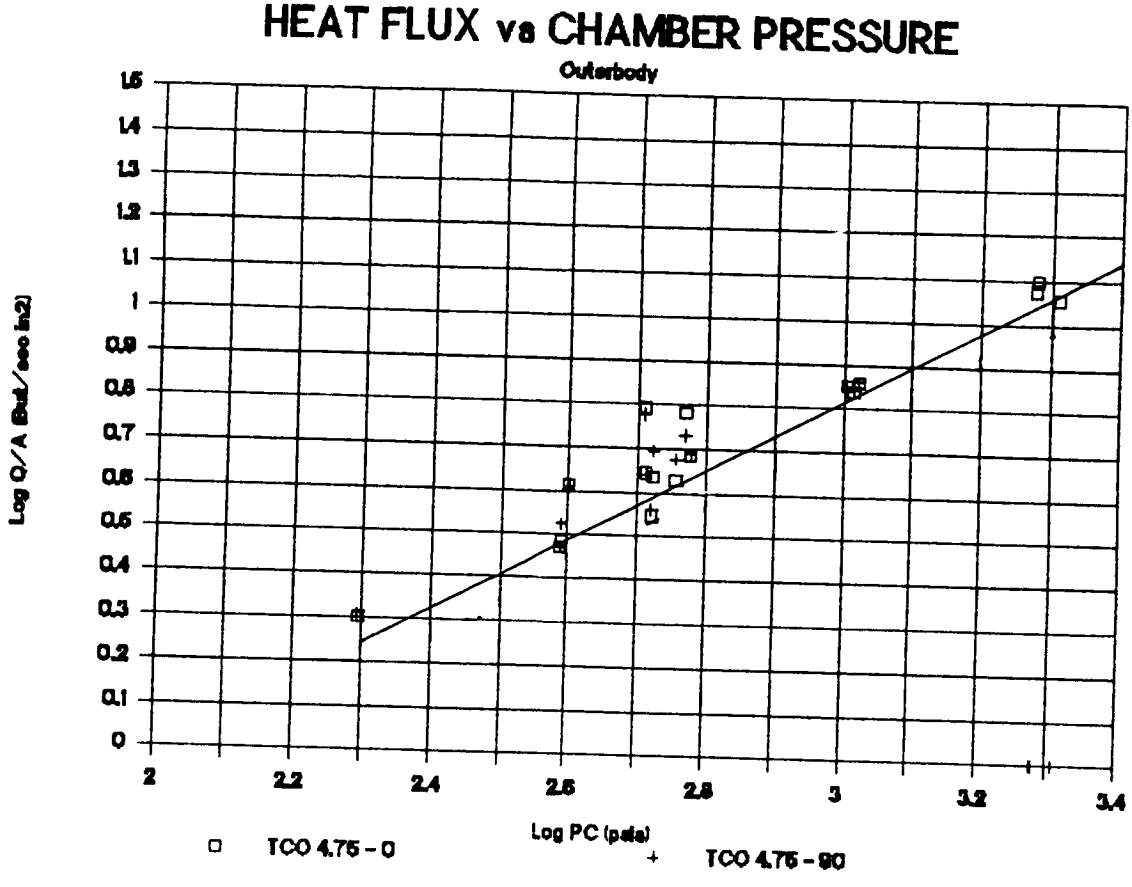

Figure 4.4.2-8. Heat Flux vs. Chamber Pressure at 4.75″

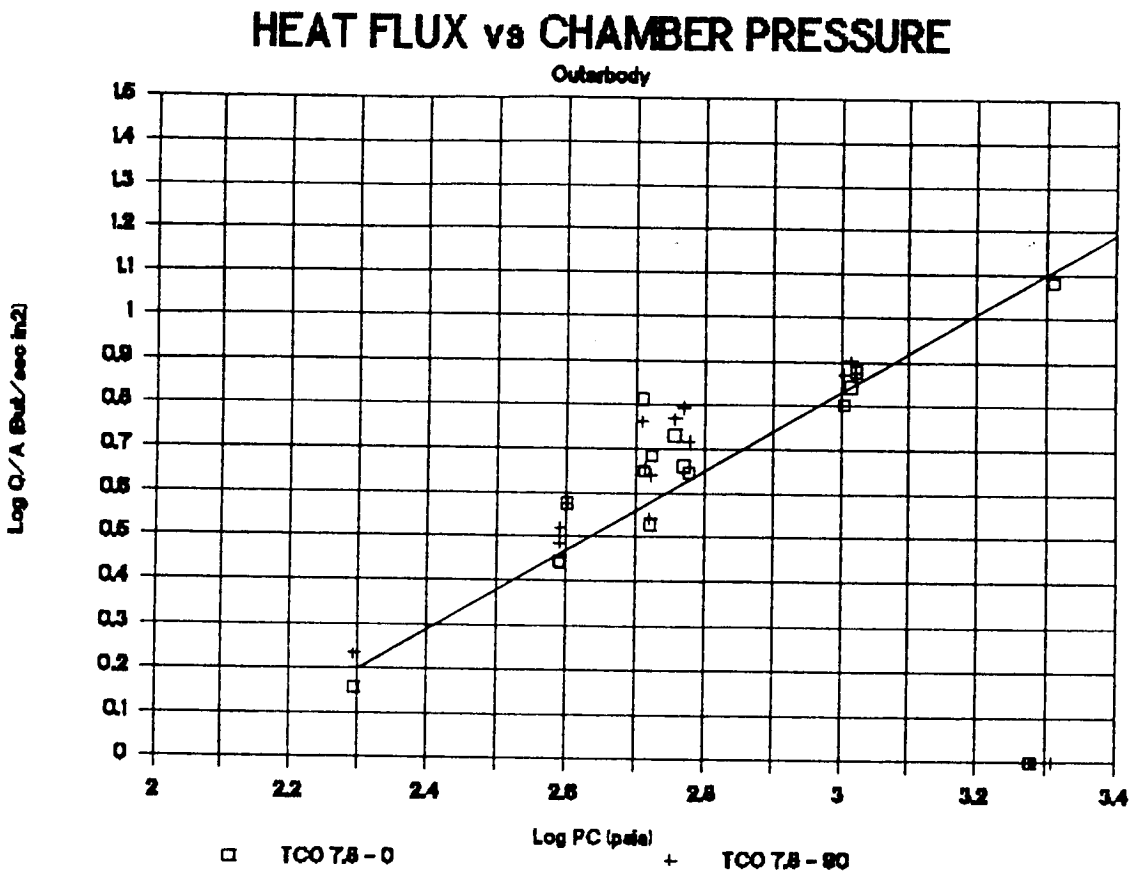

Figure 4.4.2-9. Heat Flux vs. Chamber Pressure at 7.8"

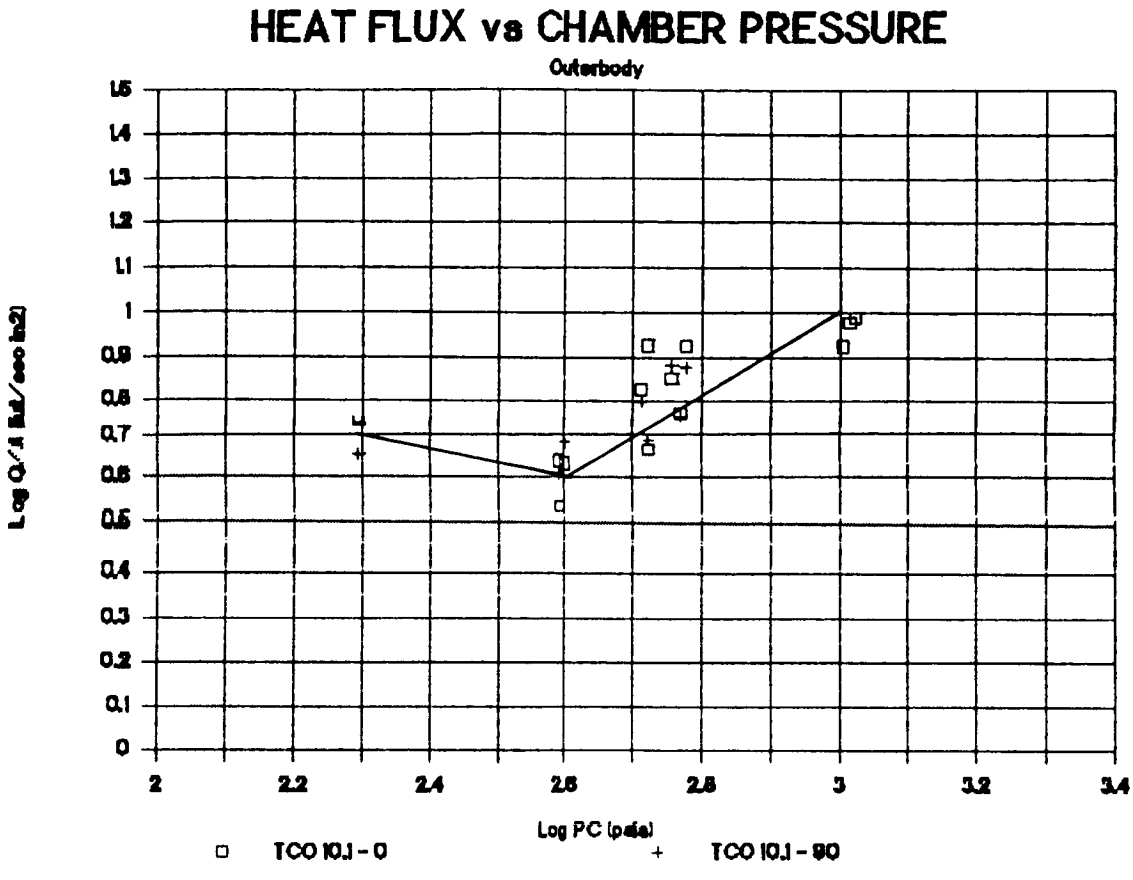

Figure 4.4.2-10. Heat Flux vs. Chamber Pressure at 10.1"

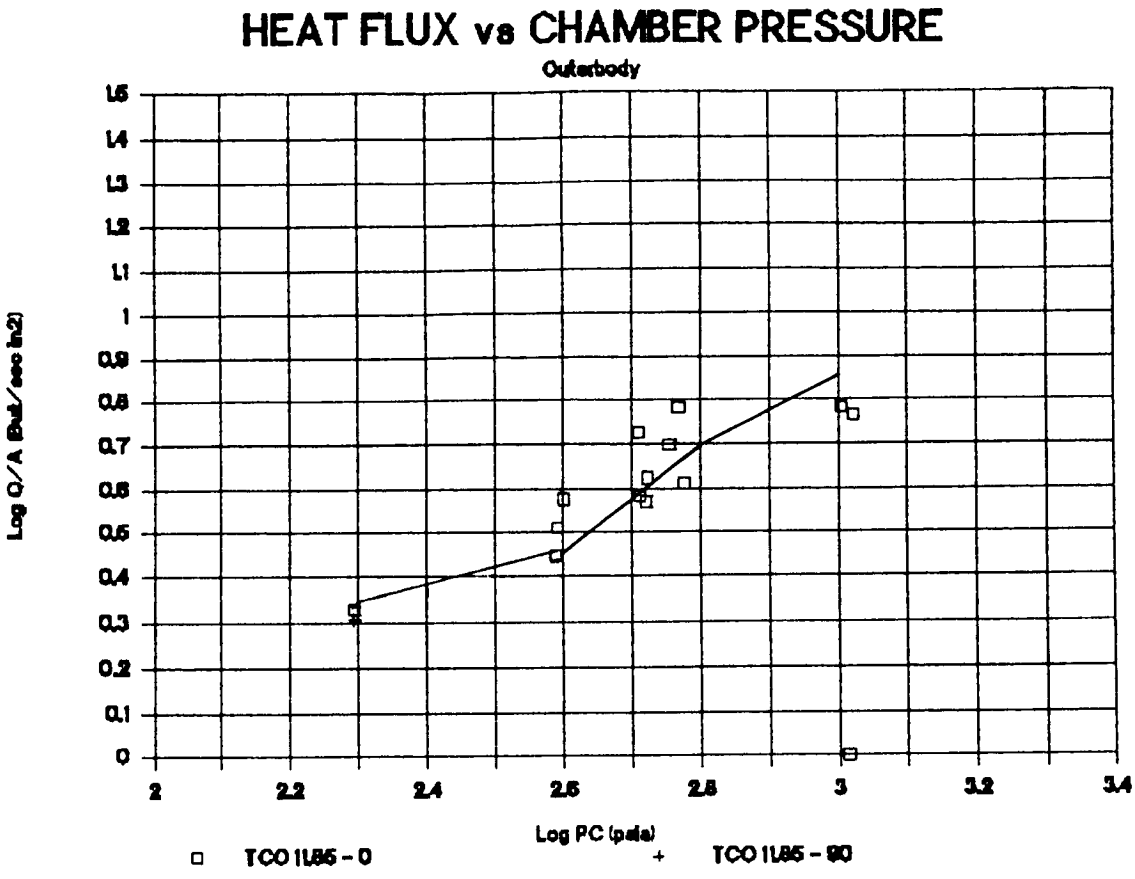

Figure 4.4.2-11. Heat Flux vs. Chamber Pressure at 11.85"

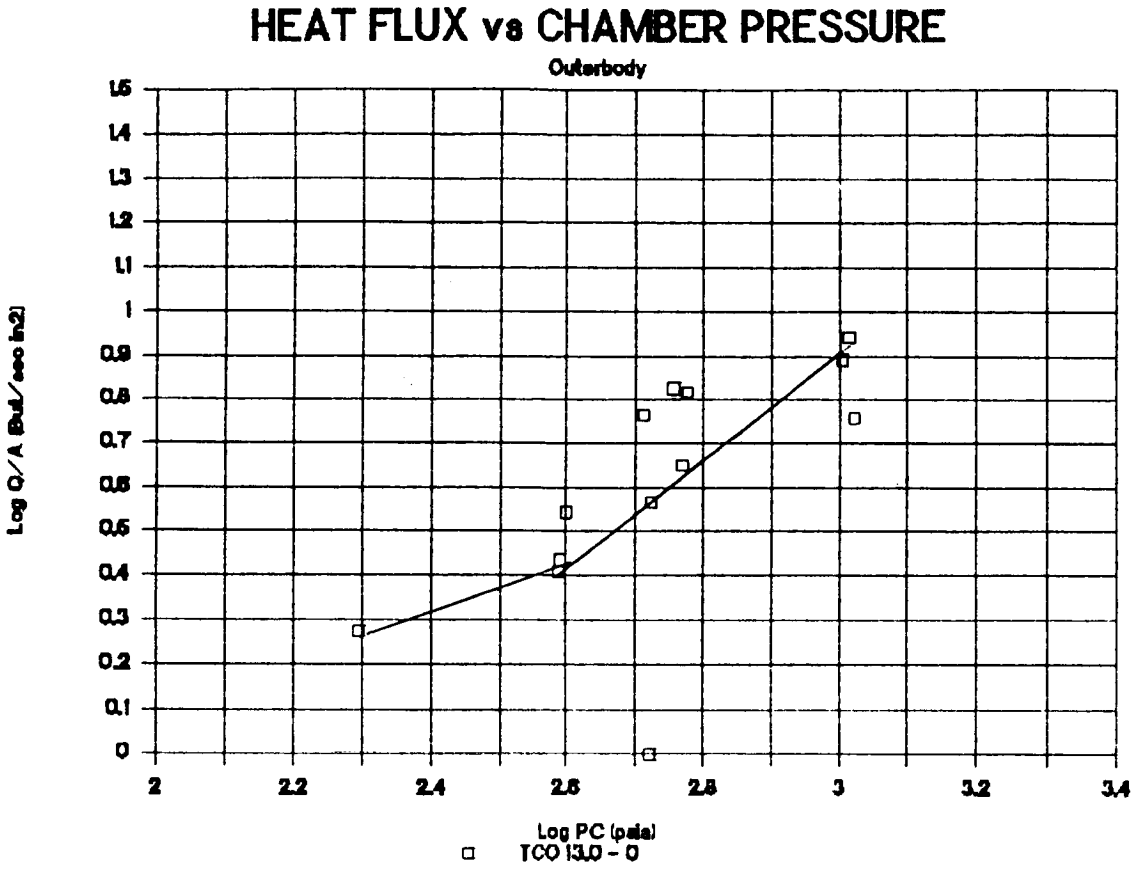

Figure 4.4.2-12. Heat Flux vs. Chamber Pressure at 13.0"

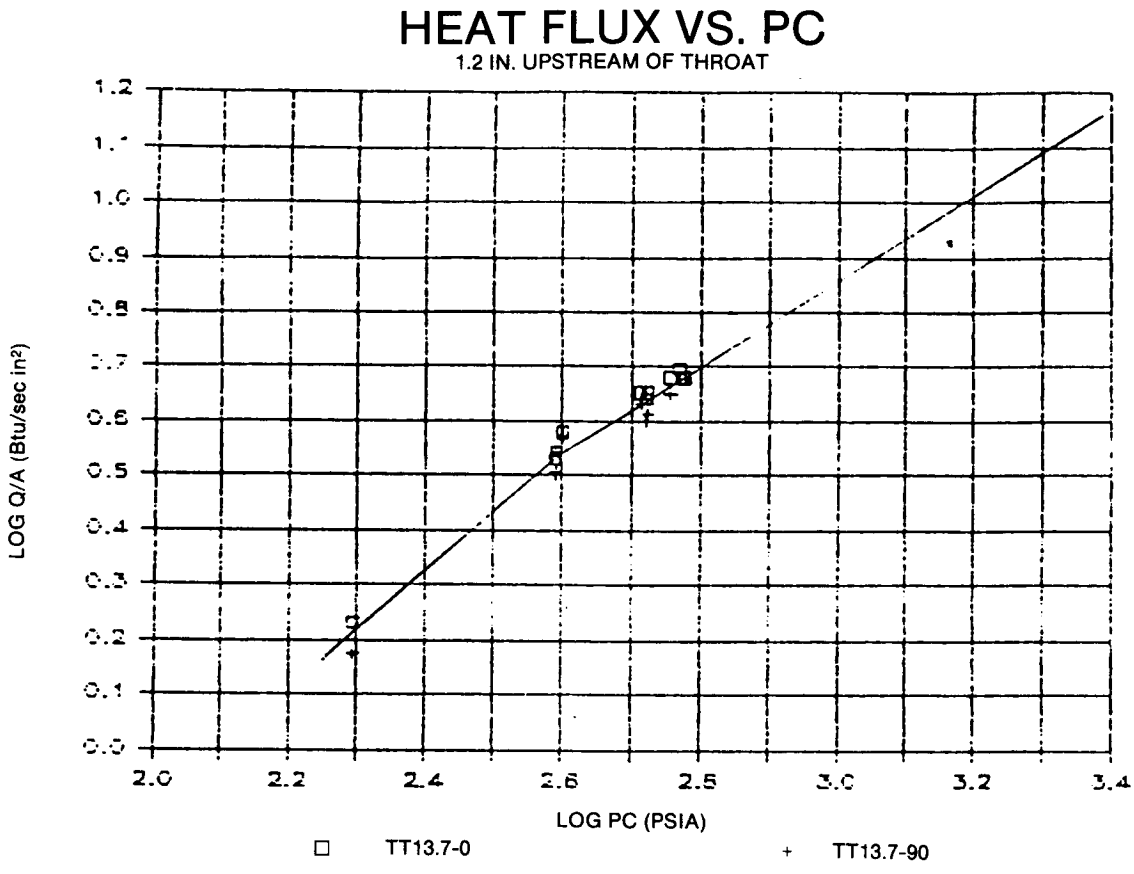

Figure 4.4.2-13. Heat Flux vs. Chamber Pressure at Throat - 13.7

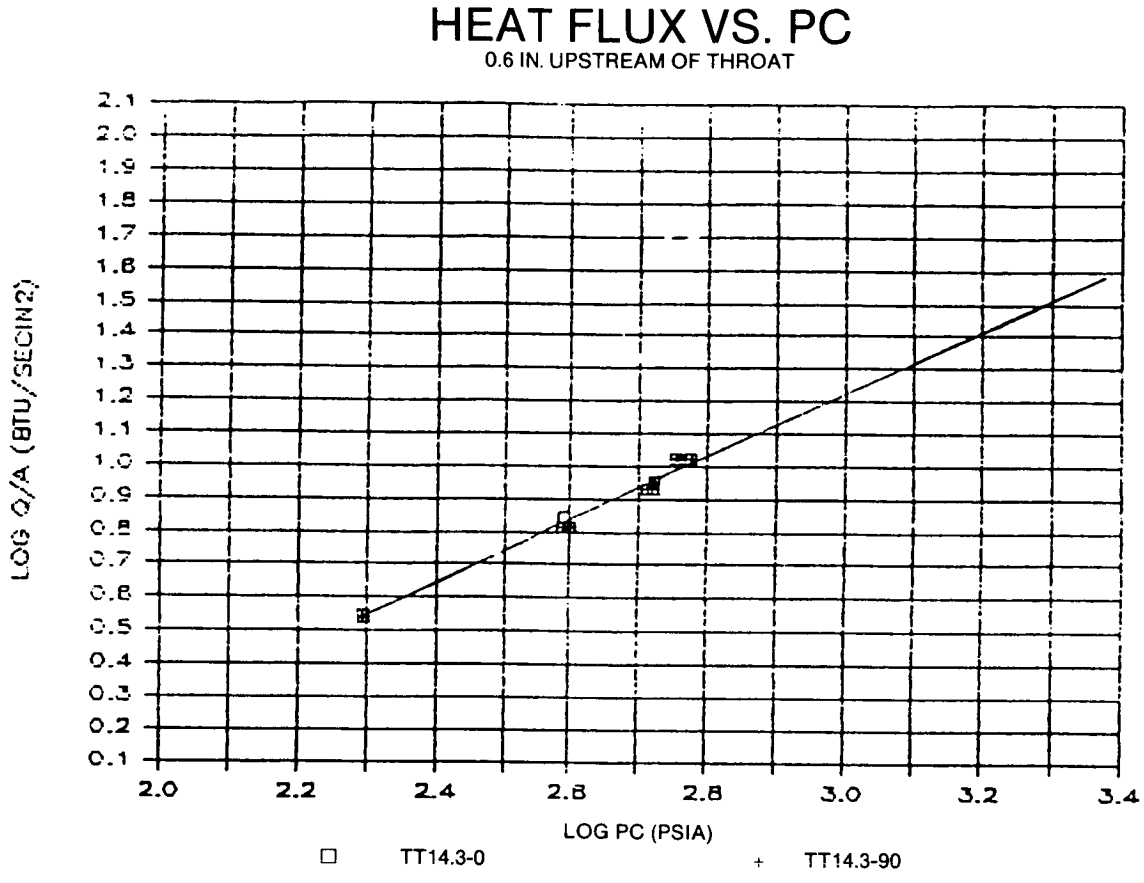

Figure 4.4.2-14. Heat Flux vs. Chamber Pressure at Throat - 14.3

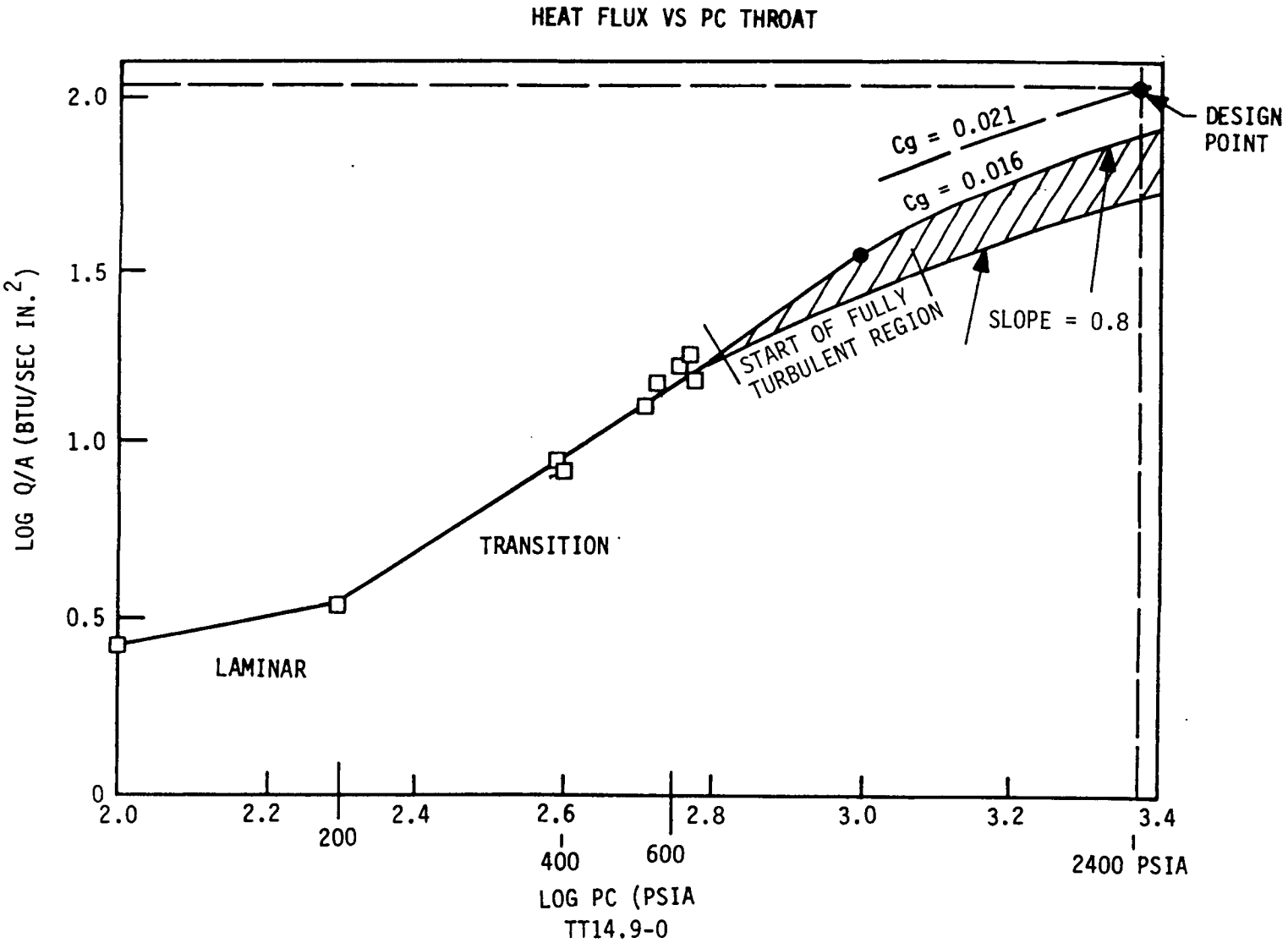

Figure 4.4.2-15. Heat Flux vs. Chamber Pressure at Throat - 14.9

TABLE 4.4.2-II

OUTERBODY HEAT FLUX VALUES

Location	Predicted Fluxes from Low PC Tests	Actual Fluxes from High PC Tests	% Δ
0.75	14.1	13.12	-7.5
2.8	12.6	12.1	-4.1
10.1	12.6		
11.85	8.7		

C-3

Figures 4.4.2-16 through 4.4.2-18 give the pipe flow heat transfer correlation coefficient (Cg) axial profiles for various MR levels. The Cg value is obtained from the measured heat flux as follows:

$$Cg: \quad = \frac{\Phi_w \; Re_f^{0.2} \; Pr_f^{0.6}}{\rho_f \mu_e \, cp_f \, (T_{aw} - T_w)}$$

Φ_w = measured heat flux from thermocouple transient analysis

Re = Reynolds number, $\rho_f \mu_e D/\mu_f$

Pr = Prandte number

ρ = Density

μ_e = Freestream velocity

c_p = specific heat

T_{aw} = Theoretical adiabatic wall temperature

T_w = Wall temperature corresponding to Φ_w

Subscript f devotes property evaluation at a film temperature defined as the average of adiabatic wall and actual wall temperatures. A cg of 0.026 corresponds to the simplified Bartz equation.

All the Cg values appear to fall within a definitive region, averaging 0.04 for the outerbody and dropping off to 0.01 at the entrance to the throat. The Cg's were calculated at a 800 degree F wall temperature. A listing of the values are given in Table 4.4.2-III. Figure 4.4.2-15 presents the throat heat flux and includes the Cg throat values. Based on the consistency of the Cg data, actual heat fluxes at the throat were in the range of 60-80 Btu/sec in^2, Predicted valves have been in the range of 100 Btu/sec in^2.

4.4.3 LH_2 Cooled Throat Performance

The LH_2 cooled throat hardware was designed to mate with the heat sink chamber. The nozzle contour was designed to allow full flow at chamber pressures above 400 psia. A 15 degree half angle nozzle exit cone with a 10:1 expansion ratio was selected in order to obtain coolant bulk temperatures in the

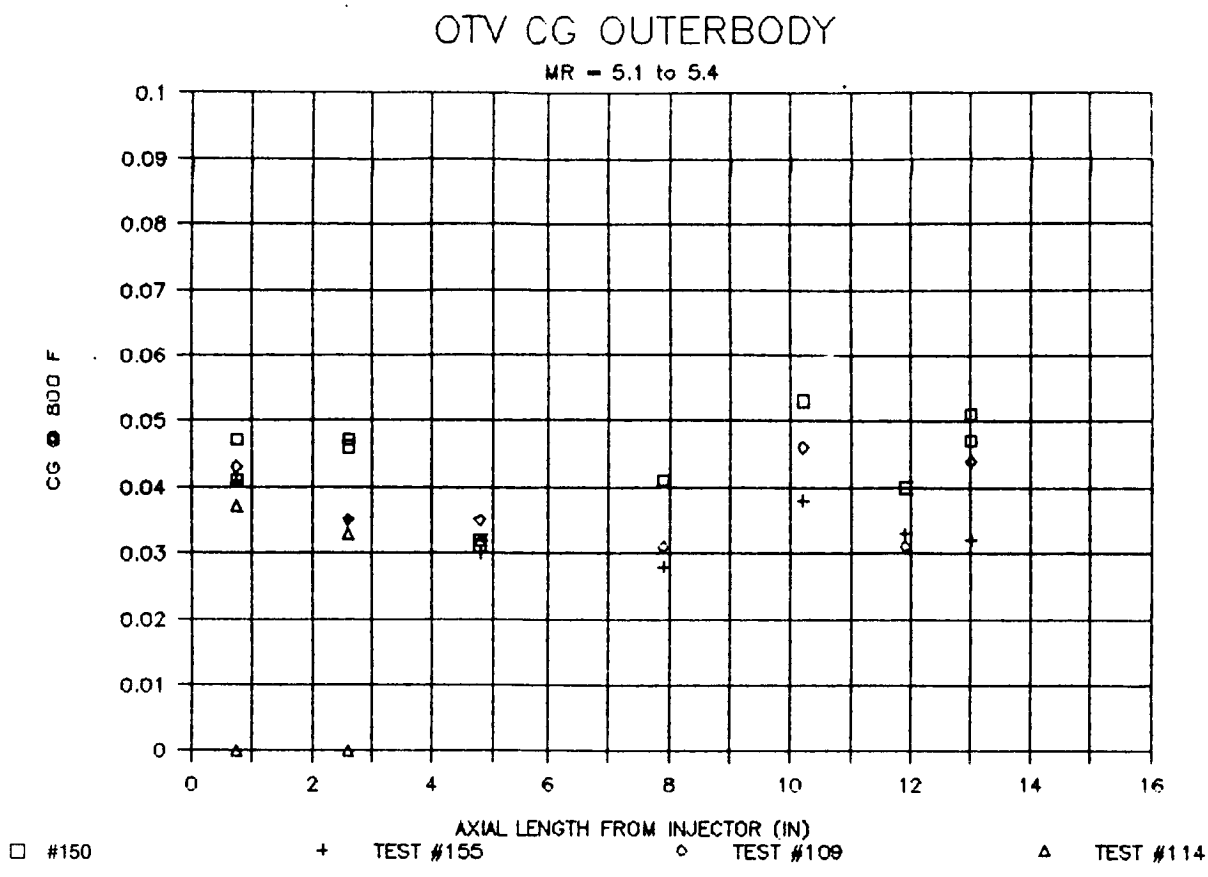

TC #	CG
0.75	0.041
2.60	0.042
4.75	0.035
7.80	0.036
10.10	0.044
11.85	0.039
13.0	0.039

Figure 4.4.2-16. OTV CG Profile Outerbody at MR = 5

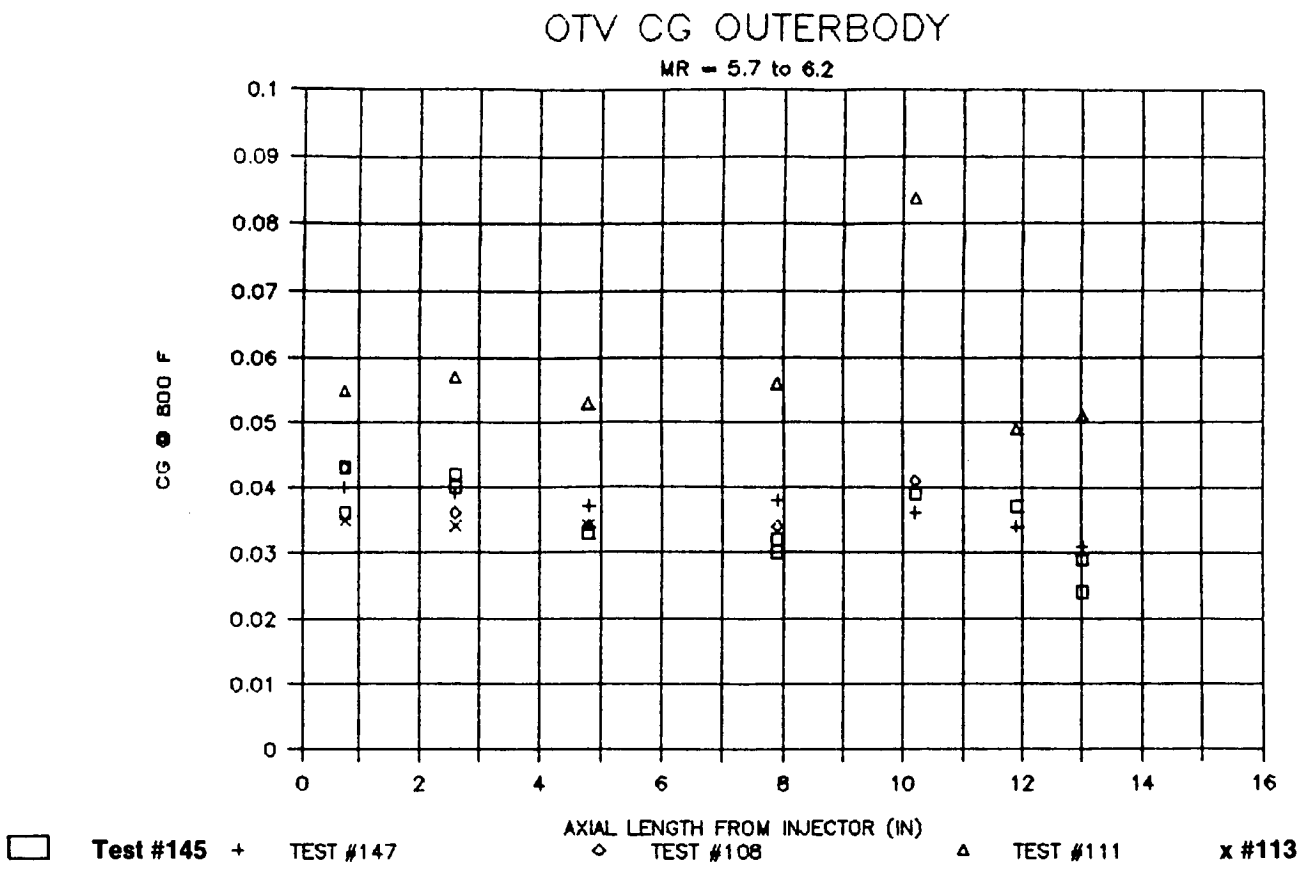

Figure 4.4.2-17. OTV CG Profile Outerbody at MR = 6

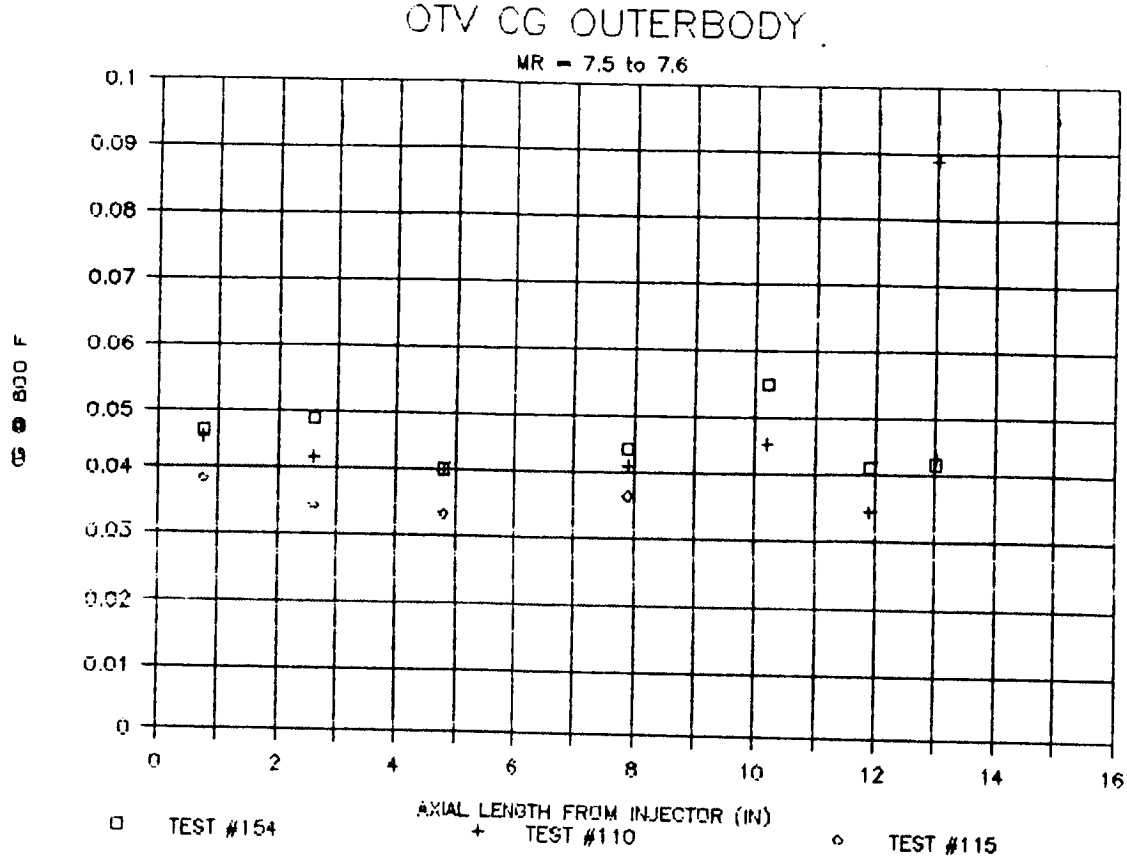

Figure 4.4.2-18. OTV CG Profile Outerbody at MR = 7.5

Table 4.4.2-III. OTV Hot Fire Tests - CG @ 800°F

OTV HOT-FIRE TESTS
NON-REACTIVE CG @800 F

TEST NO.		140	144	145	146	147	149	150	151	154	155	108	109	110	111	113	114	115
MR		4.10	4.40	5.80	8.30	6.20	4.20	5.30	6.50	7.50	5.40	6.07	5.11	7.64	5.68	6.20	5.21	7.56
PC		197	390	391	400	517	600	570	588	529	526	1032	1009	1051	513	1907	1895	2044
CENTERBODY TCB																		
0.50	90	0.073	0.051	0.049	0.049	0.041	0.044	0.043	0.041	0.046	0.041	0.068	0.076	0.062	0.064	0.081	0.082	0.100
2.30	90	0.052	0.042	0.044	0.054	0.041	0.043	0.050	0.051	0.048	0.041	0.044	0.036	0.048	0.071	---	0.037	0.044
4.50	0	0.037	0.026	0.034	0.042	0.032	0.027	0.039	0.043	0.041	0.031	---	---	---	---	---	---	---
4.50	90	0.035	0.030	0.033	0.037	---	0.026	0.038	0.041	---	---	0.030	0.032	0.034	0.037	0.028	0.028	0.031
7.50	0	0.036	0.028	0.031	0.037	0.029	0.033	0.039	0.043	0.039	0.029	0.031	0.030	0.028	0.030	0.032	0.032	0.029
7.50	90	0.042	0.034	0.032	0.031	---	0.038	0.045	0.040	---	---	---	---	---	---	---	---	---
11.30	0	0.037	0.028	0.033	0.035	0.029	---	---	0.044	0.037	---	0.036	0.033	0.030	0.027	0.036	0.034	0.033
12.10	0	0.033	0.029	0.034	0.036	0.033	0.033	0.043	0.046	0.042	0.033	---	---	---	---	---	---	---
12.10	90	0.029	0.027	0.030	0.031	---	0.031	0.030	0.045	---	---	0.029	0.032	0.030	0.037	0.032	0.033	0.031
12.50	0	0.043	---	0.026	0.044	0.032	0.028	0.041	0.051	0.053	0.030	0.044	0.034	0.048	0.050	0.044	0.042	0.040
OUTERBODY TCO																		
0.75	0	0.054	0.043	0.043	0.050	0.040	0.045	0.047	0.048	0.047	0.041	0.043	0.043	0.046	0.055	0.035	0.037	0.038
0.75	90	0.046	0.038	0.036	0.046	---	0.041	0.041	0.038	---	---	---	---	---	---	---	---	---
2.60	0	0.046	0.036	0.042	0.057	0.039	0.036	0.047	0.045	0.049	0.035	0.036	0.035	0.043	0.057	0.034	0.033	0.034
2.60	90	0.045	0.036	0.040	0.052	---	0.035	0.046	0.042	---	---	---	---	---	---	---	---	---
4.75	0	0.037	0.030	0.033	0.052	0.037	0.036	0.032	0.047	0.040	0.030	0.034	0.035	0.040	0.053	0.034	0.032	0.033
4.75	90	0.034	0.028	0.033	0.045	---	0.035	0.034	0.038	---	---	---	---	---	---	---	---	---
7.80	0	0.025	0.028	0.030	0.047	0.038	0.033	0.041	0.036	0.045	0.028	0.034	0.031	0.041	0.056	---	---	---
7.80	90	0.028	0.029	0.032	0.042	---	0.037	0.041	0.044	---	---	---	---	---	---	---	---	---
10.10	0	---	0.055	---	0.043	0.036	0.050	0.063	0.055	0.055	0.038	0.041	0.046	0.046	---	---	---	---
10.10	90	0.041	0.042	0.039	0.045	---	0.045	0.053	0.053	---	---	---	---	---	---	---	---	---
11.85	0	0.040	0.030	0.037	0.050	0.034	0.032	0.040	0.050	0.041	0.033	---	0.031	0.034	0.049	---	---	---
11.85	90	0.036	---	---	---	---	---	---	---	---	---	---	---	---	---	---	---	---
13.00	0	---	0.020	0.029	0.035	0.031	0.045	0.051	0.054	0.043	0.032	---	0.044	0.044	0.051	---	---	---
13.00	90	---	0.029	0.024	0.034	---	0.037	0.047	0.045	---	---	---	---	---	---	---	---	---

throat region which simulate the flight engine design where the coolant enters at a higher area ratio. Overall bulk temperature rise in the cooled throat hardware is determined by monitoring the thermocouples placed in the LH_2 inlet and exit manifolds. This only allows an estimation of the temperature rise at the throat. A graph of the bulk temperatures for tests #108 to #115 are shown versus time in Figure 4.4.3-1.

Thermal analysis of the throat section geometry utilized ATC's SCALER program for regeneratively cooled channels. SCALER (Reference 5) integrates the coolant energy and momentum equations and calculates local wall temperatures at selected locations along the flow path. Two-dimensional conduction effects around rectangular channels are accounted for by a coupled fin model of the wall. Different coolant heat transfer coefficients are associated with each fin in order to represent channel curvature effects and the variation with wall temperature. SCALER includes a design mode which defines channel depths based on wall temperature criteria. The coolant channels were sized to provide a gas side wall temperature in the range of 1260 to 1460 R at maximum pressure. Resulting backside wall temperatures were predicted to be in the 500 to 700 R range. Temperatures were measured on the backside wall at the throat, 1 inch upstream, and 1 inch downstream. Readings were obtained from two thermocouples at each location. The plots in Figure 4.4.3-2 through 4.4.3-4 show the temperatures to be in the 500 to 600 R range.

The pressure drops through the regeneratively cooled channels were predicted using SCALER. The flight engine has a split fuel flow scheme where 83% of the flow is used to cool the throat. Separate plumbing was used in the test facility to deliver the required LH_2 flow to the throat based on the GH_2 flow to the injector. Actual LH_2 flowrates, pressures, and temperatures were input into the SCALER model to predict the expected pressure drops. The calculated friction factor is a function of surface roughness and Reynolds number. Inspection of the channels indicated a surface roughness of 25-40 microinches. Analysis of the pre-fire test data closely matched the pressure drops observed at a surface roughness equal to the average of the observed ranged (Figure 4.4.3-5) During the firing, changes in coolant temperature are reflected in the friction factor as the gas viscosity changes the Reynolds number. Surface roughness typically input in chamber design are in the range of 63 to 120 microinches. Comparison with the actual test data

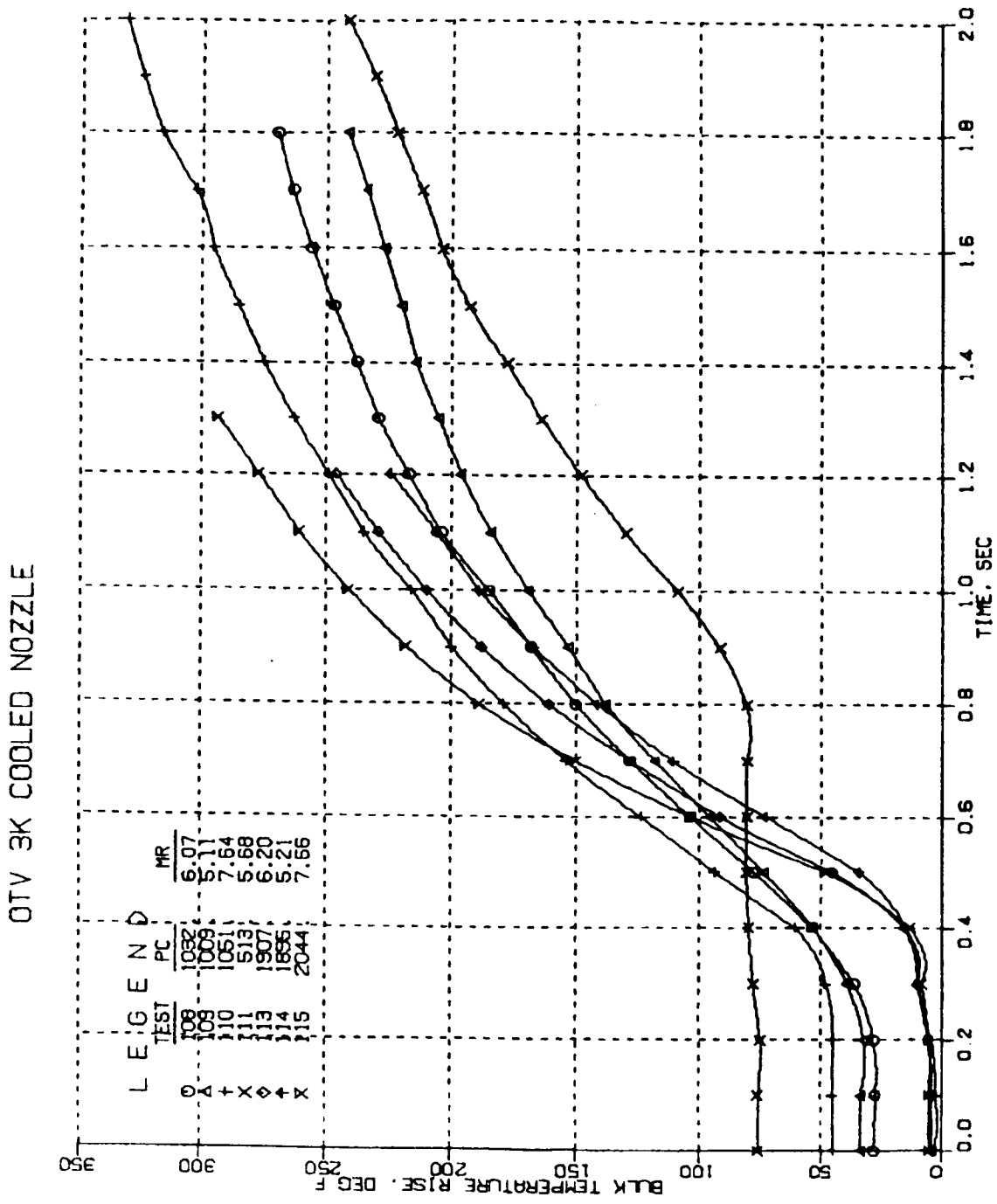

Figure 4.4.3-1. Bulk Temperature Rise - OTV Nozzle

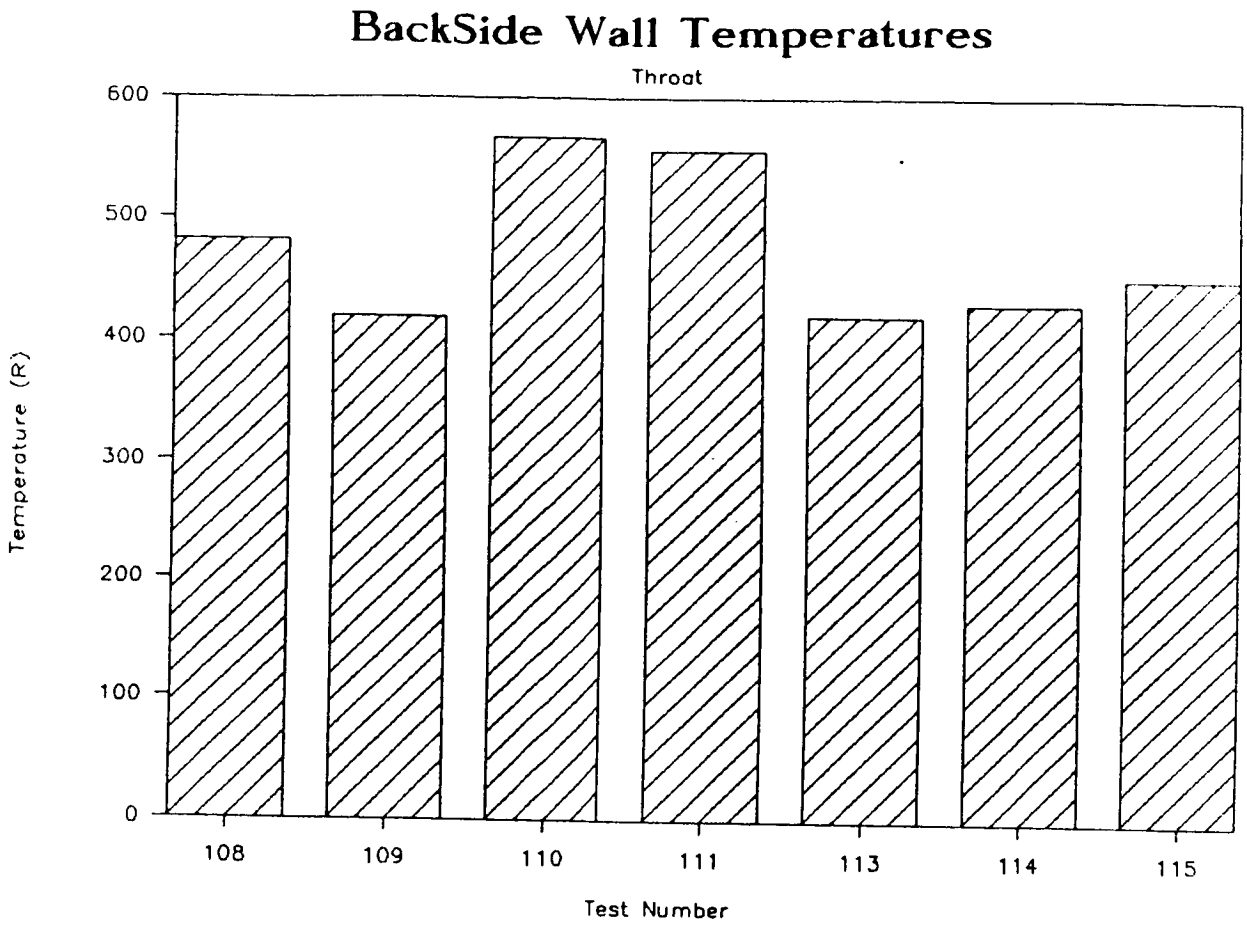

Figure 4.4.3-2. Backside Wall Temperature - Throat

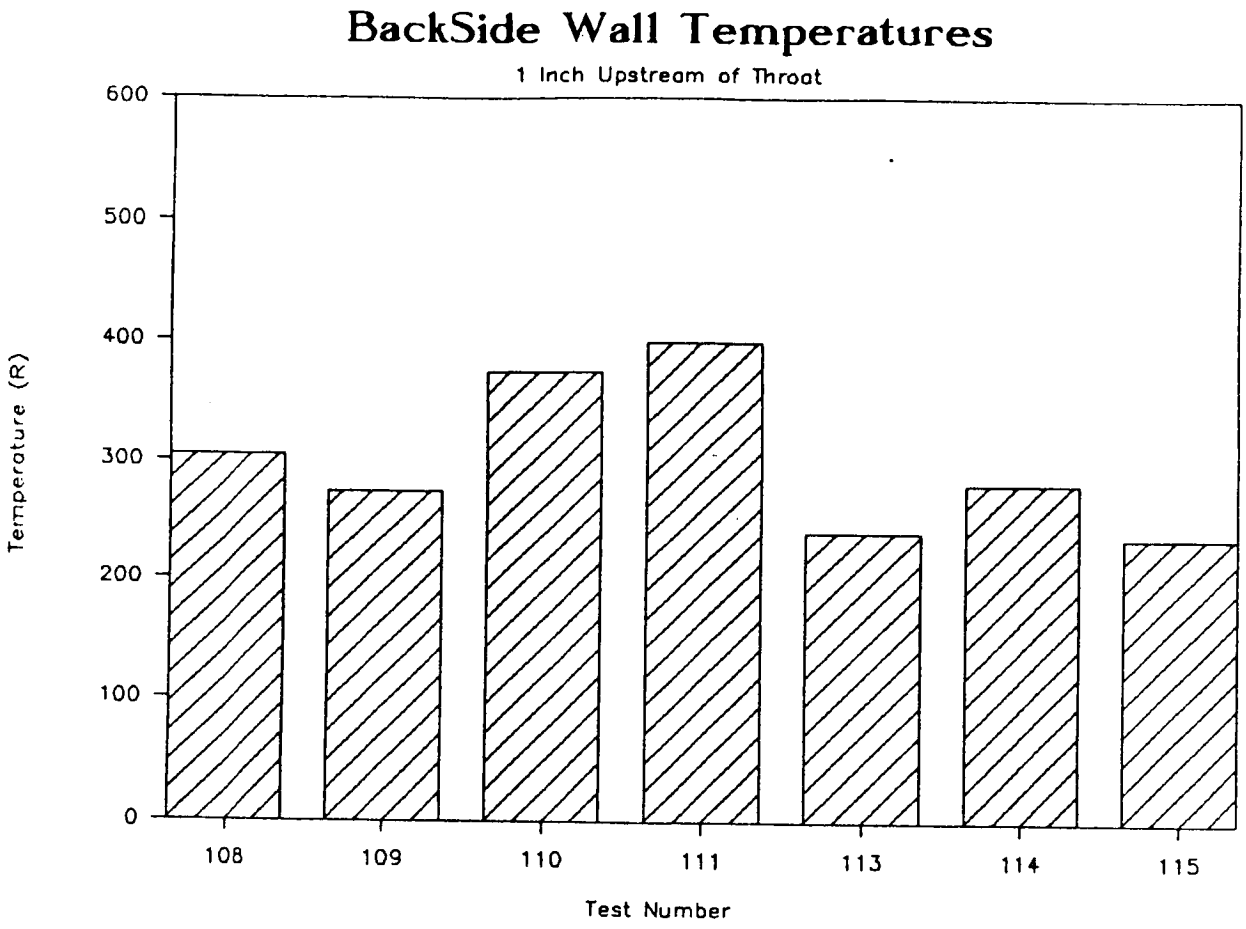

Figure 4.4.3-3. Backside Wall Temperature - 1" Upstream of Throat

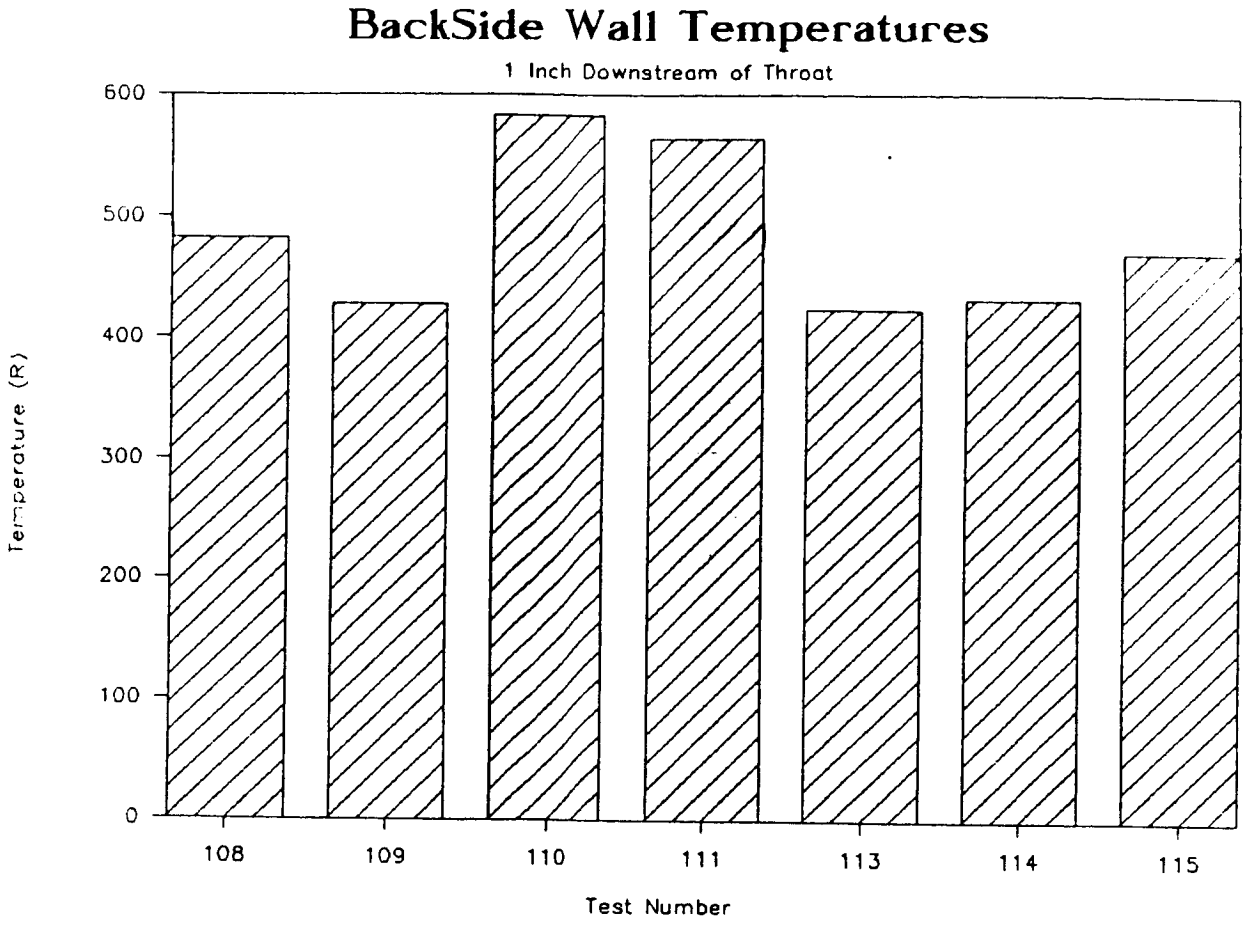

Figure 4.4.3-4. Backside Wall Temperature - 1" Downstream of Throat

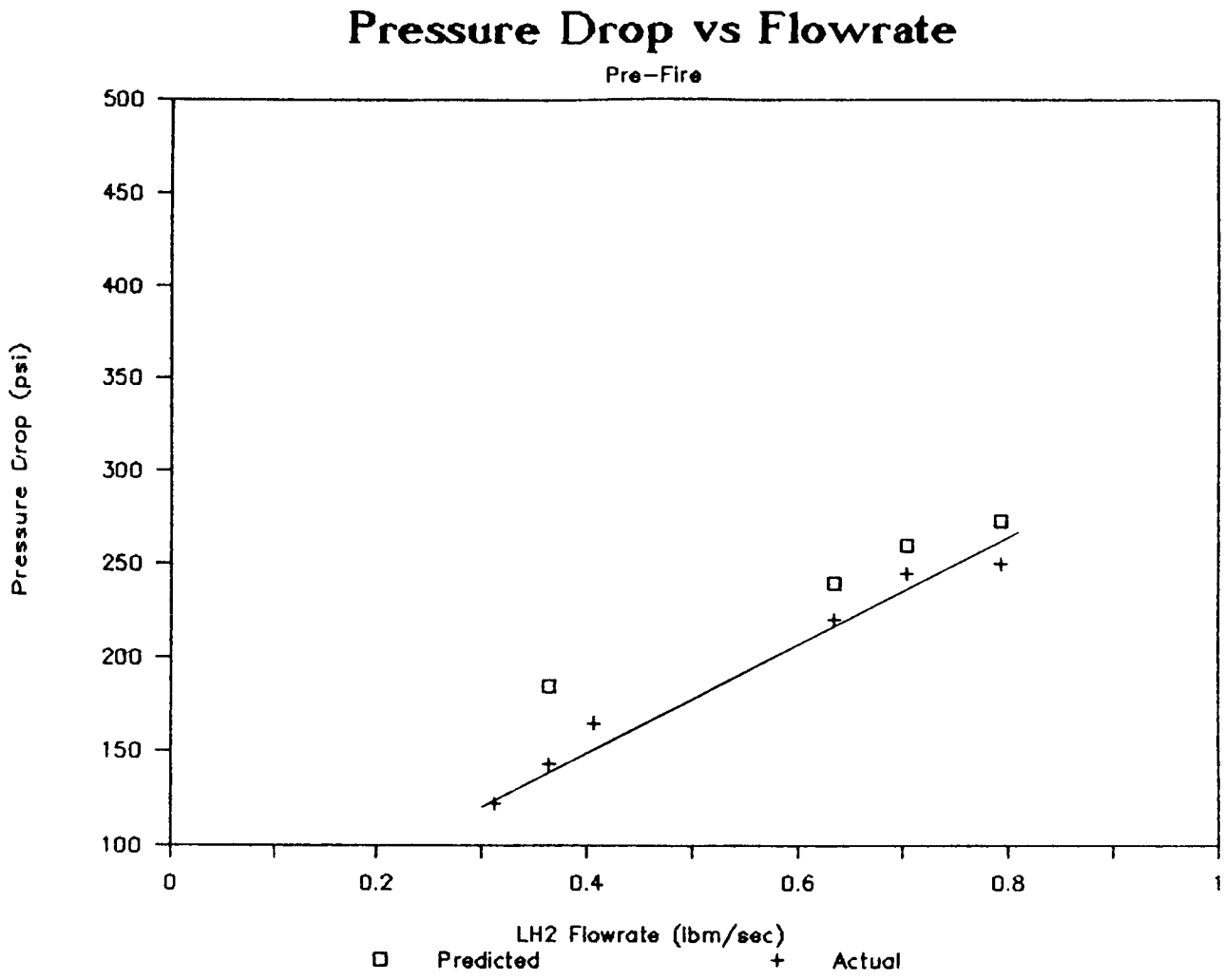

Figure 4.4.3-5. Pressure Drop vs. Flowrate - Prefire

(Figure 4.4.3-6) concurred with a 63 microinch roughness which indicates pressure drop predictions have been on the conservative side. Since the hydrogen coolant was warm enough to compress like a gas and the flow rate was proportional to chamber pressure, the hydrogen velocity was essentially constant and the pressure drop directly proportional to the hydrogen flow rate.

Heat load versus LH_2 flowrate is shown in Figure 4.4.3-7.

4.5 Thrust Chamber Performance

4.5.1 Specific Impulse Data

Specific impulse information on delivered vs ODE predictions are presented in this section for the low (Pc = 200 to 600) and high (Pc = 500 to 2000) series of tests. The low Pc tests were run from chamber pressures of 200 to 600 with the MR varying from 3 to 8. With the test stand configuration and control valves, a 3 second duration test was felt necessary to achieve steady state conditions. A full 4 to 5 second duration was achieved for the 200 & 400 psia chamber pressure tests. Plots from the ODE computer model predictions are shown with the Isp delivered data in Figure 4.5.1-1. Also included in this figure are Isp data from the igniter low pressure tests series (Pc = 100 to 300 psia). Isp data are not represented for the 500 and 600 Pc tests as those at 600 did not reach steady state conditions and those at 500 Pc are marginal.

The ODE curves shown in Figure 4.5.1-1 are uncorrected for heat loss to the heat sink chamber. Test stand modifications made to the test stand between the low and high Pc series of tests replaced the control regulator valves in an effort to achieve steady state conditions within 1.5 seconds. Of the high Pc series of tests, those at 500 and 1000 achieved durations of 1.6 to 1.8 seconds. The tests at 2000 Pc only achieved durations of 1 to 1.3 seconds, and did not reach steady state conditions.

The Isp data are presented for Pc = 500, 1000, and 2000 in Figures 4.5.1-2, -3, and -4, respectively. The top curve on each plot is the ODE computer model predictions without corrections for heat loss to the heat sink centerbody and chamber. The second dashed curve is the ODE data with corrections

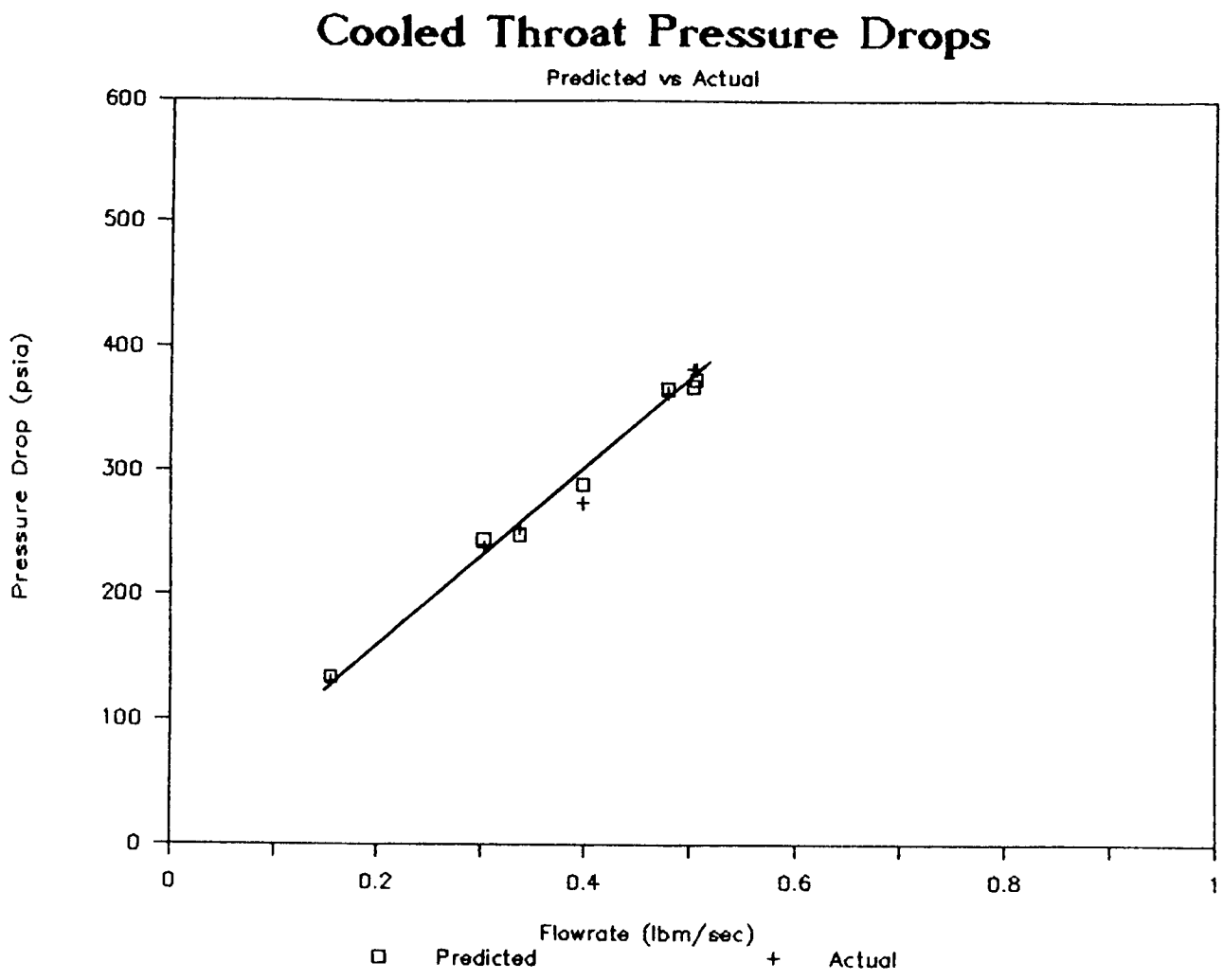

Figure 4.4.3-6. Pressure Drop vs. Flowrate - Postfire

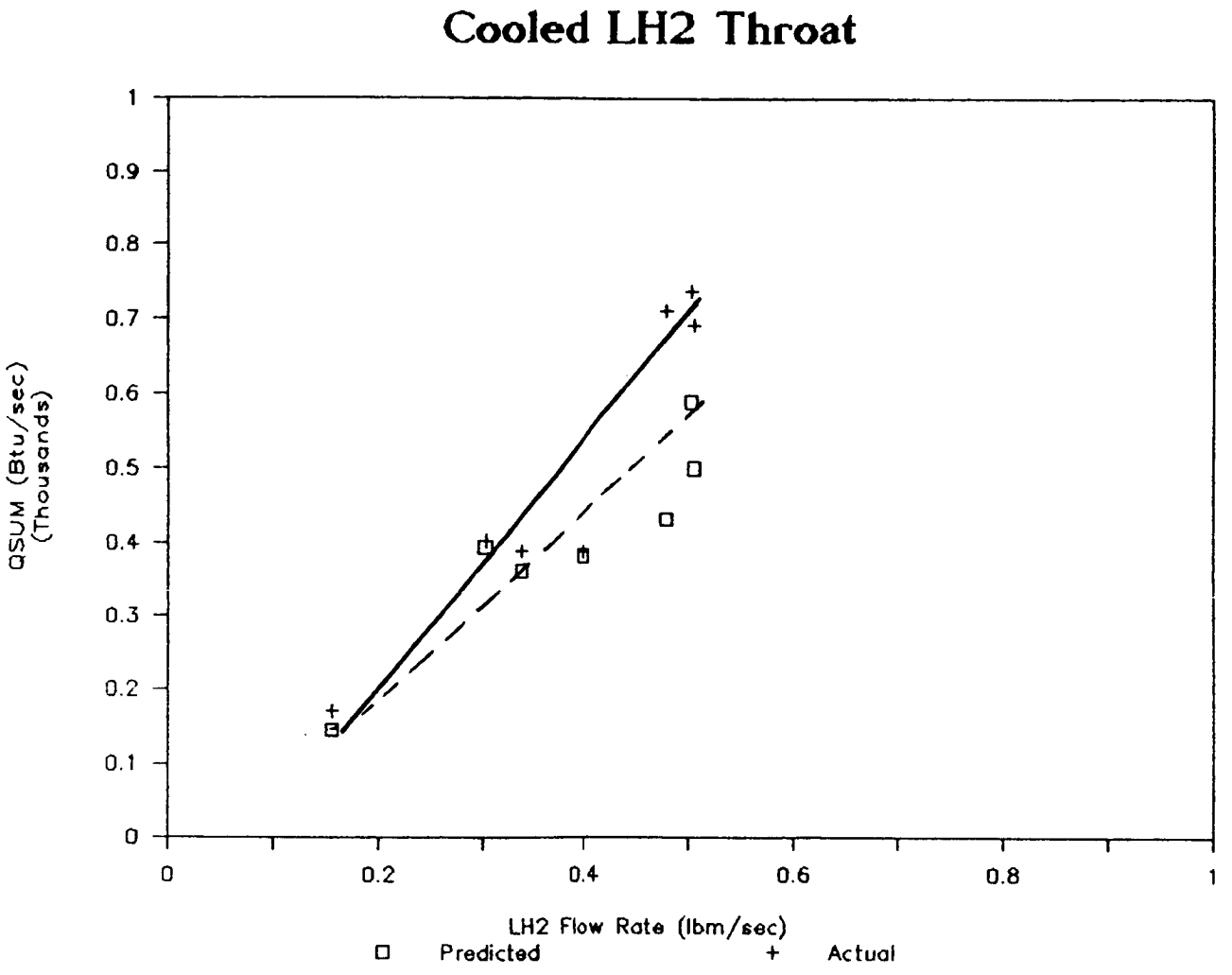

Figure 4.4.3-7. Cooled LH_2 Throat - Heat Load vs. Flowrate

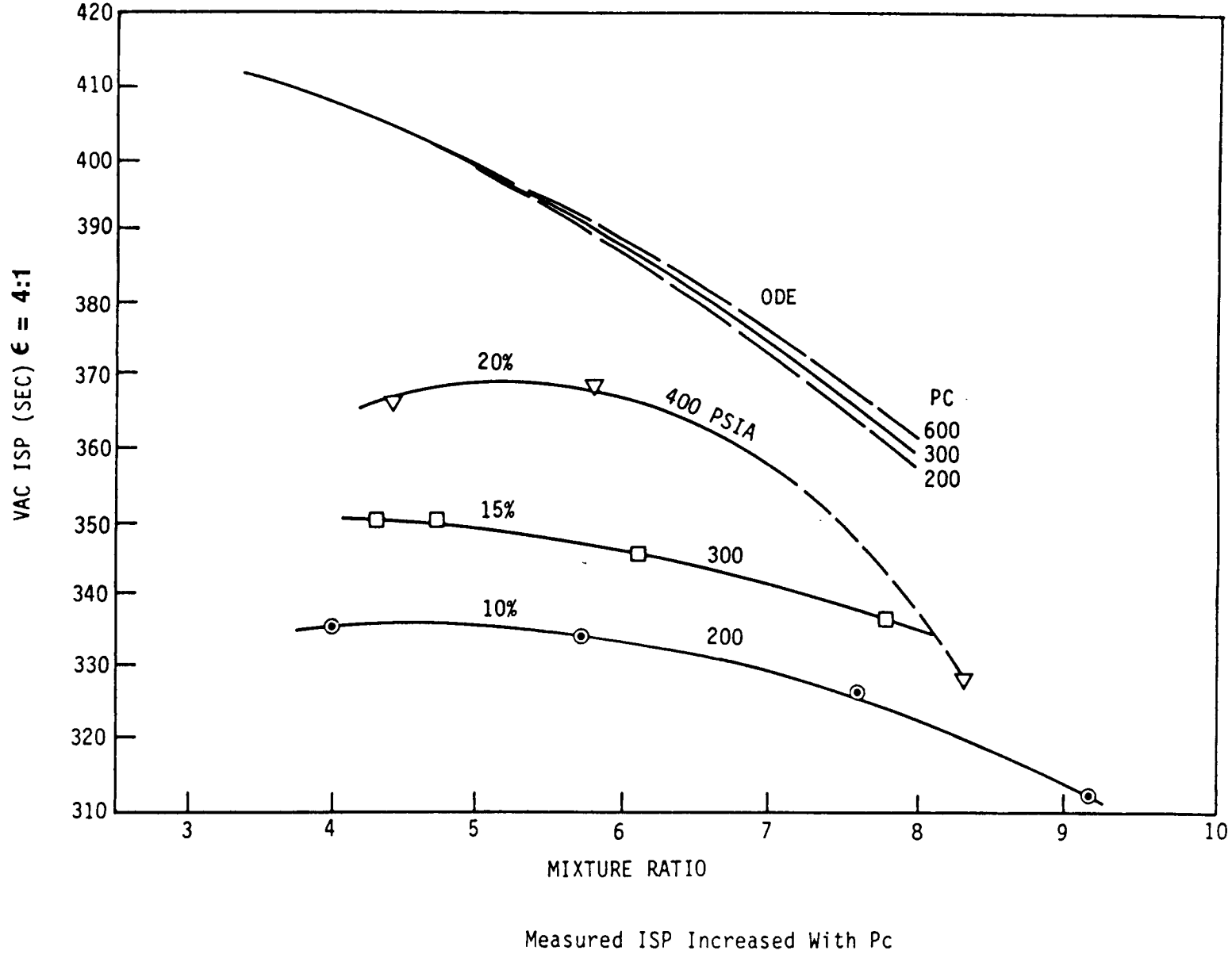

Measured ISP Increased With Pc

Figure 4.5.1-1. Isp vs. MR for PC Range of 200 to 400 psia

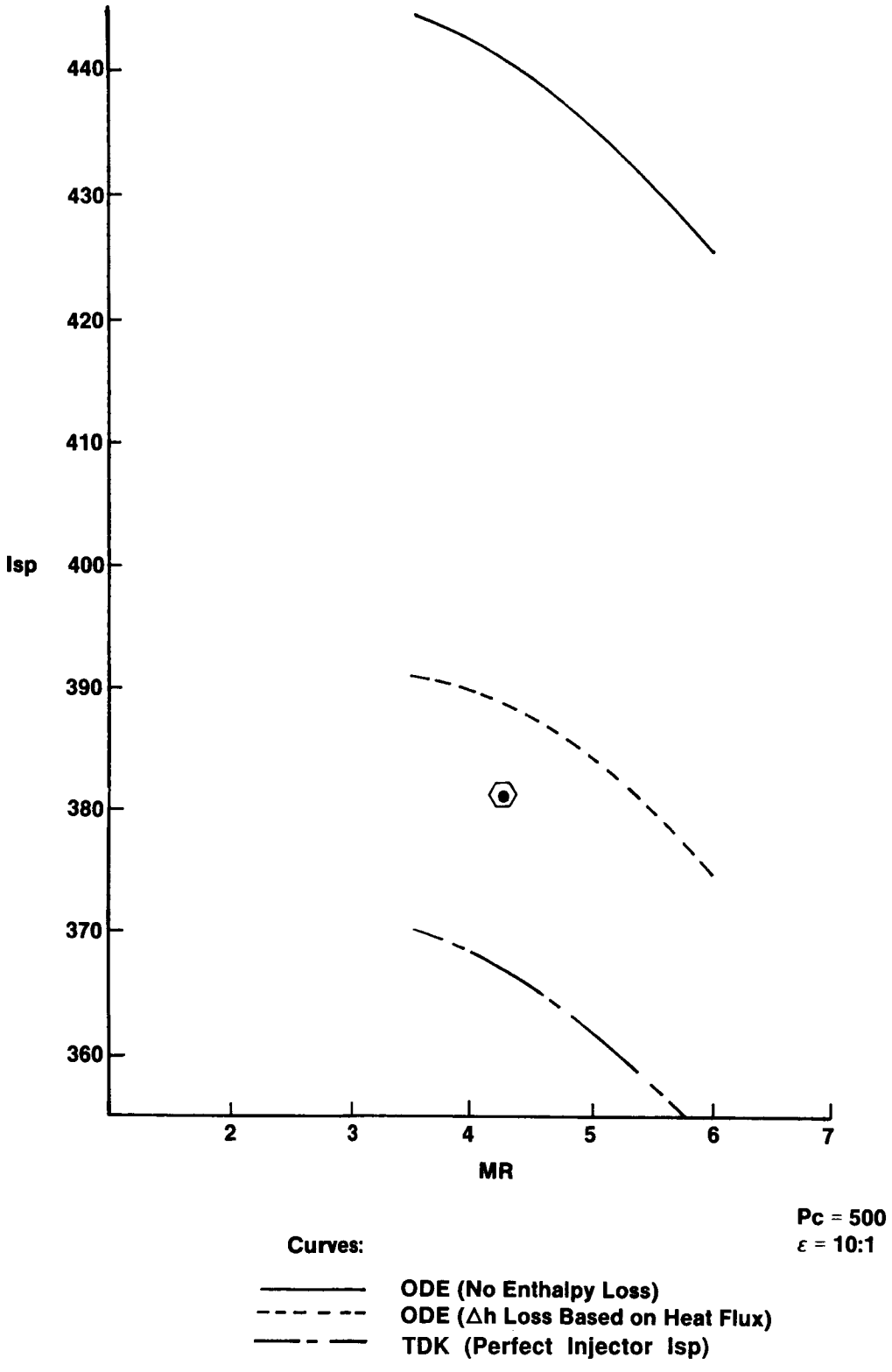

Figure 4.5.1-2. Isp vs. MR for PC = 500 psia

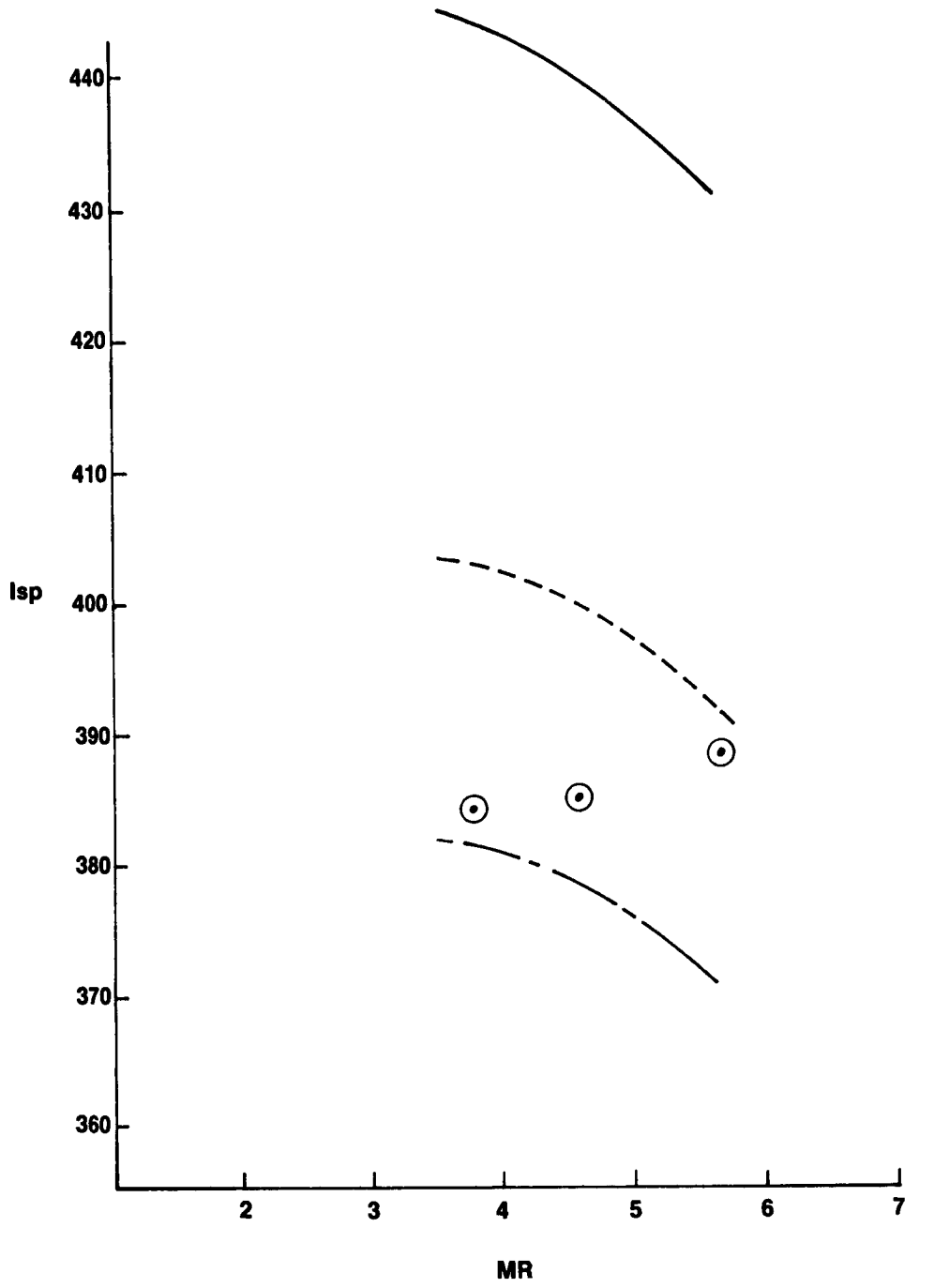

Figure 4.5.1-3. Isp vs. MR for PC = 1000 psia

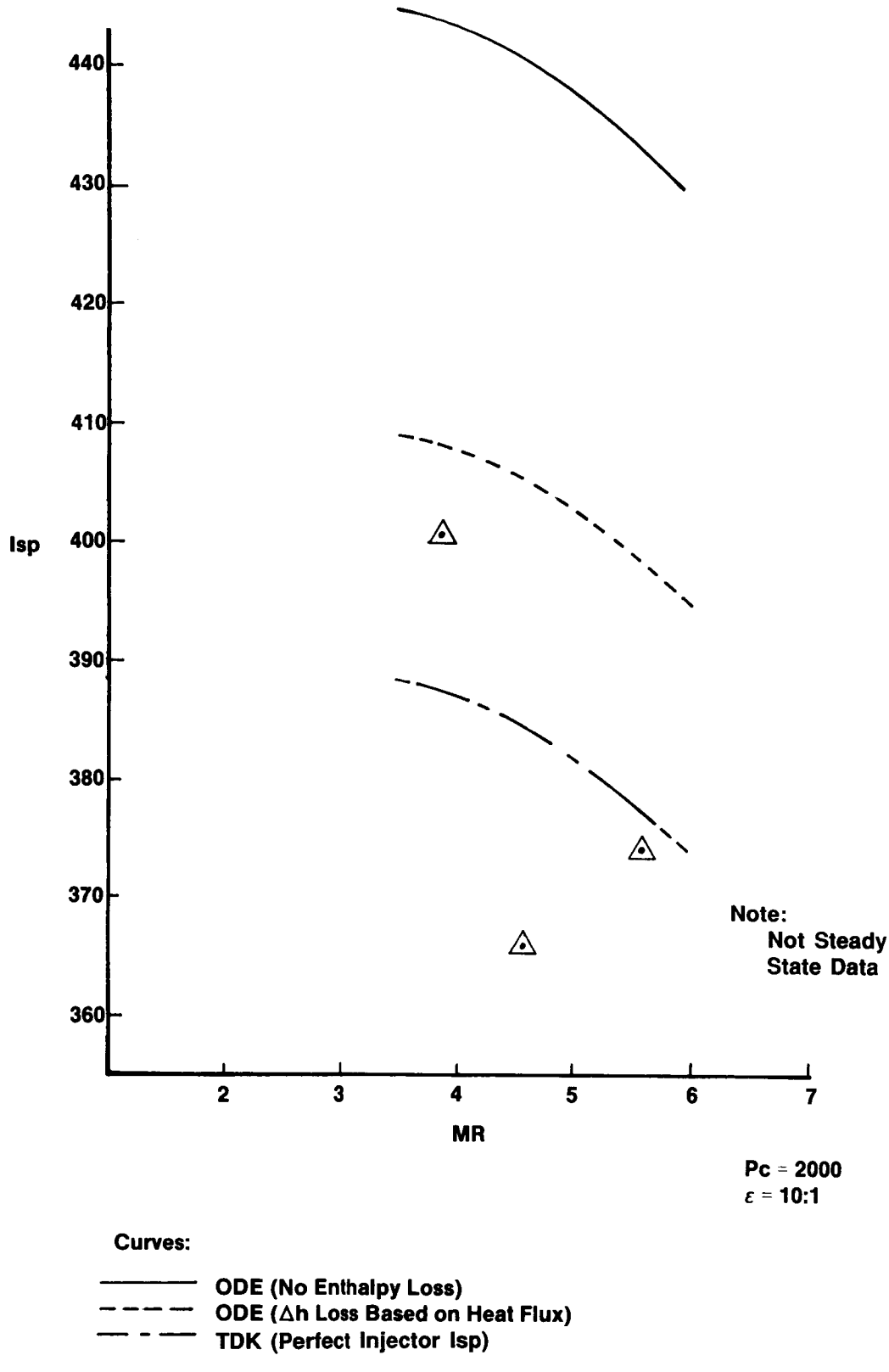

Figure 4.5.1-4. Isp vs. MR for PC = 2000 psia

for this heat loss. The heat loss to the chamber walls and to the centerbody was derived by first determining the heat flow at specific thermocouple locations and by assuming the heat flow to be circumferentially constant at each thermocouple location. The heat flux utilized was the instantaneous data presented in Section 4.4.

The heat loss term input to the ODE computer code is Δh, defined as:

$$\Delta h \text{ (Btu/lbm)} = Q_{tot} / \dot{w}_t$$

where: Q_{tot} = Heat flux (Btu/s)

$\dot{w}_t$ = Total propellant flowrate (lbm/s)

The heat loss for the high Pc series of tests is greater (approximately 40 seconds) than it was for the low Pc series of tests (approximately 20 seconds), due to the higher heat fluxes observed. The third dashed curve indicates the predicted Perfect Injector Performance which is defined as:

$$Isp_{\text{perfect injector}} = Isp_{ODE} - \text{losses}$$

where: losses =
chamber heat loss +
kinetics loss +
nozzle divergence loss +
nozzle boundary layer loss =
nozzle heat loss +
nozzle friction loss

The TDK computer program was used to determine these performance losses. The modules used are shown in Table 4.5.1-I.

Tables 4.5.1-I through 4.5.1-III list the output from these modules for two representative tests at chamber pressures of 500 and 1000 psia. Overall ERE values (Isp - Delivered/ Isp - Perfect Injector) for the high Pc test series

Table 4.5.1-I TDK Computer Program Modules Used in OTV Performance Analysis

Module	Performance Parameter Obtained
ODE	Isp and C* for equilibrium conditions
ODE with Δh term	Isp and C* accounting for heat loss to centerbody and chamber walls
ODK	Kinetics loss
TDE	Divergence loss
BLM	Nozzle heat and friction losses

TABLE 4.5.1-II

ERE CALCULATION FOR TEST #147

Test #147

PC	=	517 psia
MR	=	6.16
$\dot{w}$	=	1.639 lbm/sec
Δh	=	915 Btu/lbm
ϵ	=	4:1

Isp (ODE)	386.1 (sec)
Isp loss due to reduced propellant enthalpy	20.6
	365.5
Isp (ODK)	
Kinetic Loss	1.0
	364.5
Nozzle Boundary Layer Losses: (TDE/BLM):	
Friction	1.7
Heat Loss + Divergence Efficiency	6.5
Perfect Injector Isp	356.3
Isp Delivered	356.2

ERE = 356.2/356.3 = 99.97%

TABLE 4.5.1-III

ERE CALCULATION FOR TEST #108

Test #108

PC	=	1035 psia
MR	=	4.6
$\dot{w}$	=	3.216 lbm/sec
Δh	=	1127 Btu/lbm
ϵ	=	10:1

Isp (ODE)	440.25 (sec)
Isp loss due to reduced propellant enthalpy	40.25
	400.00
Isp (ODK)	
Kinetic loss	1.33
	398.67

Nozzle Bondary Layer Losses (TDE/BLM):

Friction	2.6
Heat Loss	8.81
Divergence Efficiency	8.5
Perfect Injector Isp	378.76
Isp Delivered	385.2

ERE = 385.2/378.76 = 101.7%

are given in Table 4.5.1-IV. ERE efficiencies in the range of 100.7 to 104.8% for Pc = 500 and 1000 psia were achieved in the steady state tests. The ERE values greater than 100% were attributable to uncertainties up to 20% in the estimation of Δh term. The TDK computer program itself is accurate to within 1% (Reference 4).

Reduction of the initial data from the high Pc test series indicated anomalous flowrates. Inspection of the test facility resulted in the following compiled list of possible causes of flowrate anomalies.

- Incorrect venturi diameter
- Close proximity of fuel venturi flowmeter to control valve. (Approximately 6 inches)
- Distance from point of flowrate calculation to injector delivery point. (Approximate 6 feet)
- Compression of fuel and oxidizer in respective lines.
- Temperature drop and resulting density changes from venturi flowmeter to injector manifold.

During tear down of the test stand, the venturis were removed and inspected. The recommended venturi to be used for the high Pc series of tests had not been installed. This had been missed during the test stand preparations for the cooled throat tests and was not discovered until testing was complete. This affected the injector flow and mixture ratio values for the high Pc series of tests. The data was recalculated using the proper venturi dimension and is the test data presented.

Compression of the fuel and oxidizer in their respective lines between the venturi flowmeter and the injector manifold was a concern, especially for the short duration tests. Based on the flowrate, temperatures, and test duration, a certain portion of the fuel and oxidizer went into filling the line until equilibrium was reached. A correction was made to the flowrates to compensate for this line filling. This correction had increasing effect on the flowrates from 500 to 2000 Pc as the test durations decreased from 1.8 seconds to 1.6 seconds. No other corrections were made to the presented data.

TABLE 4.5.1-IV

ERE Performance

Test#	Perfect Injector Isp (sec)	Delivered Isp (sec)	ERE (%)
108	379	385	101.7
109	382	384	100.5
110	371	389	104.8
111	367	381	103.8
113	384	366	95.3
114	388	402	103.6
115	377	374	99.2

4.5.2 Characteristic Chamber Velocity Data

Characteristic chamber velocity (C *) data on delivered vs ODE predictions are presented in this section for the low (PC = 200 to 600) and high (Pc = 500 to 2000) series of tests. The low Pc tests were run from chamber pressures of 200 to 600 with the MR varying from 3 to 8. With the test stand configuration and control valves, a 3 second duration test was felt necessary to achieve steady state conditions. A full 4 to 5 second duration was achieved for the 200 and 400 psia chamber pressure tests. Plots from the ODE computer model predictions are shown with the C* delivered data in Figure 4.5.1-1. Also included in the figure are C* data from the igniter low pressure tests series (Pc = 100 to 300 psia). C* data are not presented for the 500 and 600 PC tests as those at 600 did not reach steady state conditions and those at 500 Pc are marginal.

The ODE curves shown in Figure 4.5.2-1 are uncorrected for heat loss to the heat sink chamber. Test stand modifications made to the test stand between the low and high Pc series of tests replaced the control regulator valves in an effort to achieve steady state conditions within 1.5 seconds. Of the high Pc series of tests, those at 500 and 1000 achieved durations of 1.6 to 1.8 seconds. The tests at 2000 Pc only achieved durations of 1 to 1.3 seconds, and did not reach steady state conditions.

The C* data are presented for Pc = 500, 1000, and 2000 in Figures 4.5.2-2, -3, and -4, respectively. The top curve on each plot is the ODE computer model predictions without corrections for heat loss to the heat sink chamber. The second dashed curve is the ODE data with corrections for heat loss to the chamber. This heat loss was determined as described in Section 4.5.1. The heat loss for the high Pc series of tests is greater (approximately 40 seconds) than it was for the low Pc series of tests (approximately 20 seconds), due to the higher heat fluxes observed. Data points from the tests indicate C* efficiencies (C*-del/C*-ODE) in the range of 100.3 to 103.2% for Pc = 500 and 1000 psia tests, where steady state was achieved (Table 4.5.2-I). C* efficiencies greater than 100% are attributable to flowrate corrections as described in Section 4.5.1.

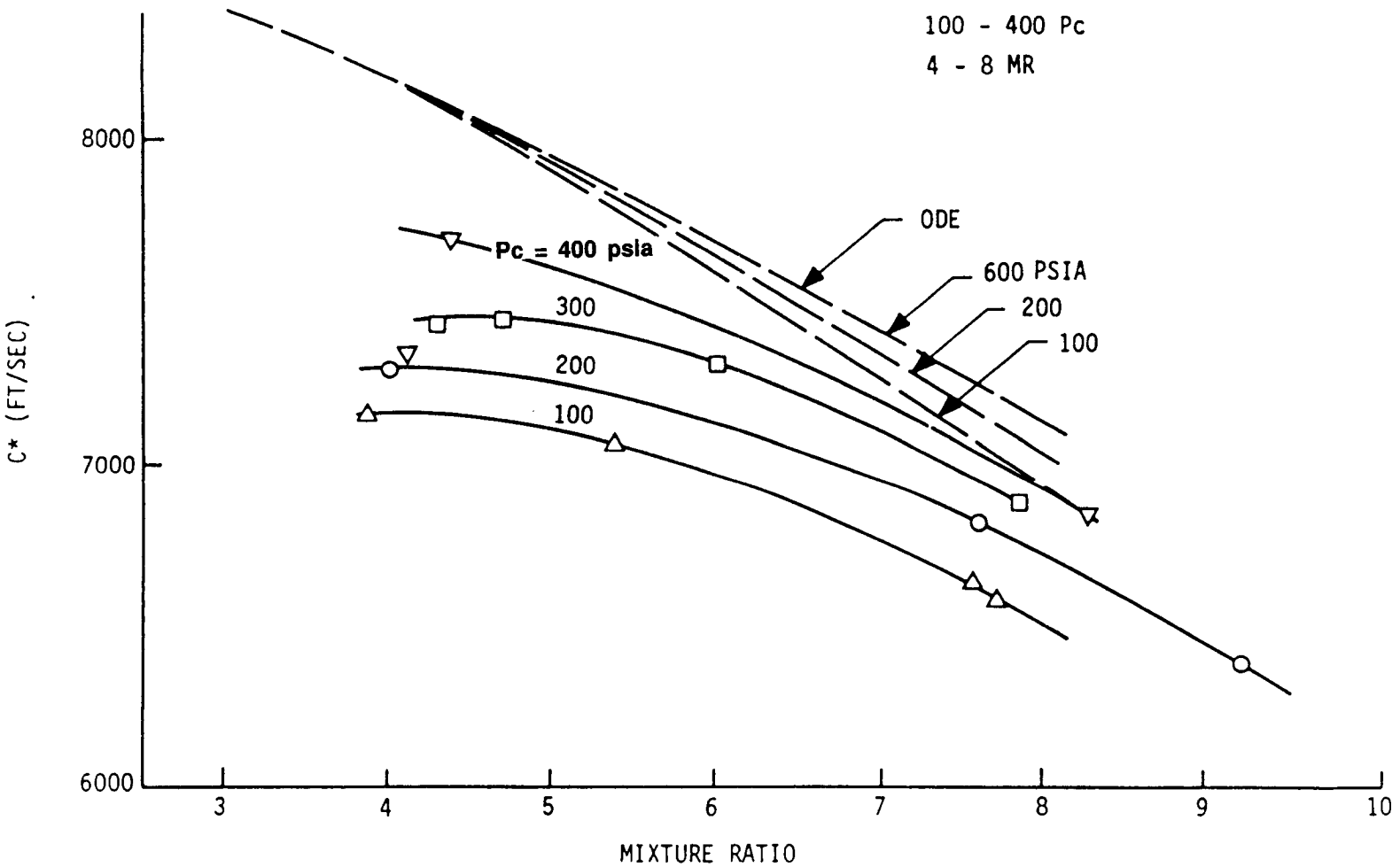

Uncorrected C* Data

Figure 4.5.2-1. C * vs. MR for PC Range of 200 to 400 psia

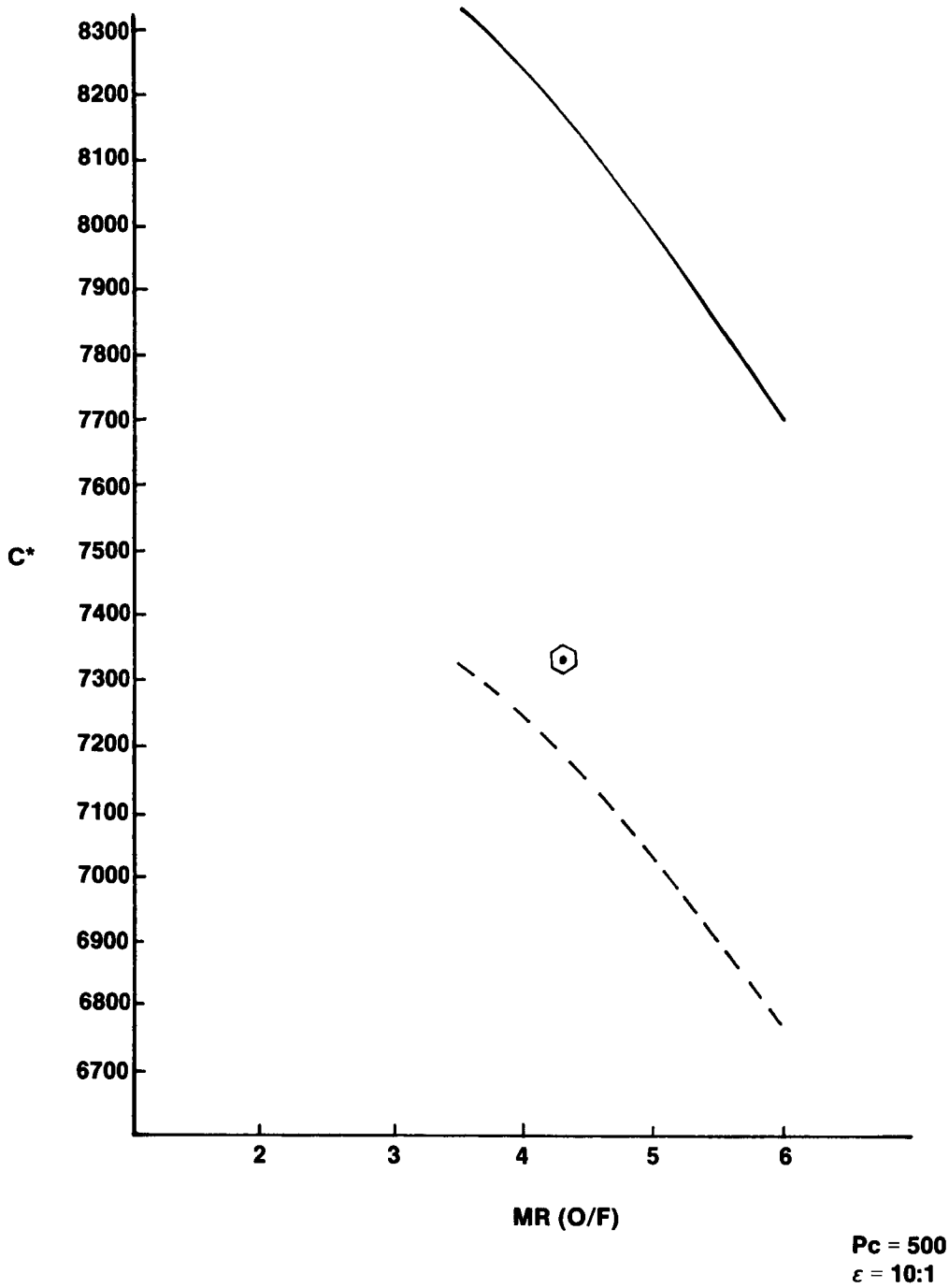

Figure 4.5.2-2. C * vs. MR for PC = 500 psia

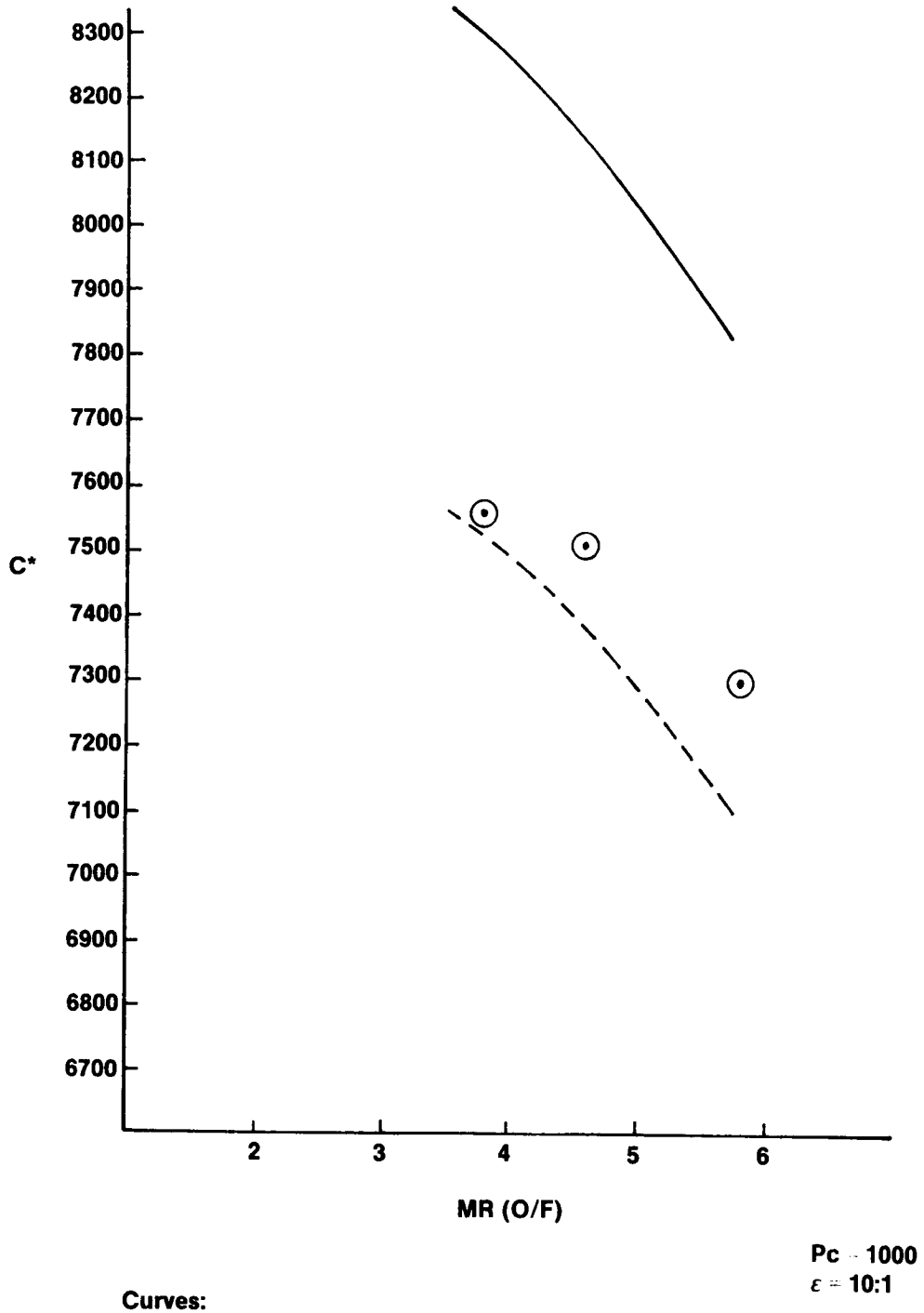

Figure 4.5.2-3. C * vs. MR for PC = 1000 psia

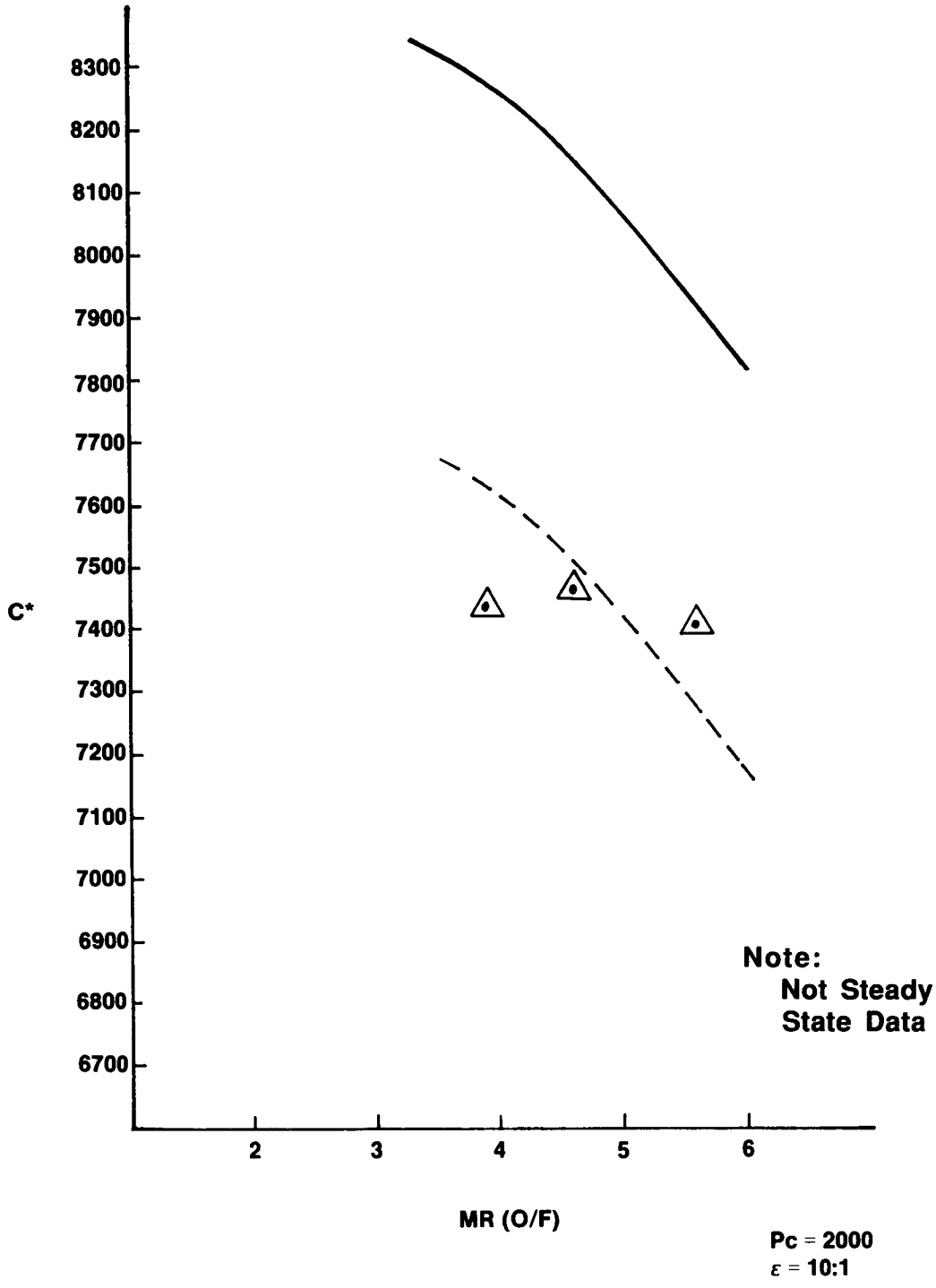

Figure 4.5.2-4. C * vs. MR for PC = 2000 psia

TABLE 4.5.2-I

C* Performance

Test #	TDK C*ODE (fps)	Delivered C*(fps)	% C*
108	7545	7569	100.3
109	7380	7576	102.5
110	7100	7316	103.0
111	7109	7338	103.2
113	7515	7485	99.6
114	7630	7459	97.8
115	7280	7426	102.0

5.0 Results And Conclusions

5.1 Post-Test Photographs

Photographs of the injector and chamber have been included to document the post test condition of the hardware. The injector face is shown in Figures 5.1-1 with a closeup of the elements in Figure 5.1-2. The injector face is in good condition with no evidence of erosion around the elements. The condition of the centerbody can be noted in Figure 5.1-1 and 5.1-3. Erosion of the centerbody was noted at approximately 2.6 inches out from the face of the injector. It is not known at this time what specifically caused the erosion of the centerbody. Possible causes include:

- Misalignment of the copper segments
- Injector element providing higher heat fluxes than predicted
- Contamination of the injector causing localized hot spots
- Contamination of the Hydrogen bleed holes preventing
- adequate cooling of the centerbody.

In order to understand the cause of the damage to the centerbody and higher than predicted heat fluxes, the injector will need to be re-cold flowed. This will given an opportunity to compare the Kw values of the injector with those obtained prior to hot fire testing. This will indicate if any contamination in the injector manifolds or elements has occured. Cold flow tests will also give an opportunity to visually inspect the injector flow pattern and bleed holes. If the spray is non-uniform, this may have been the cause of localized hot spots. This also will give an indication of the possible presence of contamination. If no contamination is present, then redesign of the injector element will be necessary to provide a more benign environment for the chamber walls.

Figure 5.1-4 shows the throat from the chamber view. Figure 5.1-5 is a view of the throat from the outer view. No damage to the copper hardware is noted.

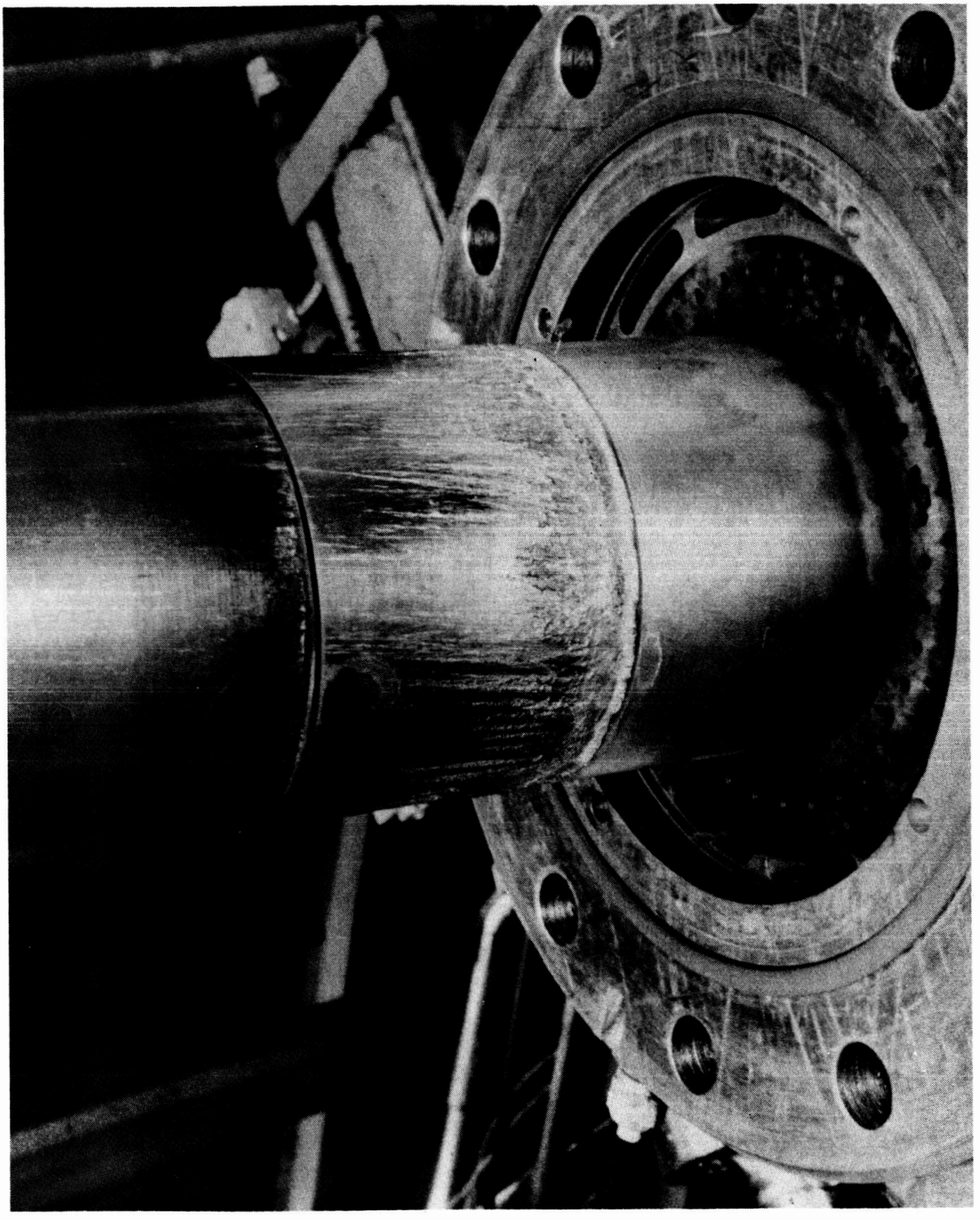

Figure 5.1-1. Injector Face

Figure 5.1-2. Closeup of Injector Face

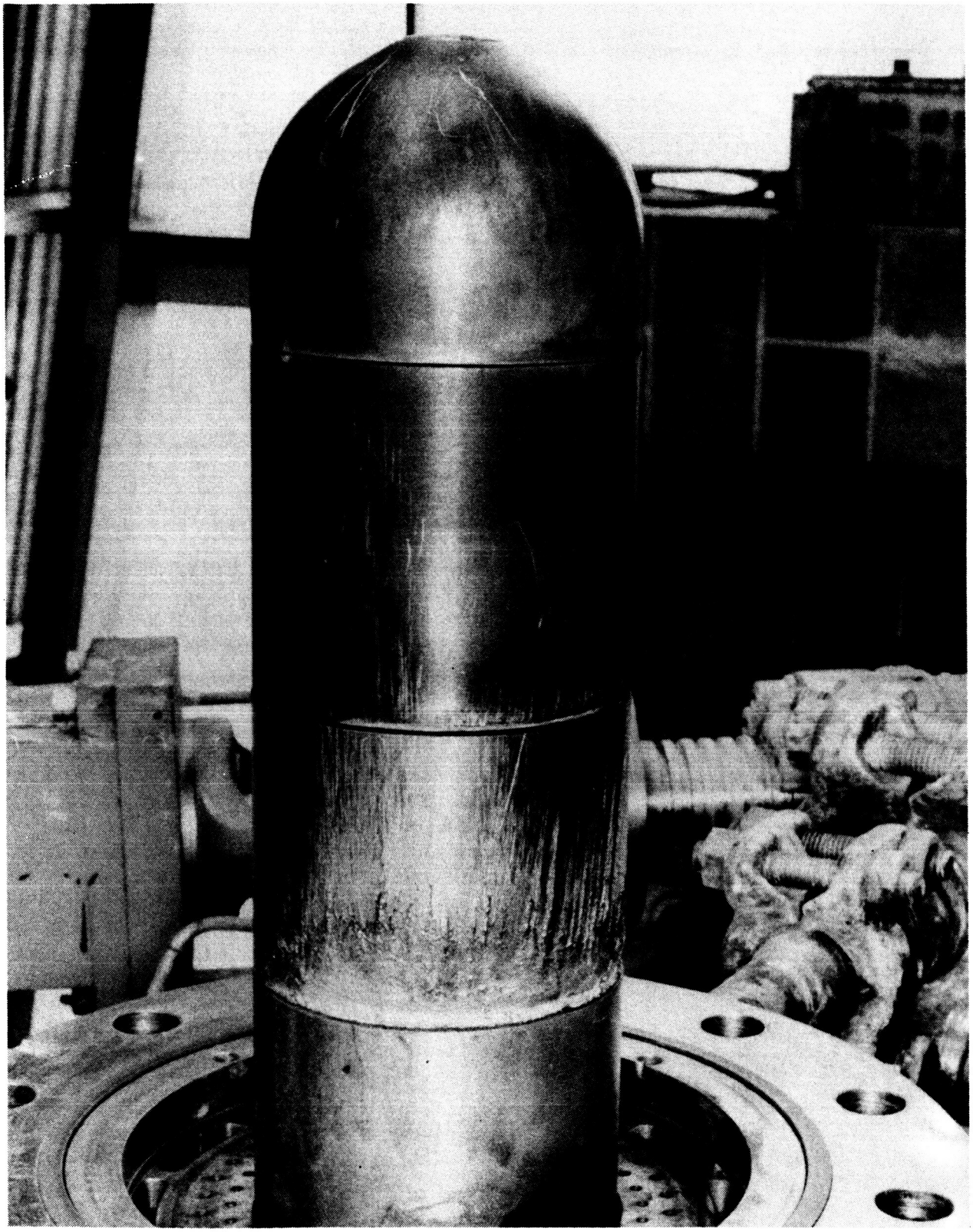

Figure 5.1-3. Centerbody Hardware

Figure 5.1-4. Throat from Chamber View

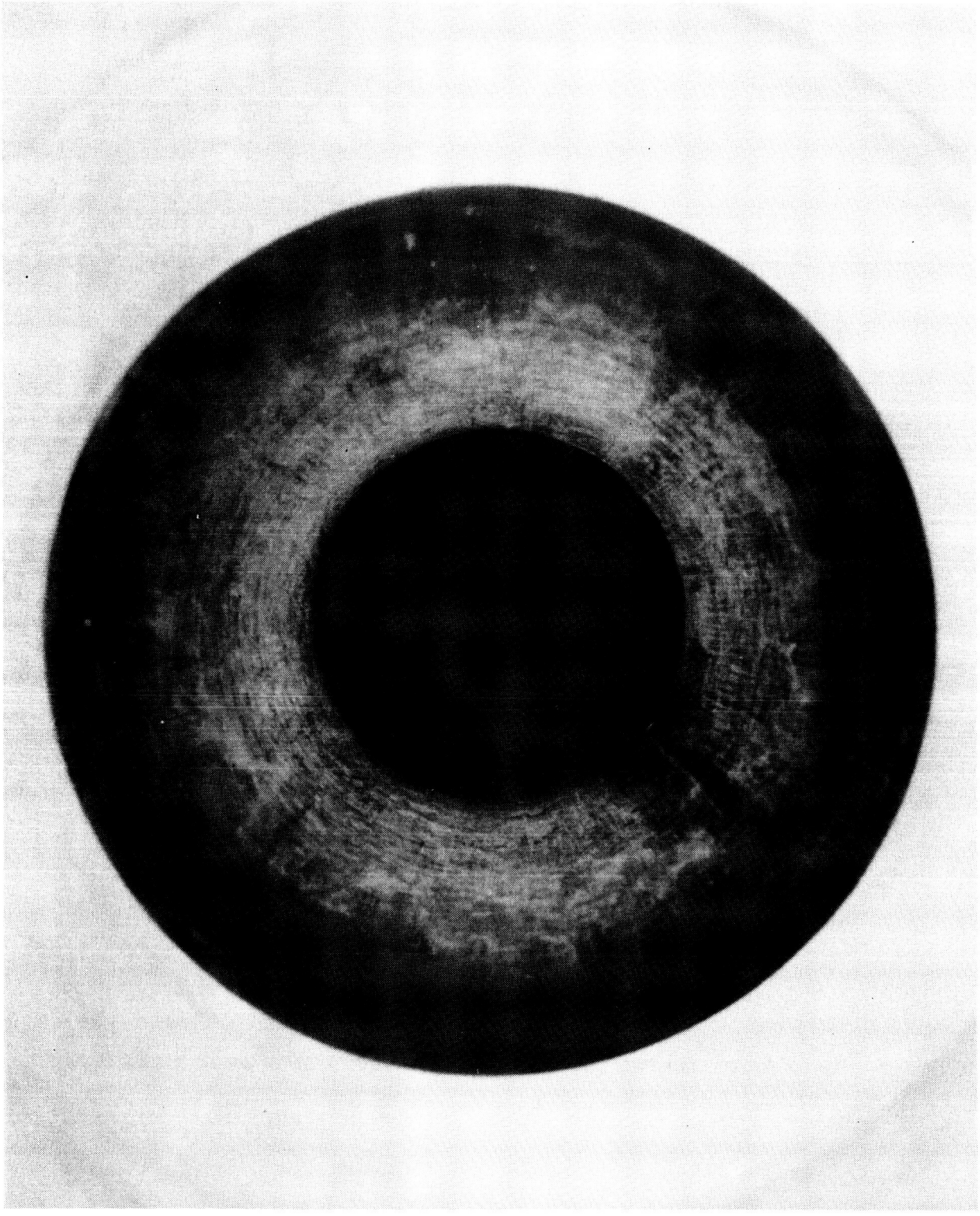

Figure 5.1-5. Throat from Nozzle View

5.2 Conclusions

The objective of this program has been to develop and verify the design of a Thrust Chamber Assembly (TCA) to be used in Aerojet's OTV engine dual propellant expander cycle. The dual propellant expander cycle utilizes preheated hydrogen to drive the turbopumps and preheated oxygen to drive the oxygen turbopumps thereby eliminating the need for interpropellant seals. The Aerojet OTV TCA concept consists of a hydrogen cooled chamber, an annular injector, and an oxygen cooled centerbody. To provide adequate heating of the propellants without utilizing regenerators, a high heat flux regenerative cooled combustion chamber and centerbody were baselined for the TCA design.

Injector element selection was based on meeting the Isp requirement of 490 seconds. A pre-mix "I" triplet element pattern was selected based on previously demonstrated high mixing efficiencies with energy release efficiencies (ERE) approaching 100% in a relatively short mixing length of 7 inches.

Analysis supported a "mini" channel design for hydrogen regenerative cooling of the combustion chamber. To meet the cycle life requirement of 500, minimization of the wall and differential temperatures was necessary. Minimization of the temperatures was achieved by the machining of 0.01" wide channels with 0.011" wide lands at a maximum aspect ratio of 10. The gas-side wall was 0.02" thick. Plating techniques for Ni-Co, a high strength nickel alloy, were developed which resulted in a lightweight, thin (0.018") closeout. Demonstration of the fabricability issues were achieved with the completion of a LH2 regenerative cooled throat segment.

Verification of the design was achieved with hot fire testing of a heatsink version of the chamber with only the throat section using hydrogen cooling. Hydraulic performance of the injector and cooled throat were verified by water flow testing prior to TCA assembly. The cooled throat was proof tested to 3000 psia to verify the integrity of the co-deposited EF Nickel-Cobalt closeout.

Fourteen heat sink tests were completed at chamber pressures of 85 to 359 psia. The injector face was modified to add more face coolant flow and ten more tests were run at chamber pressures of 197 to 620 psia. The cooled throat was installed and seven more tests run at pressures up to 2275 psia.

Results of the chamber thermal characteristics indicated outerbody flux levels on the order of 13 Btu/sec in**2 for the 2000 Pc tests. This was 10% lower than what was predicted based on the lower Pc tests using the relationship of Flux = Pc** 0.8. However, based on the overall design requirement of flux levels equal to 10 Btu/in2 in the barrel section of the chamber, the outerbody flux was 23% higher.

Centerbody flux levels were exceptionally high for the higher Pc tests. Two particularly hot areas were noted, 0.5 inches from the face of the injector, and on the tip of the centerbody. These flux levels averaged 40 to 60% higher than what was predicted from the low Pc set of tests and roughly 69% higher than the design flux level of 10 Btu/in2.

The flux levels measured in the throat indicated levels of 60 to 80 against the design flux of 100. This gave confidence to the testing with the regeneratively cooled nozzle. Performance of this component compared favorably with the analytical predictions.

Variations in heat flux proved to be proportional to the chamber pressure for the centerbody and the outerbody. Mixture ratio effects were not noticeable as the plots indicated in Sections 4.4.1 and 4.4.2. This supports the intent to operate the thrust chamber assembly over a wide range of operating conditions with a minimum wall temperature variation during operations.

Performance data from the low Pc set of tests indicated an injector element ERE of virtually 100%. This parameter is difficult to assess for high Pc set of tests due to the uncorrectable flow measurement anomalies which include:

- Close proximity of fuel venturi flowmeter to control valve (Approximately 6 inches).
- Control valve may have had some influence on the flow through the venturi.
- Distance from point of flowrate calculation to injector delivery point (Approximate 6 feet).

- Absence of thermocouple prevents accurate estimation of the temperature drop and resulting density changes from venturi flowmeter to injector manifold. Longer duration tests may have given propellant temperatures a chance to equalize, shorter tests probably had more of a temperature drop, thus more impact on flow calculation.

Heat flux levels for the outerbody were within 25% of the design goal at this element efficiency. Further refinement of the element can be made to improve wall compatibility and should be pursued. A large data base of test conditions is necessary to assess the data scatter in the three tests within the 1000 and 2000 psia chamber pressure range.

The gas-gas injector proved to be stable over the range of operating conditions of chamber pressure from 100 to 2000 and mixture ratio ranges from 3 to 8. Injector parameters of CdA and pressure drop were consistent over the range of tests.

5.3 Recommendations

Further work is recommended to continue characterization of the injector element design. By slight modifications to the injection angles of the fuel circuit, it should be possible to lessen the heat flux thereby improving wall compatibility without degradation of combustion performance.

Any follow-on test program should add more thermocouples to the outerbody and centerbody to ensure that heat flux readings are not being based on localized hot spots. Examination of the hardware gave no indication of streaks despite the indicated localized high heat fluxes.

Longer test durations would enable steady state conditions to be achieved at the higher chamber pressures. The control valves in the test stand did not respond as quickly as desired. Due to the slow ramp-up times during the tests, temperature shutdowns occurred very shortly after the nominal thrust levels were obtained. Investigation into higher response control valves or an alternative approach to propellant flow control would allow the ramp time to be shortened.

REFERENCES

1. Fang, J.J., "Application of Combustion Time-Lag Theory to Combustion Stability Analysis of Liquid and Gaseous Propellant Rocket Engines", AIAA paper No. 84-0510, AIAA 22nd Aerospace Sciences Meeting, January 1984.

2. Frey, H., and Nickerson, G.R., Two-Dimensional Kinetic Reference Program, prepared by Dynamic Science, Contract NAS 9-10391, December 1970.

3. Calhoon, D., Ito, J., and Kors, D., "Investigation of Gaseous Propellant Combustion and Associated Injector/Chamber Design Guidelines," prepared by Aerojet TechSystems Company, Contract NAS 3-14379.

4. Chemical Propulsion Information Agency, "JANNAF Rocket Engine Performance Prediction and Evaluation Manual," April 1975.

5. R.L. Ewen, Modification of the SCALER Program for the Low Thrust I_{sp} Sensitivity Study, TAR 9751:0646, Aerojet Liquid Rocket Co., 9 April 1981.